

THE INTERACTION OF METAL CARBONYL COMPOUNDS WITH
ORGANIC POLYMERS AND MONOMERS

A Thesis presented for the degree of Doctor of Philosophy

at



by

Michael P. Lyons B.Sc.

under the supervision of Dr. Conor Long

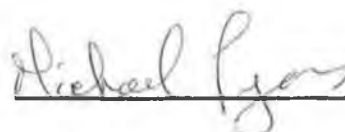
School of Chemical Sciences

October 1993

To
My Parents

Declaration

I, the undersigned, declare that the work presented in this thesis represents the sole work of the author, carried out at Dublin City University under the supervision of Dr. Conor Long.

A handwritten signature in dark ink, appearing to read 'Michael Lyons', is written over a horizontal line.

Michael P. Lyons

Acknowledgements

I would like to express my sincerest gratitude to Dr. Conor Long for his knowledge, encouragement and supervision over the last three years. I thank my fellow postgraduates, the academic and technical staff at DCU, for their help and friendship throughout.

Also, thanks to my classmates Helen, Mark, James, Catherine, Eithne, and Margaret, and many other postgrads including Declan, Stephen, Peter, Cormac, Shane, James, Tia, Fiona, and many others including Boris and Gilly, for their friendship.

To my friends Tony, Kevin, and Declan, what can I say? - I made it!

I especially thank past and present members of 'The Conor Long Research Group' namely Graham, Gerry, Barry, Celia, Irene, Maureen, Mary and Ciara.

I acknowledge the financial support received from Waterford County Council, Eolas and DCU.

I would like to thank my family, namely, Breeda (and Conor), Louise A., Patrick (Sinead, and Louise), Eugene, Laurence, Sean, Rudy, Fiona, Eric, and Jovita, for their never ending love and encouragement.

Finally, I thank my parents for their infinite love and support (financial and otherwise) throughout my 'extended' education.

Table of Contents

Contents	Page
Title Page	(i)
Dedication	(ii)
Declaration	(iii)
Acknowledgements	(iv)
Table of Contents	(v)
Abstract	(xii)

Chapter 1

Introduction.

1.1	Introduction.	2
1.1.1	Photolysis of Metal Carbonyl Compounds.	6
1.1.2	Low Temperature Matrix Isolation.	9
1.1.3	Laser Flash Photolysis.	10
1.2	References.	13

Chapter 2

Flash Photolysis of $M(CO)_6$, ($M = W, Mo, \text{ or } Cr$), and Poly(StyCr(CO)₃) in Toluene Solution.

2.1	Synthesis and Catalytic Reactions of Phosphine Containing Catalysts.	18
2.2	Photolysis of Metal Carbonyl Compounds in Polymer Matrices.	23
2.2.1	Laser Flash Photolysis of Metal Carbonyl Compounds in the presence of Monomeric and Polymer-bound Pyridines in Solution.	28
2.3	Results and Discussion.	32
2.3.1	Laser Flash Photolysis of $W(CO)_6$ in the presence of Monomeric and Polymeric Phosphine Units in Toluene.	32
2.3.1.1	Electronic Excitation Spectrum of $W(CO)_6$ in Toluene Solution.	33
2.3.1.2	Second Order Reaction Rates for the Reaction of $W(CO)_5(S)$ with Phosphine Units.	36
2.3.1.3	Activation Parameters for the Reaction of $W(CO)_5(\text{toluene})$ with Various Phosphine Units.	37
2.3.2	Laser Flash Photolysis of $Mo(CO)_6$ in the presence of Monomeric and Polymeric Phosphine Units in Toluene Solution.	40

2.3.2.1	Second Order Reaction Rates for $\text{Mo(CO)}_5(\text{S})$ with Phosphine Units.	41
2.3.2.2	Activation Parameters for the Reaction of $\text{Mo(CO)}_5(\text{toluene})$ with Various Phosphine Units.	42
2.3.3	Laser Flash Photolysis of Cr(CO)_6 in the presence of Monomeric and Polymeric Phosphine Units in Toluene Solution.	45
2.3.3.1	Second Order Reaction Rates for $\text{Cr(CO)}_5(\text{S})$ with Phosphine Units in Toluene Solution.	46
2.3.3.2	Activation Parameters for the Reaction of $\text{Cr(CO)}_5(\text{toluene})$ with Various Phosphine Units in Toluene Solution.	48
2.3.4	Discussion.	51
2.4	Laser Flash Photolysis of M(CO)_6 in the presence of Various Homopolymers in Toluene Solution.	53
2.4.1	Laser Flash Photolysis of M(CO)_6 , ($\text{M} = \text{W, Mo, or Cr}$) in the presence of Various Molecular Weight Polystyrenes (with and without free PPh_3) in Toluene.	54
2.4.1.1	Comparison of Transient UV/visible Absorption Spectra for the Reaction of Cr(CO)_6 with Polystyrene Ligands made <i>via</i> Two Different Synthetic Routes.	57
2.4.2	Laser Flash Photolysis of M(CO)_6 , ($\text{M} = \text{W, Mo, or Cr}$) in the presence of Various Molecular Weight Poly- α -Methylstyrenes in Toluene.	62

2.4.3	Laser Flash Photolysis of $M(CO)_6$ ($M = W, Mo, \text{ or } Cr$) in the presence of Various Molecular Weight (PMMA) Polymethylmethacrylates in Toluene.	66
2.4.4	Summary.	68
2.5	Laser Flash Photolysis of Polystyrene-anchored Chromium-tricarbonyl in the presence of Free Triphenylphosphine in Toluene Solution.	69
2.5.1.1	Activation Parameters for the Reaction of $P-(S:StyCr(CO)_2(S))$ with Triphenylphosphine in Toluene.	73
2.5.2	Discussion.	75
2.6	Conclusion.	75
2.7	References.	79

Chapter 3

Laser flash photolysis of $StyCr(CO)_3$, $CpMn(CO)_2(\eta^2-C_8H_{14})$, and $MeCpMn(CO)_2(\mu-Sty)Cr(CO)_3$.

3.0	Introduction.	84
3.1	(Arene) $Cr(CO)_2$ - π -olefin Complexes.	85
3.2	Mononuclear $CpMn$ - π -olefin Compounds.	92
3.3	Hetero-binuclear $CpMn$ - π -olefin Compounds.	96

3.3	Results and Discussion.	98
3.3.1	Laser Flash Photolysis of $\text{StyCr}(\text{CO})_3$ in Cyclohexane Solution.	98
3.3.3.1	Electronic Excitation Spectrum of $\text{StyCr}(\text{CO})_3$.	99
3.3.1.2	Primary Photoproduct.	101
3.3.1.3	Activation Parameters for the reaction of $\text{StyCr}(\text{CO})_2(\text{S})$ with CO.	105
3.3.1.4	Formation of $\text{Sty}_2\text{Cr}_2(\text{CO})_5$.	109
3.3.1.5	Activation parameters for the formation of $\text{Sty}_2\text{Cr}_2(\text{CO})_5$.	113
3.3.1.6	Infrared Monitored Photolysis of $\text{StyCr}(\text{CO})_3$.	116
3.3.1.7	Attempted Homopolymerisation of $\text{StyCr}(\text{CO})_3$ by UV/vis Irradiation.	119
3.3.1.8	Summary.	122
3.3.2	Laser Flash Photolysis of $\text{CpMn}(\text{CO})_2(\eta^2\text{-C}_8\text{H}_{14})$ in Cyclohexane Solution.	123
3.3.2.1	Electronic Excitation Spectrum of $\text{CpMn}(\text{CO})_2(\eta^2\text{-C}_8\text{H}_{14})$.	125
3.3.2.2	Primary Photoproduct.	126
3.3.2.3	Activation Parameters for the reaction of $\text{CpMn}(\text{CO})_2(\text{S})$ with CO.	132
3.3.2.4	Formation of $(\text{CO})_2\text{CpMn}(\mu\text{-CO})\text{MnCp}(\text{CO})(\eta^2\text{-C}_8\text{H}_{14})$.	135
3.3.2.5	Activation Parameters for the formation of $(\text{CO})_2\text{CpMn}(\mu\text{-CO})\text{MnCp}(\text{CO})(\eta^2\text{-C}_8\text{H}_{14})$.	140

3.3.2.6	Infrared Monitored Photolysis of $\text{CpMn(CO)}_2(\eta^2\text{-C}_8\text{H}_{14})$.	143
3.3.2.7	Summary.	144
3.3.3	Laser Flash Photolysis of $\text{MeCpMn(CO)}_2(\mu\text{-Sty})\text{Cr(CO)}_3$ in Cyclohexane Solution.	146
3.3.3.1	Electronic Excitation Spectrum of $\text{MeCpMn(CO)}_2(\mu\text{-Sty})\text{Cr(CO)}_3$.	147
3.3.3.2	Primary Photoproduct.	148
3.3.3.3	Activation Parameters for the reaction of CO with $\text{MeCpMn(CO)}_2(\mu\text{-Sty})\text{Cr(CO)}_2(\text{S})$.	154
3.3.3.4	Formation of $\{\text{MeCpMn(CO)}_2(\mu\text{-Sty})\text{Cr(CO)}_2\}_2(\mu\text{-CO})$.	158
3.3.3.5	Activation Parameters for the formation of $\{\text{MeCpMn(CO)}_2(\mu\text{-Sty})\text{Cr(CO)}_2\}_2(\mu\text{-CO})$.	161
3.3.3.6	Infrared Monitored Photolysis of $\text{MeCpMn(CO)}_2(\mu\text{-Sty})\text{Cr(CO)}_3$.	165
3.3.3.7	^1H NMR Monitored Photolysis of $\text{MeCpMn(CO)}_2(\mu\text{-Sty})\text{Cr(CO)}_3$.	167
3.3.3.8	Summary.	167
3.3.3.9	Conclusion.	168
3.4	References.	171

Chapter 4

The Crystal and Molecular Structure of $\text{MeCpMn(CO)}_2(\mu\text{-Sty})\text{Cr(CO)}_3$.

4.1	Introduction.	176
4.2	Data collection for $\text{MeCpMn(CO)}_2(\mu\text{-Sty})\text{Cr(CO)}_3$.	177
4.3	Molecular structure of $\text{MeCpMn(CO)}_2(\mu\text{-Sty})\text{Cr(CO)}_3$.	181
4.4	References.	191

Chapter 5

Experimental Section.

5.1	Materials.	194
5.2	Equipment and Procedures.	194
5.3	Synthetic Procedures.	207
5.4	Synthesis of the Homopolymer Complexes.	210
5.5	Synthesis of the Copolymer Complexes.	212
5.6	References.	214
	Appendix A	215
	Appendix B	222
	Appendix C	229
	Appendix D	236

The Interaction of Metal Carbonyl Compounds with Organic Polymers and Monomers.

Michael P. Lyons

Abstract

The photochemistry of W(CO)_6 , Mo(CO)_6 , and Cr(CO)_6 in the presence of monomeric and polymeric triphenylphosphine ligands was investigated in toluene solution, using laser flash photolysis with 355nm excitation. The mechanism and kinetics of interaction of the primary photoproducts $\text{M(CO)}_5(\text{toluene})$ ($\text{M} = \text{W, Mo, or Cr}$) with the various monomeric ligands were investigated. Interaction of the metal carbonyl photofragments with various homopolymers is also discussed. The polymerisation methods used resulted in polymers with either cyano end-groups or methyl end-groups. The nature of the end-group proved to be important in interpreting the observed reaction kinetics. The root mean square (rms) end-to-end distances of the polymer chains were also considered in rationalising the observed trends.

The solution photochemistry of StyCr(CO)_3 , $\text{CpMn(CO)}_2(\eta^2\text{-C}_8\text{H}_{14})$, and $\text{MeCpMn(CO)}_2(\mu\text{-Sty})\text{Cr(CO)}_3$, ($\text{Sty} = \text{Styrene}$; $\text{Cp} = \text{Cyclopentadienyl}$) was investigated in room temperature cyclohexane solution using laser flash photolysis with 355nm excitation. In StyCr(CO)_3 , the effect of an olefin substituent on the arene ring, on the reactivity of the photochemical intermediates produced was investigated. In the manganese complexes, olefinic ligands were directly coordinated to the metal centre, and the subsequent photochemistry was studied.

The crystal and molecular structure of $\text{MeCpMn(CO)}_2(\mu\text{-Sty})\text{Cr(CO)}_3$ is also presented. This complex contains a styrene unit in an unusual bridging role between the two metal centres.

Chapter 1

Introduction.

1.1 Introduction.

The history of organotransition metal chemistry dates back to the early 1800's, when the first transition metal salt was prepared. Since then development in the area has been very extensive. The principal reason for such development was the great potential of these organometallic species as catalysts in industrial reactions. Many important discoveries were made, including the Ziegler and Wacker processes [1]. Ziegler developed the efficient polymerisation of ethylene using a combination of TiCl_4 and AlCl_3 under very mild conditions. This process was discovered simultaneously by Natta in Italy. These catalysts were often used for the production of various monomers which, in turn were used as precursors to new polymers and plastics.

An increasing demand for polymers and plastics led to the discovery of more efficient cost-effective ways to synthesise monomers with improved catalyst recovery. From the 1950's to the mid-1970's rapid expansion took place in the petrochemicals industry, with the use of olefins and dienes containing C_2 - C_5 carbon units as feedstocks.

Because of the limited supply of petrochemical resources and also their ever-increasing costs, recent years have seen a shift towards finding new feedstocks [2]. The importance of carbon monoxide in catalysis, coupled to its wide availability has led to its increasing use as a feedstock in the form of 'synthesis gas' or syngas, which is a mixture of carbon monoxide and hydrogen. It is mainly produced from reforming of natural gas and naphtha, but may also be obtained from coal or heavy petroleum fractions. These investigations are at a relatively early stage, and many of the well

documented homogeneous catalytic processes are still in operation.

The major advantage of homogeneous catalysis is the great selectivity enabling the synthesis of pure products. An example is the Wilkinson catalyst $\text{RhCl}(\text{PPh}_3)_3$, used for hydrogenation of olefins [3]. Advantages over heterogeneous systems include greater activity and specificity and the greater number of active sites exposed. Problems are however encountered in separating the catalyst from the product; loss of activity of the catalyst species, and the unstable nature of some homogeneous catalytic systems.

This could be overcome by embedding the catalytically active species onto a polymer support. Incorporating these homogeneous catalysts onto the polymer backbone effectively 'heterogenises' them. This may be carried out by reaction steps which maintain the structure and function of the homogeneous complex. These catalysts offer higher selectivity at relatively mild operating conditions [4]. Activity and selectivity of the heterogenised catalysts may be controlled by attachment of different ligands and by varying the solvent. Heterogeneous catalysts are in general less active and of lower selectivity compared to their homogeneous analogues but are easily separated from reaction products.

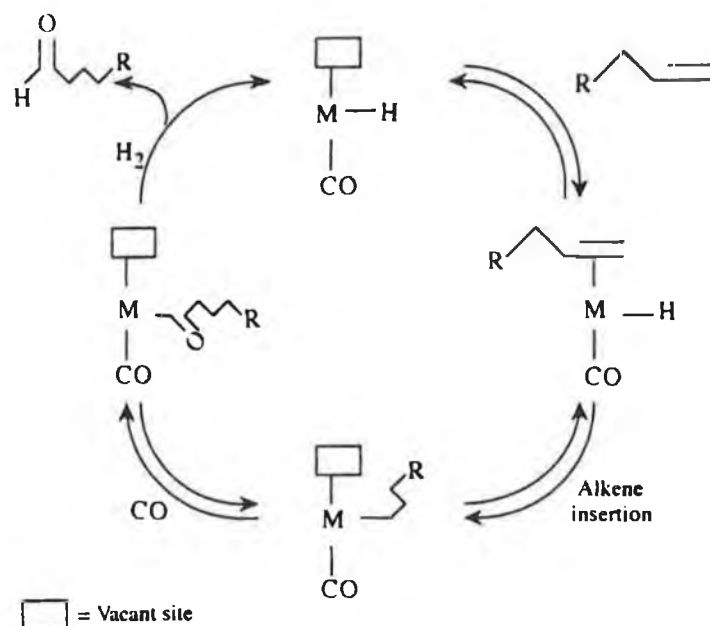
Haag and Whitehurst were the first to immobilise a homogeneous catalyst onto a solid support [5]. Grubbs and Kroll [6], in their work on reduction of olefins with a polymer-supported rhodium catalyst showed that activity greatly increased over a surface reduction reaction with $\text{RhCl}(\text{PPh}_3)_3$ and also, specificity for the polymer-bound catalyst was much higher. The catalytic species may be chemically immobilised by attaching to various donor sites on the support. Phosphine anchors are by far the most popular [see for example refs. 7-10], but others have been used *e.g.* pyridine type

donors [11].

Improved separation of catalyst from products has been achieved by thermal methods also [9]. A polyethylene bound catalyst was prepared which is insoluble at room temperature. At elevated reaction temperature, catalysis is very efficient, and separation of the reaction product is achieved by returning to room temperature, where the insoluble catalyst precipitates from solution. The possibility of coordinating more than one catalytic species to the support allows sequential multi-step catalytic reactions. This was first exploited by Pittman and Smith [44] who performed cyclooligomerisation reactions on butadiene followed by various hydrogenation or hydroformylation reactions. The wide variety and availability of polymer supports, attachable donor ligands, and transition metal catalysts allows the development of 'finely-tuned' catalysts which may participate in very specific catalytic sequences [12].

A relatively simple catalytic cycle is shown in Figure 1.1.1, demonstrating alkene hydroformylation using the homogeneous catalyst HCo(CO)_4 [2]. In the sequence, this species is monodecarbonylated to generate vacant sites for the alkene and H_2 . The metal-alkyl is formed by alkene insertion, and the alkyl undergoes a migratory insertion to give the corresponding acyl metal carbonyl. This is cleaved by H_2 to give the aldehyde product, with regeneration of the catalyst.

Figure 1.1.1:



Many different transition metals have been used in catalysis including ruthenium [13], niobium and tantalum [14].

The catalytically active species may be immobilised by several methods including chemical bonding, as used for phosphine and pyridine donors, high temperature vapour deposition [15] and physical impregnation [16]. Functionalising polymers by vapour deposition yields catalytic metal species with high surface to mass ratios, which result in improved catalyst efficiency.

Physically impregnated metallic species have potential uses as indicators for gas permeability in polymeric species, an important aspect in the food and drug industry and in soft contact lenses.

Chemically modified polymers have found many uses, the more recent include the preparation of optical materials of low specific gravity and high refractive index [17], and radiation sensitive polymers suitable for use in graphical [18] and biological [19] applications among others. Because of the increasing number of applications for these polymers and plastics, the quantities currently being synthesised are very substantial. In 1991, the

demand for styrene alone (as a precursor to various polymers) amounted to 13.7 million tons, and is projected to reach 19.3 million tons by the year 2000 [45]. This increase in demand has been attributed to the use of styrene polymers in the rapidly expanding electronic and communications industry. Growing in line with the increasing demand for polymers is the very big problem of plastic litter [20]. Because of this, investigations are now centering on the area of degradable polymers, principally by photochemical methods. Tenhaeff and Tyler [21] have produced polymers with metal-metal centres along the polymer backbone. Upon UV irradiation the metal-metal bonds are cleaved, resulting in degradation of the polymers.

Despite the significant advantages of polymer-supported systems over their homogeneous analogues, the latter is still used in nearly all processes *e.g.* the Wacker process. This involves the synthesis of acetaldehyde by oxidation of ethylene using a palladium dichloride catalyst [2]. There are many disadvantages for heterogenised systems including heat transfer, low activity and selectivity, and the requirement of high temperatures (and high pressures).

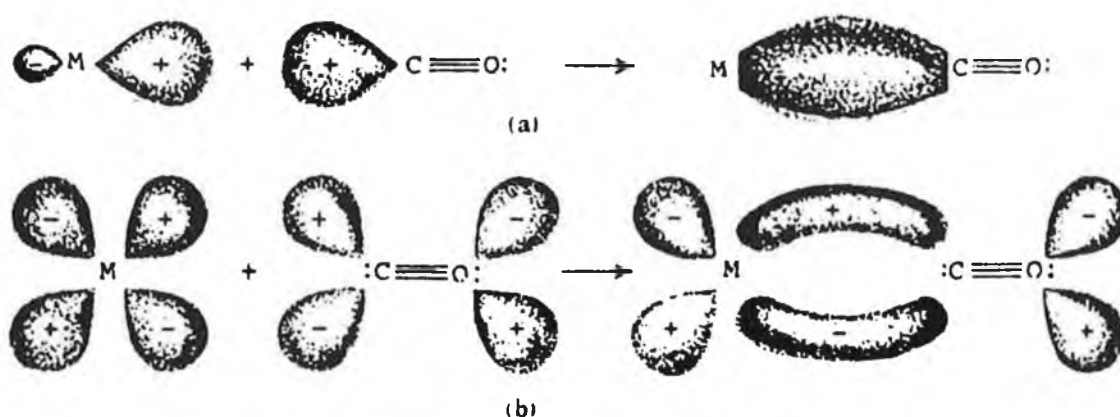
1.1.1 Photochemistry of Metal Carbonyl Compounds.

In many reactions involving transition metal carbonyl compounds and substrates, the primary reaction is photo-ejection of a CO molecule to generate a highly reactive intermediate. As in many of the reactions discussed, the main concern was with the efficient production of product with good catalyst recovery. Very little attention has been given to the nature of reactive intermediates in these processes. A detailed understanding of the

reaction intermediate may provide invaluable information towards overall improvement of catalyst systems.

Firstly, the nature of the metal-CO bond must be considered. This bond has both σ and π characteristics, as shown in Figure 1.1.2. The carbon lone-pair overlaps with the metal $d\sigma$ orbitals and may donate electron density to the metal as in (a). Reinforcing this metal-CO σ bond is the fact that the non-bonding $d\pi$ orbitals on the metal overlap with the π^* antibonding orbitals of the CO, and back-donation efficiently stabilises the filled $d\pi$ set (b). The metal is relieved of its excess electron density.

Figure 1.1.2:

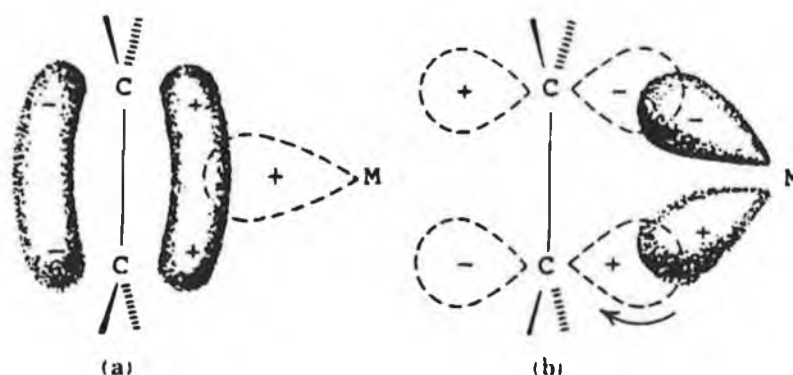


Irradiation of the metal-CO bond promotes an electron from the π bonding orbital to the σ orbital which is metal-CO antibonding. This gives rise to a situation unfavourable to back-donation and higher electron density remains on the metal, eventually resulting in cleavage of the metal-CO σ bond. The quantum yield for the dissociation of CO is very high, making transition metal carbonyl compounds ideal precursors to catalytically active species.

Relevant to this thesis also is metal-olefin π -bonding, because complexes

containing metal-olefin π -bonds have been synthesised and investigated. The explanation of this type of bond was put forward by Dewar, Chatt and Duncanson [22] proving the existence of Zeise's platinum salt. Interaction of an olefin bond with a metal is shown in Figure 1.1.3. The filled π orbital of the coordinated ethylene overlaps with a $d\sigma$ acceptor orbital on the metal atom (a), while the filled metal $d\pi$ orbital overlaps with the π^* antibonding orbital of the olefin (b). The result is a relatively strong bond between the two centres. Overall the carbon-carbon double bond strength is reduced, resulting in a longer C=C bond length. Two coordination modes are possible; the C=C bond may be oriented perpendicular to the molecular plane, or it may be in the molecular plane [1].

Figure 1.1.3:



In a system where both metal-CO and metal-olefin bonds exist together, labilisation of one or the other may occur when irradiated.

Identification of the structure and reactivity of the intermediates produced in photochemical reactions has been monitored mainly by low temperature matrix isolation and laser flash photolysis.

1.1.2 Low Temperature Matrix Isolation.

Dispersing metal complexes in inert matrices at low temperatures was first carried out in the 1950's [23]. Temperatures are normally lower than 60K, and typical matrices include argon and methane [30]. Highly reactive photofragments may be stabilised at reduced temperatures, allowing their chemistry to be investigated. The technique has been used, for example, for the characterisation of unstable olefin-coordinated species such as $\text{Ni}(\text{C}_2\text{H}_4)$ and $\text{Ni}(\text{C}_2\text{H}_4)_2$ by IR spectroscopy [24]. The photofragments produced have been shown to react with what were once considered 'inert' matrices *e.g.* argon in $\text{Cr}(\text{CO})_5(\text{argon})$ [25]. Hooker and Rest investigated the photochemistry of some Group 6 metal hexacarbonyls [26], tricarbonyls [27], and several dinuclear complexes [34] in polyvinyl chloride (PVC) matrices from 12-298K. They concluded that the polymer matrices were very suitable to matrix isolation studies. They also noticed that the photoejected CO molecules did not diffuse away from the metal, as recombination was observed on warming the matrix. Irradiation at 298K resulted in an interaction with the PVC matrix. Similar trends were observed on irradiation of $\text{Fe}(\text{CO})_5$ in PVC, PTFE and LDPE matrices [28]. On warming from 12 to 60K, interaction of the iron carbonyl photofragment with the matrix was observed, indicating that it is a very reactive unsaturated intermediate, supporting previous investigations [29]. Low temperature solvent glasses have also been used to investigate these reactive intermediates. Bitterwolf *et al.* irradiated Group 6 metal hexacarbonyls and several half-sandwich complexes in Nujol mulls at 77K and observed the formation of the monodecarbonylated photoproducts and

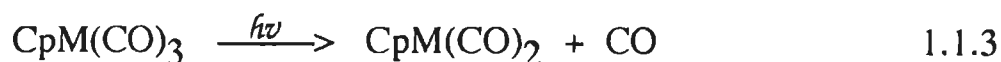
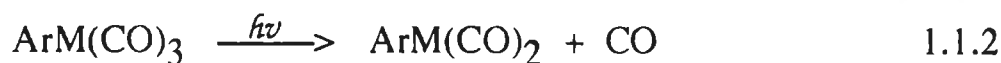
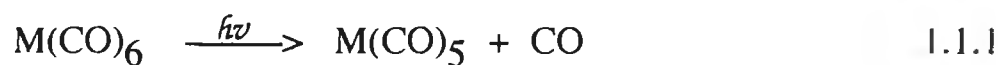
free CO [31]. Annealing of the mulls containing $M(CO)_5$ and free CO resulted in regeneration of the parent complex. Annealing of mulls containing cyclopentadienylmanganese carbonyl resulted in the formation of a dinuclear species. Low temperature solutions of liquefied noble gases have also been used to examine the nature of 'non-classical' dihydrogen or dinitrogen complexes [32]. Liquid xenon is most commonly used.

Gas phase reactions have also been studied because the photochemistry of complexes may be monitored without any influence from solvent [33].

1.1.3 Laser Flash Photolysis.

Flash photolysis was first introduced in the 1950's by Norrish and Porter [35]. The underlying principle is that by exposure of a sample to a high intensity pulse of monochromatic radiation, it is possible to generate a relatively high concentration of a transient species. This transient species is normally very unstable and decays to form other products. By monitoring these subsequent reactions using UV/vis or IR detection, one may determine the kinetics involved. Using infrared detection, structural information is also obtainable. The advantages of lasers include; (i) the monochromatic nature of the beam; (ii) the high intensity and (iii) the short pulse duration. Nasielski *et al.* [36] were the first to monitor the photoproducts on irradiation of $Cr(CO)_6$ using conventional flash photolysis with UV/vis detection.

Irradiation of $M(CO)_6$, $ArM(CO)_3$ ($M = W, Mo, \text{ or } Cr; Ar = C_6H_6$) or $CpM(CO)_3$ ($M = Mn; Cp = C_5H_5$) results almost always in photodissociation of a CO ligand as shown in Reactions 1.1.1 to 1.1.3.



The quantum yields for dissociation of CO are 0.67 [37], 0.72 [38] and 0.65 [39] respectively. Photodissociation of a ligand other than CO was also observed in ArM(CO)_3 [40], where displacement of the arene ring occurred. However, the quantum yield for this photoprocess was significantly lower. Arene displacement was found to be the predominant thermal reaction. The high quantum yield for dissociation of CO allows determination of the interaction kinetics of photogenerated intermediates with various ligands including norbornadiene [41] and 'token' solvent ligands [42]. However, the instantaneous ejection of a CO molecule produces a species which is highly reactive, especially if we consider Cr(CO)_5 . The sub-nanosecond photochemistry of this species is still unresolved, but there is a substantial amount of information in the literature [43]. Studies were carried out on the reactivity of this species in the presence of various solvents and ligands, but not (to our knowledge) when ligands were attached to polymer supports. Such metal carbonyl compounds may be incorporated onto polymer supports relatively easily, and these 'heterogenised' complexes have been extensively used in catalysis. Attachment of the metal to the support usually involves a one-step reaction. The catalytic reactions have been extensively characterised, while very little research has been carried out on the mechanism and kinetics of attachment of the metal to the support. Also, as regards the polymer support, the effect of different polymerisation methods

and/or molecular weight on the reaction kinetics has not received attention. More than one metallic species may be incorporated into these systems. Efforts to improve catalytic ability led to the synthesis of both mixed-metal (for sequential multi-step catalysis), and mixed-ligand complexes.

Mixed-ligand complexes containing both CO and π -bonding ligands have been known for some time. Irradiation of such compounds may lead to the ejection of either ligand to generate a coordinatively unsaturated intermediate. These compounds have widespread application as precursors to a variety of products *via* relatively simple pathways. However, the mechanism and kinetics of the intermediate reactions have not been well documented.

Part of this thesis is concerned with the mechanism and kinetics of interaction of Group 6 metal carbonyl photofragments with various polymeric supports. The effect of different polymerisation methods as well as the molecular weight of the support was also considered. The general aim of these investigations is centred on comprehending the fast reaction solution photochemistry of such metal-polymer systems, with a view to overall improvement of these 'heterogenised' catalysts.

We are also concerned with the photoprocesses of mixed-ligand complexes, notably CO and π -olefin ligands. The effect of attaching an electron-withdrawing group to a η^2 - π -coordinated olefin is also investigated.

1.2 REFERENCES

- 1 Yamamoto, A.; *Organotransition Metal Chemistry: Fundamental Concepts and Applications*, Wiley-Interscience, New York, 1986.
- 2 Parshall, G. W.; *Homogeneous Catalysis*, Wiley-Interscience, New York, 1980.
- 3 Halpern, J., in *Organotransition Metal Chemistry*; Ishii, Y.; Tsutsui, M. (eds.), Plenum Press, New York, 1975.
- 4 Swan, J. D.; Black, D. St. C.; *Organometallics in Organic Synthesis*, Chapman and Hall, London, 1974.
- 5 Haag, W.; Whitehurst, D. D.; *Belg. Pat.* 721,686, 1969.
- 6 Grubbs, R. H.; Kroll, L. C.; *J. Am. Chem. Soc.* **93**, 3062, 1971.
- 7 Evans, G. O.; Pittman, C. U. Jr.; McMillan, R.; Beach, R. T.; Jones, R.; *J. Organomet. Chem.* **67**, 295, 1974.
- 8 Sanner, R. D.; Austin, R. G.; Wrighton, M. S.; Honnick, W. D.; Pittman, C. U. Jr.; *Inorg. Chem.* **18**(4), 928, 1979.
- 9 Bergbreiter, D. E.; Chandran, R.; *J. Am. Chem. Soc.* **109**, 174, 1987.
- 10 Pittman, C. U. Jr.; Quock, N. G.; *J. Organomet. Chem.* **153**, 85, 1978.
- 11 (a) Creaven, B. S.; Long, C.; Russell, G.; Hamilton, J.; McQuillan, G. P.; *Inorg. Chim. Acta* **146**, 25, 1988; (b) Elman, B.; Moberg, C.; *J. Organomet. Chem.* **294**, 117, 1985; (c) Card, R. J.; Liesner, C. E.; Neckers, D. C.; *J. Org. Chem.* **44**(7), 1095, 1979; (d) Card, R. J.; Neckers, D. C.; *Inorg. Chem.* **17**(9), 2345, 1978; (e) Menger, F. M.; McCann, D. J.; *J. Org. Chem.* **50**, 3928, 1985; (f) Potts, K. T.; Usifer, D. A.; *Macromol.* **21**, 1985, 1988; (g) Biedermann, H. G.; Graf, W.;

- Chem. Ztg.* **98(11)**, 563, 1974; (h) Kelly, J. M.; Long, C.; *J. Organomet. Chem.* **235**, 315, 1982.
- 12 Pittman, C. U. Jr. in *Comp. Organomet. Chem.*; Wilkinson, G.; Stone, F. G. A.; Abel E. W. (eds.), Pergamon Press, Oxford, **8**, 553, 1982.
 - 13 (a) Pertici, P.; Vitulli, G.; Carlini, C.; Ciardelli, F.; *J. Mol. Catal.* **11**, 353, 1981; (b) Pittman, C. U. Jr.; Wilemon, G. M.; *J. Org. Chem.* **46**, 1901, 1981.
 - 14 Chang, B. H.; Lau, C. P.; Grubbs, R. H.; Brubaker, C. H. Jr.; *J. Organomet. Chem.* **281**, 213, 1985.
 - 15 Francis, C. G.; Timms, P. C.; *J. Chem. Soc., Chem. Commun.* 466, 1977.
 - 16 (a) Shaver, A.; Gao, J. P.; Butler, I. S.; *Appl. Organomet. Chem.* **3**, 425, 1989; (b) Shaver, A.; Gao, J. P.; Butler, I. S.; *Appl. Organomet. Chem.* **2**, 9, 1988; (c) Markwell, R. D.; Butler, I. S.; Gao, J. P.; Shaver, A. S.; *Appl. Organomet. Chem.* **6**, 693, 1992; (d) Hooker, R. H.; Rest, A. J.; Whitwell, I.; *J. Organomet. Chem.* **266**, C27, 1984.
 - 17 Doi, H.; Sakagami, T.; EP 322,614, 1989.
 - 18 (a) Wright, R. E.; EP 0,095,269, 1983; (b) Wagner, H. M.; Pubrick, M. D.; GB 2,106,522, 1983.
 - 19 Pispisa, B.; Paradossi, G.; Palleschi, A.; Desideri, A.; *J. Phys. Chem.* **92**, 3422, 1988.
 - 20 Scott, G.; *J. Photochem. Photobiol. A: Chem.* **51**, 73, 1990.
 - 21 (a) Tenhaeff, S.; Tyler, D. R.; *Organometallics* **10**, 473, 1991; (b) Tenhaeff, D.; Tyler, D. R.; *Organometallics* **10**, 1116, 1991.
 - 22 (a) Dewar, M. J. S.; *Bull. Soc. Chim. Fr.* C71, 1951; (b) Chatt, J.; Duncanson, L. A.; *J. Chem. Soc.* 2939, 1953.

- 23 Whittle, E.; Dows, D. A.; Pimentel, G.; *J. Phys. Chem.* **22**, 1954, 1943.
- 24 (a) Ozin, G. A.; *Acc. Chem. Res.*; **10**, 2, 1977; (b) Moskovits, M.; Ozin, G. A.; *Cryochemistry*, Wiley-Interscience, New York, 1976.
- 25 Perutz, R. N.; Turner, J. J.; *J. Am. Chem. Soc.* **97**, 4791, 1975.
- 26 Hooker, R. H.; Rest, A. J.; *J. Organomet Chem.* **249**, 137, 1983.
- 27 Hooker, R. H.; Rest, A. J.; *J. Chem. Soc., Dalton Trans.* 761, 1984.
- 28 Hooker, R. H.; Rest, A. J.; *Appl. Organomet. Chem.* **4**, 141, 1990.
- 29 Poliakoff, M.; Turner, J. J.; *J. Chem. Soc., Dalton Trans.* 2276, 1974.
- 30 Rest, A.; Sodeau, J. R.; Taylor, D. J.; *J. Chem. Soc., Dalton Trans.* 651, 1978.
- 31 Bitterwolf, T. E.; Lott, K. A.; Rest, A. J.; Mascetti, J.; *J. Organomet. Chem.* **419**, 113, 1991.
- 32 (a) Gadd, G. E.; Upmacis, R. K.; Poliakoff, M.; Turner, J. J.; *J. Am. Chem. Soc.* **108**, 2547, 1986; (b) Upmacis, R. K.; Poliakoff, M. A.; Turner, J. J.; *J. Am. Chem. Soc.* **108**, 3645, 1986; (c) Turner, J. J.; Simpson, M. B.; Poliakoff, M.; Maier II, W. B.; Graham, M. A.; *Inorg. Chem.* **22**, 911, 1983.
- 33 Zheng, Y.; Wang, W.; Lin, J.; She, Y.; Fu, K.J.; *J. Phys. Chem.* **96**, 9821, 1992.
- 34 Hooker, R. H.; Rest, A. J.; *J. Chem. Soc., Dalton Trans.* 1121, 1990.
- 35 Norrish, R. G. W.; Porter, G.; *Nature*, **164**, 658, 1949.
- 36 Nasielski, J.; Kirsch, P.; Wilputte-Steinert, L.; *J. Organomet. Chem.* **29**, 269, 1971.
- 37 Nayak, S. K.; Burkley, T. J.; *Organometallics* **10**, 3745, 1991.
- 38 Wrighton, M. S.; Haverty, J. L.; *Z. Naturforsch.* **30b**, 254, 1975.

- 39 Giordano, P.; Wrighton, M. S.; *Inorg. Chem.* **16**(1), 160, 1977.
- 40 (a) Strohmeier, W.; von Hobe, D.; *Z. Naturforsch.* **18b**, 770, 1963;
(b) Strohmeier, W.; von Hobe, D.; *Z. Naturforsch.* **18b**, 981, 1963.
- 41 Zhang, S.; Dobson, G.; *Inorg. Chem.* **29**, 598, 1990.
- 42 (a) Wieland, S.; Van Eldik, R.; *J. Phys. Chem.* **94**, 5865, 1990; (b)
Zhang, S.; Dobson, G.; Zang, V.; Bajaj, H. C.; Van Eldik, R.; *Inorg.
Chem.* **29**, 3477, 1990; (c) Simon, J. D.; Xie, X.; *J. Phys. Chem.* **91**,
5538, 1987; (d) Langford, C. H.; Moralejo, C.; Sharma, D. K.;
Inorg. Chim. Acta **126**, L11, 1987.
- 43 Turner, J. J.; in *Photoprocesses in Transition Metal Complexes,
Biosystems and other Molecules, Expt. and Theory*; Kochanski, E.
(ed.), 125, 1992.
- 44 Pittman, C. U. Jr.; Smith, L. R.; *J. Am. Chem. Soc.* **97**(7), 1750,
1975.
- 45 Kalton, M.; *Chem. Brit.* 291, 1993.

Chapter 2

**Flash Photolysis of $M(CO)_6$, ($M = W, Mo, \text{ or } Cr$), and
Poly($StyCr(CO)_3$) in Toluene Solution.**

2.1 Synthesis and Catalytic Reactions of Phosphine Containing Catalysts.

Problems associated with soluble transition metal catalysts may sometimes be overcome by embedding them in an insoluble support. Such “hybrid” catalysts combine the virtues of homogeneous and heterogeneous catalysts. However, with solid supports, the reactants and products will need to be soluble, so as to ensure good catalyst efficiency and ultimately, ease of separation of the product.

A method has been developed which involves chemically binding a transition metal complex to a solid support, to generate a heterogeneous catalyst. Silica and alumina [1] supports are widely used, where the transition metal complex is fixed on the solid surface. More popular supports include those which possess a chemically-bonded pendant phosphine group [2]. Phosphine-containing polymers may be prepared in two ways:

- (i) by substitution reactions on preformed polystyrene;
- (ii) by copolymerisation of monomers such as *p*-diphenylphosphinostyrene with, for example, styrene.

Research in this area has been extensively covered by Pittman [3] and coworkers. In 1974, he described the preparation of both linear and cross-linked phosphinated polymeric ligands [3a], as well as subsequent incorporation of various metal carbonyls, by both thermal and photochemical methods. Catalytic studies carried out on ‘new’ heterogeneous cobalt derivatives found them to be active in the hydroformylation of 1-pentene at relatively low pressure, much below that required for $\text{Co}_2(\text{CO})_8$

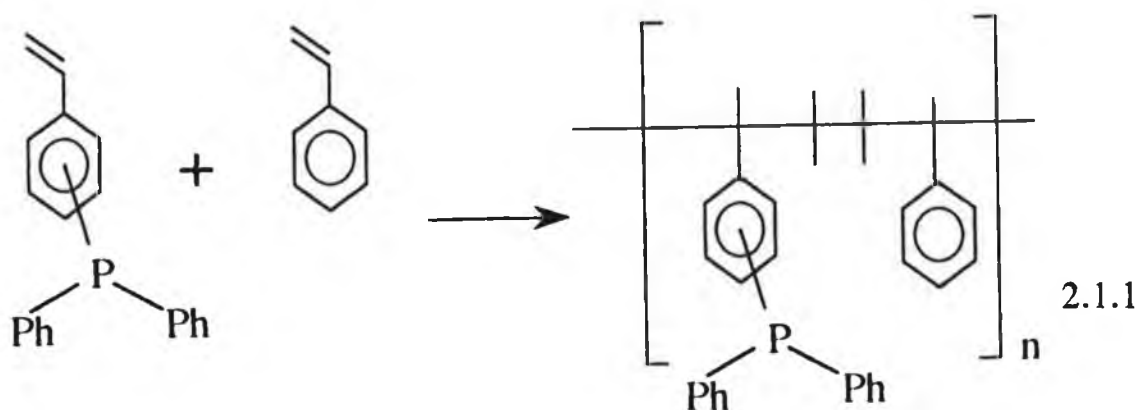
and similar to results reported for the diphosphine substituted homogeneous analogue $\text{Co}_2(\text{CO})_6(\text{PPh}_3)_2$. The polymeric catalysts were recovered by filtering the reaction mixture in air, followed by washing.

The ability to carry out sequential multi-step reactions was also investigated [3b]. This involved supporting two different catalysts on a polymer backbone, for example, the immobilisation of nickel and rhodium, followed by a study of the resultant catalytic activity. However the proximity of coordinatively unsaturated sites in solution may lead to problems. For instance, if the metal centres are too close or their concentration is too high, then metal-metal interactions may be promoted, reducing catalytic activity with the disappearance of active sites. When phosphines are immobilised along the polymer support, the possibility of more than one of these interacting with the metal is reduced, *e.g.* palladium [3c]. In homogeneous situations, this would normally result in catalyst agglomeration and deactivation.

An important feature of metal carbonyl phosphines is the relative photostability of the metal-phosphine bond. Our studies are based on using phosphines as anchors for transition metal catalysts on polymer supports because, upon exposure to light, a ligand other than the phosphine will usually be photoejected [3d] to generate an immobilised, coordinatively unsaturated metal centre. Sanner *et al.* concluded that the polymer anchored- $\text{Fe}(\text{CO})_n$ lost a carbonyl ligand when irradiated, thus generating a highly reactive metal centre available for catalysis.

Other metals anchored to phosphine units include ruthenium [3e], where the activated metal centre plays a catalytic role in the hydroformylation of 1-

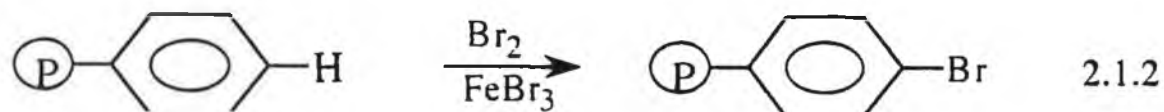
pentene. Capka and coworkers [4] looked at various hydrogenation, hydrosilylation, and hydroformylation of olefins catalysed by polymer-supported rhodium complexes. The polymer support used was a phosphinated polystyrene-divinylbenzene resin. These resins also found uses in organic synthesis. Camps [5] treated a 3:1 copolymer of styrene: *p*-diphenylphosphinostyrene (2% dvb) with benzyl chloride, to produce the polymer bound *p*-styryldiphenyl-benzyl-phosphonium chloride. This was reacted with a base, and then benzaldehyde added. Finally, the resultant polymeric species was removed and variable quantities of *cis*-, *trans*-, stilbene, benzyl alcohol, benzoic acid, and benzaldehyde were recovered. There are two ways of functionalising various resins. Firstly, *p*-DPPS monomer is prepared (see Chapter 5). This may then be copolymerised with an olefinic comonomer [6, 7, 14] as in Reaction 2.1.1.



A cross-linking agent may be added if required. The mole ratio of comonomers may be varied, allowing one to control the proportion of phosphine groups in the final polymeric material. The polymerisation reaction may be carried out in bulk, solution, emulsion, or in suspension.

An alternative procedure [3, 8-10] for preparing phosphine containing

polymers would be to react a halogenated (cross-linked) vinyl aromatic polymer with butyl lithium as shown in Reactions 2.1.2 -2.1.3.



Halogenated diphenylphosphine is then introduced to produce the supported polymeric diphenylphosphinostyrene resin (Reaction 2.1.4).

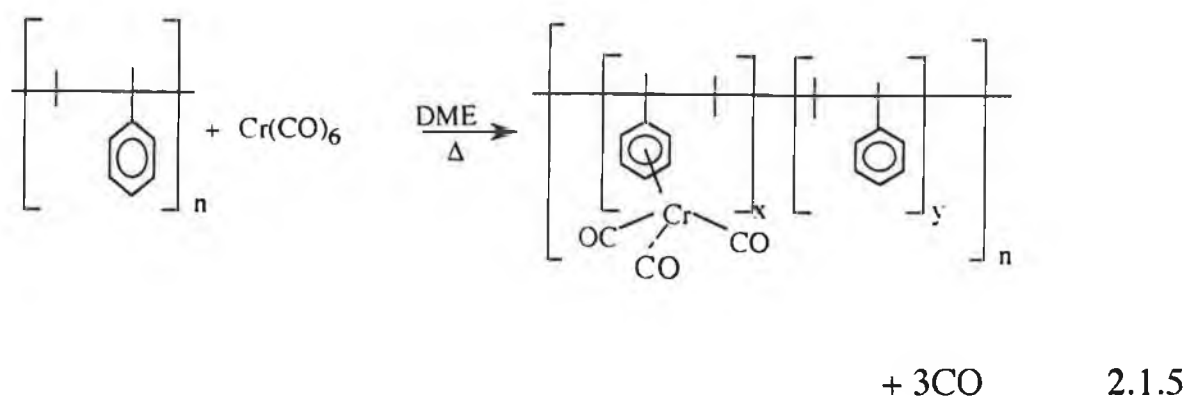


The functionalisation of polymeric resins in this way has received much attention [8-13]. It also allows for a more complete characterisation of the polymer.

Another very useful technique for the metallation of polymeric species is the dispersion of very fine metallic particles onto the polymer. Metals with high surface to mass ratios have been used as heterogeneous catalysts in industry for over 150 years [15, 16]. Draper described the formation of ultra fine metal particles from the corresponding metal carbonyl compounds [17].

Functionalisation of a polymeric species may also be achieved by a direct

reaction with the metal carbonyl compound [18, 19]. Polystyrene reacted with chromium hexacarbonyl in refluxing dimethoxyethane (DME) to produce a polymer in which about 32% of the benzene rings were complexed with chromium tricarbonyl moieties (Reaction 2.1.5),



As already mentioned, attachment and activation of a potential catalytic centre may be achieved by photochemical as well as thermal methods. Photochemical investigations previously carried out on some metal carbonyl systems in the presence of polymeric ligands [20, 21] have exhibited some interesting trends. We have looked at the photochemistry of Group 6 metal carbonyls in the presence of polymeric species. The photochemistry of the Group 6 metal carbonyl compounds has been well documented [see for example refs. 22-27]. However, the effect of a polymer support on the photochemistry of these compounds has received little attention.

2.2 Photolysis of Metal Carbonyl Compounds in Polymer Matrices.

Solution photolysis of $M(CO)_6$ ($M = W, Mo, \text{ or } Cr$), yields the “naked” $M(CO)_5$ fragment [28,29], which is rapidly solvated (Reaction 2.1.6 - 2.1.7).



In the presence of a coordinating ligand, L , the more stable ligated species is formed [23-28], (Reaction 2.1.8)



In 1961, Massey and Orgel [30] observed that methylmethacrylate polymers which were impregnated with metal hexacarbonyls, became yellow upon exposure to ultra-violet irradiation. This was the first evidence published for the interaction of a metal carbonyl photofragment with a polymer matrix. The researchers proposed that the metal pentacarbonyl was stabilised by interaction with neighbouring ester groups or isolated carbon-carbon double bonds. The evolved carbon monoxide was trapped in the rigid matrix, so eventually the original colourless $M(CO)_6$ was regenerated. McIntyre [31] also observed the formation of a yellow species on irradiating $Cr(CO)_6$ in

polystyrene. The two research groups noticed the increasing stability of the yellow pentacarbonyl product as the temperature was reduced. Shaver *et al.* [32] embedded some monomeric carbonyl complexes in various donor and non-donor polymer supports and exposed them to UV irradiation over long time periods. It was noticed that irradiation of the metal complexes in donor containing polymer matrices resulted in the formation of metal pentacarbonyl polymeric analogues, *via* interaction with donor sites along the polymer backbone. The reactions were monitored by infrared spectroscopy. Infrared data in the $\nu(\text{CO})$ stretching region was reported for $\text{M}(\text{CO})_6$ ($\text{M} = \text{W}, \text{Mo}, \text{or Cr}$), $\text{CpMn}(\text{CO})_3$, $\text{ArCr}(\text{CO})_2\text{L}$ [$\text{L} = \text{CO}$ or $\text{P}(n\text{-Bu})_3$], $(\eta^6\text{-C}_6\text{H}_5\text{NH}_2)\text{Cr}(\text{CO})_3$, $(\eta^6\text{-}o\text{-C}_6\text{H}_4(\text{NH}_2)(\text{CH}_3)\text{Cr}(\text{CO})_3)$, $\text{CpFe}(\text{CO})\text{LR}$ [$\text{L} = \text{CO}$ or PPh_3 ; $\text{R} = \text{CH}_3$ or COCH_3], embedded in poly(methylmethacrylate) (PMMA), polystyrene (PS), polystyrene-poly(methylmethacrylate) (PS-PMMA), or polystyrene-polyacrylonitrile (PS-AN) films. The workers concluded that these matrices appeared, on the whole, to approximate the solvents ethyl acetate, toluene, toluene-ethyl acetate, and toluene-acetonitrile respectively, with respect to the $\nu(\text{CO})$ vibrational band behaviour. Polystyrene and other polymers have a window of low absorbtivity in the region of the IR spectrum where bands due to the terminal stretching carbonyl vibrations of metal carbonyls are detected.

For the Group 6 $\text{M}(\text{CO})_6$ complexes embedded in both donor and non-donor polymer matrices, additional new peaks were observed in the $\nu(\text{CO})$ stretching region. An important point to note is that minimum interaction occurs between the metal carbonyls and the matrices during the embedding

procedure, except in the case of PS-AN.

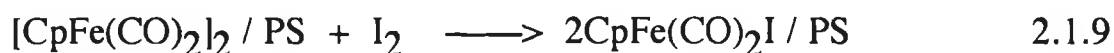
The $M(CO)_6$ complexes in PS, PMMA and PS-AN were irradiated in the region 250 - 270nm. In the case of the PS films, the $\nu(CO)$ bands due to the metal hexacarbonyl compounds decrease in intensity and no new peaks appear. However, when no filter was used (except quartz), irradiation of $W(CO)_6$ in PS led to a much faster decrease in intensity of the parent $\nu(CO)$ band in conjunction with the appearance of three very weak new bands at 2074, 1931, and 1897cm^{-1} , immediately after irradiation. No $\nu(CO)$ frequencies were quoted for the analogous Mo or Cr compounds. These observations are consistent with the stability of the appropriate $M(CO)_5(\text{Polymer})$ species, *i.e.* the $W(CO)_5(\text{Polymer})$ species decomposes at a slower rate than the $Mo(CO)_5(\text{Polymer})$ or $Cr(CO)_5(\text{Polymer})$ analogues. Irradiation of $ArCr(CO)_3$ in PS, PMMA, and PS-AN, (pyrex filter) led to new bands due to $Cr(CO)_6$ in PS and PMMA. Also, new bands have been observed in PS (very weak) and PMMA (moderate), which have not been assigned. Irradiation of $CpMn(CO)_3$ in the three matrices (pyrex filter) led to a decrease in the parent $\nu(CO)$ frequencies. New bands appear in PS (strong) and PMMA (weak), and are stable for several days. Their positions are in agreement with those reported for $CpMn(CO)_2$. These observations support a trend accross the periodic table whereby iron-olefin complexes are more stable than manganese-olefin complexes, which in turn are more stable than their tungsten, molybdenum, or chromium-olefin counterparts.

In an ensuing article [33], Shaver and coworkers looked at the photochemistry of some iron, molybdenum, and manganese dimers in PS, PMMA, and PS-AN films. The infrared carbonyl stretching frequencies of

the dimers in PS, PMMA, and PS-AN matrices gradually decreased in intensity and no new $\nu(\text{CO})$ bands were detected. The rate of decrease in intensity was much slower in PMMA than in PS for all three dimers. Irradiation of $[\text{CpFe}(\text{CO})_2]_2$ and $\text{Mn}_2(\text{CO})_{10}$ in PS-AN gave rise to strong new peaks, consistent with the formation of $\text{Cp}_2\text{Fe}_2(\text{CO})_3(\text{PS-AN})$ and $\text{Mn}_2(\text{CO})_9(\text{PS-AN})$ respectively.

In PS, photogenerated CO would diffuse from the film, leaving coordinatively unsaturated intermediates which are unstable under the reaction conditions (room temperature, continued irradiation) and in the absence of stabilising donors. Such a process would lead to the gradual decrease in intensity observed. PMMA is much less permeable than PS, hence the relatively slow photodecomposition of the dimers embedded in PMMA. The molybdenum analogue is very reactive and the coordinatively unsaturated intermediate decomposes very rapidly in the absence of donor sites. Oxidation of these dimers by iodine (Reactions 2.1.9 - 2.1.11) was fastest in PS (thin film), followed by PS (thick film), then PS-AN. However, virtually no oxidation took place in PMMA. These differences are related to the rates of diffusion of iodine into the films, and hence illustrate the importance of polymer microstructure in determining the chemistry of metal supported systems.

It is worth noting that this iodine oxidation reaction in PS demonstrates an additional method of transforming organometallic complexes embedded in plastics, and also that these systems might be useful as indicators of gas permeability in various polymers.



Further work [34] described the study of addition reactions of iridium and ruthenium compounds embedded in polystyrene with various ligands, the reactions being monitored by IR spectroscopy. Upon irradiation of the matrix in the presence of various ligands, the photofragments produced exhibited bands which were in good agreement with those $\nu(\text{CO})$ stretches for the corresponding products in similar solvents. The environment surrounding complexes embedded in PS is very similar to that in toluene solution. However, Shaver's results suggest that the PS matrix may modify the relative rates of reactions by hindering the diffusion of large gaseous molecules in the plastic. This provides a greater selectivity not possible with corresponding solvents. The distribution of such organometallic complexes in the polymer films was subsequently studied [35]. A uniform distribution is important because the efficiency of these reactions is dependent on the cross-section of the reactive site. The thickness of the film is also an important parameter. Also, high concentrations of metal carbonyl embedded in the matrix can lead to problems such as unwanted side reactions and the formation of concentration gradients. The workers found that the PMMA

films generally have lower variances in distribution of the metal carbonyl, compared to PS films. Again it was shown that PMMA films were the most stable and that the PS-AN and PMMA films also stabilise the metal carbonyl substrates.

The coordinatively unsaturated photofragments have increased stability at lower temperatures. Hooker and Rest [36] recently looked at the photochemistry of $\text{Fe}(\text{CO})_5$ in poly(vinyl-chloride) (PVC), polytetrafluoroethylene (PTFE) and low-density polyethylene (LDPE) films at 12 - 298K, monitoring the reactions by IR spectroscopy. Irradiation of $\text{Fe}(\text{CO})_5$ in LDPE led to weak interactions between $\text{Fe}(\text{CO})_4$ and the polymer or solvent. However, these interactions were considered very weak since the parent $\text{Fe}(\text{CO})_5$ was regenerated on warming from 12 to 120K. Bonding of the photofragments to the PVC matrices was quite strong, the temperature being raised to 180K in order to observe regeneration of the parent.

In LDPE films at room temperature, irradiation of $\text{Fe}(\text{CO})_5$ led to the formation of $\text{Fe}(\text{CO})_4(\text{olefin})$ type complexes. Other photoproducts were observed in PVC matrices at 298K, and Hooker proposed these were because of binding of the $\text{Fe}(\text{CO})_4$ fragment to some unsaturated units in the polymer.

2.2.1 Laser Flash Photolysis of Metal Carbonyl Compounds in the presence of Monomeric and Polymer-bound Pyridines in Solution.

The catalytic ability of many polymer-supported transition metal complexes

has been well documented [1-3]. However, the synthetic route leading to the formation of these polymer-supported metal complexes has received little attention. As already outlined, one method of immobilising a transition metal complex involves the generation of a coordinatively unsaturated site, which may interact with a pendant donor on the polymer support. The process occurs on a fast timescale, making laser flash photolysis a suitable technique for elucidation of the kinetics and mechanism of interaction of such species. Russell [20] used laser flash photolysis to investigate the interaction of $W(CO)_6$ with various monomeric and polymer-bound pyridine ligands in toluene solution. Copolymers of styrene and 4-vinylpyridine were prepared in 5:1 and 10:1 mole ratios respectively and the kinetics of interaction with photogenerated $W(CO)_5(\text{toluene})$ evaluated. The respective rates of reaction were compared to that obtained for the interaction of $W(CO)_5(\text{toluene})$ with free pyridine, so as to determine the effect of the polymer support present in solution. The second order rate constants for the reaction of $W(CO)_5(\text{toluene})$ with the various ligands are tabulated in Table 2.3.1.

Table 2.3.1: Second order rate constants for the reaction of $W(CO)_5(\text{toluene})$ with various pyridine ligands at 298K [20].

Ligand	$k_2 \text{ (dm}^3\text{mol}^{-1}\text{s}^{-1}\text{)}$
Pyridine	$0.9 (\pm 0.1) \times 10^3$
5/1 Copol [†]	$3.2 (\pm 0.3) \times 10^3$
10/1 Copol	$1.4 (\pm 0.1) \times 10^3$

[†] Refers to the mole ratio of styrene to 4-vinylpyridine.

Surprisingly, the second order rate constants for the copolymers are higher than those for free pyridine in toluene solution. A difference would have been expected in the second order rates because of possible diffusional constraints arising from the polymers in solution, but then one would expect k_2 to be higher for the monomeric pyridine. The higher pyridine loading in the (5:1; Styrene:4-Vinylpyridine) copolymer has the highest second order rate. Russell concluded that this was because of a higher effective pyridine concentration in a polymer with higher loading of bound pyridine. It was proposed that the tungsten hexacarbonyl diffused into the polymer coils, where the effective pyridine concentration was higher than that of free pyridine in solution, resulting in higher rates for the polymeric systems.

Similarly, in Pittman's work on the polystyrene anchored rhodium hydroformylation catalyst [3f], it was noticed that catalytic activity decreased as the ratio of bound phosphine units to rhodium increased. It was suggested that the effective concentration of bound phosphines was greater in the immobilised system compared to free triphenylphosphine, and subsequently occupied a greater proportion of the catalytic sites, thus reducing catalytic activity.

To determine if the trends observed by Russell were unique to the $W(CO)_6$ system, an investigation of the interaction of $Cr(CO)_6$ with various pyridine ligands was carried out [21]. Copolymers of styrene and 4-vinylpyridine were prepared in 5:1, 10:1, 30:1, and 40:1 mole ratios respectively. The second order rate constants for the reaction of $Cr(CO)_5$ (toluene) with the various copolymers, 4-methylpyridine, and free pyridine were determined (Table 2.3.2). Again the second order rates for the polymeric systems are

higher than those for the free pyridines in solution.

Table 2.3.2: Second order rate constants for the reaction of $\text{Cr}(\text{CO})_5(\text{toluene})$ with various pyridine ligands at 298K [21].

Ligand	$k_2 \text{ (dm}^3\text{mol}^{-1}\text{s}^{-1}\text{)}$
Pyridine	$0.75 (\pm 0.1) \times 10^5$
4-Mepyrindine	$0.92 (\pm 0.1) \times 10^5$
5:1 Copol [†]	$0.96 (\pm 0.1) \times 10^5$
10:1 Copol	$1.44 (\pm 0.1) \times 10^5$
30:1 Copol	$1.07 (\pm 0.1) \times 10^5$
40:1 Copol	$3.52 (\pm 0.3) \times 10^5$

[†] Refers to the mole ratio of styrene to 4-vinylpyridine.

From the trend observed, Farrell concluded that the process was not unique to the tungsten metal system. Because the second order rate constants increased as the loading of pendant donor groups decreased, it was proposed that the polymer support (as well as the pendant sites) contributed in some way to the kinetics observed. Values of ΔG^\ddagger determined by the workers for the various reactions were the same within experimental error.

These studies provide important information on the reaction kinetics of metal carbonyls with polymeric supports containing pendant pyridine donor sites.

The aims of part of the work in this thesis were, firstly, to see if the trends observed by Russell and Farrell were obeyed when phosphines were used as

anchors on the polymer support. Secondly, the process was investigated using homopolymers (without pendant sites) to see if any interaction occurred. Thirdly, the nature of the support and also the polymerisation method used was varied, to determine the importance of the end-groups on the support. Finally, the molecular weight of the various copolymers and homopolymers was considered in all cases.

2.3 Results and Discussion.

2.3.1 Laser Flash Photolysis of $W(CO)_6$ in the presence of Monomeric and Polymeric Phosphine Units in Toluene.

Laser flash photolysis at 355nm of $W(CO)_6$ in toluene at room temperature produces the coordinatively unsaturated $W(CO)_5$ intermediate. Within the duration of the flash (10ns), this coordinates to the solvent (S) to produce $W(CO)_5(S)$. In the presence of a coordinating ligand, L, the more stable ligated adduct $W(CO)_5(L)$ is then formed. Since the ligand was present in large excess, the reaction with $W(CO)_5(S)$ follows pseudo first order kinetics. Toluene was chosen as the solvent principally because of its chemical similarity to polystyrene. By keeping the two similar, it was hoped there would be minimal interference from solvent with the photogenerated metal-polymer interaction being monitored. Toluene is also a 'good' solvent for polystyrene polymers at 298K, the theta temperature being ~173K, at which the polymer chains adopt unperturbed conformations [37]. Another

advantage is the high solubility of the copolymers in it.

2.3.1.1 Electronic Excitation Spectrum of W(CO)_6 in Toluene Solution.

The UV/vis spectrum of W(CO)_6 in toluene is shown in Figure 2.3.1.1. The shoulder at 340nm and the very intense band at 320nm were assigned to LF ($\pi \rightarrow \pi^*$) and MLCT ($\sigma \rightarrow \pi^*$) transitions respectively. Similar spectra were obtained for molybdenum and chromium hexacarbonyls.

Figure 2.3.1.1: UV/visible absorption spectrum of W(CO)_6 in toluene.

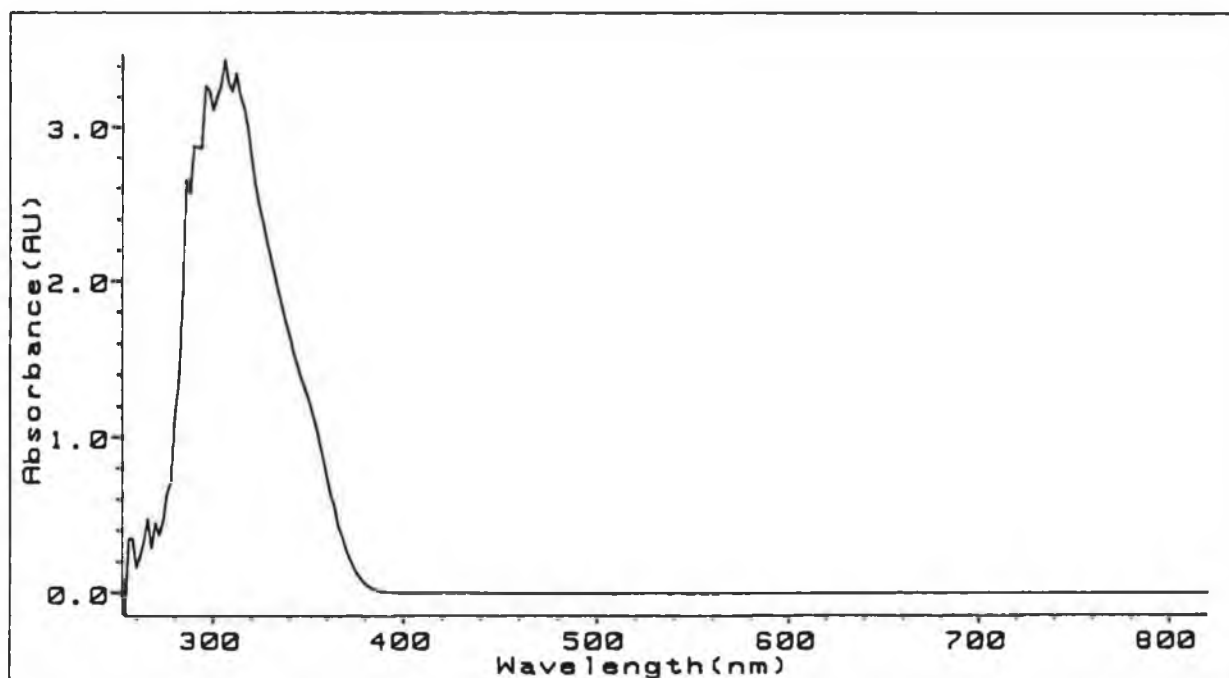


Figure 2.3.1.2 shows the transient UV/vis difference spectrum recorded at various time intervals after flash photolysis. The trace at $0\mu\text{s}$ is the absorption profile of $\text{W(CO)}_5(\text{toluene})$. This decays to produce $\text{W(CO)}_5(\text{PPh}_3)$, with λ_{max} at 420nm. The rate of this reaction was monitored at 430nm. The isobestic point at 400nm is indicative of a clean conversion of the solvated to ligated analogue. Figure 2.3.1.3 is a three-dimensional representation of this changing absorbance profile [38].

Figure 2.3.1.2: Transient UV/vis difference absorption spectrum for W(CO)_6 with PPh_3 in toluene.

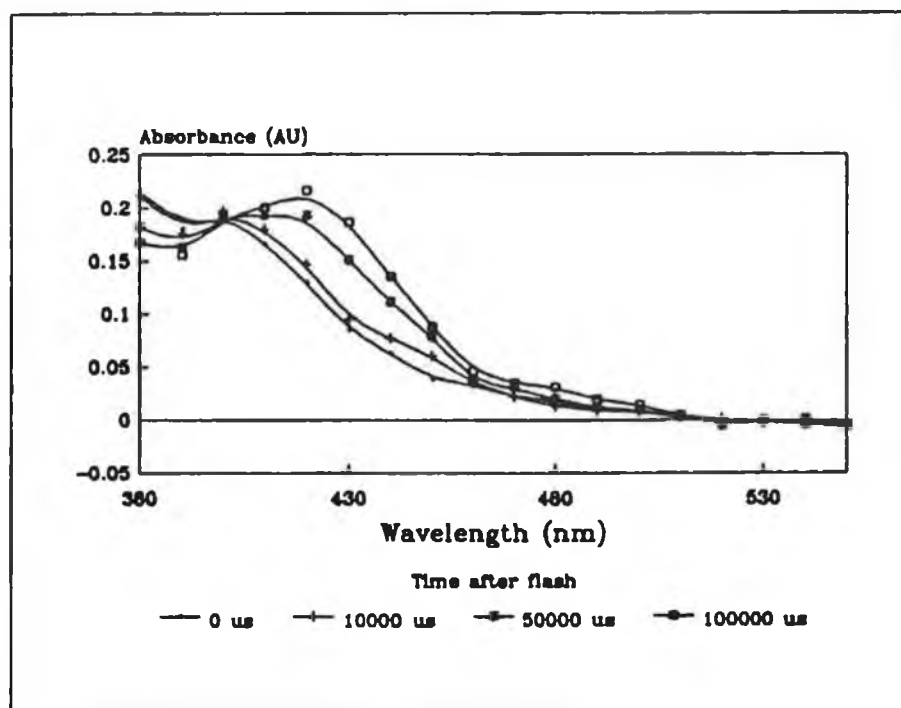
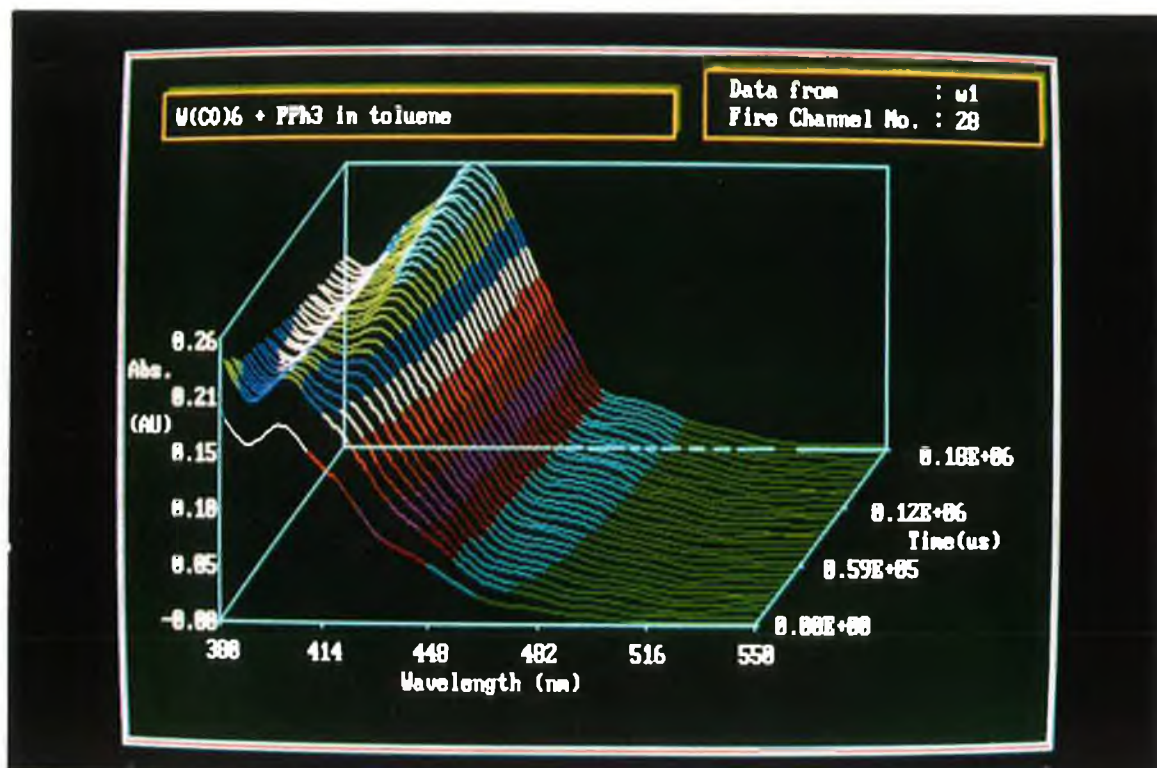


Figure 2.3.1.3: A three-dimensional representation of the change in absorbance with time for $\text{W}(\text{CO})_6$ with PPh_3 in toluene.



To effectively compare results for the copolymer systems with previous work, copolymers of styrene and *p*-diphenylphosphinostyrene (S:*p*-DPPS) were prepared in 5:1, 10:1, 20:1, and 30:1 mole ratios respectively, and the molecular weight of each determined (Chapter 5). Lower loadings of phosphines were not used because a large weight of copolymer would be required to maintain the same phosphine concentration throughout the investigation, which could possibly introduce unwanted viscosity effects. The concentration of phosphine in the polymeric ligands was determined by microanalysis [39].

2.3.1.2 Second Order Reaction Rates for the Reaction of $\text{W(CO)}_5(\text{S})$ with Phosphine Units.

The second order rate constants (k_2) for the reaction of L with $\text{W(CO)}_5(\text{S})$ were determined by plotting the observed rate constant (k_{obs}) against the concentration of phosphine units for each of the different systems, as shown in Figure 2.3.1.4. The values are tabulated in Table 2.3.1.1. The observed rate constant, and subsequently k_2 , increases as the loading of phosphine units on the polymer decreases. A higher rate would be expected in a situation where ligand concentration is higher. Restrictions imposed by the polymer backbone would also possibly lead to slower rates for the polymeric systems. The rate for the reaction of various metal carbonyl photofragments with polymer-bound pyridines was higher than that for the corresponding monomeric pyridine [20, 21].

Figure 2.3.1.4: Plot of k_{obs} (s^{-1}) versus phosphine unit concentration [M] for W(CO)_6 with various phosphine units in toluene.

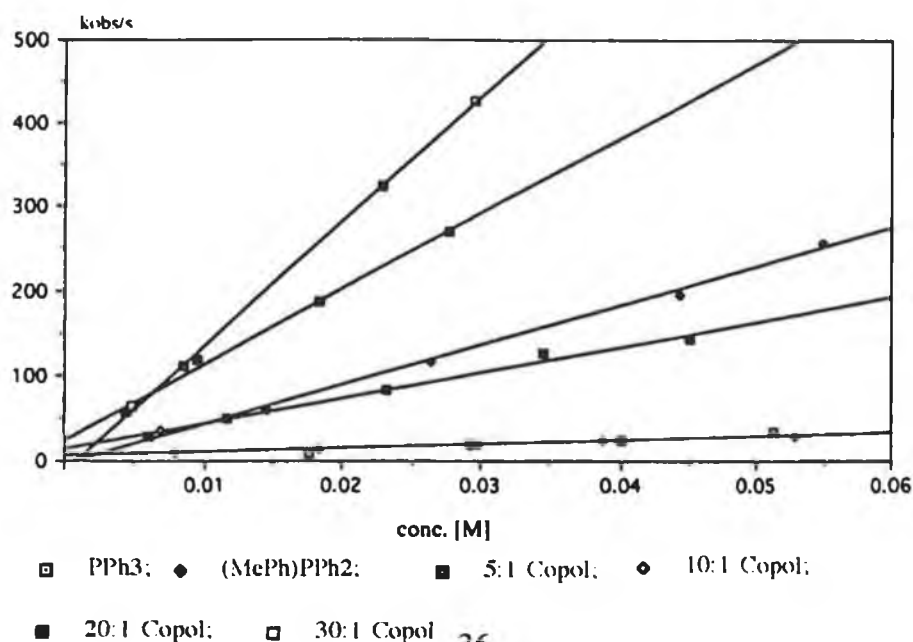


Table 2.3.1.1: Second order rate constants for the reaction of $W(CO)_5(\text{toluene})$ with various phosphine units at 298K.

Ligand	k_2 ($\text{dm}^3\text{mol}^{-1}\text{s}^{-1}$)
PPh_3	$6.6 (\pm 0.7) \times 10^2$
$(MePh)PPh_2$	$4.2 (\pm 0.4) \times 10^2$
(5:1);(S: <i>p</i> -DPPS)	$2.9 (\pm 0.3) \times 10^3$
(10:1);(S: <i>p</i> -DPPS)	$4.6 (\pm 0.5) \times 10^3$
(20:1);(S: <i>p</i> -DPPS)	$8.9 (\pm 0.9) \times 10^3$
(30:1);(S: <i>p</i> -DPPS)	$1.5 (\pm 0.1) \times 10^4$

2.3.1.3 Activation Parameters for the Reaction of $W(CO)_5(\text{toluene})$ with Various Phosphine Units.

The activation parameters for the different systems were determined, to see if there was a difference in the spontaneity of the various reactions. These were calculated from the Arrhenius and Eyring equations [40]. Usually the second order rate constant k_2 is used when determining the activation parameters so as to consider the effect of ligand concentration. In these experiments, approximately the same concentration of phosphine units was used in all cases, but the concentration of polymer varied. Because of this, ΔS^\ddagger may not be correct but will be relative.

The experimental data for the Arrhenius and Eyring plots are tabulated in Appendix A. Representative Arrhenius and Eyring plots are shown in Figure 2.3.1.3.1 and Figure 2.3.1.3.2 respectively. A summary of the activation parameters is given in Table 2.3.1.3.1.

Table 2.3.1.3.1: Activation Parameters for the reaction of $W(CO)_5$ (toluene) with various phosphine units.

LIGAND	E_a^\ddagger (a)	ΔH^\ddagger (a)	ΔS^\ddagger (b)	ΔG^\ddagger (a)
PPh_3	26	24	-143	67
$(MePh)PPh_2$	44	41	-84	66
(5:1);(S:p-DPPS)	28	26	-124	63
(10:1);(S:p-DPPS)	28	26	-119	61
(20:1);(S:p-DPPS)	33	30	-106	62
(30:1);(S:p-DPPS)	35	32	-90	59

(a) $\pm 2 \text{ kJmol}^{-1}$

(b) $\pm 25 \text{ Jmol}^{-1}\text{K}^{-1}$

The values of ΔG^\ddagger are the same within experimental error, and overall, no change in the activation energy occurs for the different reactions. The values of ΔS^\ddagger are negative, indicating an associative mechanism.

Figure 2.3.1.3.1: Arrhenius plot for the reaction of $\text{W(CO)}_5(\text{toluene})$ with PPh_3 (see Appendix A for data).

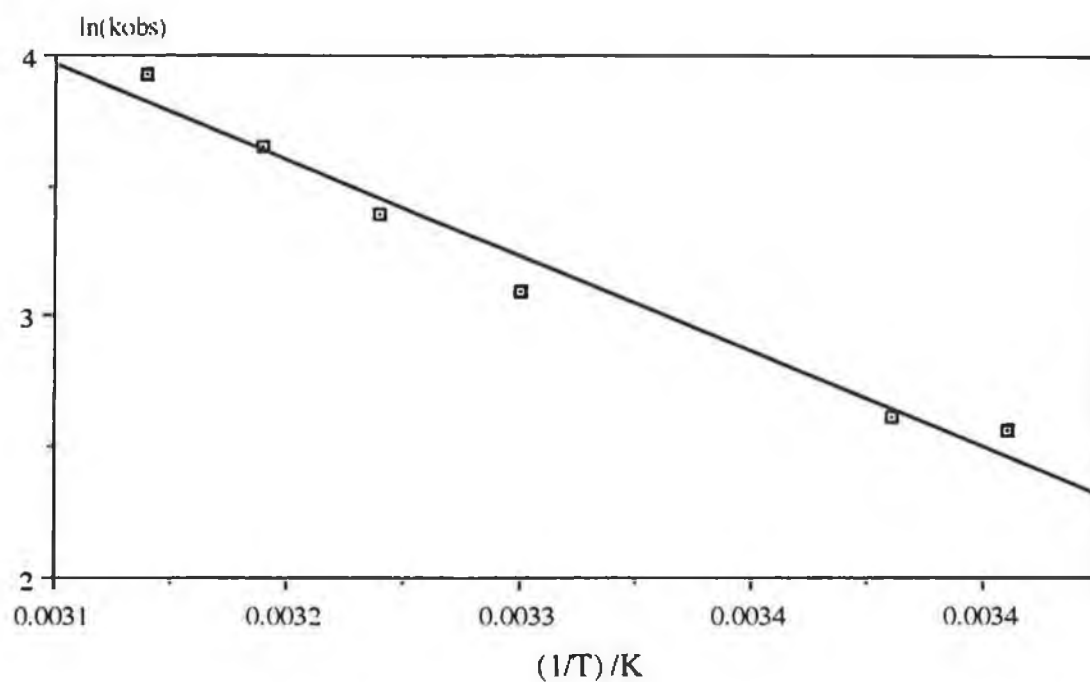
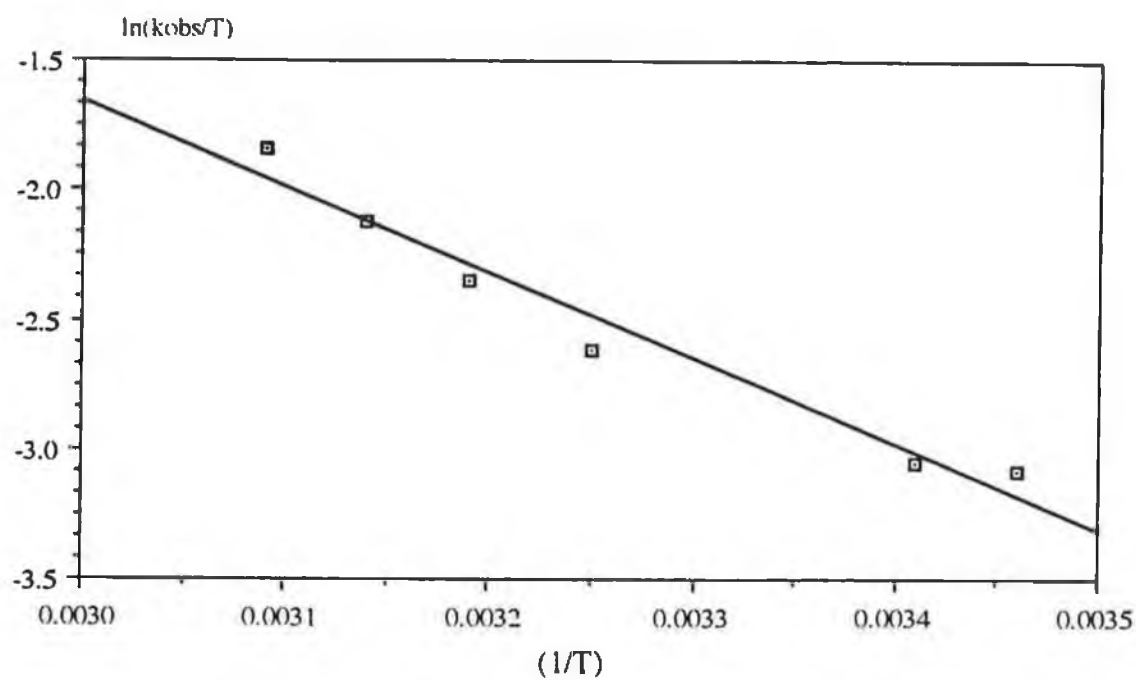


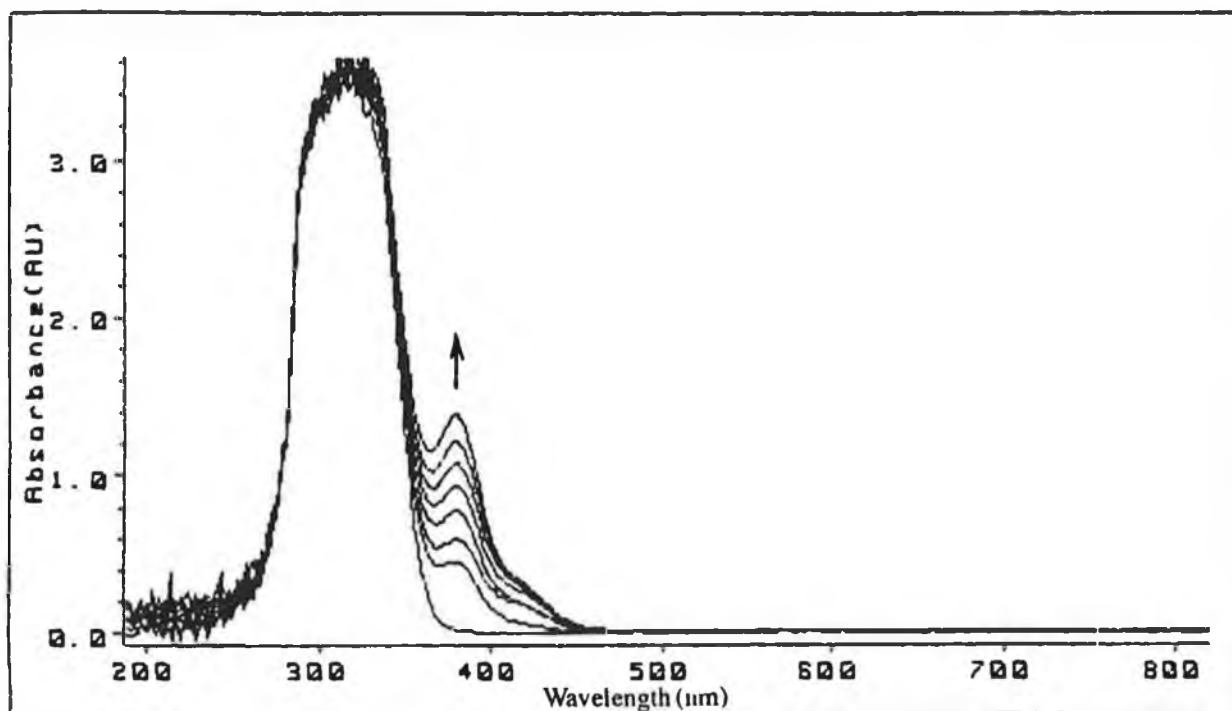
Figure 2.3.1.3.2: Eyring plot for the reaction of $\text{W(CO)}_5(\text{toluene})$ with PPh_3 (see Appendix A for data).



2.3.2 Laser Flash Photolysis of Mo(CO)_6 in the presence of Monomeric and Polymeric Phosphine Units in Toluene Solution.

Figure 2.3.2.1 shows the changing UV/vis spectrum upon flash photolysis of a sample of Mo(CO)_6 with (20:1);(S:*p*-DPPS) in toluene. On irradiation, a CO molecule is photoejected to generate the coordinatively unsaturated Mo(CO)_5 photofragment which is rapidly solvated. The solvent molecule is displaced by the ligand to form $\text{Mo(CO)}_5(\text{L})$ ($\text{L} = \text{S}:\textit{p}$ -DPPS), with an absorption at 380nm. The intensity of this band increases with increased exposure to the laser pulse, as does the shoulder at 410nm. These are a combination of MLCT ($\sigma \rightarrow \pi^*$) and LF ($\pi \rightarrow \pi^*$) transitions.

Figure 2.3.2.1: Changes observed in the UV/vis spectrum of Mo(CO)_6 with (20:1);(S:*p*-DPPS) in toluene.



2.3.2.1 Second Order Reaction Rates for $\text{Mo(CO)}_5(\text{S})$ with Phosphine Units.

The second order rate constants (k_2) were determined as before (Section 2.3.1.2). Figure 2.3.2.2 is a plot of k_{obs} versus phosphine concentration. Again, as the phosphine loading decreases, the respective rates increase. Table 2.3.2.1 contains the values for Mo(CO)_6 with the various ligands. The observed rates are higher than those for the tungsten system. This is mainly as a result of the stability of the $\text{M(CO)}_5(\text{toluene})$ species on going down the group.

Figure 2.3.2.2: Plot of k_{obs} (s^{-1}) versus phosphine concentration [M] for Mo(CO)_6 with various phosphines in toluene solution.

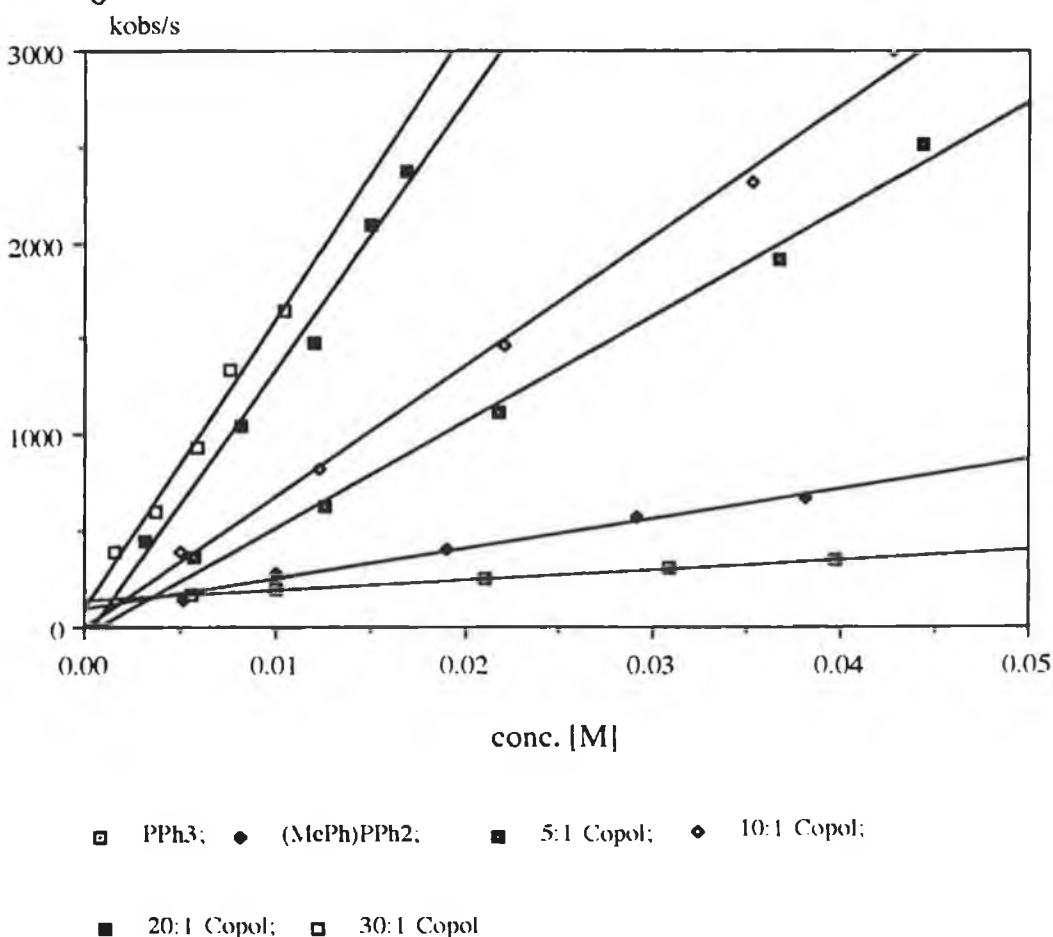


Table 2.3.2.1: Second order rate constants (k_2) for the reaction of $\text{Mo(CO)}_5(\text{toluene})$ with various phosphine units at 298K.

Ligand	k_2 ($\text{dm}^3\text{mol}^{-1}\text{s}^{-1}$)
PPh_3	$5.2 (\pm 0.5) \times 10^3$
$(\text{MePh})\text{PPh}_2$	$1.6 (\pm 0.2) \times 10^4$
(5:1);(S: <i>p</i> -DPPS)	$5.5 (\pm 0.6) \times 10^4$
(10:1);(S: <i>p</i> -DPPS)	$6.8 (\pm 0.7) \times 10^4$
(20:1);(S: <i>p</i> -DPPS)	$1.4 (\pm 0.1) \times 10^5$
(30:1);(S: <i>p</i> -DPPS)	$1.5 (\pm 0.1) \times 10^5$

As was observed for the tungsten system, the second order rate constants for the reaction of $\text{Mo(CO)}_5(\text{toluene})$ with the copolymers increased as the loading of phosphine decreased.

2.3.2.2 Activation Parameters for the Reaction of $\text{Mo(CO)}_5(\text{toluene})$ with Various Phosphine Units.

Activation parameters were determined as described in Section 5.2.4.3. Table 2.3.2.2.1 summarises the activation parameters obtained for these systems. The experimental data for the Arrhenius and Eyring plots is presented in Appendix B. Representative plots are shown in Figure 2.3.2.2.1 and Figure 2.3.2.2.2.

Table 2.3.2.2.1: Activation parameters for the reaction of $\text{Mo(CO)}_5(\text{toluene})$ with various phosphine ligands.

LIGAND	E_a^\ddagger (a)	ΔH^\ddagger (a)	ΔS^\ddagger (b)	ΔG^\ddagger (a)
PPh_3	34	32	-92	59
$(\text{MePh})\text{PPh}_2$	36	34	-84	59
(5:1);(S:p-DPPS)	38	36	-68	56
(10:1);(S:p-DPPS)	36	34	-70	55
(20:1);(S:p-DPPS)	36	34	-71	55
(30:1);(S:p-DPPS)	47	44	-37	55

(a) $\pm 2 \text{ kJmol}^{-1}$

(b) $\pm 25 \text{ Jmol}^{-1}\text{K}^{-1}$

As for the tungsten system, the values of ΔG^\ddagger are the same within experimental error for the different reactions. The values of ΔS^\ddagger are on average more positive than those reported for W(CO)_6 .

Figure 2.3.2.2.1: Arrhenius plot for the reaction of $\text{Mo(CO)}_5(\text{toluene})$ with PPh_3 , (see Appendix B for data).

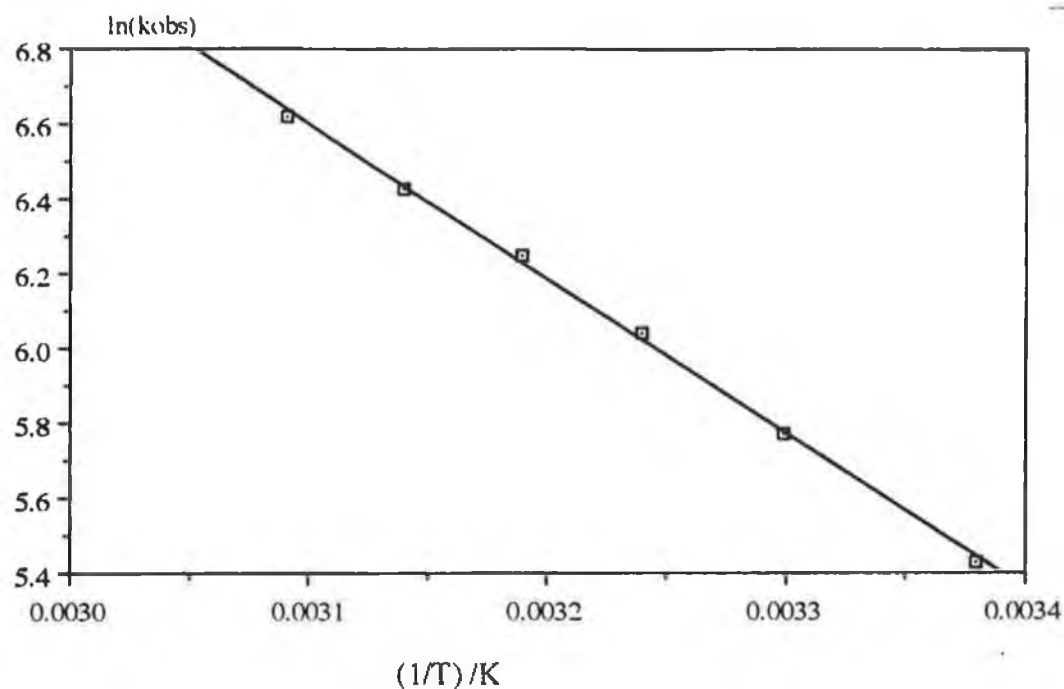
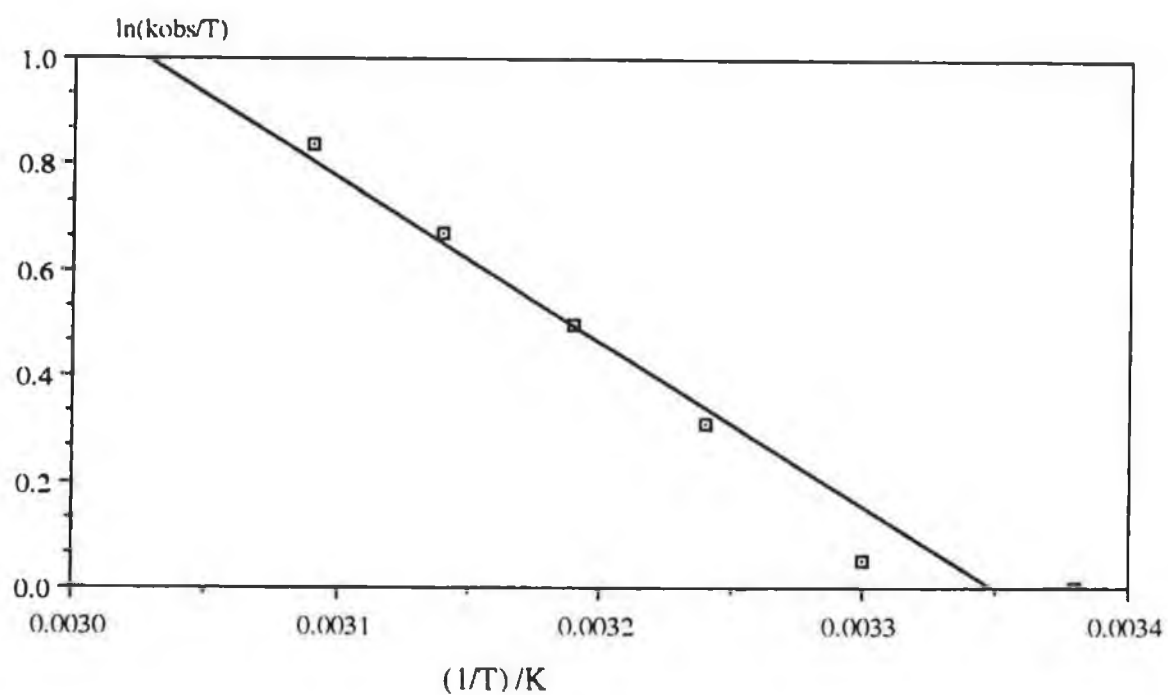


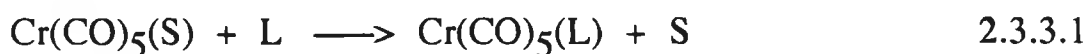
Figure 2.3.2.2.2: Eyring plot for the reaction of $\text{Mo(CO)}_5(\text{toluene})$ with PPh_3 , (see Appendix B for data).



2.3.3 Laser Flash Photolysis of $\text{Cr}(\text{CO})_6$ in the presence of Monomeric and Polymeric Phosphine Units in Toluene Solution.

Chromium hexacarbonyl is the most widely studied of the three metals in Group 6. This is largely attributed to the fact that this system is very reversible in comparison to either the molybdenum or tungsten analogues. Its photochemistry has been very well documented, but there are still some unresolved problems [41].

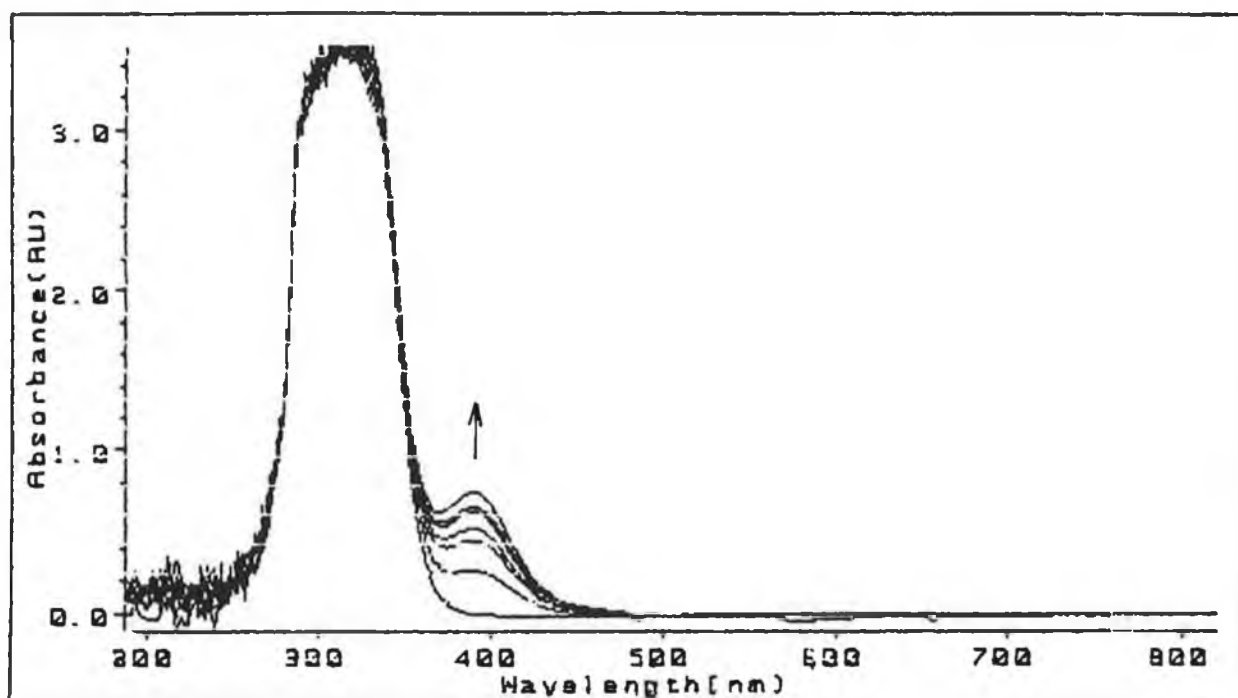
Flash photolysis (at 355nm) of $\text{Cr}(\text{CO})_6$ in toluene solution produces the coordinatively unsaturated $\text{Cr}(\text{CO})_5$ species, which is rapidly solvated. In the presence of the coordinating phosphine ligand, L, the solvent molecule is displaced to form the more stable $\text{Cr}(\text{CO})_5(\text{L})$ adduct, as shown in Reaction 2.3.3.1. Figure 2.3.3.1 shows the changes observed in the UV/vis spectrum upon flash photolysis of a sample of $\text{Cr}(\text{CO})_6$ and (30:1);(S:*p*-DPPS) in toluene. The product has an absorption maximum at 390nm.



L = Phosphine,

S = Toluene.

Figure 2.3.3.1: Changes observed in the UV/vis spectrum on flash photolysis of $\text{Cr}(\text{CO})_6$ with (30:1);(S:*p*-DPPS) in toluene.



2.3.3.1: Second Order Reaction Rates for $\text{Cr}(\text{CO})_5(\text{S})$ with Phosphine Units in Toluene Solution.

The observed rate constants, and subsequently the second order rate constants, for the chromium system were higher than those for molybdenum, which in turn were higher than those for the tungsten. Figure 2.3.3.2 is a plot of k_{obs} versus phosphine concentration for the reaction of $\text{Cr}(\text{CO})_5(\text{toluene})$ with various phosphine ligands, and Table 2.3.3.1 contains the data. As already observed, the rates are higher for lower phosphine loadings.

Figure 2.3.3.2: Plot of k_{obs} (s^{-1}) versus phosphine concentration [M] for the reaction of $\text{Cr}(\text{CO})_5(\text{toluene})$ with various phosphine ligands.

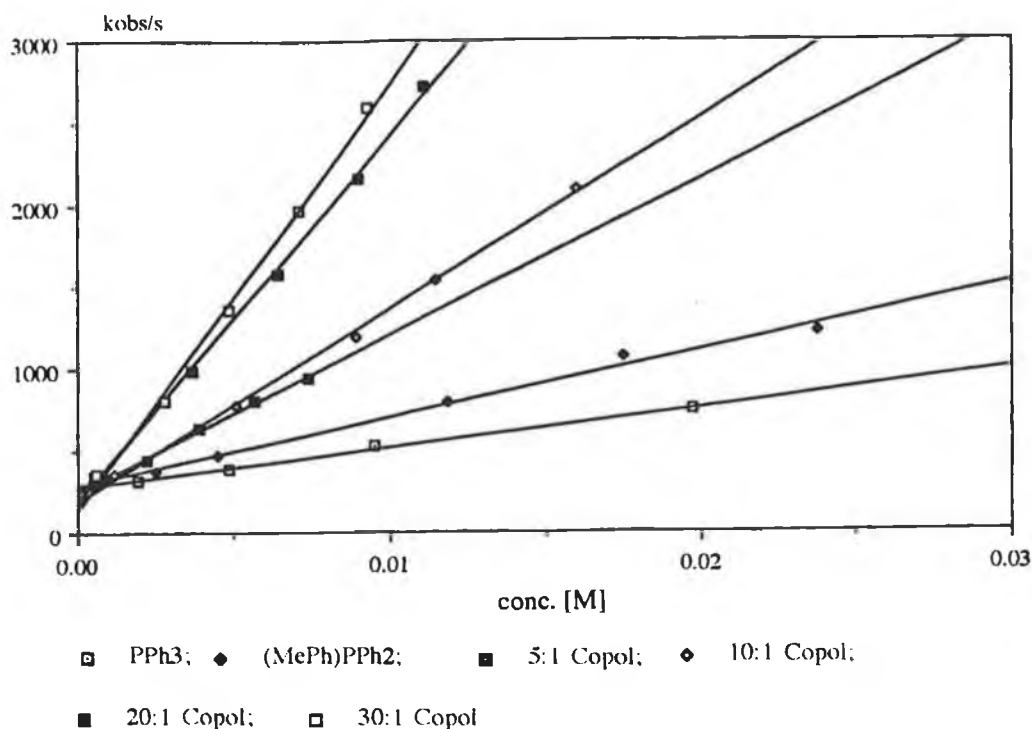


Table 2.3.3.1: Second order rate constants (k_2) for the reaction of $\text{Cr}(\text{CO})_5(\text{toluene})$ with various phosphine units at 298K.

Ligand	k_2 ($\text{dm}^3\text{mol}^{-1}\text{s}^{-1}$)
PPh_3	$2.4 (\pm 0.3) \times 10^4$
$(\text{MePh})\text{PPh}_2$	$4.1 (\pm 0.4) \times 10^4$
(5:1);(S: <i>p</i> -DPPS)	$1.0 (\pm 0.1) \times 10^5$
(10:1);(S: <i>p</i> -DPPS)	$1.2 (\pm 0.1) \times 10^5$
(20:1);(S: <i>p</i> -DPPS)	$2.2 (\pm 0.2) \times 10^5$
(30:1);(S: <i>p</i> -DPPS)	$2.6 (\pm 0.3) \times 10^5$

2.3.3.2 Activation Parameters for the Reaction of $\text{Cr}(\text{CO})_5(\text{toluene})$ with Various Phosphine Units in Toluene Solution.

Activation parameters were calculated as described in Section 5.2.4.3. For the chromium system, Table 2.3.3.2.1 details the results obtained in the presence of the various ligand systems. The experimental data for the Arrhenius and Eyring plots is presented in Appendix C. Representative plots are shown in Figure 2.3.3.2.1 and Figure 2.3.3.2.2.

Table 2.3.3.2.1: Activation parameters for the reaction of $\text{Cr}(\text{CO})_5(\text{toluene})$ with various phosphine ligands.

LIGAND	E_a^\ddagger (a)	ΔH^\ddagger (a)	ΔS^\ddagger (b)	ΔG^\ddagger (a)
PPh_3	40	37	-68	57
$(\text{MePh})\text{PPh}_2$	44	42	-52	57
(5:1);(S:p-DPPS)	41	38	-62	57
(10:1);(S:p-DPPS)	41	39	-55	55
(20:1);(S:p-DPPS)	25	22	-110	55
(30:1);(S:p-DPPS)	34	31	-78	55

(a) $\pm 2 \text{ kJmol}^{-1}$

(b) $\pm 25 \text{ Jmol}^{-1}\text{K}^{-1}$

Again, no change in ΔG^\ddagger was observed. The negative values of ΔS^\ddagger indicate the associative nature of the transition state. However, the values for the chromium system are on average more positive than those for molybdenum, which are in turn, more positive than for tungsten. This trend is in agreement with the fact that S_N2 attack to the smaller chromium atom is unfavourable, compared to the other metal centres.

Figure 2.3.3.2.1: Arrhenius plot for the reaction of $\text{Cr}(\text{CO})_5(\text{toluene})$ with PPh_3 , (see Appendix C for the data).

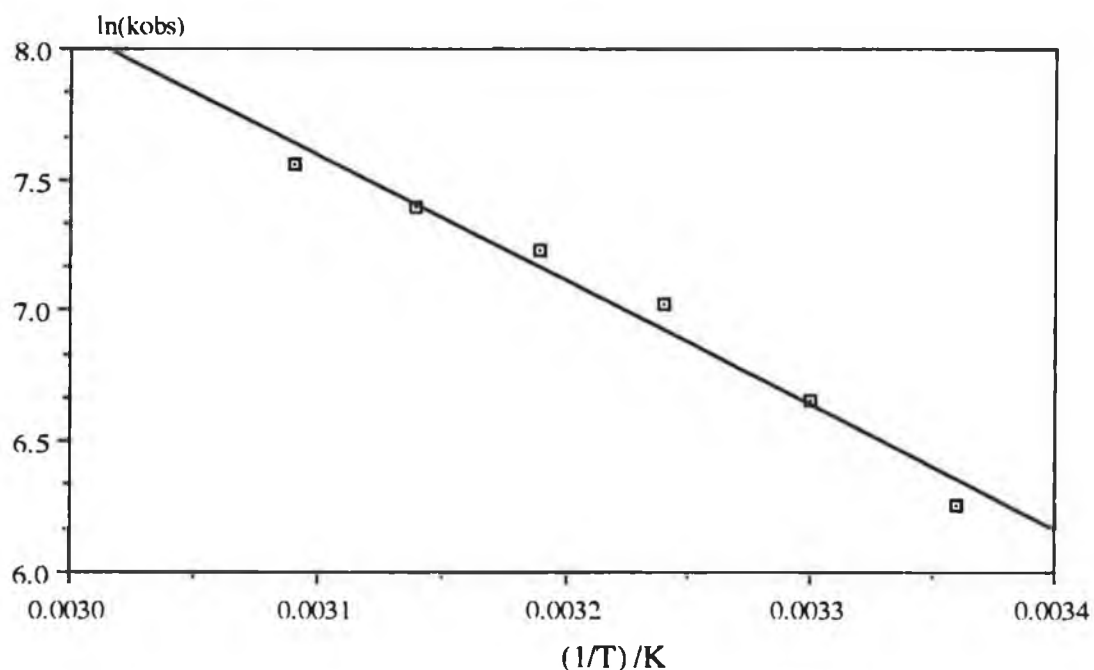
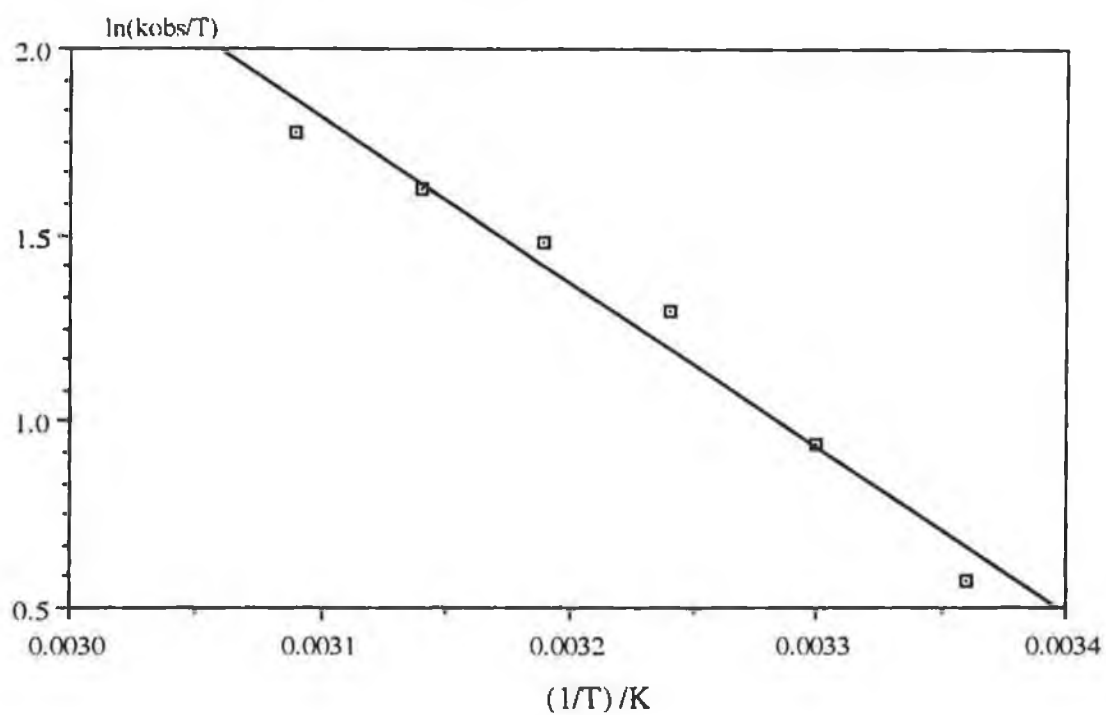


Figure 2.3.3.2.2: Eyring plot for the reaction of $\text{Cr}(\text{CO})_5(\text{toluene})$ with PPh_3 (see Appendix C for the data).



2.3.4 Discussion

The mechanism and kinetics of interaction of $M(CO)_6$, $M = W, Mo, \text{ or } Cr$, with various phosphine units was investigated. It was of interest to study these photoprocesses as previous investigations [20, 21] with various metal carbonyls, in the presence of monomeric and polymeric pyridines showed higher rates in systems where the loading of donor atoms on the polymer were lower. This is contrary to what one would expect, because of the physical restrictions imposed by the polymer coils in solution.

The second order rate constants for the reaction of $M(CO)_6$ with the various phosphine ligands were determined. The rates increased as the phosphine loading decreased, as observed in previous investigations carried out by Russell and Farrell. The activation parameters were determined, and overall, values of ΔG^\ddagger are the same within experimental error. The values of ΔS^\ddagger are negative, indicating an associative mechanism for the transition state.

Therefore, other parameters must be considered to explain the unusual chemistry observed in these systems. A scheme was proposed (Scheme 2.3.4.1) which included the interaction of $M(CO)_5(\text{toluene})$ with either a phosphine unit or the polymer support. When the concentration of phosphine ligand is high (as in free PPh_3), the solvent is displaced to form $M(CO)_5(\text{phosphine})$, (I). When the polymer concentration is high, $M(CO)_5(\text{polymer})$ is formed, (II), which may interact with immobilised phosphines, (III). A rate law for the formation of $M(CO)_5(\text{phosphine})$ was derived.

In a pseudo first order process, the observed rate constant depends on the

ligand concentration;

$$k_{\text{obs}} = k_2[\text{Ligand}]$$

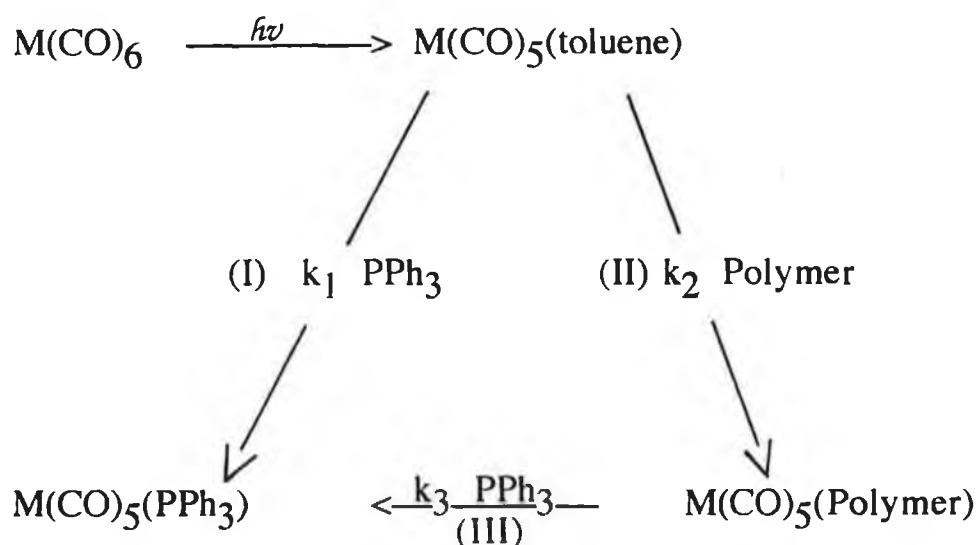
Assuming a steady state concentration of $\text{M}(\text{CO})_5(\text{Copol})$;

the rate law corresponding to this mechanism is;

$$\text{Rate} = \{k_1[\text{PPh}_3] + k_2[\text{Copol}]\}(\text{M}(\text{CO})_5(\text{S})), \text{ where}$$

$$k_{\text{obs}} = k_1[\text{PPh}_3] + k_2[\text{Copol}]$$

Scheme 2.3.4.1:



Clearly, the polymer support greatly affects the reaction kinetics in solution, and because of the unusual effects observed in these experiments, and also the small volume of work carried out in this area, it was decided to investigate the interaction of metal carbonyl photofragments with several homopolymers.

2.4 Laser Flash Photolysis of $\text{M}(\text{CO})_6$ in the presence of Various Homopolymers in Toluene Solution.

If interaction of the homopolymers with metal carbonyl photofragments occurred, this would provide further evidence for the involvement of the polymer support (in copolymer systems). The molecular weight of the homopolymers was varied, and the effects of molecular weight, and the presence of free triphenylphosphine (where indicated) on the photochemical reaction were investigated. The procedures for molecular weight determinations are given in Chapter 5.

The linear homopolymers chosen were polystyrene (PS), poly- α -methylstyrene (P- α -MS), and polymethylmethacrylate (PMMA). PS was chosen because it was used as the support for the copolymers discussed earlier (Section 2.3). P- α -MS homopolymer coils are more expanded than PS coils in solution because of steric hindrance associated with the rather large methyl groups. By comparison of the results for PS and P- α -MS, the effect of having such methyl groups on the polymer support may be investigated. PMMA was chosen because it possesses lone pairs along the backbone, which may therefore interact with the $\text{M}(\text{CO})_5$ photofragment. Experiments were also undertaken to determine if an end-group reaction occurred between the homopolymers and the respective photofragments. In all cases, root mean square (rms) end-to-end distances are quoted for the homopolymers. This treatment allows neglect of intramolecular chain entanglements in solution and also energy transfer between the solvent

molecules and the polymer chains [42].

2.4.1 Laser Flash Photolysis of $M(CO)_6$, ($M = W, Mo, \text{ or } Cr$) in the presence of Various Molecular Weight Polystyrenes (with and without free PPh_3) in Toluene.

The linear polystyrenes with molecular weights in the range 3940 -79800 were prepared by free radical polymerisation using azobisisobutyronitrile (AIBN) as initiator (see Chapter 5). The photochemistry of $M(CO)_6$ with various molecular weight polystyrenes, both in the presence and absence of free PPh_3 , was studied to see if the homopolymer in solution affected the rate of reaction of $M(CO)_5(S)$ with the PPh_3 . In these experiments, concentration of metal hexacarbonyl, PPh_3 (where used) and the amount of polymer was maintained constant, the only variable being the molecular weight of the polymer used. The observed rate constants, with and without PPh_3 , are tabulated in Table 2.4.1.1. The values in parentheses are those obtained without free PPh_3 present.

Table 2.4.1.1: Data for the determination of the effect of PS (varying molecular weight) in the presence (and absence) of free PPh_3 [2×10^{-2} M] on the photoreaction at 298K.

rms Dist. (Å)	k _{obs} /s		
	W(CO) ₆ (#)	Mo(CO) ₆ (#)	Cr(CO) ₆ (#)
PS (62.77)	45 (46)	566 (234)	2631 (804)
PS (93.59)	27 (28)	487 (166)	1780 (745)
PS (112.69)	23 (22)	367 (134)	1179 (726)
PS (235.58)	15 (10)	333 (123)	791 (567)
PS (282.5)	12 (7)	310 (107)	646 (488)

(#) Values in parentheses were obtained in the absence of PPh_3 .

In the W(CO)_6 system, k_{obs} for the photoreaction with and without PPh_3 are identical, and thus indicates that there is no interreaction between $\text{W(CO)}_5(\text{toluene})$ and PPh_3 under these conditions. The rates are very slow, principally because of the stability of $\text{W(CO)}_5(\text{toluene})$. On going down a group in the periodic table, the stronger the interaction of the 'naked' metal photofragment with toluene. $\text{W(CO)}_5(\text{toluene})$ is much more stable than $\text{Cr(CO)}_5(\text{toluene})$, and will therefore react more slowly with the ligand present.

For the Mo(CO)_6 analogue, k_{obs} in the presence of PPh_3 is higher than that observed for the same reaction without PPh_3 . This indicates an interaction between the molybdenum photofragment and PPh_3 .

In the chromium system, the observed rate constants are also greater with free PPh_3 present. For lower molecular weights, the values differ by a factor of three, while in the presence of high molecular weight PS, the values differ by a factor of 1.5.

More important is the variation in k_{obs} with molecular weight of polymer. In all cases, the lower molecular weight PS homopolymers have faster observed rate constants compared to the higher molecular weight analogues. The higher the molecular weight for a given weight of polymer, means that there will be less polymer coils in solution, compared to the same weight of a lower molecular weight polystyrene. The photofragment may either be reacting with the polymer coils in solution, or perhaps the end-groups.

Free-radical polymerisation using AIBN as initiator results in polymers with cyano end-groups, as shown in Figure 2.4.1.5. The AIBN molecule may be thermally or photochemically cleaved, to produce two cyanopropyl radicals. These are extremely reactive and react with monomers containing a double bond, to form an active centre which is capable of reacting with further molecules to give a macromolecular chain. The polymerisation reaction is terminated principally by 'combination', where two growing chains join together to form a single polymer molecule, with cyanopropyl groups at each end. Termination may also be achieved between a growing chain and a radical which has not reacted with any monomer molecule, especially when monomer concentration is high.

Each nitrogen atom of the cyano group has a lone pair of electrons which may coordinate to a metal centre. A low molecular weight polymer will have a high concentration of cyano groups compared to the same weight of

a high molecular weight analogue, and will therefore possess greater ability to interact with $M(CO)_5(\text{toluene})$.

By carrying out similar experiments using polymers prepared by other synthetic routes (which will have different end-groups), the influence of the end-group in directing subsequent chemistry may be established.

2.4.1.1 Comparison of Transient UV/visible Absorption Spectra for the Reaction of $Cr(CO)_6$ with Polystyrene Ligands made *via* Two Different Synthetic Routes.

Transient UV/vis absorption difference spectra obtained for the reaction of $M(CO)_5(\text{toluene})$ with the various PS polymers (prepared using AIBN) exhibited different maxima, depending on the polymer molecular weight. This supported the differing rates obtained for the reaction of the metal carbonyl photofragments with various molecular weight polymers (Table 2.4.1.1). Spectra obtained for the reaction of $Cr(CO)_6$ and PS of various molecular weight, are shown in Figures 2.4.1.1 and 2.4.1.2. In Figure 2.4.1.1 (mol. wt. PS = 3940), the absorption pattern at $0\mu s$ has a maximum at 480nm. The spectrum 15000 μs later shows the grow-in of $Cr(CO)_5(PS)$, with maximum at 400nm. In Figure 2.4.1.2 (mol. wt. = 79800), the spectrum $0\mu s$ after the flash has a maximum at 460nm, while λ_{max} for $Cr(CO)_5(PS)$ is at 460nm, 15000 μs after the flash. This is quite a substantial

shift to lower energy. Of interest also is the fact that the absorption spectra for both at $0\mu\text{s}$ are slightly different, perhaps indicating that something other than $\text{Cr}(\text{CO})_5(\text{toluene})$ is being formed in the laser flash.

Figure 2.4.1.1: Transient UV/vis difference spectrum for $\text{Cr}(\text{CO})_6$ with PS (mol. wt. = 3940, AIBN init.) in toluene.

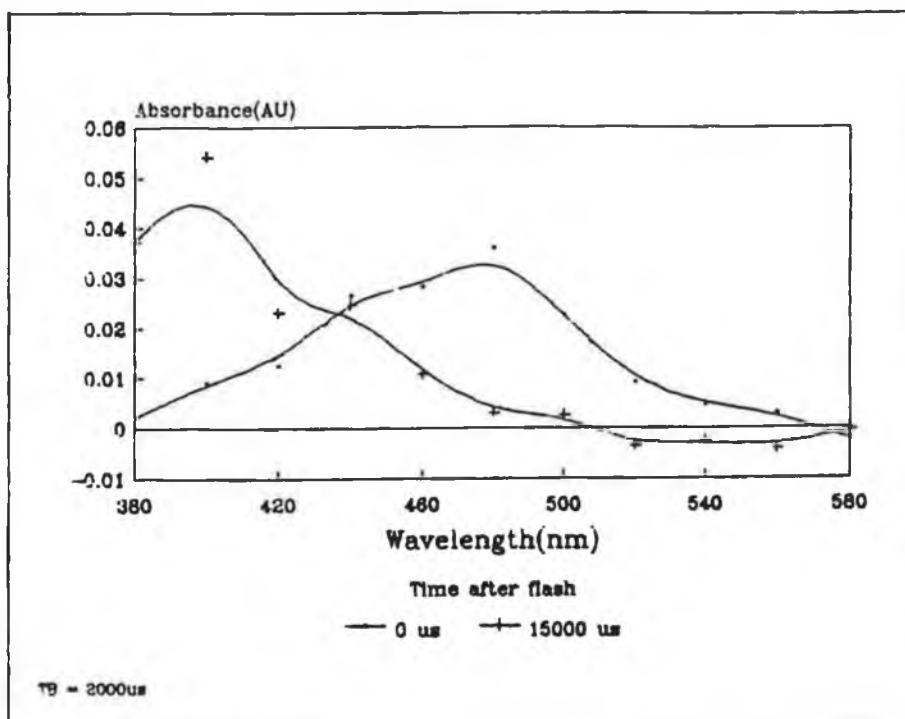
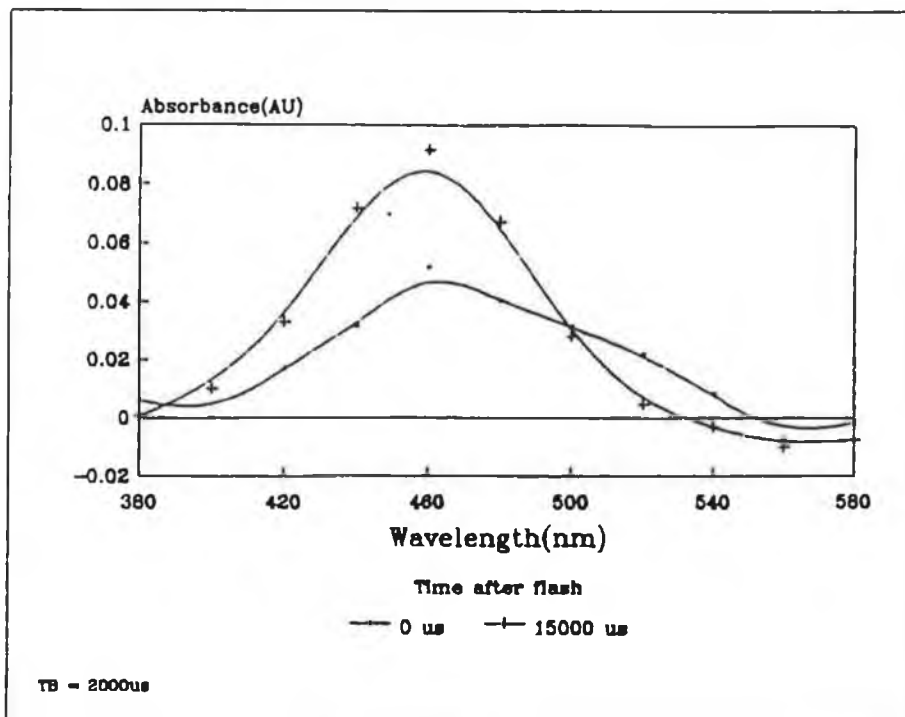


Figure 2.4.1.2: Transient UV/vis difference spectrum for $\text{Cr}(\text{CO})_6$ with PS (mol. wt. = 79800, AIBN init.) in toluene.



To investigate the importance of the end-group, the experiments were repeated using PS which had been prepared by anionic polymerisation (see Section 5.3.3.2). These polystyrene polymers do not in effect have potentially 'reactive' end-groups, as shown in Figure 2.4.1.6. The 'living' polymer is terminated using ethanol, whereupon a proton is extracted from the solvent molecule to produce a polymer with a saturated end-group.

The transient UV/vis difference spectra obtained for two different molecular weight PS polymers are shown in Figures 2.4.1.3. and 2.4.1.4. No shift in the absorption spectrum is observed for these systems, the maximum in both at approximately 460nm.

Figure 2.4.1.3: Transient UV/vis difference spectrum for $\text{Cr}(\text{CO})_6$ with PS (mol. wt. = 3600, anionic polym.) in toluene.

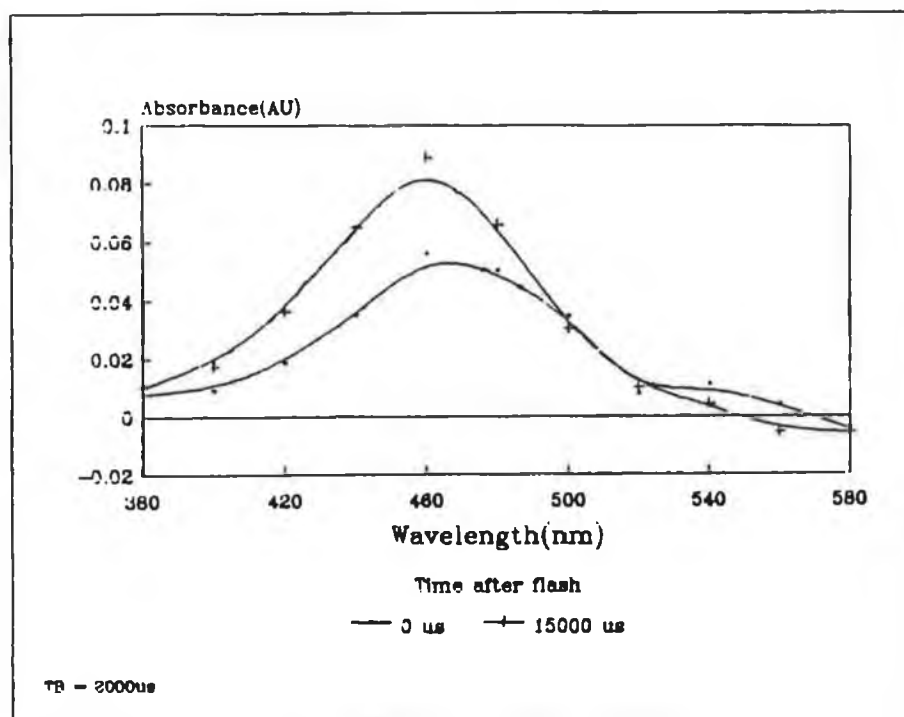
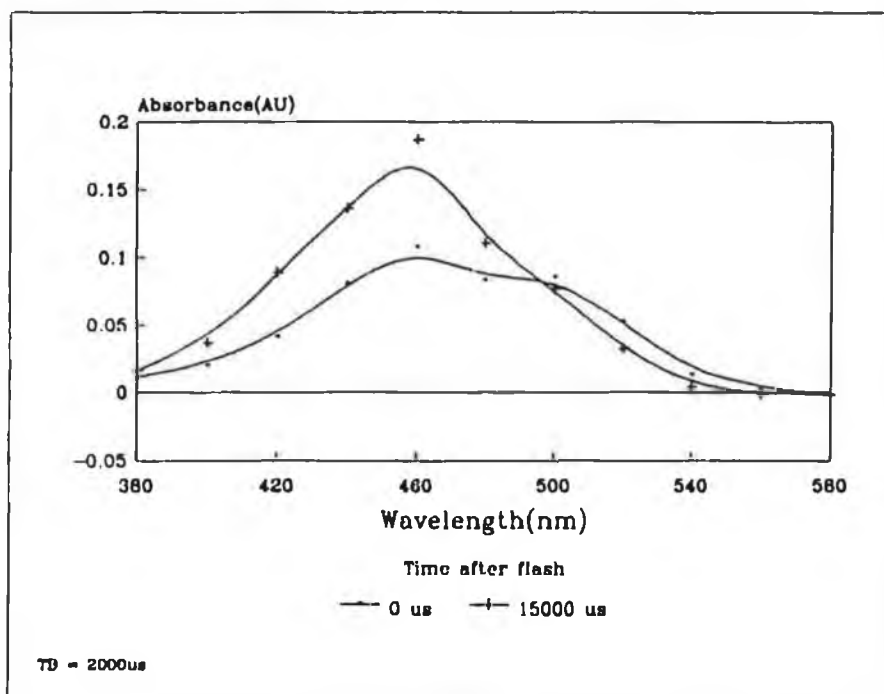


Figure 2.4.1.4: Transient UV/vis difference spectrum for $\text{Cr}(\text{CO})_6$ with PS (mol. wt. = 68000, anionic polym.) in toluene.



The nature of the end-group in polymer chains is important. The polymers prepared using AIBN as the free-radical initiator have cyano end-groups. These cyano groups may displace the solvent in $M(CO)_5(\text{toluene})$ to form a more stable $M(CO)_5(\text{cyano})$ species. Because a low molecular weight polymer will have a high concentration of these 'reactive' end-groups, compared to the same weight of a high molecular weight analogue, the greater will be the extent of interaction with the metal carbonyl photofragment, and thus explains the increase in observed rate constants in the lower molecular weight PS experiments. Therefore, the shift observed in λ_{max} for the polymers prepared in this way is possibly because of an increased end-group reaction between the photofragment and the cyano groups.

Polymers prepared by anionic polymerisation have saturated end-groups. Comparison of the photochemistry of these polymers with polymers containing 'reactive' end-groups suggests minimum interaction between the $M(CO)_5(\text{toluene})$ species and the saturated ends-groups (anionic polym.). No shift in λ_{max} was observed for the range of polymers prepared in this manner. Investigation of the dependency of k_{obs} on the polymer rms end-to-end distance yielded irreproducible results, also indicating no end-group interaction.

Figure 2.4.1.5: A typical PS chain produced by free radical (AIBN) polymerisation.

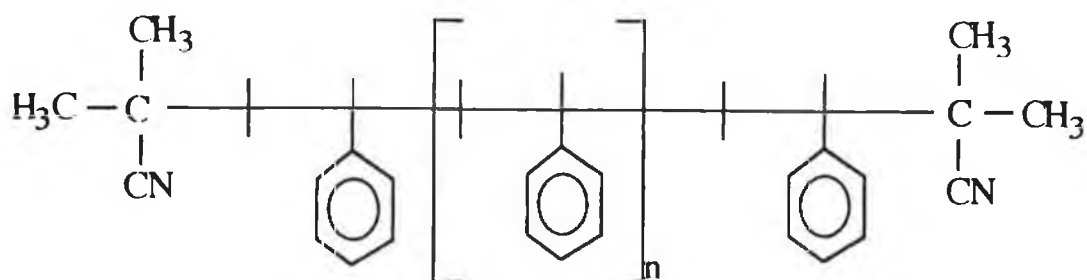
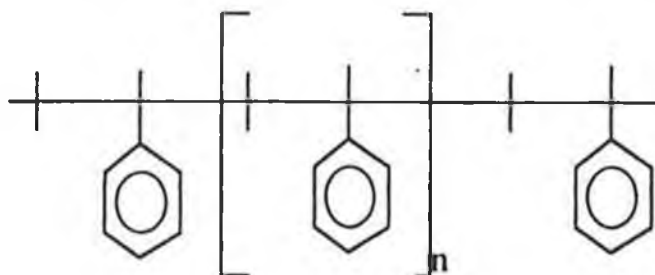


Figure 2.4.1.6: A typical PS chain produced by anionic polymerisation.



2.4.2 Laser Flash Photolysis of $\text{M}(\text{CO})_6$, ($\text{M} = \text{W}, \text{Mo}, \text{or Cr}$) in the presence of Various Molecular Weight Poly- α -Methylstyrenes in Toluene.

These polymers were prepared by anionic polymerisation and the respective molecular weights, and subsequently the rms end-to-end distances, were determined by gel permeation chromatography (Chapter 5). The aim was to examine the effect of a methyl group attached to the polymer, which resulted in more expanded coils in solution. Methyl groups are bulky, and sterically, interaction of the coordinatively unsaturated photofragment with the polymeric ligand would be unfavourable.

Figures 2.4.2.1 to 2.4.2.3 show the transient UV/vis difference spectra

obtained for the reaction of $\text{W(CO)}_5(\text{S})$, $\text{Mo(CO)}_5(\text{S})$ or $\text{Cr(CO)}_5(\text{S})$ with P- α -MS (mol. wt. = 43000) respectively. Little change is observed for the reaction with W(CO)_6 , even after 100ms. For the Mo(CO)_6 system, the grow-in of $\text{Mo(CO)}_5(\text{P-}\alpha\text{-MS})$ from $\text{Mo(CO)}_5(\text{toluene})$ is observed at 420nm. In the Cr(CO)_6 analogue, a slight shift to higher energy was observed on going from $\text{Cr(CO)}_5(\text{toluene})$ (λ_{max} at 470nm) to $\text{Cr(CO)}_5(\text{P-}\alpha\text{-MS})$ (λ_{max} at 450nm).

Figure 2.4.2.1: Transient UV/vis difference spectrum for W(CO)_6 with P- α -MS in toluene.

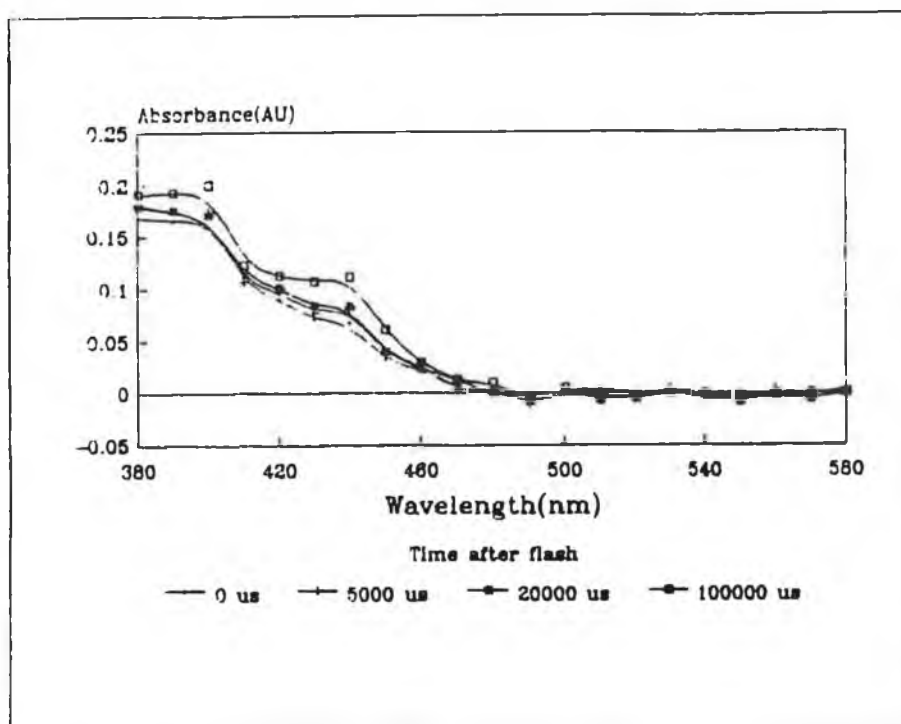


Figure 2.4.2.2: Transient UV/vis difference spectrum for Mo(CO)_6 with P- α -MS in toluene.

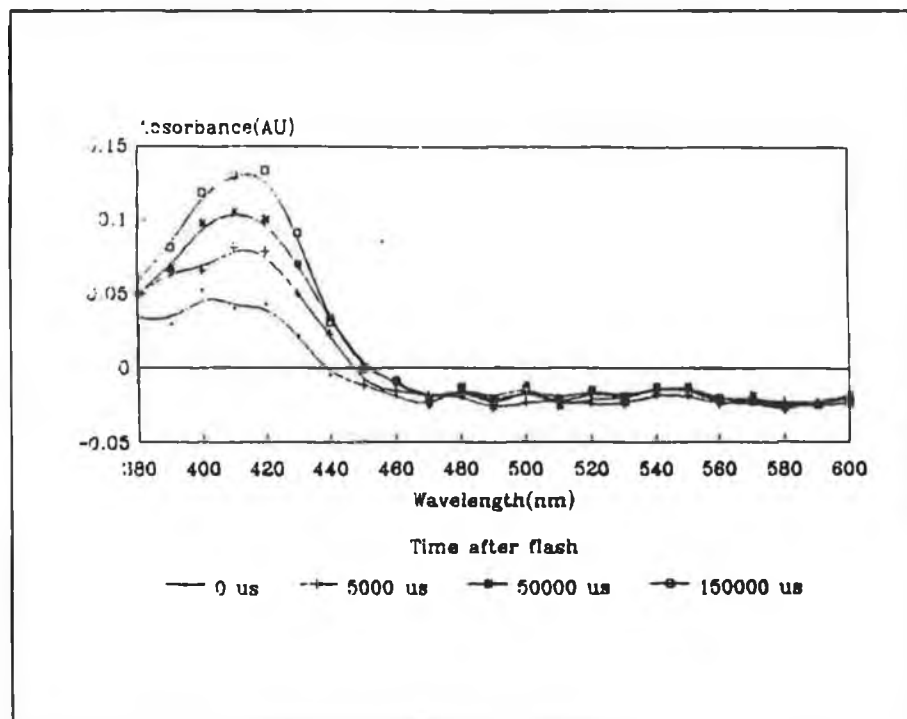
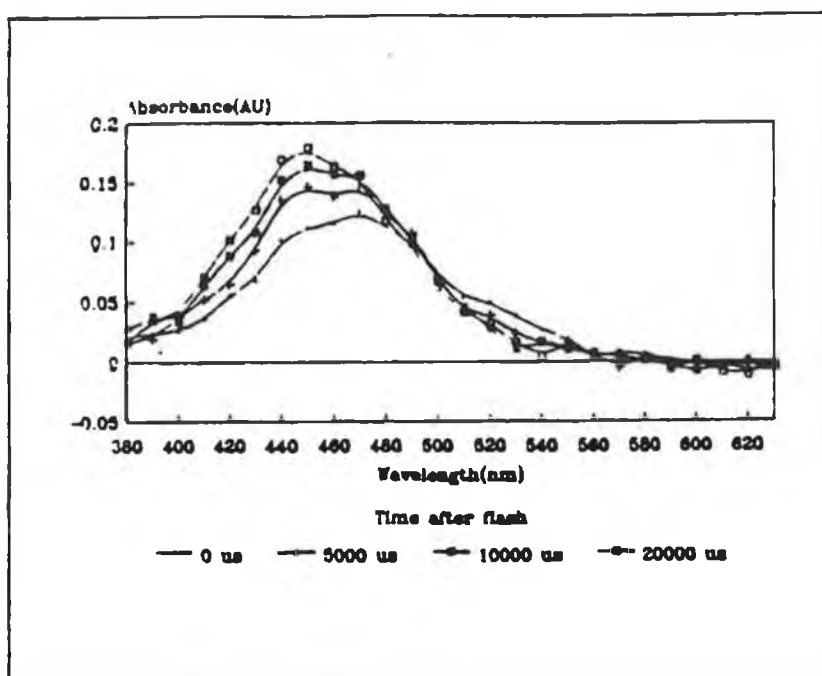


Figure 2.4.2.3: Transient UV/vis difference spectrum for Cr(CO)_6 with P- α -MS in toluene.



The observed rate constants for the reaction of the various poly- α -methylstyrene ligands with the metal carbonyl photofragments were determined and tabulated in Table 2.4.2.1. For the $W(CO)_6$ system, the data obtained suggests that there is little or no reaction between the polymer and the photofragment. This was attributed to the stability of the solvated adduct $W(CO)_5(\text{toluene})$. This supports the information obtained from the transient absorption spectrum (Figure 2.4.2.1), where very little change in absorbance was detected.

The observed rate constants for the photoreactions of $Mo(CO)_6$ and $Cr(CO)_6$ with poly- α -methylstyrenes are much slower than those for the corresponding reactions with polystyrene. The presence of a large number methyl groups causes expansion of the polymer coils, thus hindering coordination to the photofragment.

Overall, on comparing these results to those obtained for the analogous interaction with PS (Table 2.4.1.1), this work indicates that there is little spectroscopic or kinetic evidence for the formation of $M(CO)_5(\text{polymer})$. This again supports the idea that the effects observed with the AIBN initiated polymers are principally because of interactions with the end-groups.

Table 2.4.2.1: k_{obs} for the reaction of $\text{M}(\text{CO})_5(\text{toluene})$ with various molecular weight poly- α -methylstyrenes in toluene.

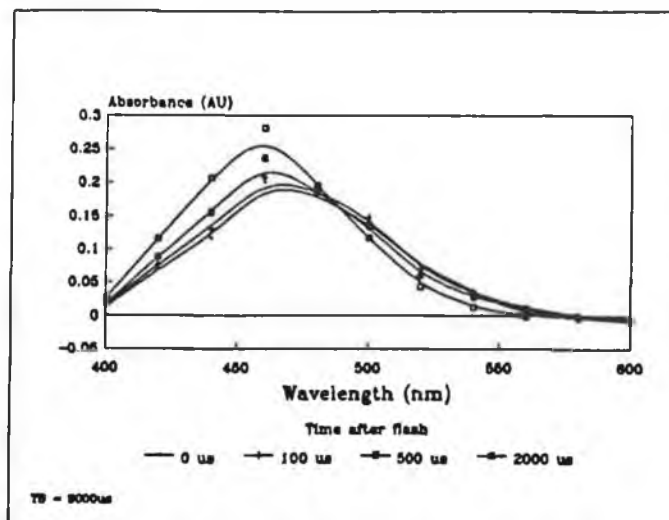
rms Dist. (Å)	k_{obs}/s		
	$\text{W}(\text{CO})_6$	$\text{Mo}(\text{CO})_6$	$\text{Cr}(\text{CO})_6$
85.4	8.4	57.5	210
108.4	7.8	55	184
145.9	6.8	49.3	—
167	6.4	45.3	118.3
179.4	6.2	43.5	104
207.4	5.5	—	87

2.4.3 Laser Flash Photolysis of $\text{M}(\text{CO})_6$ ($\text{M} = \text{W}, \text{Mo}, \text{or Cr}$) in the presence of Various Molecular Weight (PMMA) Polymethylmethacrylates in Toluene.

These polymers were prepared by free radical polymerisation using AIBN so the reaction kinetics are complicated by possible coordination to cyano end-groups. However, PMMA homopolymers have oxygen atoms on the backbone, which have lone pairs of electrons capable of strongly interacting with the photofragments. Shaver *et al.* [32] noticed that, even in the preparatory stage of embedding organometallic complexes in PS-AN, interaction between the two species occurred.

The transient UV/vis absorption spectra for the chromium system is shown in Figure 2.4.3.1. The grow-in of $\text{Cr}(\text{CO})_5(\text{PMMA})$ from $\text{Cr}(\text{CO})_5(\text{toluene})$ is observed at 460nm.

Figure 2.4.3.1: Transient UV/vis difference spectrum for $\text{Cr}(\text{CO})_6$ with PMMA (mol. wt. = 98000) in toluene.



The observed rate constants for the three metal systems are tabulated in Table 2.4.3.1. As seen for the the photochemical reactions with other polymers, the reactivity of the $\text{W}(\text{CO})_5(\text{toluene})$ species towards the polymer is lowest, compared to $\text{Mo}(\text{CO})_5(\text{toluene})$ or $\text{Cr}(\text{CO})_5(\text{toluene})$. Interaction of the molybdenum and chromium fragments with PMMA is faster, but possible end-group reactions cannot be ruled out because of the linear relationship between k_{obs} and the polymer rms end-to-end distance.

Table 2.4.3.1: k_{obs} for the reaction of $\text{M}(\text{CO})_5(\text{toluene})$ with PMMA (various rms end-to-end dist.) in toluene.

rms Dist. (Å)	k_{obs}/s		
	$\text{W}(\text{CO})_6$	$\text{Mo}(\text{CO})_6$	$\text{Cr}(\text{CO})_6$
96	27.7	278	1142
173	12.3	253	902
258	9.9	130	584
313	6.9	116	427

2.4.4 Summary.

Laser flash photolysis of $M(CO)_6$ ($M = Mo$ or Cr) with PS (AIBN init.), in the presence and absence of free PPh_3 in toluene have shown that observed rate constants were affected by the polymer in solution. UV/vis spectra revealed the production of slightly different photoproducts, which were dependent on polymer rms end-to-end distance. Subsequent investigation using PS (anionic polym) exhibited lower reaction rates for interaction of the metal carbonyl photofragment with the polymer. This indicated that a possible interaction occurred between the $M(CO)_5$ (toluene) species and the cyano end-groups in polymers prepared by free radical polymerisation.

The kinetic data obtained for the tungsten system suggests that the interaction of tungsten photofragments with all the homopolymers studied was negligible. This was possibly due to electronic effects, as steric hindrance may be ruled out because of the similarity in ionic radii for both molybdenum and tungsten. Also, $W(CO)_5$ (toluene) is relatively stable so conversion to the polymeric analogue will be slow.

In all the homopolymer systems studied, the observed rate constant for the reaction of the coordinatively unsaturated molybdenum and chromium photofragments with polymer was linearly dependent on polymer rms end-to-end distance. This provides a new method for the determination of polymer molecular weight. However, the nature of the end-group in polymer chains must be given consideration.

Dependencies on rms end-to-end distances were also noticed in a study of the cyclization rate constants for pyrene end-labelled polystyrene [43].

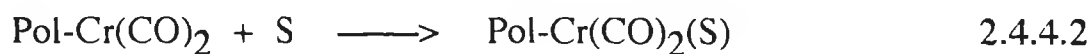
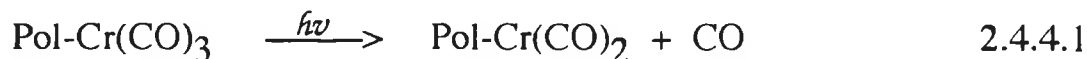
In P- α -MS and PS (anionic polym.) there are effectively no end-groups present and minimal interaction with $\text{M}(\text{CO})_5(\text{toluene})$ was observed. The small variations in the observed rates may correspond to the decay of a water complex $\text{M}(\text{CO})_5(\text{H}_2\text{O})$, formed by interaction of the coordinatively unsaturated pentacarbonyl with traces of water impurities present in the system. This process happens on a fast timescale, hence it was not observed by Hooker *et al.* in experiments carried out on much longer timescales. In conclusion, interaction of $\text{M}(\text{CO})_5(\text{toluene})$ with the 'reactive' end-groups of a copolymer or homopolymer prepared using AIBN initiation, contributes significantly to the reaction kinetics.

2.5 Laser Flash Photolysis of Polystyrene-anchored Chromium-tricarbonyl in the presence of Free Triphenylphosphine in Toluene Solution.

To investigate if a similar end-group reaction occurred when the metal itself was immobilised on the polymer support, several copolymers were prepared with chromiumtricarbonyl units directly attached. The monomers (styrene and styrenechromiumtricarbonyl) were polymerised using AIBN as initiator, and characterised by infrared spectroscopy and GPC (see Chapter 5).

Flash photolysis of polymer-bound chromiumtricarbonyl in toluene produces the coordinatively unsaturated dicarbonyl photofragment as shown in Reaction 2.4.4.1. This coordinates rapidly to the solvent (Reaction

2.4.4.2). In the presence of free PPh₃, the solvent is displaced to form the polymer-bound-Cr(CO)₂(PPh₃) adduct, as in Reaction 2.4.4.3.

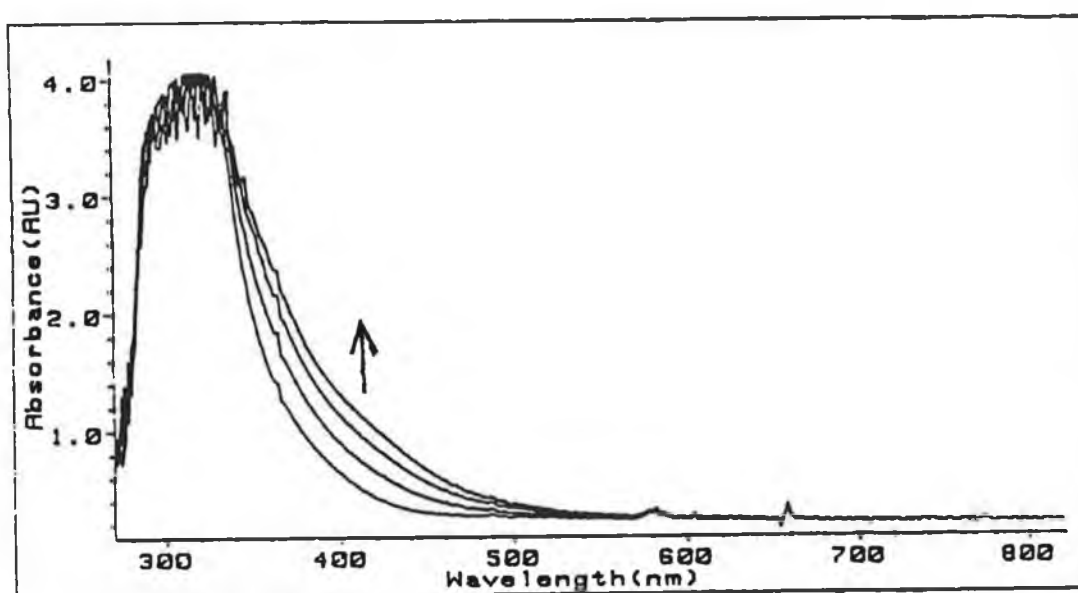


The molecular weight, and consequently, the rms end-to-end distance provides an indication of the number of 'reactive' end-groups in these copolymers, and this parameter was used to investigate if the photofragments interacted with the end-groups. If such an interaction significantly affected the reaction kinetics, a linear relationship between k_{obs} and the rms end-to-end distance should exist.

Five different copolymers were prepared in mole ratios of 3:1, 5:1, 10:1, 20:1, and 30:1 styrene to styrenechromiumtricarbonyl (S:StyCr(CO)₃) respectively. Flash photolysis experiments were carried out in the presence of a large excess of PPh₃. Reasons for this were (a) the concentration of metal carbonyl in solution is low, (to prevent problems with laser flash photolysis experiments), so any impurities present would greatly affect the kinetics, (b) to minimise the interaction between coordinatively unsaturated centres and the polymer backbone, as observed by Farrell [21] and, (c) to ensure pseudo first order conditions.

Changes observed in the UV/vis spectrum of polystyrene-anchored chromiumtricarbonyl are shown in Figure 2.5.1.1. In the visible region, there is an overall increase in intensity, due to the formation of the poly-(S:StyCr(CO)₂(PPh₃)) photoproduct.

Figure 2.5.1: Changes observed in the UV/vis spectrum upon flash photolysis of P-(S:StyCr(CO)₃) with PPh₃ in toluene.



The observed rate constants for the reaction of P-(S:StyCr(CO)₂(toluene)) with different PPh₃ concentrations were obtained, and from these the second order rate constants were calculated. The values are tabulated in Table 2.5.1. The rms end-to-end distances are also included.

The k_2 values for the reaction of the 3:1 and 5:1 copolymers with PPh₃ are significantly less than those for the corresponding 10:1, 20:1 and 30:1 analogues. However, the concentration of metal in solution is so low (for the

3:1 and 5:1 copolymers), that the validity of these figures is questionable. The values obtained for the 10:1, 20:1 and 30:1 systems are essentially the same within experimental error. This is in good agreement with the results obtained by Farrell for the reaction of $\text{Pol-Cr(CO)}_2(\text{S})$ with free pyridine as the incoming ligand.

Interestingly, the observed rate constants were independent of the rms end-to-end distance of the prefunctionalised copolymers. This suggests that no significant reaction takes place between the immobilised chromium photofragments and the cyano end-groups of the supports, to which they are attached.

Table 2.5.1: k_2 for the reaction of $\text{P-(S:StyCr(CO)}_3\text{)}$ with PPh_3 at 298K.

Ligand	$k_2 \text{ (dm}^3\text{mol}^{-1}\text{s}^{-1}\text{)}$
(3:1);(S:StyCr(CO) ₃)	$2.9 (\pm 0.3) \times 10^3$
(5:1);(S:StyCr(CO) ₃)	$1.2 (\pm 0.1) \times 10^3$
(10:1);(S:StyCr(CO) ₃)	$1.8 (\pm 0.2) \times 10^5$
(20:1);(S:StyCr(CO) ₃)	$2.7 (\pm 0.3) \times 10^5$
(30:1);(S:StyCr(CO) ₃)	$2.4 (\pm 0.3) \times 10^5$

2.5.1.1 Activation Parameters for the Reaction of P-(S:StyCr(CO)₂(S)) with Triphenylphosphine in Toluene.

The activation parameters were determined as already described (Section 5.2.4.3). The values are tabulated in Table 2.5.1.1.1. The values for the 3:1 and 5:1 copolymers are different from the other systems, which again casts doubt on the results for these two copolymers.

Table 2.5.1.1.1: Activation parameters for the reaction of P-(S:StyCr(CO)₂(toluene)) with PPh₃ [2 x 10⁻² M].

LIGAND	E _a [‡] (a)	ΔH [‡] (a)	ΔS [‡] (b)	ΔG [‡] (a)
3:1 Copol*	52	50	-41	61
5:1 Copol	103	95	115	61
10:1 Copol	73	71	51	55
20:1 Copol	70	67	51	52
30:1 Copol	66	63	38	52

(a) ± 2 kJmol⁻¹

(b) ± 25 Jmol⁻¹K⁻¹

* Refers to the mole ratio of Styrene to StyCr(CO)₃.

The positive nature of ΔS[‡] indicates a dissociative mechanism for the interaction of P-(S:StyCr(CO)₂(toluene)) and PPh₃. ΔG[‡] is the same within experimental error for the three copolymer species. The data for the Arrhenius and Eyring plots is tabulated in Appendix D. Representative plots are shown in Figures 2.5.1.1.1 and 2.5.1.1.2 for the Arrhenius and Eyring plots respectively.

Figure 2.5.1.1.1: Arrhenius plot for the reaction of (30:1); (S:StyCr(CO)₂(S)) with PPh₃ [2×10^{-2} M], (see Appendix D for data).

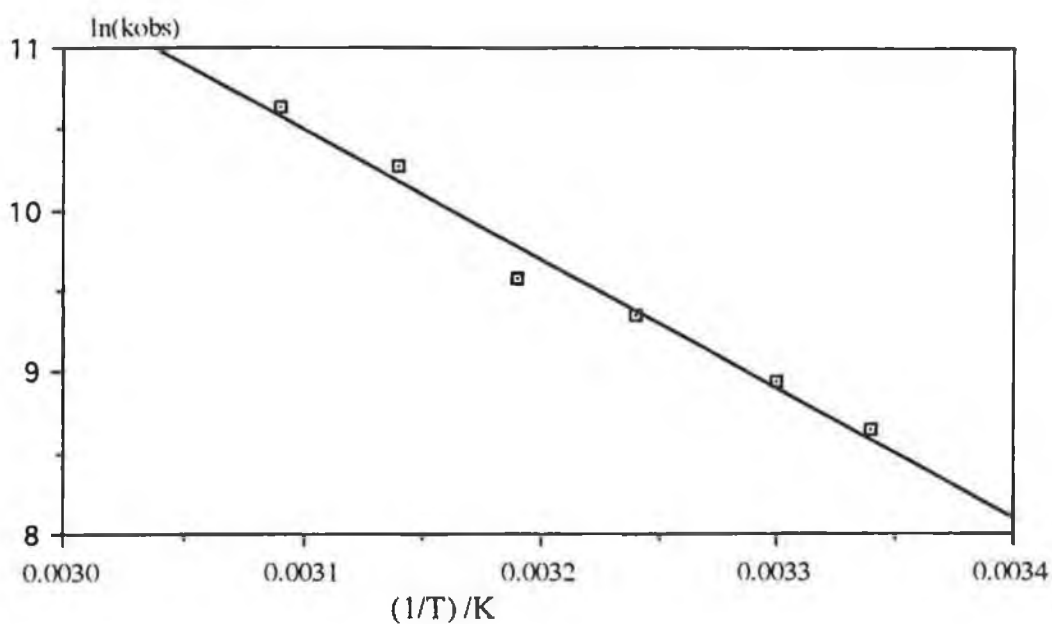
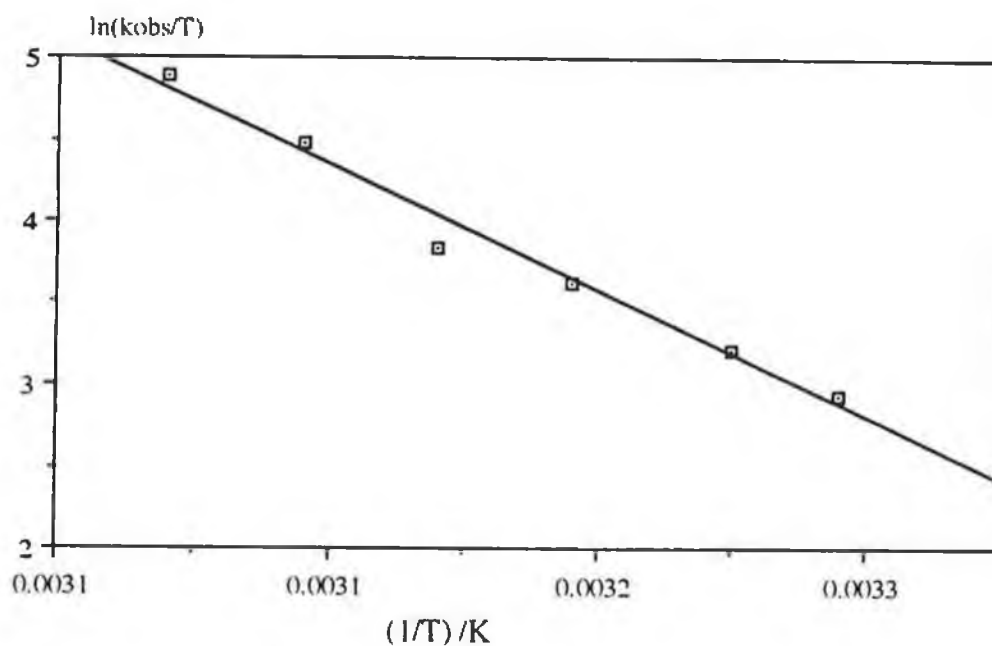


Figure 2.5.1.1.2: Eyring plot for the reaction of (30:1);(S:StyCr(CO)₂(S)) with PPh₃ [2×10^{-2} M], (see Appendix D for data).



2.5.2 Discussion.

The reaction of free PPh_3 with various styrene-styrenechromium tricarbonyl copolymers was investigated. No correlation between the observed rate constants and polymer rms end-to-end distance was detected. Thus, no significant interaction occurred between the chromium photofragments and the end-groups of the polymer supports to which they were immobilised. This is possibly because of the reduced mobility of the metal photofragments when immobilised, compared to the metal hexacarbonyl systems, where a greater freedom of motion exists. The results obtained for the 3:1 and 5:1 systems are not very reproducible. The concentration of metal carbonyl is so low that any impurities present greatly affect the reaction kinetics. For the 10:1, 20:1, and 30:1 copolymers, values of ΔG^\ddagger are the same within experimental error. The positive nature of ΔS^\ddagger suggests a dissociative mechanism for the transition state. This is understandable considering the 'crowded' nature of the metal surrounded by the polymer, making coordination to the bulky ligand difficult.

2.6 Conclusion.

'Reactive' end-groups on polymer supports may interact with photogenerated $\text{M}(\text{CO})_5(\text{toluene})$, to produce metal-polymer complexes. Homopolymers or copolymers prepared using AIBN as initiator contain cyano end-groups, which have lone pairs of electrons. Such moieties are

capable of stabilising $M(CO)_5$ photofragments. In low molecular weight polymers there is a high concentration of cyano groups, compared to the same weight of a high molecular weight analogue, resulting in a dependency of the observed reaction rate on the polymer molecular weight. This results in a greater interaction between the $M(CO)_5(\text{toluene})$ photofragment and the low molecular weight species.

The dependence of the observed rate of reaction on polymer molecular weight (or rms end-to-end distance) presents a possible method for determining the molecular weight of polymers, of unknown molecular weight. Standard plots of k_{obs} versus rms end-to-end distance (for polymers of known molecular weight) may be constructed. Knowing k_{obs} for the reaction of $M(CO)_5(\text{toluene})$ with the polymer of unknown molecular weight (or rms end-to-end distance), its rms end-to-end distance may be determined from the standard plot. However, the same method of polymerisation must be employed for both sets of polymers.

The flash photolysis of $M(CO)_6$ ($M = W, Mo, \text{ or } Cr$) in the presence of monomeric and polymeric phosphine units was investigated. Observed rate constants, and subsequently the second order rates, were higher for the copolymers with lower phosphine loading. The trend observed was not as a result of differences in ΔG^\ddagger for each system, as the values were the same within experimental error. The cyano end-groups on the polymer as well as phosphine contribute to the observed rate constant, resulting in an overall dependency on the copolymer rms end-to-end distance. Interaction of the copolymer with the metal carbonyl photofragment was *via* an associative pathway.

Laser flash photolysis of W(CO)_6 in the presence of various homopolymers have indicated that little or no interaction takes place between the metal photofragment and the polymeric ligand. This has been attributed to the steric problems associated with combining the large tungsten species to the bulky ligand. Also, $\text{W(CO)}_5(\text{toluene})$ is much more stable than the corresponding molybdenum or chromium analogues, so reaction with the ligand will be much slower.

The photochemical investigation of PS homopolymers with and without 'reactive' end-groups in the presence of M(CO)_6 ($\text{M} = \text{Mo}$ or Cr), have indicated that an interaction occurs with a potentially reactive end-group as well as along the polymer backbone. Thus, the nature of the end-group is an important consideration when carrying out photochemical studies on organometallic species in polymer environments.

The presence of a methyl group, as in the poly- α -methylstyrenes, along the polymer support sterically hinders coordination to the Mo(CO)_5 and Cr(CO)_5 photofragments, and, this was supported by the spectroscopic and kinetic evidence obtained for these systems.

The observed rates of reaction for the photofragments with PMMA were higher because of a stronger coordination to the oxygen lone pair electrons. Also, a dependency on the rms end-to-end distance was found for these systems and, because these PMMA homopolymers were prepared using AIBN as initiator, interaction of $\text{M(CO)}_5(\text{toluene})$ with the end-groups also contributes to k_{obs} .

Photoactive metal units were then immobilised on polymer supports to see if an end-group interaction was possible in such a situation. Immobilisation of

-Cr(CO)₃ moieties onto PS supports, followed by investigation of the reaction kinetics with PPh₃, revealed no change in the second order rate constant for the different metal loadings. The reaction was also found to be independent of the copolymer rms end-to-end distance. The activation parameters were determined, and no change in ΔG^\ddagger for the different reactions was observed. The interaction was *via* a dissociative mechanism. The immobilised chromiumtricarbonyl moiety was much more restricted compared to the hexacarbonyl in solution. This, along with steric hindrance, contributed to the different transition states on interaction of the photofragment with triphenylphosphine.

2.7 REFERENCES

- 1 (a) Burton, J. J.; Garten, R. L.; in *Advanced Materials in Catalysis*, Academic Press, New York, 1977; (b) Iwasawa, Y.; Yamagishi, M.; Ogasawara, S.; *J. Chem. Soc., Chem. Commun.* 246, 1982; (c) Iwasawa, Y.; Yamagishi, M.; Ogasawara, S.; *J. Chem. Soc., Chem. Commun.* 871, 1980; (d) Iwasawa, Y.; Hamamura, H.; *J. Chem. Soc., Chem. Commun.* 130, 1983; (e) Yermakov, Y. I.; Kuznetsov, B. N.; Zakharov, V. P.; *Catalysis by Supported Metal Complexes. Studies in Surface Science and Catalysis*, Elsevier, New York, **8**, 1981.
- 2 (a) Pittman, C. U. Jr.; in *Comp. Organomet. Chem.*; Wilkinson, G.; Stone, F. G. A.; Abel, E. W. (eds.), Pergamon Press, Oxford, **8**, 553, 1982; (b) Grubbs, R. H.; Kroll, L. C.; *J. Am. Chem. Soc.* **93**(12), 3062, 1971.
- 3 (a) Evans, G. O.; Pittman, C. U. Jr.; McMillan, R.; Beach, R. T.; Jones, R.; *J. Organomet. Chem.* **67**, 295, 1974; (b) Pittman, C. U. Jr.; Smith, L. R.; *J. Am. Chem. Soc.* **97**(7), 1749, 1975; (c) Pittman, C. U. Jr.; Quock, N. J.; *J. Organomet. Chem.* **153**, 85, 1978; (d) Sanner, R. D.; Austin, R. G.; Wrighton, M. S.; Honnick, W. D.; Pittman, C. U. Jr.; *Inorg. Chem.* **18**(4), 928, 1979; (e) Pittman, C. U. Jr.; Wilemon, G. M.; *J. Org. Chem.* **46**, 1901, 1981; (f) Pittman, C. U. Jr.; Smith, L. R.; Hanes, R. M.; *J. Am. Chem. Soc.* **97**, 1742, 1975.
- 4 Capka, M.; Svoboda, P.; Cerny, M.; Hetfleja, J.; *Tett. Lett. No.* **50**, 4787, 1971.
- 5 Camps, F.; Castells, J.; Font, J.; Vela, F.; *Tett. Lett. No.* **20**, 1715, 1971.

- 6 (a) McKinley, S. V.; Rakshys, J. W.; US Pat. 3,708,462, 1973; (b) McKinley, S. V.; Rakshys, J. W.; *J. Chem. Soc., Chem. Commun.* 134, 1972.
- 7 Manassen, J.; *Israel J. Chem.* **8**, 4p, 1970.
- 8 Nonaka, Y.; Takahashi, S.; Hagihara, N.; *Mom. Inst. Sci. Ind. Res. Osaka Univ.* **31**, 23, 1974.
- 9 Farrall, M. J.; Frechet, M. J.; *J. Org. Chem.* **41**(24), 3877, 1976.
- 10 Regen, S. L.; Lee, D. P.; *J. Org. Chem.* **40**(11), 1669, 1975.
- 11 Collman, J. P.; Hegedus, L. S.; Cooke, M. P.; Norton, J. R.; Dolcetti, G.; Marquardt, D. N.; *J. Am. Chem. Soc.* **94**(5), 1789, 1972.
- 12 Heitz, W.; Michels, R.; *Angew. Chem., Internat. Edit.* **11**(4), 298, 1972.
- 13 Yamamoto, A.; *Organotransition Metal Chem.: Fundamental Concepts and Applications*, Wiley-Interscience, New York, 1986.
- 14 Doi, H.; Sakagami, T.; EP 322,614, 1989.
- 15 Bond, G. C.; *Catalysis by Metals*, Academic Press, New York, 1963.
- 16 Thomas, J. M.; Thomas, W. J.; *Introduction to the Principles of Heterogeneous Catalysis*, Academic Press, London, 1967.
- 17 Draper, C. W.; *Metall. Trans. A*; **11A**(2), 349, 1980.
- 18 (a) Pittman, C. U. Jr.; Kim, B. T.; Douglas, W. M.; *J. Org. Chem.* **40**, 590, 1975; (b) Pittman, C. U. Jr.; Grube, P. L.; Ayers, O. E.; McManus, S. P.; Rausch, M. D.; Moser, G. A.; *J. Polym. Sci., Part A-1*, **10**, 379, 1972.
- 19 Rausch, M. D.; Moser, G. A.; Zaiko, E. J.; Lipman, A. L. Jr.; *J. Organomet. Chem.* **23**, 185, 1970.
- 20 Russell, G.; *Ph.D. Thesis*, Dublin City University, 1990.

- 21 Farrell, G.; *Ph.D. Thesis*, Dublin City University, 1992.
- 22 (a) Geoffrey, G. L.; Wrighton, M. S.; *Organometallic Photochemistry*, Academic Press, New York, 1979; (b) Wrighton, M. S.; *Chem. Rev.* **74**, 401, 1974.
- 23 (a) Zhang, S.; Dobson, G.; *Inorg. Chem.* **26**, 620, 1987; (b) Hodges, P. M.; Jackson, S. A.; Jacke, J.; Poliakoff, M.; Turner, J. J.; Grevels, F. W.; *J. Am. Chem. Soc.* **112**, 1234, 1990.
- 24 Zhang, S.; Dobson, G.; Brown, T. L.; *J. Am. Chem. Soc.* **113**, 6908, 1991.
- 25 Marx, D. E.; Lees, A. J.; *Inorg. Chem.* **26**, 620, 1987.
- 26 (a) Xie, X.; Simon, J. D.; *J. Am. Chem. Soc.* **112**, 1130, 1990; (b) O' Driscoll, E.; Simon, J. D.; *J. Am. Chem. Soc.* **112**, 6580, 1990; (c) Joly, A.; Nelson, K. A.; *J. Phys. Chem.* **93**, 2876, 1989.
- 27 Grevels, F. W.; Jacke, J.; Klotzbucher, W. E.; Ozkar, S.; Skibbe, V.; *Pure Appl. Chem.* **60**(7), 1017, 1988.
- 28 Kelly, J. M.; Long, C.; Bonneau, R.; *J. Phys. Chem.* **87**(17), 3344, 1983.
- 29 Wang, L.; Zhu, X.; Spears, K. G.; *J. Phys. Chem.* **93**, 2, 1989.
- 30 Massey, A. G.; Orgel, L. E.; *Nature*, 1387, 1961.
- 31 McIntyre, J. A.; *J. Phys. Chem.* **74**(11), 2403, 1970.
- 32 Shaver, A.; Butler, I. S.; Eisenberg, A.; Gao, J. P.; Xu, Z. H.; Fong, B.; Uhm, H.; Klein, D.; *Appl. Organomet. Chem.* **383**, 1987.
- 33 Shaver, A.; Gao, J. P.; Butler, I. S.; *Appl. Organomet. Chem.* **2**, 9, 1988.
- 34 Shaver, A.; Gao, J. P.; Butler, I. S.; *Appl. Organomet. Chem.* **3**, 425, 1989.

- 35 Markwell, R. S.; Butler, I. S.; Gao, J. P.; Shaver, A.; *Appl. Organomet. Chem.* **6**, 693, 1992.
- 36 (a) Hooker, R. H.; Rest, A. J.; *Appl. Organomet. Chem.* **4**, 141, 1990;
(b) Hooker, R. H.; Rest, A. J.; Whitwell, I.; *J. Organomet. Chem.* **266**, C27, 1984.
- 37 Margerison, D.; East, G. C.; *Introduction to Polymer Chem.*, Pergamon Press, Oxford, 1967.
- 38 Sheridan, N.; M.Sc. Thesis, Dublin City University, 1991.
- 39 Microanalysis carried out at Microanalytical Laboratory, UCD, Dublin.
- 40 Atkins, P. W.; *Physical Chemistry*, Oxford University Press, 1986.
- 41 Turner, J. J.; in *Photoprocesses in Transition Metal Complexes, Biosystems and other Molecules, Expt. and Theory*; Kochanski, E. (ed.), 125, 1992.
- 42 (a) Kuhn, W.; *Kolloid-Z.* **68**, 2, 1934; (b) Schulz, G. V.; Cantow, H.-J.; Meyerhoff, G.; *J. Polym. Sci.* **10**(1), 79, 1953.
- 43 (a) Redpath, A. E. C.; Winnick, M. A.; *J. Am. Chem. Soc.*; **104**, 5604, 1982; (b) Horie, K.; Schnabel, W.; Mita, I.; Ushiki, H.; *Macromolecules* **14**, 1422, 1981.

Chapter 3

**Laser flash photolysis of $\text{StyCr}(\text{CO})_3$, $\text{CpMn}(\text{CO})_2(\eta^2\text{-C}_8\text{H}_{14})$,
and $\text{MeCpMn}(\text{CO})_2(\mu\text{-Sty})\text{Cr}(\text{CO})_3$.**

3.0 Introduction.

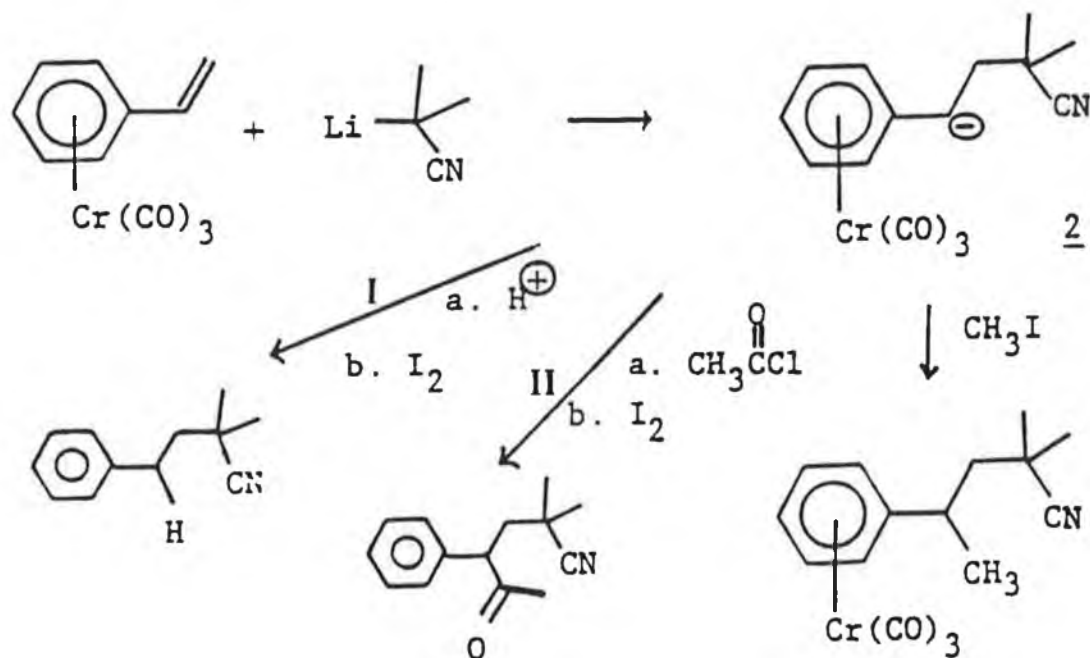
The history of metal-olefin complexes dates back to 1827 when a Danish chemist, W. C. Zeise [1] synthesised the platinum-ethylene complex $K[Pt(C_2H_4)Cl_3].H_2O$. However, the mode of coordination of ethylene to the metal fragment was not fully established until 1950. Since then, hundreds of complexes of this type have been prepared [2].

Not surprisingly, the number and type of reactions of these metal-olefin complexes is vast. The most famous are in catalysis, namely Ziegler and Wacker processes [3]. Ziegler performed the very efficient polymerisation of ethylene using catalyst systems composed of $TiCl_4$ or $TiCl_3$ mixed with organo-aluminium compounds such as $AlEt_3$ and $AlEt_2Cl$, intermediates in the reaction being metal-olefins. Many of the newer processes involve metal carbonyl compounds for the preparation of particular products [4]. Activation is usually accomplished by photochemical displacement of a carbon monoxide (CO) ligand from the metal. These photochemical substitution reactions have been extensively used as a convenient method for preparing particular products, but the nature of the reaction intermediates has not been given a great deal of attention [5]. Other olefin-containing metal carbonyl compounds of interest are (arene) $M(CO)$ - π -complexes. The presence of an olefin substituent on the arene ring in (arene) $Cr(CO)_2$ - π -complexes allows facile addition and conversion reactions which are both stereospecific and selective.

3.1 (Arene)Cr(CO)₂- π -olefin Complexes.

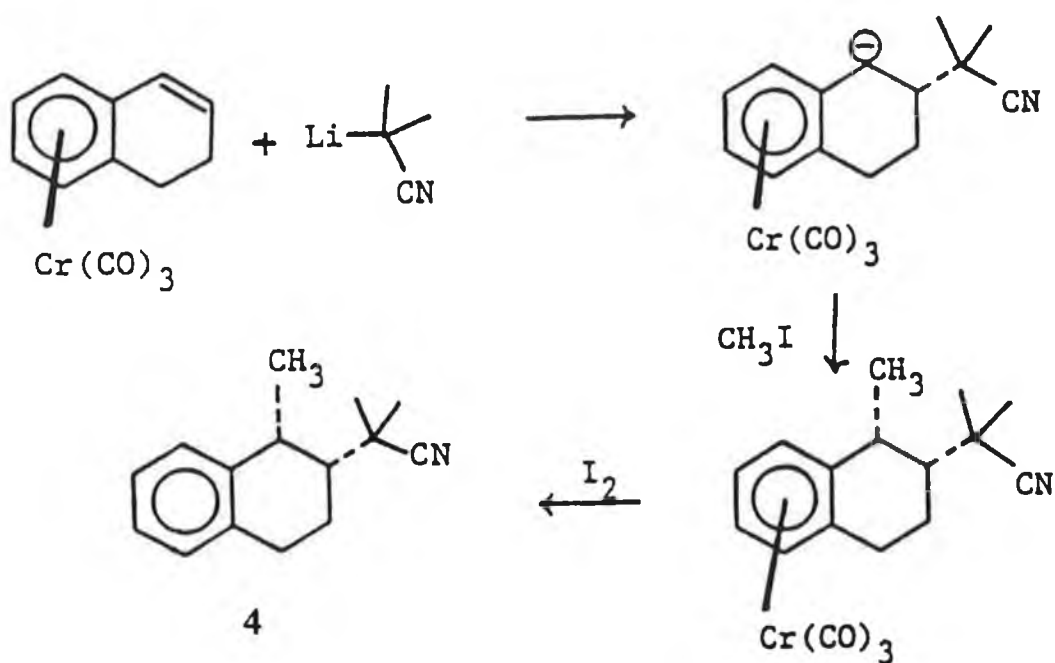
Coordination of an arene ring to a transition metal *via* the arene π orbitals produces a significant electron deficiency within the arene ring. Semmelhack [6] subjected arene-substituted (styrene)chromiumtricarbonyl (StyCr(CO)₃) complexes to nucleophilic attack to determine if attack occurred at the β -styrene position, or directly to the arene ring. Addition of 2-lithio-2-methylpropionitrile to StyCr(CO)₃ proceeds slowly at -30°C to produce anion 2 (Scheme 3.1.1), which may be trapped by a variety of electrophiles. Iodine oxidation of 2 as in I and II results in fragmentation of the -Cr(CO)₃ moiety.

Scheme 3.1.1.



A similar addition reaction for $(\eta^6\text{-1,2-dihydronaphthalene})\text{Cr}(\text{CO})_3$ produces the single isomer 4 shown in Scheme 3.1.2. The reaction proceeds in 65% yield, attack having occurred at the β -styrene position. Subsequently, the high degree of selectivity induced by vinylic substituents allows the relatively simple preparation and isolation of several organic complexes.

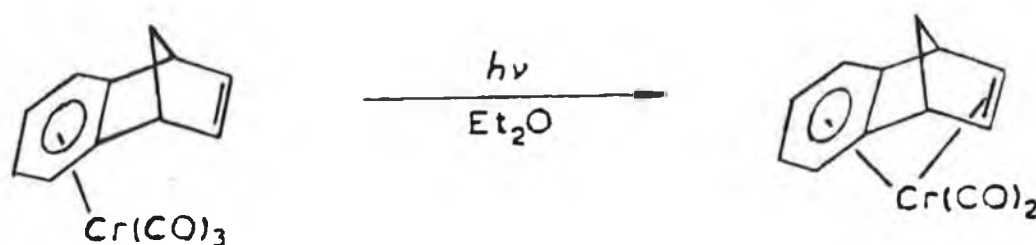
Scheme 3.1.2:



Photochemical as well as chemical methods have been used in the synthesis of novel $(\text{arene})\text{Cr}(\text{CO})_2\text{-}\pi\text{-olefin}$ complexes. Several $(\text{alkenylarene})\text{Cr}(\text{CO})_3$ complexes were prepared by Trahanovsky and Hall [7a], and these were irradiated to produce the monodecarbonylated analogues which underwent intramolecular cyclisation. Scheme 3.1.3 shows

the conversion of *syn*-(η^6 -benzonorbornadiene)Cr(CO)₃ to the cyclised adduct (η^8 -benzonorbornadiene)Cr(CO)₂.

Scheme 3.1.3:

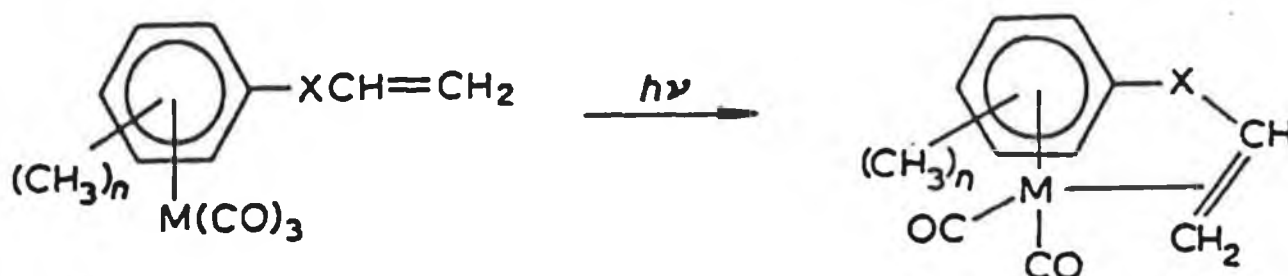


The workers found that stable (η^8 -alkenylbenzene)Cr(CO)₂ complexes may be formed by photolysis of the corresponding (arene)Cr(CO)₃, if the carbon-carbon double bond is attached to the benzene ring by two or three methylene groups, or a methylene group and an oxygen atom, or is part of a bicyclic system which causes the carbon-carbon double bond to be in good orientation for complexation.

Nesmeyanov *et al.* [8] synthesised similar chelate compounds of chromium, molybdenum and tungsten. A two or three atom bridge between the arene and the olefinic group was again found to be most suited to intramolecular cyclisation. The general preparation for linear π -olefin complexes is shown in Scheme 3.1.4. Conversions were most successful for chromium, followed by molybdenum, and tungsten, yielding only very small amounts of the

cyclised adduct even after prolonged irradiation.

Scheme 3.1.4:

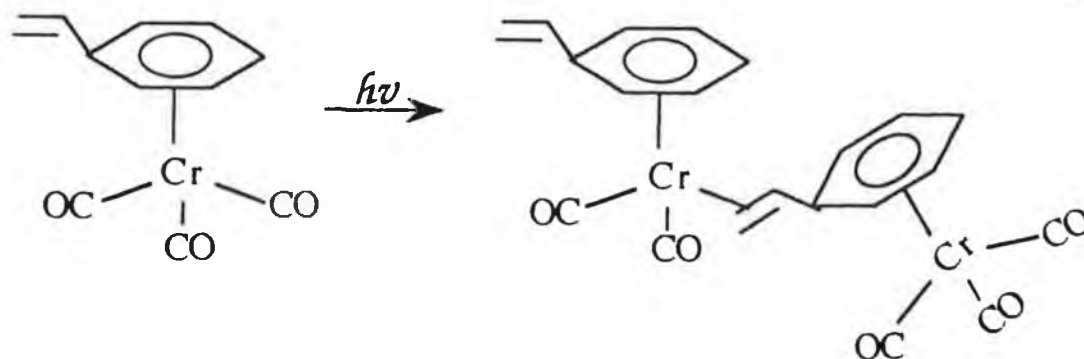


(M = Cr, Mo, W; $n = 0, 2, 3, 5$;

X = OCH₂, CH₂CH₂, CH₂OCH₂, (CH₂)₃, (CH₂)₄

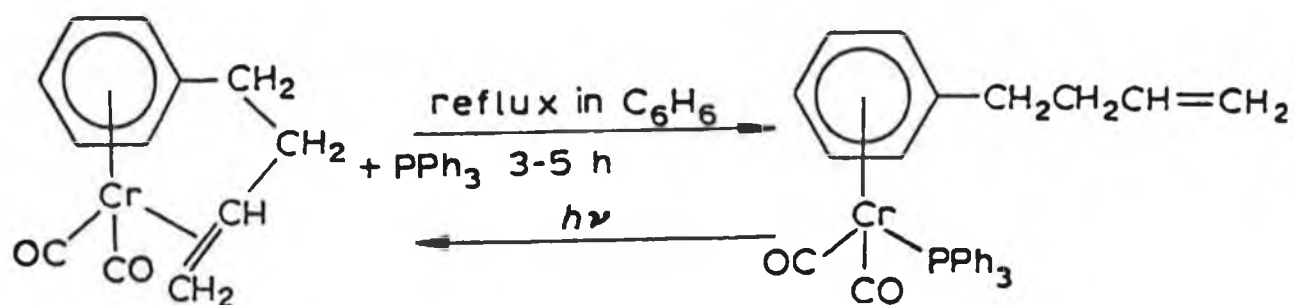
Longer bridges had strong destabilising effects, especially if the bridges possessed oxygen atoms. When a one-unit bridge was used, as in (allylbenzene)Cr(CO)₃, only decomposition occurred. When no bridge was used as in StyCr(CO)₃ and StyMo(CO)₃, μ -olefin bridged dinuclear complexes were produced as shown in Scheme 3.1.5. These complexes are formed because of the electron withdrawing action of the (arene)M(CO)₃ moiety attached to the vinyl group. These complexes are very unstable and replacement of the μ -olefin link with PPh₃ occurs within minutes upon heating in benzene.

Scheme 3.1.5:



The (alkenylarene)Cr(CO)₂ chelates are far more stable than their respective parent analogues (except those with the olefin directly linked to the arene), being much more resilient towards heat, oxidation and ligand substitution. Refluxing for several hours is required before the η^2 -coordinated ligand is displaced by PPh₃. Interestingly, UV irradiation of the product leads to recovery of the starting material (Scheme 3.1.6)

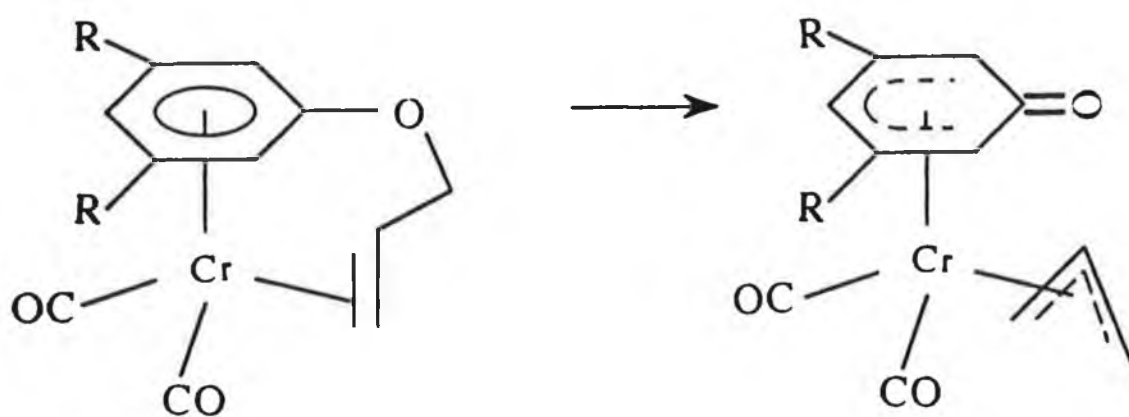
Scheme 3.1.6:



Coordination of the vinyl group to the metal by intramolecular cyclisation leads to the formation of chiral complexes. Nesmeyanov concluded that the vinyl group was oriented parallel (or near parallel) to the plane of the arene ring in cyclised chelates. The chelates formed were rigid structures, and no rotation parallel to the vector adjoining the chromium to the centroid of the arene ring occurred.

Surprisingly, when $(\eta^8\text{-allylphenylether})\text{Cr}(\text{CO})_2$ or its 3, 5-dimethyl derivative was irradiated, in the presence and absence of PPh_3 [7b], the corresponding isomeric $(\pi\text{-allyl})(6\text{-oxocyclohexadienyl})\text{Cr}(\text{CO})_2$ complex was formed (Scheme 3.1.7). This is a novel route to the synthesis of η^3 -allylic complexes.

Scheme 3.1.7:



An interesting feature of the chemistry of $\text{StyCr}(\text{CO})_3$ and its analogues is their very poor tendency to homopolymerise [10, 11], when compared to the relatively simple styrene polymerisation. Khand *et al.* [12] investigated the reactions of various (arene) substituted $\text{StyCr}(\text{CO})_3$ compounds with

phenylacetylenehexacarbonyldicobalt, and compared the results to similar investigations with the metal-free styrene derivatives. Most of the substituted $\text{StyCr}(\text{CO})_3$ compounds behaved in a manner similar to the corresponding styrene analogues (without the $\text{Cr}(\text{CO})_3$ moiety attached), with the production of both (1, 4-diarylbutadiene) $\text{Cr}(\text{CO})_3$ and (2-phenyl-5-arylcyclopentanone) $\text{Cr}(\text{CO})_3$ with similar yields. Reaction of simple alkenes with the acetylene complex generally produced the cyclopentanone derivative, whereas the presence of an electron withdrawing group on the alkene favoured production of the diene complexes. As a result, the authors expected more of the diene complex to be formed in the presence of the strongly electron withdrawing $\text{Cr}(\text{CO})_3$ moiety. However, this was not reflected in the experiments.

Clearly, the synthetic and photochemical permutations associated with (alkenylarene) $\text{M}(\text{CO})_3$ complexes are large. The primary process in many of the reactions outlined here is the expulsion of a CO ligand, followed by interaction with solvent and subsequently, some site of unsaturation or an adjacent ligand. The mechanism and kinetics of such processes in many non-olefin containing (arene) $\text{Cr}(\text{CO})_3$ complexes has received much attention [see for example refs. 13 -17].

Howell and Burkinshaw [18], and Grevels *et al.* [19] reviewed the mechanisms and kinetics of interaction of olefins with Group 6 metal hexacarbonyls. To our knowledge, no investigations into the mechanisms and kinetics of CO loss in (alkenylarene) $\text{Cr}(\text{CO})_3$ compounds have been published. We have synthesised the simplest alkenylarene derivative, $\text{StyCr}(\text{CO})_3$, and investigated its fast reaction solution photochemistry. We

have also used it as a model for elucidation of the photochemistry in the manganese-chromium dinuclear complex $\text{MeCpMn(CO)}_2(\mu\text{-Sty})\text{Cr(CO)}_3$ which has been synthesised. In this complex, we were interested in determining if the photoactivity resided at the manganese centre or the chromium centre, by comparison with the various model compounds synthesised.

3.2 Mononuclear $\text{CpMn-}\pi\text{-olefin}$ Compounds.

$\text{CpMn-}\pi\text{-olefin}$ complexes are readily synthesised by a photochemical substitution mechanism which postulates the photoejection of a CO molecule from CpMn(CO)_3 , and replacement by the $\pi\text{-olefin}$ donor [21]. The parent complex CpMn(CO)_3 has been the subject of numerous investigations, one reason being its very high thermal stability [23], in contrast to its great synthetic capabilities using photochemical substitution [2c, 20]. The substituted analogues have very different reactivities from the Cp or (MeCp) metal carbonyl compounds. The strength of the Mn-CO bond in CpMn(CO)_3 is very high compared to other metal-CO bond strengths [24] and helps to explain its observed thermal inertness. By the mid 1960's, a large number of $\text{CpMn-}\pi\text{-olefin}$ complexes had been characterised [20]. The olefin ligands included linear and cyclic mono-olefins such as C_2H_4 and C_8H_{14} , di-olefins *e.g.* butadienes, which may coordinate to one metal centre or act as a ligand bridge between two manganese atoms, or aromatic $\pi\text{-bound}$ ligands such as benzene. However, it wasn't until 1972 that the

decarbonylated intermediate CpMn(CO)_2 was first detected [22], when CpMn(CO)_3 was photolysed at 80K in methylcyclohexane / Nujol. Two sharp bands appeared in the $\nu(\text{CO})$ region of the infrared which were assigned to the CpMn(CO)_2 photofragment.

Antonova *et al.* [25] synthesised a CpMn(CO)_2 -vinylidene complex, and reacted this with P(OR)_3 ($\text{R} = \text{Et}$ or Ph), to produce the $\text{CpMn(CO)}_2(\eta^2\text{-olefin})$ analogue (Scheme 3.2.1.1). The reaction proceeded efficiently at 20°C without UV irradiation.

Scheme 3.2.1.1:



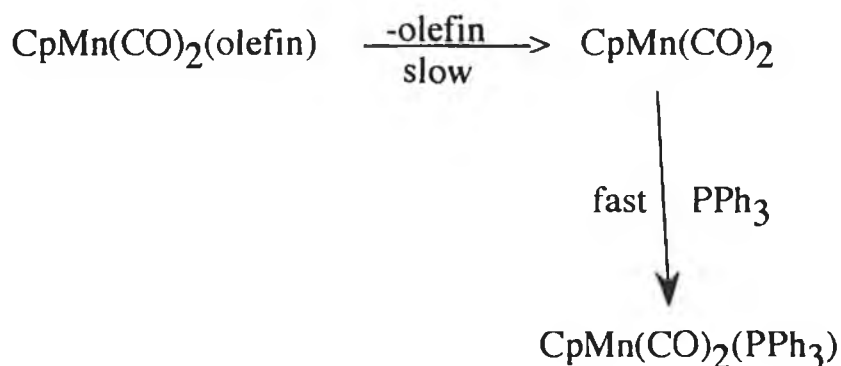
The reaction of 9-diazoanthrone with photogenerated $\text{CpMn(CO)}_2(\text{THF})$ (or the MethylCp (MeCp) derivative), proceeded very cleanly and easily to produce the $\text{CpMn(CO)}_2(\eta^2\text{-anthronylketene})$ (or $(\text{MeCp})\text{Mn(CO)}_2(\eta^2\text{-anthronylketene})$ derivative, while no reaction was observed for the ligand with the analogous tricarbonyl complexes, even under very severe conditions [26]. These reactions exhibit the potential usefulness of these compounds as intermediates and precursors, for the synthesis of organometallic species.

The substantial difference in reactivity of the $\text{CpMn(CO)}_2\text{L}$ complexes led to various kinetic studies on these systems. Angelici and Loewen [23] examined the rates at which olefin ligands in $\text{CpMn(CO)}_2(\text{olefin})$ were replaced by phosphine, amine, or sulphur ligands according to Reaction 3.2.1.2. The olefins used included ethylene, propylene and *cis*-cyclooctene.



The rate of olefin dissociation was found to be independent of L and proceeded according to an $\text{S}_{\text{N}}1$ type mechanism for the transition state (Scheme 3.2.1.2).

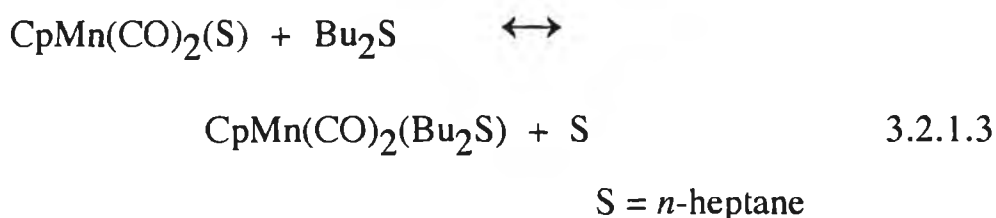
Scheme 3.2.1.2:



With non-cyclic olefins, the rate of dissociation increased in the order ethylene \ll propylene $<$ 1-pentene. For cyclic olefins, the rate of olefin dissociation increases in the order norbornadiene $<$ norbornylene \ll cyclooctene $<$ cyclopentene $<$ cycloheptene. Overall, if there is high ring

strain in the free cyclic olefin, coordination to the metal relieves the strain resulting in a stronger metal-olefin interaction. In linear olefins, steric effects of methyl groups or else their electron donating nature were attributed to the trends observed. The rate of dissociation of olefin from (MeCp)Mn(CO)₂(olefin) was found to be virtually the same as that for the non-methylated analogue.

Klassen *et al.* [27] found that the observed rate constant for coordination of dibutyl sulphide (L) to CpMn(CO)₂(S) depended on the concentration of L (Reaction 3.2.1.3).



The ease at which a CO molecule may be photoejected from the parent CpMn(CO)₃ or (MeCp)Mn(CO)₃ complexes, and indeed the high quantum efficiency of the reaction [28] has resulted in investigation of the primary photochemical processes in both the gaseous [29] and condensed phases [30]. The primary photoproducts in the gaseous state are CpMn(CO)_x, x = 2, 1. In solution, the primary photoproduct is CpMn(CO)₂ which coordinates weakly to the solvent molecules. These photofragments react with CO, parent, or other substrates to form secondary products. To our knowledge, no such photochemical studies have been reported on the mono-substituted π-olefin analogues.

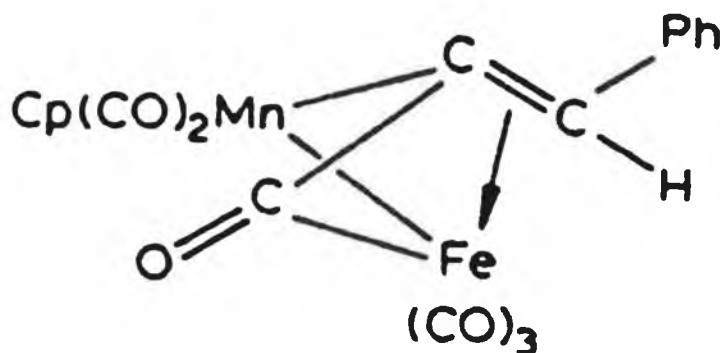
We have synthesised the CpMn-π-olefin complex CpMn(CO)₂(η²-C₈H₁₄)

and investigated its solution photochemistry. This complex was chosen because it may easily be prepared from the photolysis of CpMn(CO)_3 in THF, to produce $\text{CpMn(CO)}_2(\text{THF})$, from which the solvent is displaced by the incoming olefin ligand. *Cis*-cyclooctene was chosen as the ligand because, the crystal and molecular structure of the analogous π -olefin complex $(\text{MeCp})\text{Mn(CO)}_2(\eta^2\text{-C}_8\text{H}_{14})$ has recently been carried out [41], providing information on the various bonds between the metal centre and the ligands which may be beneficial in determining the photochemistry. This complex was also used as a model for elucidation of the photochemistry of the manganese-chromium dinuclear complex synthesised.

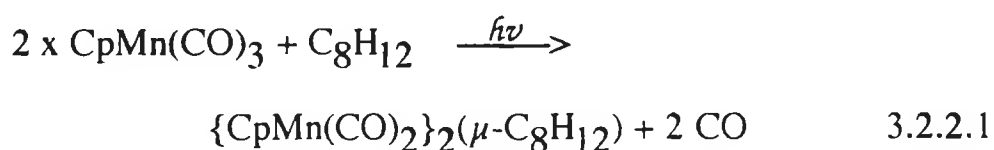
3.3 Hetero-binuclear $\text{CpMn-}\pi\text{-olefin}$ Compounds.

The great potential of CpMn(CO)_3 to undergo replacement of one, two, or three of its CO ligands *via* photochemical substitution, coupled to the almost endless choice of incoming ligand, has resulted in the synthesis of a vast number of poly-nuclear and poly-heteronuclear manganese complexes [31]. The majority contain metal-metal bonds with various bridging ligands, for example the manganese-iron complex $\{\text{Cp(CO)}_2\text{MnC(CO)CHPh}\}\text{Fe(CO)}_3$, shown in Figure 3.3.1 [32].

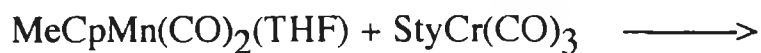
Figure 3.3.1:



There are very few examples where a dinuclear manganese complex is linked purely by a ligand [2c]. 4-Vinylpyridine (VP) was used as both an N- and π -donor bridge in the dinuclear $\{\text{MeCpMn}(\text{CO})_2\}_2(\mu\text{-VP})$ complex [33]. Kaim and Gross [47], linked two $\text{MeCpMn}(\text{CO})_2$ photofragments *via* the two nitrogen atoms of a pyrazine ring. Gross-Lannert *et al.* [48] synthesised a similar dinuclear complex using benzene(*bis*-1,4-dimethylphosphine) as the bridge. Norbornadiene (NBD), a bifunctional π -donor can act as a ligand bridge between two manganese centres [2c, 20]. 1,5-Cyclooctadiene combined with two $\text{CpMn}(\text{CO})_2$ fragments in similar fashion to form (μ -cyclooctadiene(1, 5)-*bis*-($\text{CpMn}(\text{CO})_2$)) as in Reaction 3.2.2.1 [20].



We have synthesised a mixed metal dinuclear complex, bridged by a π -donor centre. $\text{MeCpMn}(\text{CO})_2(\text{THF})$ was reacted with $\text{StyCr}(\text{CO})_3$ to produce $\text{MeCpMn}(\text{CO})_2(\mu\text{-Sty})\text{Cr}(\text{CO})_3$, as in Reaction 3.2.2.2.



The photochemistry of manganese complexes and chromium complexes have received much attention. In general, the chromium systems have faster reactivities compared to manganese systems. It was of interest to determine the photoprocess in solution when the two metal centres were combined, as in the manganese-chromium complex (as in Reaction 3.2.2.2). In this complex, there are two potential photoactive sites.

3.3 Results and Discussion.

3.3.1 Laser Flash Photolysis of StyCr(CO)_3 in Cyclohexane Solution.

Laser flash photolysis investigation of StyCr(CO)_3 was carried out in room temperature cyclohexane solution with an excitation wavelength of 355nm. Cyclohexane was chosen as the solvent because of its chemical inertness, and also for direct comparison of results with previous work on analogous systems [13, 30].

3.3.3.1 Electronic Excitation Spectrum of StyCr(CO)_3 .

The UV/vis spectrum of StyCr(CO)_3 is shown in Figure 3.3.1.1. As for BenzeneCr(CO)_3 [53], the prominent spectral feature is a sharp, intense band near 330nm, assigned to a combination of $\text{M} \rightarrow \text{Sty CT}$, with some $\text{M} \rightarrow \pi^* \text{ CO}$ character. The lowest energy absorption is a shoulder centered at 400nm, the origin of which is uncertain. The extinction coefficient of StyCr(CO)_3 in cyclohexane was calculated to be $4912 \text{ dm}^3\text{mol}^{-1}\text{cm}^{-1}$ at 355nm.

Figure 3.3.1.1: UV/vis spectrum of StyCr(CO)_3 in cyclohexane.

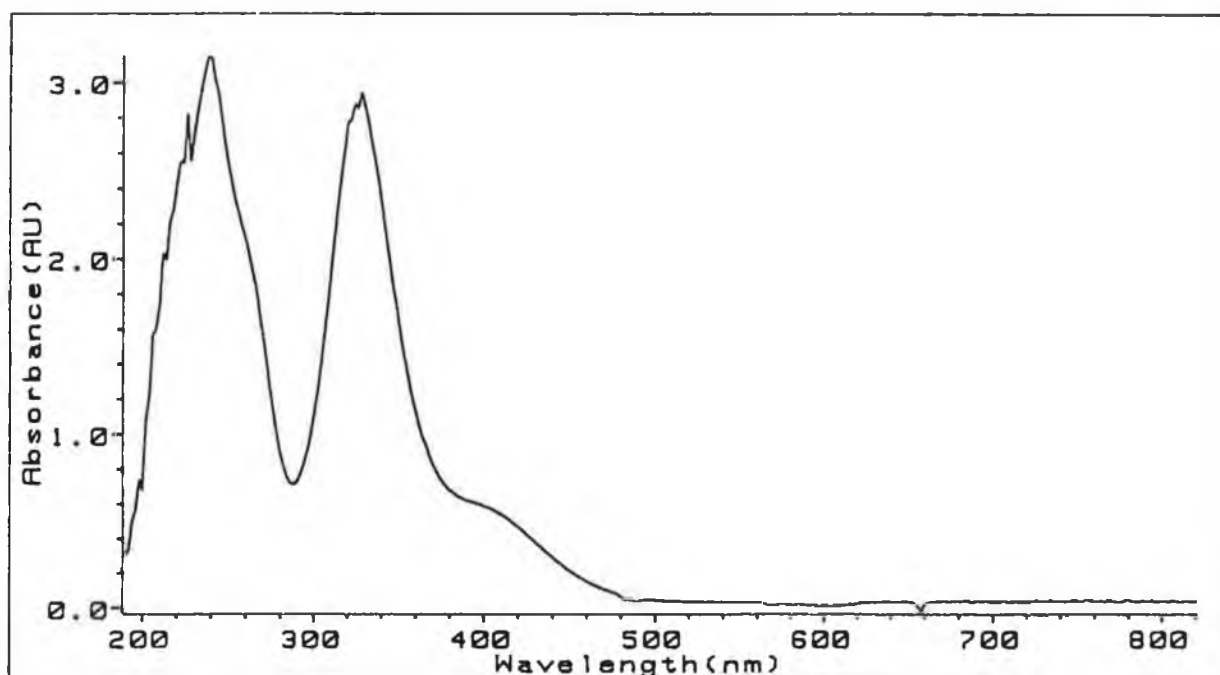
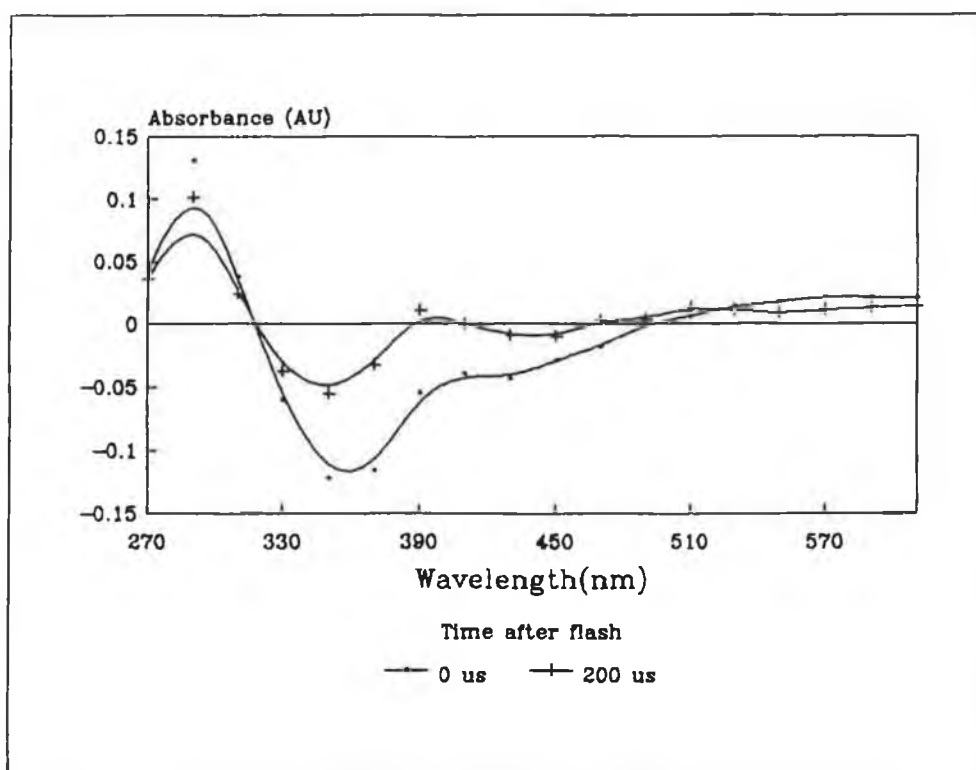


Figure 3.3.1.2 is the transient UV/vis absorption difference spectrum recorded at the time of flash and $200\mu\text{s}$ after the flash. The decay of the primary photoproduct centred at 290nm is concomitant with the grow-in of product at around 360nm. Based on previous spectroscopic work [13, 34 -

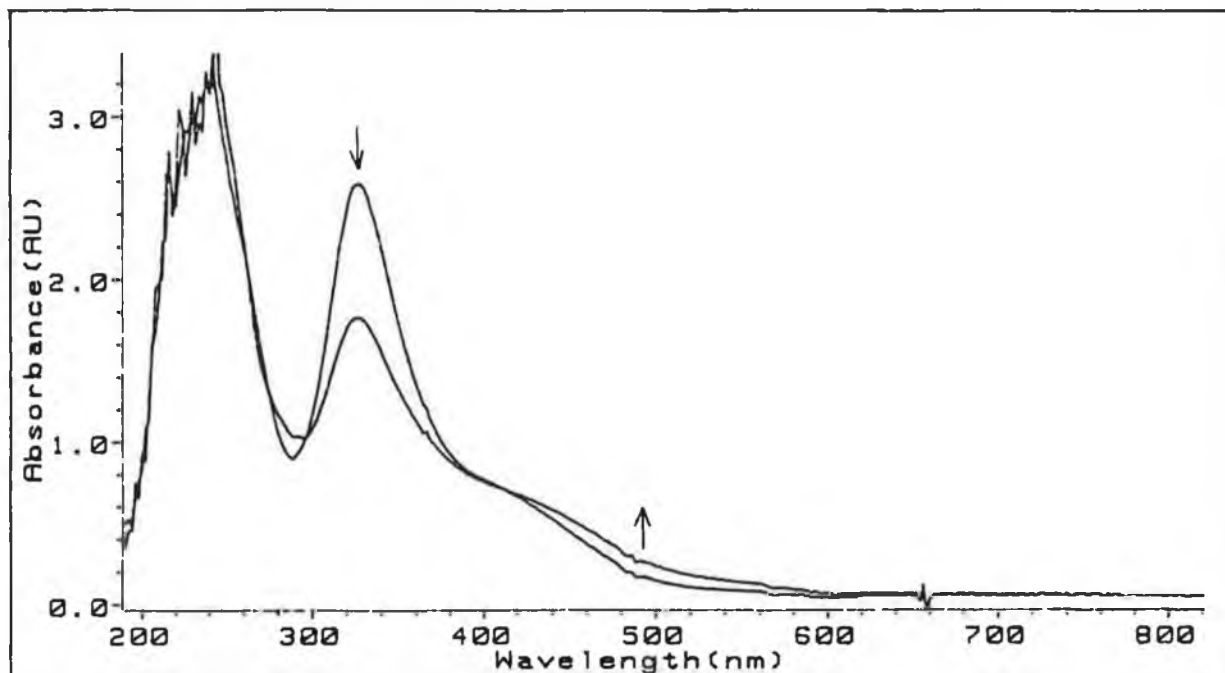
- 36] we have assigned the band at $0\mu\text{s}$ to $\text{StyCr(CO)}_2(\text{cyclohexane})$. This species was formed within the flash (10ns) and its risetime is too fast to be detected on our system (see Chapter 5). The decay of this complex was investigated.

Figure 3.3.1.2: Transient UV/vis absorption difference spectrum observed upon flash photolysis of StyCr(CO)_3 in cyclohexane under an argon atmosphere.



Flash photolysis of StyCr(CO)_3 in cyclohexane, in an atmosphere of argon is not reversible, as shown in Figure 3.3.1.3. A decrease in the parent absorption is observed at 330nm, while the shoulder at 400nm increases. There is also some weak absorption in the visible region of the spectrum.

Figure 3.3.1.3: Changes observed in the UV/vis spectrum for StyCr(CO)_3 in cyclohexane (1 atm. argon) before and after flash photolysis.



3.3.1.2 Primary Photoproduct.

The dependence of the lifetime of the solvated dicarbonyl $\text{StyCr(CO)}_2(\text{S})$ on CO was investigated. If the ejection of CO is the primary photoprocess, then its recombination with the decarbonylated parent should occur in a CO atmosphere. The transient UV/vis difference spectrum under CO is recorded at various time intervals after the flash (Figure 3.3.1.4). Flash photolysis of StyCr(CO)_3 in cyclohexane under various concentrations of CO, showed a linear dependence of $\text{StyCr(CO)}_2(\text{S})$ lifetime with $[\text{CO}]$. Figure 3.3.1.5 shows a typical trace obtained, which represents the decay of the solvated intermediate (in a carbon monoxide environment), to regenerate StyCr(CO)_3 .

Figure 3.3.1.4: Transient UV/vis absorption difference spectrum for $\text{StyCr}(\text{CO})_3$ under 1 atm. CO in cyclohexane.

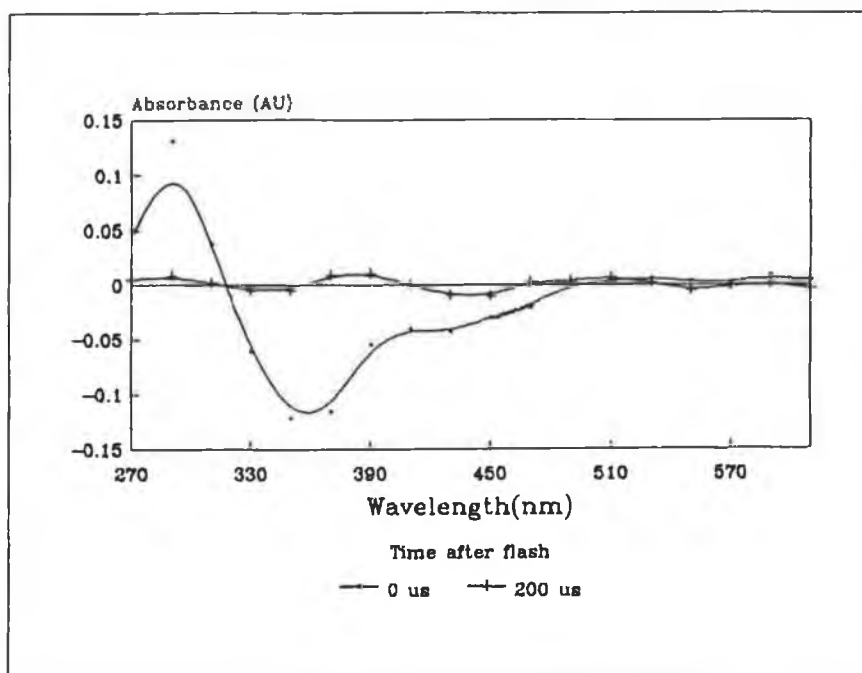
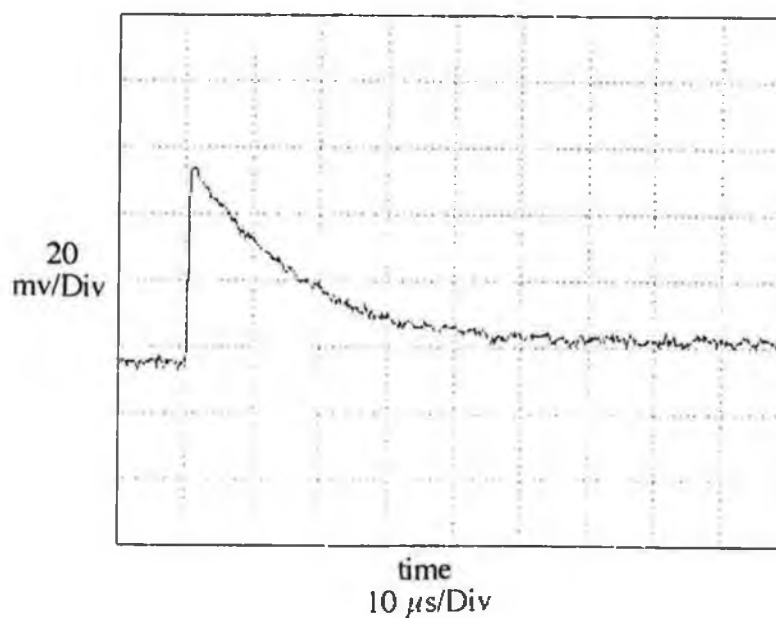
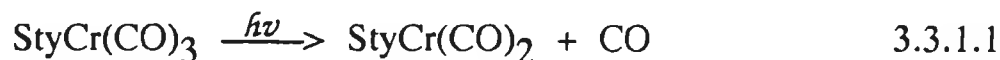


Figure 3.3.1.5: Decay of $\text{StyCr}(\text{CO})_2(\text{S})$ in the presence of $9.0 \times 10^{-3}\text{M}$ CO at a monitoring wavelength of 290nm.



The primary photoreaction in solution is therefore given by Reaction 3.3.1.1.



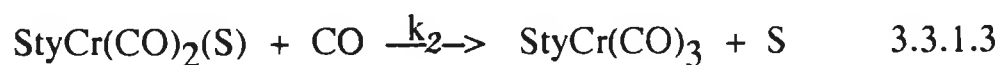
The coordinatively unsaturated dicarbonyl complex is very reactive and rapidly forms the solvated complex (Reaction 3.3.1.2).



S = Cyclohexane

The lifetime of $\text{StyCr(CO)}_2(\text{S})$ is linearly dependent on the concentration of CO, yielding a second-order rate constant for recombination (Reaction 3.3.1.3) of $7.1 \times 10^6 \text{ dm}^3 \text{ mol}^{-1} \text{ s}^{-1}$ at 298K.

In a similar study, Creaven *et al.* [13] observed the formation of $\text{AreneCr(CO)}_2(\text{S})$ as the primary photoproduct on flash photolysis of various AreneCr(CO)_3 compounds in cyclohexane and several linear alkane solvents. The rate reported for the reaction of $\text{BenzeneCr(CO)}_2(\text{S})$ with CO in cyclohexane was $9.8 \times 10^6 \text{ dm}^3 \text{ mol}^{-1} \text{ s}^{-1}$. The solvent is weakly bound, and is easily displaced by CO, hence the very fast reaction rates.



The data for the determination of the effect of CO on the lifetime of the solvated intermediate is tabulated in Table 3.3.1.1. Figure 3.3.1.6 shows the corresponding plot of observed rate constants obtained for the different CO concentrations.

Table 3.3.1.1: Data for the effect of CO on the lifetime of the primary photoproduct, $[\text{StyCr}(\text{CO})_3] = 1.3 \times 10^{-4} \text{ M}$.

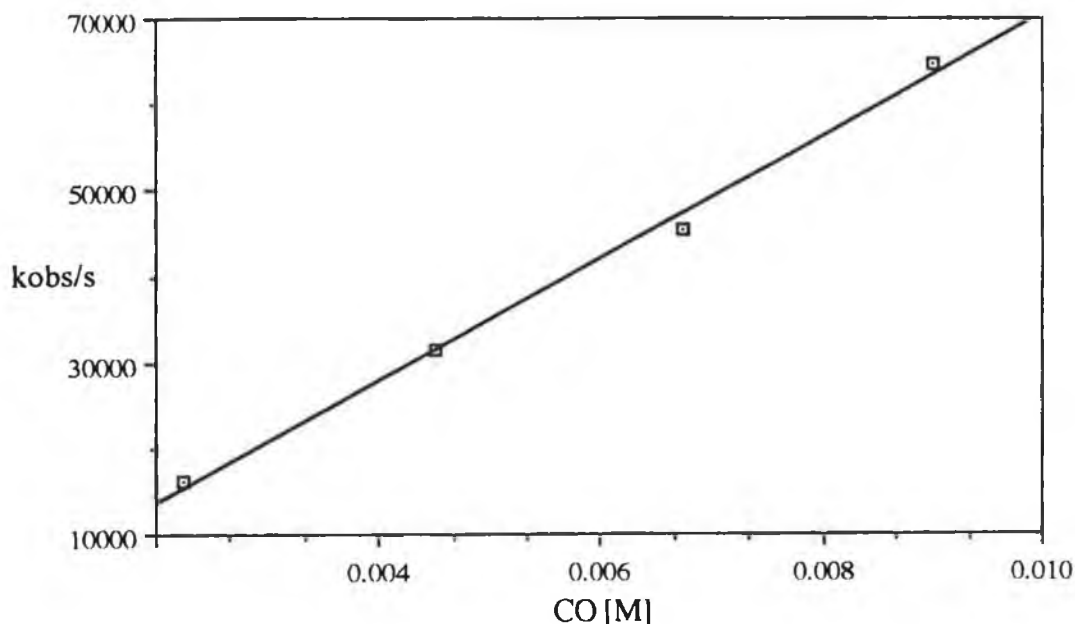
CO (E3) [M]	k _{obs} /s
2.25	16135
4.50	31480
6.75	45390
9.00	64860

$$\text{Slope} = 7.1 (\pm 0.4) \times 10^6 \text{ dm}^3 \text{ mol}^{-1} \text{ s}^{-1}$$

$$\text{Intercept} = -555 \pm 1800 \text{ s}^{-1}$$

$$\text{Correlation} = 0.99$$

Figure 3.3.1.6: Plot of k_{obs} (s^{-1}) versus $[\text{CO}]$ for $\text{StyCr}(\text{CO})_2(\text{S})$ with CO in cyclohexane at 298K.



3.3.1.3 Activation Parameters for the reaction of $\text{StyCr}(\text{CO})_2(\text{S})$ with CO.

The activation parameters for the reaction of $\text{StyCr}(\text{CO})_2(\text{S})$ with CO were calculated using Arrhenius and Eyring equations (Section 5.2.4.2). The second order rate constant k_2 was used in the calculations ($k_2 = k_{\text{obs}}/[\text{CO}]$), where $[\text{CO}] = 0.9 \times 10^{-2}\text{M}$. The activation parameters are listed in Table 3.3.1.2. The experimental data is given in Table 3.3.1.3 and the corresponding graphs in Figures 3.3.1.7 and 3.3.1.8.

Table 3.3.1.2: Activation parameters for the reaction of $\text{StyCr(CO)}_2(\text{S})$ with CO.

$$E_a^\ddagger = 37 \pm 2 \text{ kJmol}^{-1}$$

$$\Delta H^\ddagger = 35 \pm 2 \text{ kJmol}^{-1}$$

$$\Delta S^\ddagger = 3 \pm 25 \text{ Jmol}^{-1}\text{K}^{-1}$$

$$\Delta G^\ddagger = 34 \pm 2 \text{ kJmol}^{-1}$$

The activation barrier for the reaction is quite low. The nearness of the activation entropy to zero is indicative of an interchange mechanism [37 - 39]. Thus the reaction of $\text{StyCr(CO)}_2(\text{S})$ with CO involves a transition state where the CO molecule coordinates to the metal centre concomitant with loss of cyclohexane (Scheme 3.3.1.1). An interchange mechanism was also postulated for the reaction of CO with various solvated AreneCr(CO)_2 intermediates [13].

Scheme 3.3.1.1: Interchange mechanism for recombination of CO with $\text{StyCr(CO)}_2(\text{S})$.

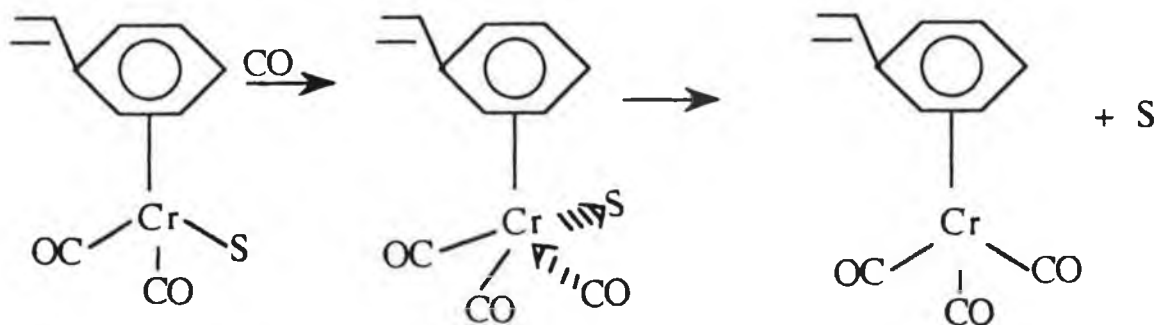


Table 3.3.1.3: Experimental data for the determination of the activation parameters for the reaction of $\text{StyCr}(\text{CO})_2(\text{S})$ with CO.

Temp (K)	(1/T)E3 (1/K)	kobs (/s)	ln(kobs/[CO])	ln((kobs/T)/[CO])
283	3.53	30154	15.02	9.37
288	3.47	39465	15.29	9.63
293	3.41	57121	15.66	9.98
298	3.36	72347	15.90	10.20
303	3.30	93199	16.15	10.43
308	3.24	111449	16.33	10.60
313	3.19	135960	16.53	10.78

Arrhenius Plot

Slope = -4470 ± 210

Intercept = 30.8 ± 0.1

Correlation = 0.99

$$E_a^\ddagger = 37 \pm 2 \text{ kJmol}^{-1}$$

Eyring Plot

Slope = -4170 ± 210

Intercept = 24.1 ± 0.1

Correlation = 0.99

$$\Delta H^\ddagger = 35 \pm 2 \text{ kJmol}^{-1}$$

$$\Delta S^\ddagger = 3 \pm 25 \text{ Jmol}^{-1}\text{K}^{-1}$$

Figure 3.3.1.7: Arrhenius plot for the reaction of $\text{StyCr(CO)}_2\text{(S)}$ with CO.

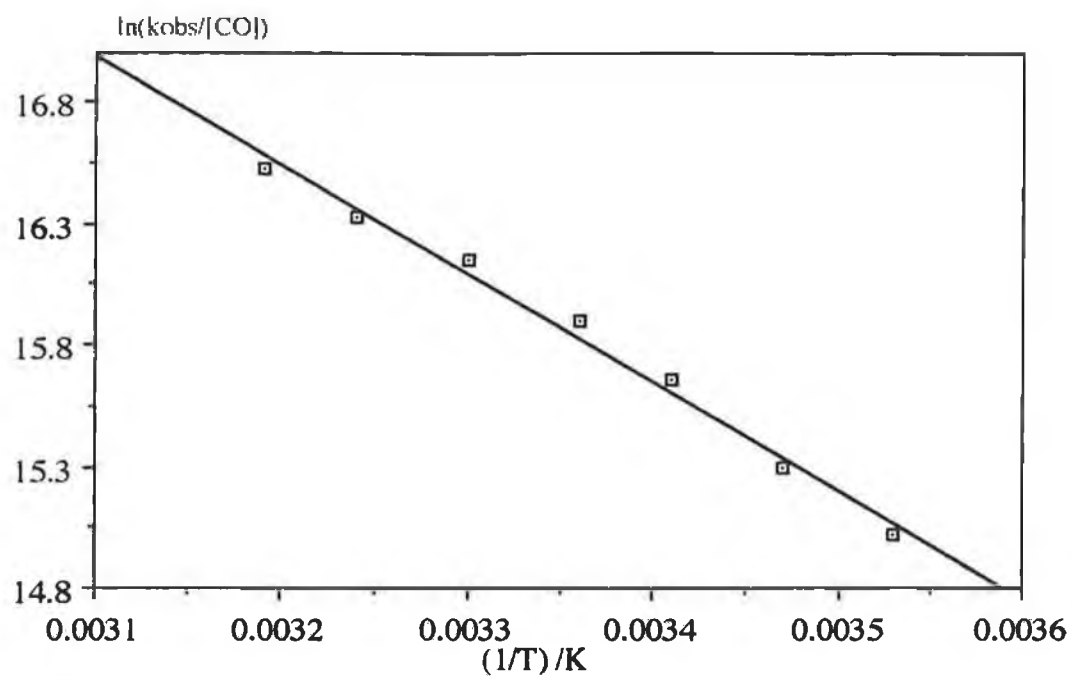
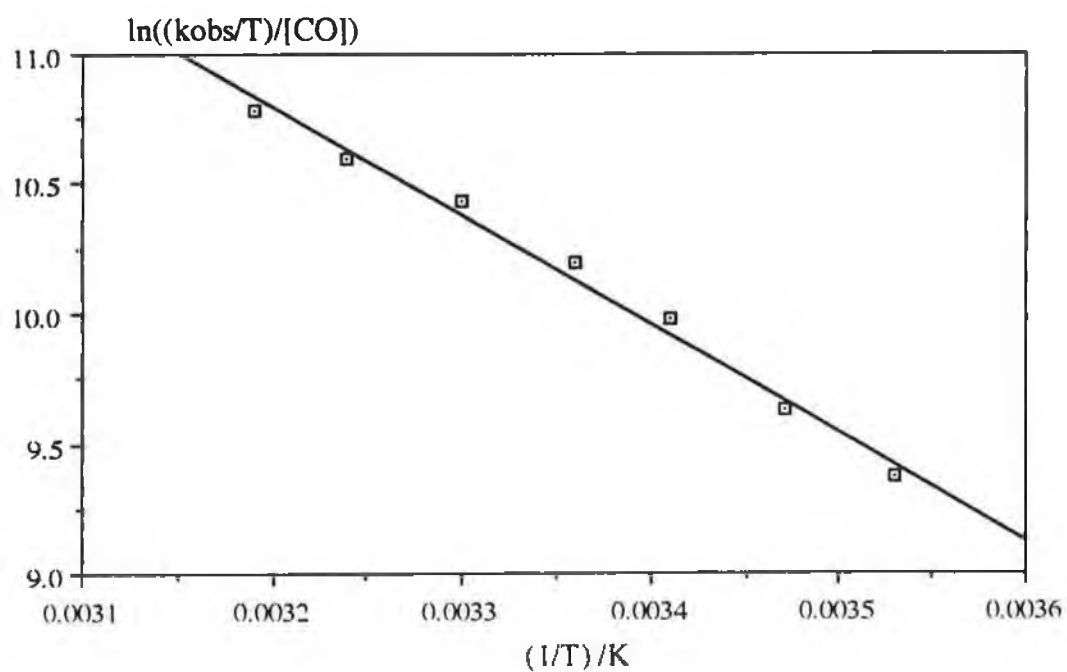


Figure 3.3.1.8: Eyring plot for the reaction of $\text{StyCr(CO)}_2\text{(S)}$ with CO.



3.3.1.4 Formation of $\text{Sty}_2\text{Cr}_2(\text{CO})_5$.

Under an argon atmosphere, the formation of a second transient species was observed. The transient UV/vis spectrum of this species is shown in Figure 3.3.1.9, with absorption maxima at 290 and 390nm.

The concentration of $\text{StyCr}(\text{CO})_3$ in solution was varied and the observed rate constants were determined at each concentration. The observed rates were plotted against parent concentration, and the slope gave an estimate of the second order rate constant for the reaction of the solvated dicarbonyl $\text{StyCr}(\text{CO})_2(\text{S})$ with parent $\text{StyCr}(\text{CO})_3$, as shown in Reaction 3.3.1.4.



The data is recorded in Table 3.3.1.4 and the corresponding plot in Figure 3.3.1.10.

Figure 3.3.1.9: Transient UV/vis absorption spectrum of the second species.

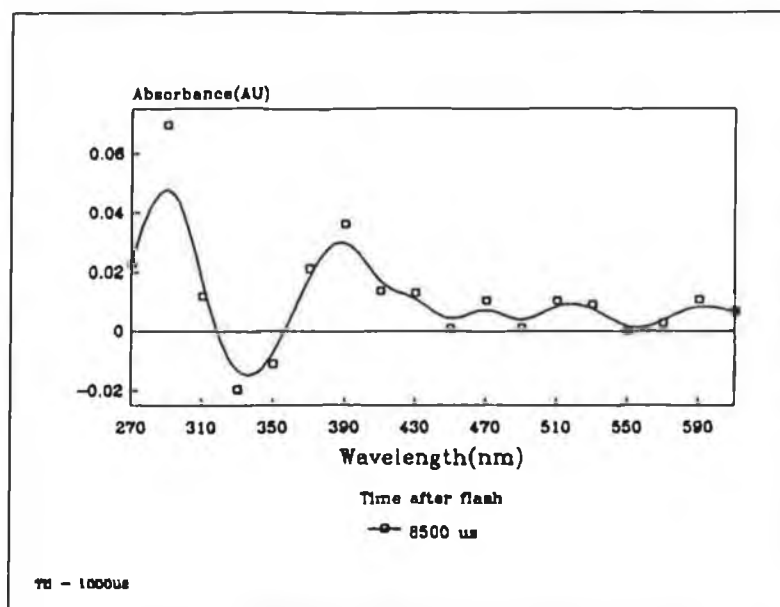


Table 3.3.1.4: Data for the determination of the effect of $\text{StyCr}(\text{CO})_3$ concentration on k_{obs} for the formation of the second species.

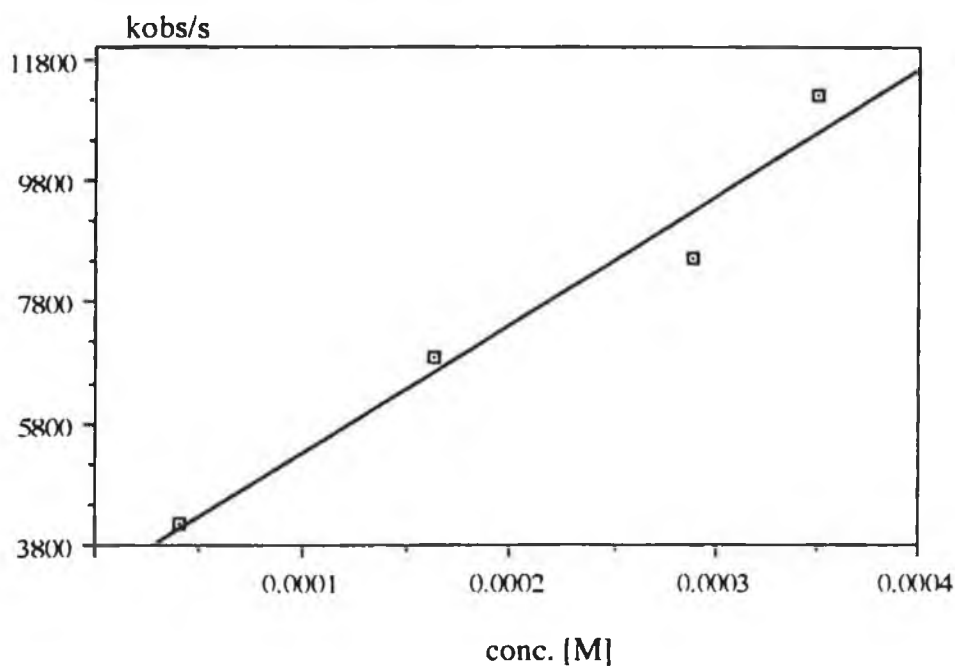
conc. (E4) [M]	kobs/s
0.9	4150
2.1	6668
3.4	8536
4.0	11206

$$\text{Slope} = 2.1 (\pm 0.3) \times 10^6 \text{ dm}^3 \text{ mol}^{-1} \text{ s}^{-1}$$

$$\text{Intercept} = 2190 \pm 710 \text{ s}^{-1}$$

$$\text{Correlation} = 0.96$$

Figure 3.3.1.10: Plot showing the change in k_{obs} with various concentrations of $\text{StyCr}(\text{CO})_3$.



The formation of the second species was suppressed under a CO atmosphere. The CO competed with parent for any available dicarbonyl solvated intermediate present. Therefore, we concluded that what was being observed was the formation of a dinuclear complex, from the interaction of the dicarbonyl fragment with the tricarbonyl (Reaction 3.3.1.4).

The second order rate constant (k_3) for the formation of this long-lived dinuclear species is $3.2 \times 10^7 \text{ dm}^3\text{mol}^{-1}\text{s}^{-1}$. An analogous interaction has been identified ($k_3 = 4.8 \times 10^7 \text{ dm}^3\text{mol}^{-1}\text{s}^{-1}$) for BenzeneCr(CO)₃ [13], where proposed coordination occurred *via* Cr-Cr interaction and a bridging carbonyl. However, IR monitored photolysis of a sample of StyCr(CO)₃ in argon degassed cyclohexane (Section 3.3.1.6) revealed the emergence of four new CO absorptions at 1970, 1935, 1903 and 1889 cm^{-1} , concomitant with a reduction in intensity of the parent $\nu(\text{CO})$ stretching frequencies (1980, 1915 cm^{-1}). No evidence for a bridging CO was observed. We believe that this is the dimeric species $(\text{CO})_2(\text{Sty})\text{Cr}(\mu\text{-Sty})\text{Cr}(\text{CO})_3$, previously isolated by Nesmeyanov *et al.* [8b], and reported to exhibit bands in the infrared $\nu(\text{CO})$ (CH_2Cl_2) at 1972, 1921, 1886, and 1869 cm^{-1} . Coordination of the unsaturated StyCr(CO)₂ photofragment to the parent occurs *via* η^2 interaction with the vinylic carbons of the parent (Reaction 3.3.1.5, Figure 3.3.1.11).

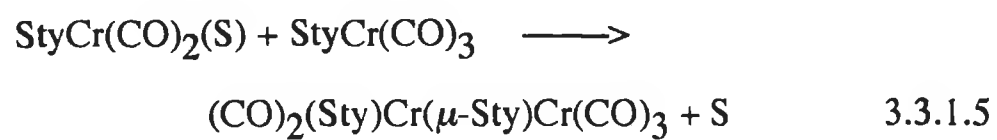
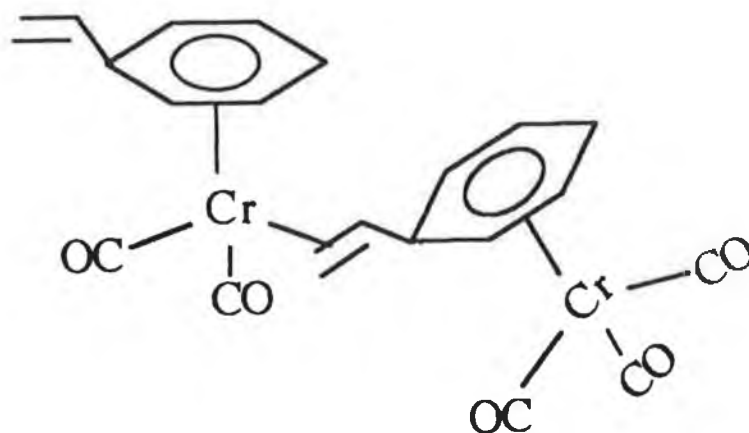


Figure 3.3.1.11: Proposed structure of $(\text{CO})_2(\text{Sty})\text{Cr}(\mu\text{-Sty})\text{Cr(CO)}_3$.



3.3.1.5 Activation parameters for the formation of $\text{Sty}_2\text{Cr}_2(\text{CO})_5$.

The activation parameters for the formation of the dinuclear species were determined from the Arrhenius and Eyring plots (Section 5.2.4.2). The second order rate constant k_3 was used in the calculations ($k_3 = k_{\text{obs}}/[\text{StyCr}(\text{CO})_3]$). The parameters are listed in Table 3.3.1.5 and the data is given in Table 3.3.1.6 with the corresponding plots in Figures 3.3.1.11 and 3.3.1.12.

Table 3.3.1.5: Activation parameters for the formation of the dinuclear species.

$$E_a^\ddagger = 30 \pm 2 \text{ kJmol}^{-1}$$

$$\Delta H^\ddagger = 27 \pm 2 \text{ kJmol}^{-1}$$

$$\Delta S^\ddagger = -11 \pm 25 \text{ Jmol}^{-1}\text{K}^{-1}$$

$$\Delta G^\ddagger = 31 \pm 2 \text{ kJmol}^{-1}$$

The more negative entropy of activation indicates a more associative transition state for the reaction of $\text{StyCr}(\text{CO})_2(\text{S})$ with $\text{StyCr}(\text{CO})_3$, compared to that for the reaction of $\text{StyCr}(\text{CO})_2(\text{S})$ with CO. The activation energy for this reaction is also lower than that for the reaction of

StyCr(CO)₂(S) with CO.

Table 3.3.1.6: Experimental data for the determination of the activation parameters for the formation of the dinuclear species, [StyCr(CO)₃] = 3.52 x 10⁻⁴ M.

Temp (K)	(1/T)E3 (1/K)	kobs (/s)	ln(kobs/[P])	ln((kobs/T)/[P])
283	3.53	5215	16.51	10.87
288	3.47	6225	16.69	11.02
293	3.41	7401	16.86	11.18
298	3.36	8897	17.04	11.35
303	3.30	10333	17.20	11.48
308	3.24	14708	17.55	11.82
313	3.19	17717	17.73	11.99

Arrhenius Plot

Slope = -3600 ± 210

Intercept = 29.1 ± 0.1

Correlation = 0.99

$$E_a^\ddagger = 30 \pm 2 \text{ kJmol}^{-1}$$

Eyring Plot

Slope = -3300 ± 220

Intercept = 22.5 ± 0.1

Correlation = 0.99

$$\Delta H^\ddagger = 27 \pm 2 \text{ kJmol}^{-1}$$

$$\Delta S^\ddagger = -11 \pm 25 \text{ Jmol}^{-1}\text{K}^{-1}$$

Figure 3.3.1.11: Arrhenius plot for the formation of the dinuclear species.

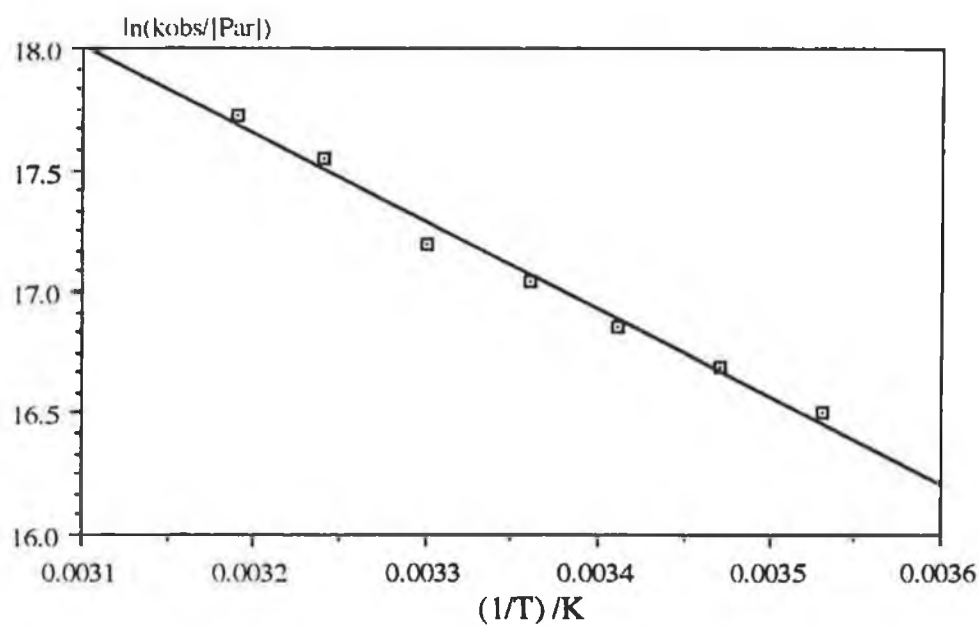
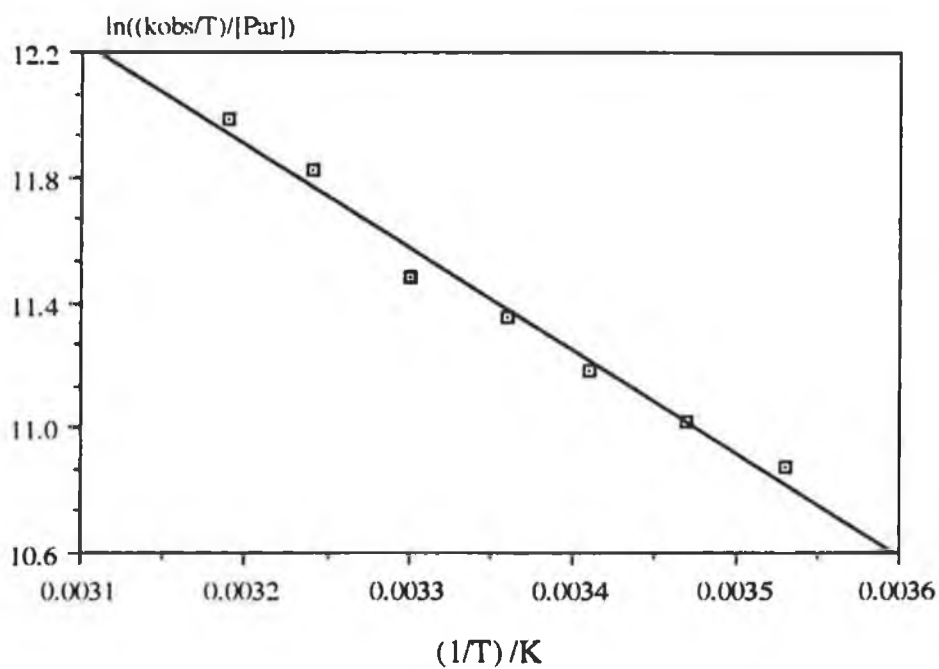


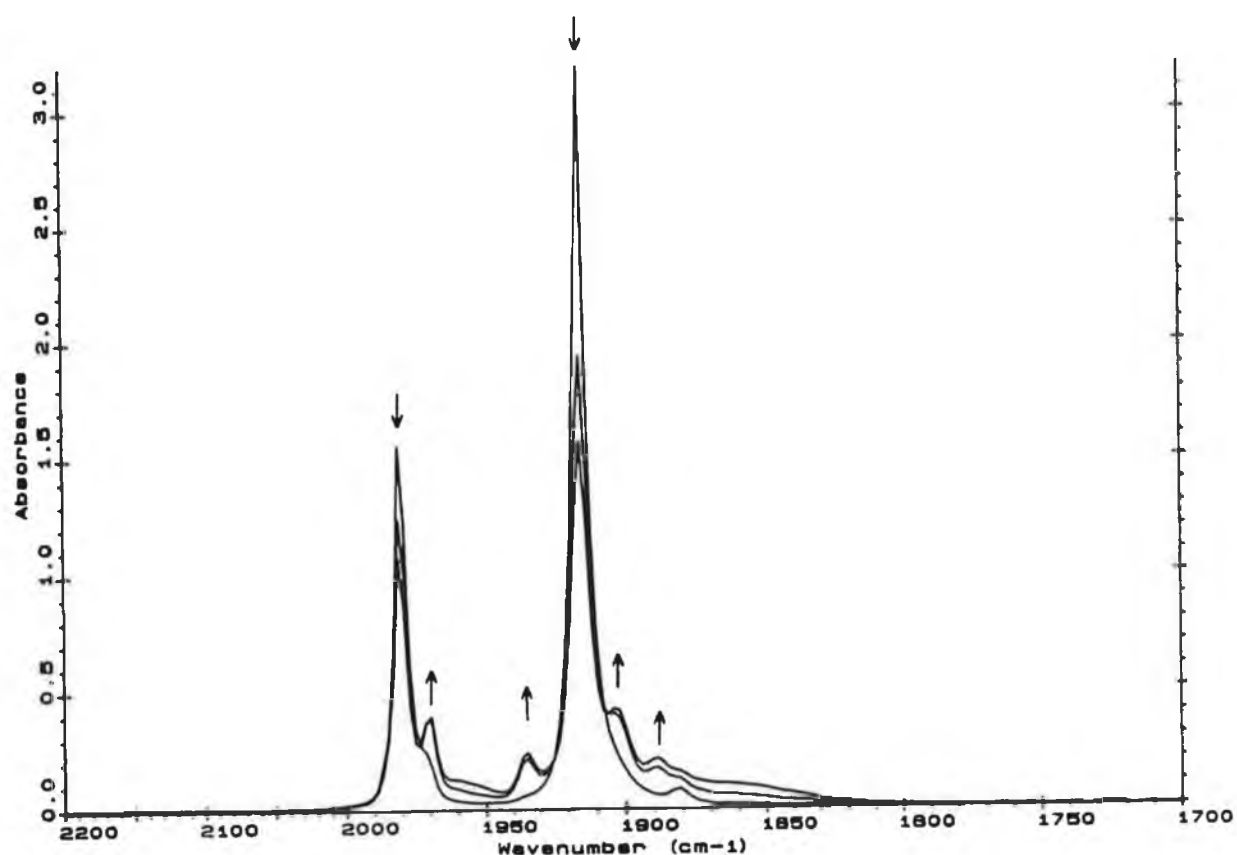
Figure 3.3.1.12: Eyring plot for the formation of the dinuclear species.



3.3.1.6 Infrared Monitored Photolysis of $\text{StyCr}(\text{CO})_3$.

$\text{StyCr}(\text{CO})_3$ was dissolved in cyclohexane and degassed with argon. IR analysis of the sample ($2200 - 1700\text{cm}^{-1}$) revealed two intense $\nu(\text{CO})$ absorptions at 1980 and 1915cm^{-1} . The sample (protected by a Corning filter; $> 80\%$ transmission at $360 < \lambda < 370\text{nm}$) was photolysed at various time intervals (in the solution cell) and the resultant changes in the $\nu(\text{CO})$ stretching region recorded as shown in Figure 3.3.1.13.

Figure 3.3.1.13: Infrared spectral changes observed upon photolysis of $\text{StyCr}(\text{CO})_3$ in cyclohexane (argon atmosphere).



After irradiating the solution for three seconds the intensity of the parent $\nu(\text{CO})$ bands decreased, and four new bands appeared at 1970, 1935, 1903, and 1889cm^{-1} . These became more intense with increased irradiation time, as the intensity of parent $\nu(\text{CO})$ bands were reduced.

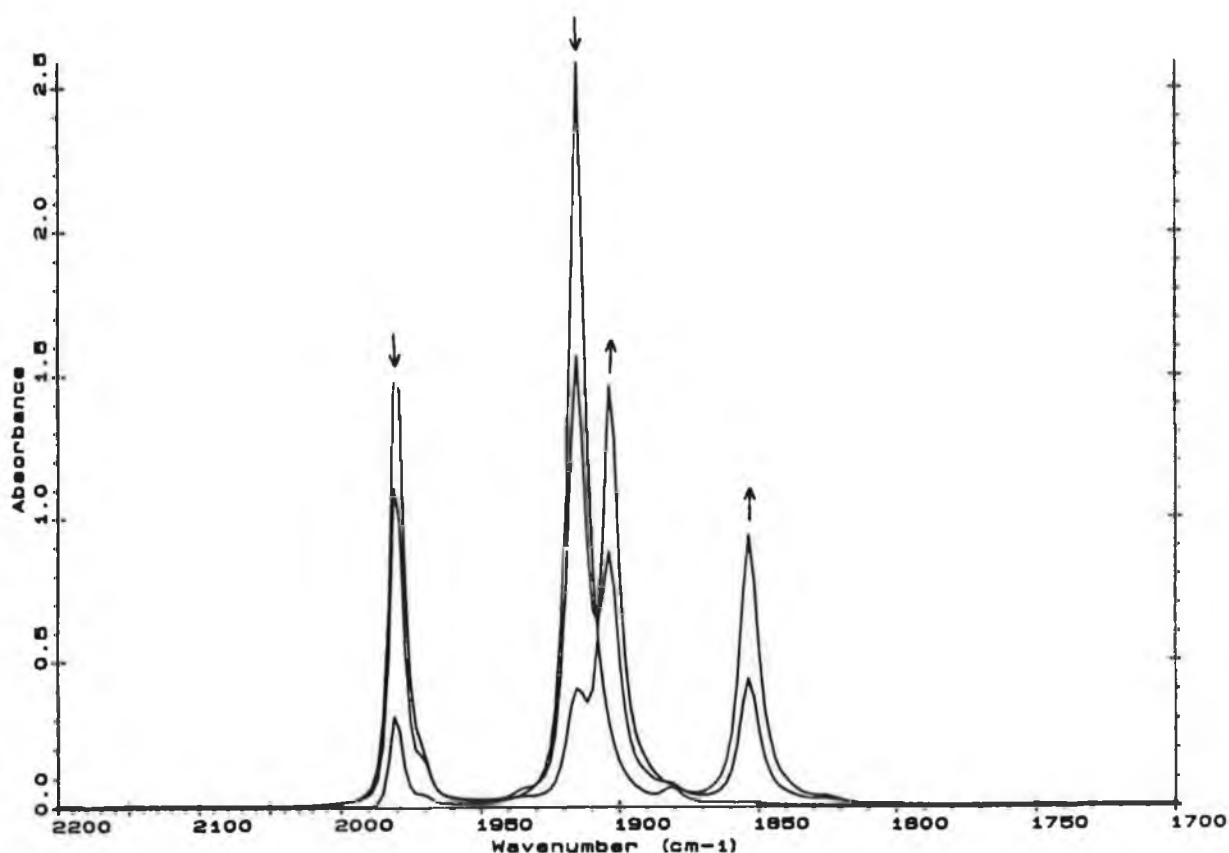
To ensure that we were observing the same process in the solution cell (argon flushed) as in the flash photolysis experiments (freeze-pump-thaw degassed), IR spectral changes for the freeze-pump-thaw degassed samples were recorded, and were found to be in excellent agreement with the former.

On photoejection of a CO molecule, $\text{StyCr}(\text{CO})_2(\text{S})$ reacts with parent to produce the μ -styrene-bridged dinuclear analogue (Section 3.3.1.2). The solution goes from yellow to a cherry colour, with precipitation of solid. The $\nu(\text{CO})$ vibrations at 1970 and 1903cm^{-1} are the tricarbonyl bands, based on their relative intensities, and proximity to the parent vibrations. The dicarbonyl bands are shifted to lower energy, located at 1921 and 1869cm^{-1} respectively. The unstable cherry-coloured dimer was isolated by Nesmeyanov *et al.* [8b], IR (CH_2Cl_2): $\nu(\text{CO})$ 1972, 1921, 1886, and 1869cm^{-1} .

The experiment was repeated in the presence of excess pyridine. The reason for this experiment was to determine the position of the $\nu(\text{CO})$ bands for $\text{StyCr}(\text{CO})_2(\text{pyridine})$, and their use as a model for infrared analysis of $\text{MeCpMn}(\text{CO})_2(\mu\text{-Sty})\text{Cr}(\text{CO})_3$ in the presence of excess pyridine (Section 3.3.3.6). Pyridine is a good base and it may efficiently donate its lone pair

of electrons on the nitrogen atom to the coordinatively unsaturated metal centre. Photolysis of StyCr(CO)_3 with excess pyridine in argon degassed cyclohexane resulted in a decrease in intensity of the parent $\nu(\text{CO})$ bands, in conjunction with the production of two new $\nu(\text{CO})$ bands at 1903 and 1853cm^{-1} . These new bands were shifted to lower energy because of a higher electron density on the metal, and were assigned to $\text{StyCr(CO)}_2(\text{pyridine})$. Figure 3.3.1.14 shows the changing IR spectrum for the reaction. The isobestic point at 1908cm^{-1} is indicative of a clean conversion from the tricarbonyl to the dicarbonyl pyridine complex.

Figure 3.3.1.14: IR spectral changes for the reaction of StyCr(CO)_3 with excess pyridine in argon degassed cyclohexane.



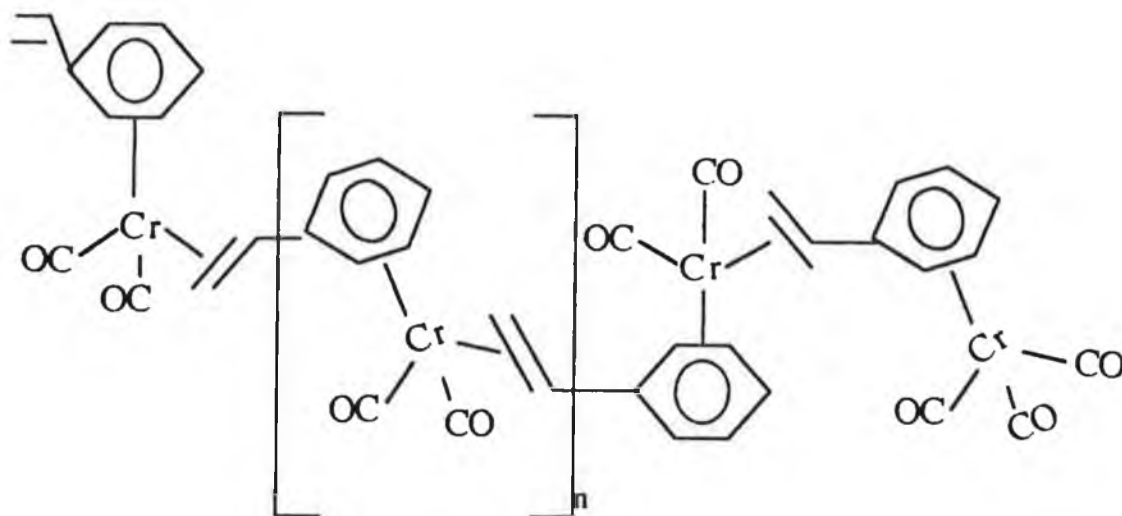
3.3.1.7 Attempted Homopolymerisation of StyCr(CO)_3 by UV/vis Irradiation.

It is well known that StyCr(CO)_3 will not undergo homopolymerisation using free radical initiation [10, 11, 49]. In fact, after heating to 100°C in the presence of AIBN, 70% of the starting material was recovered. In contrast, styrene readily homopolymerises at these conditions [50]. The instability of StyCr(CO)_3 towards acid prevented cationic polymerisation. Anionic homopolymerisation was again essentially ineffective. The $-\text{Cr(CO)}_3$ group sterically hindered the homopolymerisation reactions.

However, StyCr(CO)_3 may be easily copolymerised with various monomers including styrene and methyl acrylate [51]. Copolymerisation with vinylcymantrene [49] requires a 16.5 hour reflux, yielding 45% of copolymer. Interestingly, there was no evidence for steric inhibition in the preparation of this copolymer containing two transition metals.

Laser flash photolysis of StyCr(CO)_3 in cyclohexane (Section 3.3.1), produced the dinuclear $\text{StyCr(CO)}_2(\mu\text{-Sty})\text{Cr(CO)}_3$ complex in an argon environment. This had previously been isolated by photolysis in the non-coordinating solvent petroleum ether [8b]. Because two units may be linked in this way, the possibility of linking more units together, to form a homopolymer chain with chromium atoms along the backbone as shown in Figure 3.3.1.14 was investigated.

Figure 3.3.1.14:



The photolysis of StyCr(CO)_3 was carried out in tetrahydrofuran (THF) at -5°C for 24 hours under a constant stream of argon (Chapter 5). The reaction was monitored by infrared spectroscopy, the original yellow solution possessing strong $\nu(\text{CO})$ vibrations at 1967 and 1893cm^{-1} . This was converted to $\text{StyCr(CO)}_2(\text{THF})$ upon irradiation, $\nu(\text{CO})$ 1937 (strong) and 1894cm^{-1} (weak).

The solvent was removed, and it was hoped that the vinyl group of one unit would displace the weakly coordinated THF molecule from another centre, the end result being a chain with StyCr(CO)_2 as the repeat unit.

Infrared analysis of the yellow-green product in pentane showed $\nu(\text{CO})$

vibrations (cm^{-1}) at 2070 (v. weak), 2010 (v. weak), 1987 (v. strong), 1982 (sh.), 1955 (med.), 1940 (med.), 1911 (strong), and 1740 (broad, weak). StyCr(CO)₃ in pentane has $\nu(\text{CO})$ vibrations at 1982 and 1918cm^{-1} . TLC analysis of the residue revealed three products. Chromatography using ether/pet. ether as the eluent resulted in recovery of approximately 15% of the starting material, as identified by infrared spectroscopy.

Precipitation of the yellow-green product in pet. ether (40-60) at -80°C from chloroform did not yield any polymeric species.

From the infrared evidence produced in pentane, it is possible that some chain-like species formed. Problems associated with the system are the ease at which the parent is regenerated, and also the sensitivity of the products to air and temperature. Ideally, a non-coordinating solvent should be used but unfortunately, only two units combine in this situation and precipitate from solution.

Electronically, the feasibility of such a polymer chain is made even more difficult by the effective 'electron drain' which may occur. The $-\text{Cr}(\text{CO})_3$ moiety is electron withdrawing, and pulls electron density from the aromatic ring. This in turn tries to compensate by exerting an electron withdrawing effect on the vinylic group. This, now having reduced electron density, will not be able to coordinate as strongly to the incoming, coordinatively unsaturated StyCr(CO)₂ unit. The $-\text{Cr}(\text{CO})_2$ moiety also requires electron density. The end result would be a chain of considerable electron deficiency.

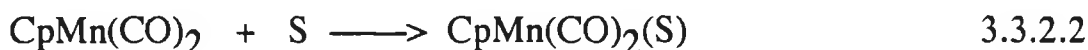
3.3.1.8 Summary.

Laser flash photolysis of StyCr(CO)_3 in cyclohexane under CO proceeds in a similar manner to that observed for the unsubstituted arene analogue [13]. The solvated dicarbonyl is produced, the lifetime of which depends on the concentration of CO present. In argon atmospheres, the dicarbonyl reacts with parent to produce a long-lived chromium dinuclear complex, linked by a μ -styrene bridge. Infrared analysis exhibited the production of four new stretches in the $\nu(\text{CO})$ region.

Attempted homopolymerisation of StyCr(CO)_3 using UV irradiation to produce a polymer with a chromium atom along the backbone was unsuccessful. This was possibly due to electronic difficulties incurred, and also the thermal and oxidative instability of the proposed product.

3.3.2 Laser Flash Photolysis of $\text{CpMn(CO)}_2(\eta^2\text{-C}_8\text{H}_{14})$ in Cyclohexane Solution.

The fast reaction solution photochemistry of CpMn(CO)_3 , and its (MeCp) analogue has been investigated [30, 36, 42]. The primary photoprocess in both systems involves photoejection of a CO molecule to produce the dicarbonyl fragment (Reaction 3.3.2.1), which rapidly coordinates the solvent (Reaction 3.3.2.2)



In the presence of a coordinating ligand, L, the solvent is displaced to produce the ligated adduct, as shown in Reaction 3.3.2.3.



where $\text{Cp} = (\eta^5\text{-C}_5\text{H}_5)$ or $(\eta^5\text{-C}_6\text{H}_7)$; $\text{S} = \text{Cyclohexane, Toluene,}$
or $n\text{-Heptane}$; $\text{L} = \text{CO, PPh}_3, \text{N}_2, \text{P(OMe)}_3, \text{or CpMn(CO)}_3$.

Under an argon atmosphere it was shown that the solvated intermediate interacted with parent, to produce the dinuclear complex $\text{Cp}_2\text{Mn}_2(\text{CO})_5$. The formation of this species was suppressed under CO, where the solvated

intermediate reacted with the CO to regenerate CpMn(CO)_3 .

The solvated intermediate was also shown to interact with various other ligands including P(OMe)_3 , N_2 or PPh_3 .

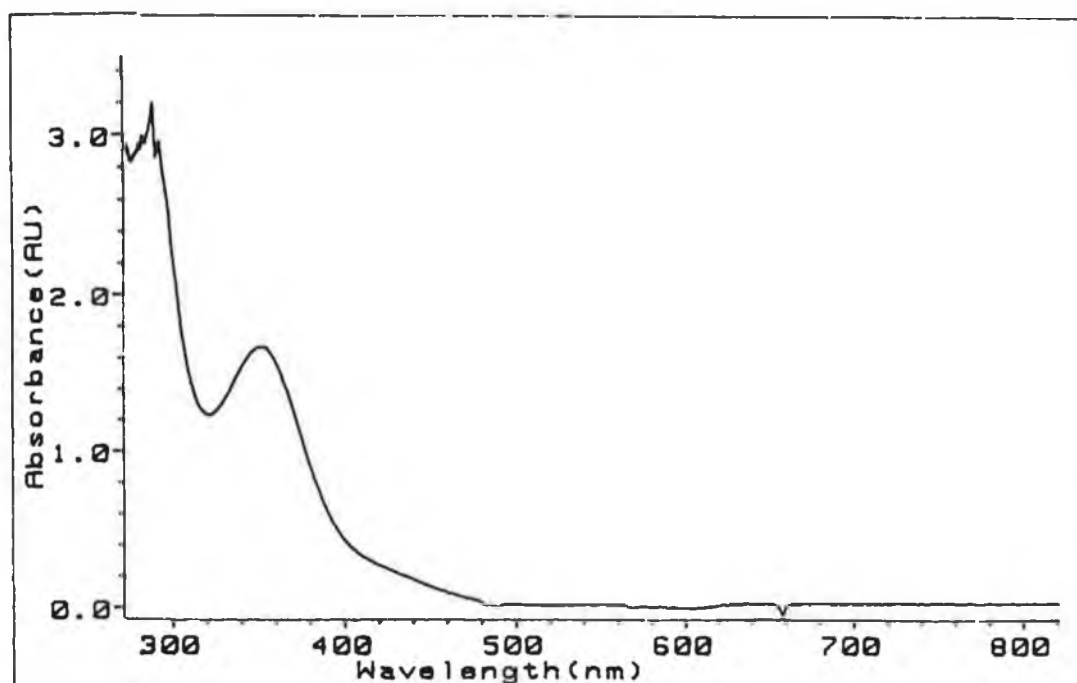
The high quantum yield for CO photodissociation in these complexes enables the efficient preparation of substituted analogues. We have prepared some manganese- π -olefin complexes *via* irradiation of the parent CpMn(CO)_3 in THF, forming the unstable $\text{CpMn(CO)}_2(\text{THF})$ intermediate, which, in the presence of an olefin-containing species (*cis*-cyclooctene or StyCr(CO)_3) forms the more stable $\text{CpMn(CO)}_2(\text{olefin})$ adduct.

Laser flash photolysis experiments on the manganese- π -olefin complex $\text{CpMn(CO)}_2(\eta^2\text{-C}_8\text{H}_{14})$ were carried out in room temperature solution at 355nm excitation. This complex was also used as a model for elucidation of the photochemistry of the manganese-chromium complex studied (Section 3.3.3). On flash photolysis of $\text{CpMn(CO)}_2(\eta^2\text{-C}_8\text{H}_{14})$ the two most likely reactions which may occur involve either the photoejection of a CO molecule, to produce the monocarbonyl solvated $\text{CpMn(CO)}(\eta^2\text{-C}_8\text{H}_{14})(\text{S})$ species, or the η^2 -coordinated *cis*-cyclooctene ligand may be labilised to produce the dicarbonyl solvated $\text{CpMn(CO)}_2(\text{S})$ adduct.

3.3.2.1 Electronic Excitation Spectrum of $\text{CpMn(CO)}_2(\eta^2\text{-C}_8\text{H}_{14})$.

The UV/vis spectrum of $\text{CpMn(CO)}_2(\eta^2\text{-C}_8\text{H}_{14})$ is shown in Figure 3.3.2.1. The lowest energy absorption band at 350nm was assigned to a combination of MLCT and LF electronic transitions. This is red-shifted approximately 20nm in comparison to the tricarbonyl analogue, whose lowest energy absorption was attributed to MLCT [40]. The extinction coefficient of $\text{CpMn(CO)}_2(\eta^2\text{-C}_8\text{H}_{14})$ in cyclohexane was calculated to be $1232 \text{ dm}^3 \text{ mol}^{-1} \text{ cm}^{-1}$ at 354nm.

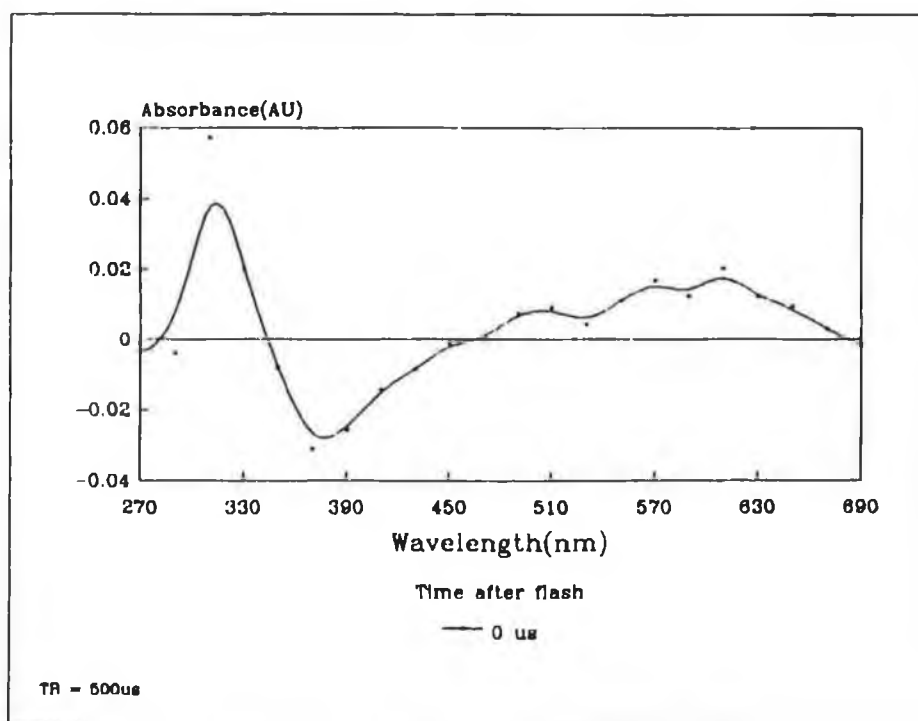
Figure 3.3.2.1: UV/vis spectrum of $\text{CpMn(CO)}_2(\eta^2\text{-C}_8\text{H}_{14})$ in cyclohexane.



3.3.2.2 Primary Photoproduct.

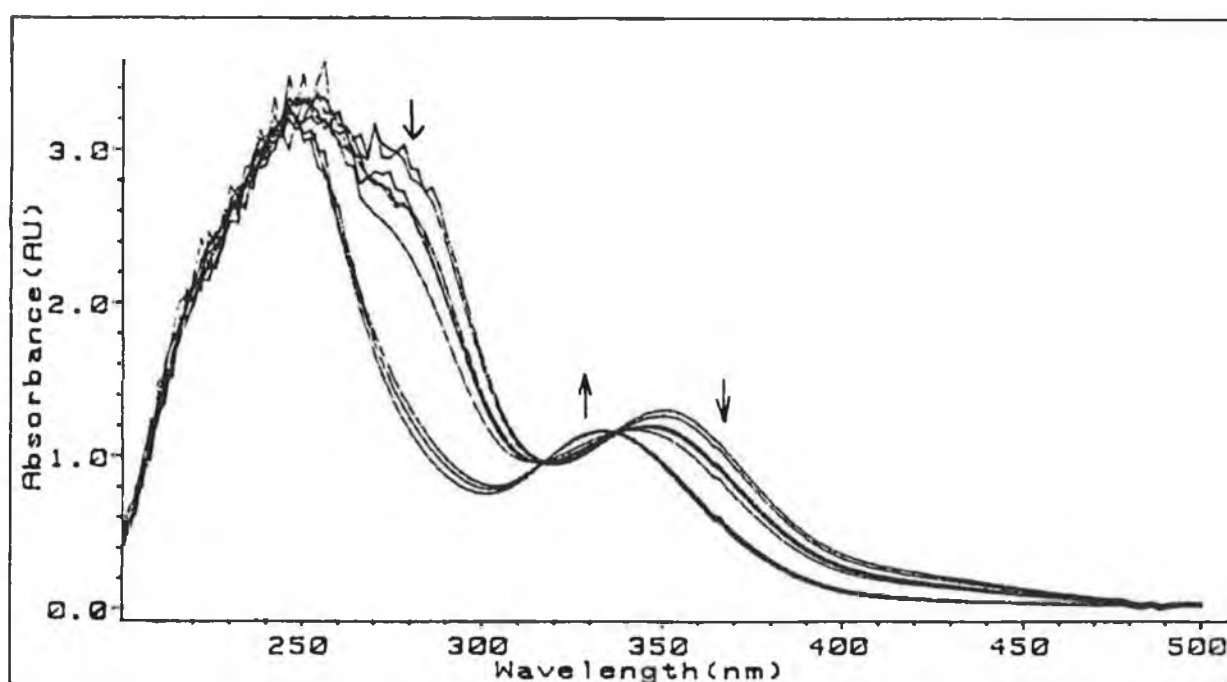
Figure 3.3.2.2 shows the UV/vis transient absorption spectrum recorded $0\mu\text{s}$ after the laser flash. The notable features are the absorption at 310nm , corresponding to the 'window' of low absorptivity in the parent complex (Figure 3.3.2.1), and the broad featureless absorption in the visible region with maximum centred at 580nm . This species is formed within the duration of the flash. On comparison with previous work in cyclohexane [30, 42] this spectrum recorded $0\mu\text{s}$ after the flash has been assigned $\text{CpMn(CO)}_2(\text{S})$ where S = cyclohexane. The rate of decay of this complex was then investigated.

Figure 3.3.2.2: Transient UV/vis absorption difference spectrum observed on flash photolysis of $\text{CpMn(CO)}_2(\eta^2\text{-C}_8\text{H}_{14})$ in cyclohexane under argon.



Changes observed in the UV/vis spectrum of the complex (Figure 3.3.2.3) under both CO and argon atmospheres have shown that the photoreaction in solution is not fully reversible. The lowest energy band at 350nm decreased in intensity, as did the shoulder centred at 270nm. Formation of a new band at 330nm suggested the formation of CpMn(CO)_3 [30, 42].

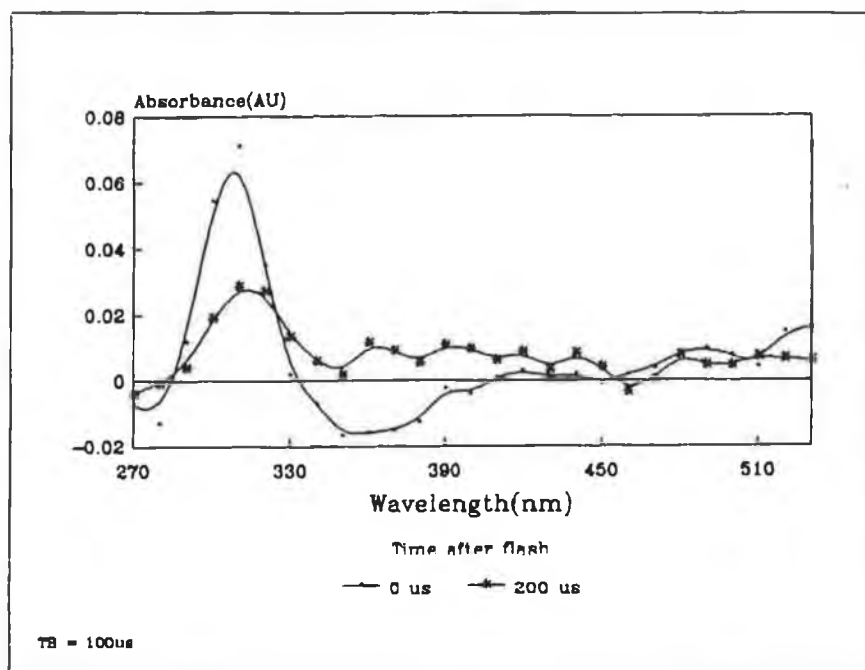
Figure 3.3.2.3: Changes observed in the UV/vis spectrum for $\text{CpMn(CO)}_2(\eta^2\text{-C}_8\text{H}_{14})$ in cyclohexane (1 atm. CO) during a flash photolysis experiment.



The dependence of the lifetime of the solvated dicarbonyl $\text{CpMn(CO)}_2(\eta^2\text{-C}_8\text{H}_{14})$ on CO was investigated. If *cis*-cyclooctene was being ejected in the flash, under CO there would be competition between it and the photoejected

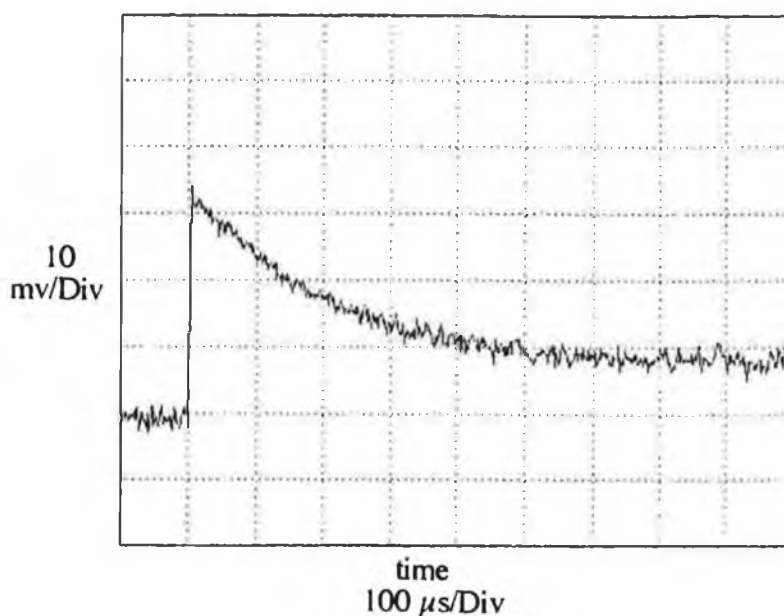
ligand for attachment to the metal carbonyl photofragment. However, the concentration of CO is much greater than that of free *cis*-cyclooctene so pseudo first order conditions may be assumed. The transient UV/vis difference spectrum under CO, recorded at various time intervals after the flash is shown in Figure 3.3.2.4. That at 0 μ s after the flash corresponds to $\text{CpMn(CO)}_2(\text{S})$, while that at 200 μ s with maximum at $\sim 320\text{nm}$ shows the grow-in of CpMn(CO)_3 .

Figure 3.3.2.4: Transient UV/vis difference spectrum for $\text{CpMn(CO)}_2(\eta^2\text{-C}_8\text{H}_{14})$ under 1 atm. CO in cyclohexane.



Flash photolysis of $\text{CpMn(CO)}_2(\eta^2\text{-C}_8\text{H}_{14})$ in cyclohexane (S) under various concentrations of CO produced $\text{CpMn(CO)}_2(\text{S})$, the lifetime of which depended linearly on $[\text{CO}]$. The higher the concentration of CO the shorter the lifetime. Figure 3.3.2.5 shows a typical transient obtained for the decay of the solvated dicarbonyl $\text{CpMn(CO)}_2(\text{S})$ under CO, monitored at 310nm.

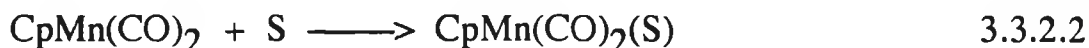
Figure 3.3.2.5: A typical transient showing the decay of $\text{CpMn(CO)}_2(\text{S})$ under CO, at a monitoring wavelength of 310nm.



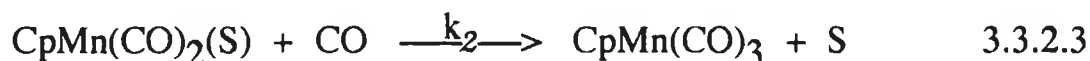
Thus, the primary photoprocess is the displacement of the η^2 -coordinated ligand according to Reaction 3.3.2.1.



In cyclohexane the very reactive metal carbonyl photofragment weakly coordinates to the solvent as in Reaction 3.3.2.2.



Similar reactions in alkane [30, 42] and aromatic solvents [36] have been documented for various manganese carbonyl compounds. In the presence of a more strongly coordinating ligand such as CO, the solvent is displaced to form the tricarbonyl adduct (Reaction 3.3.2.3).

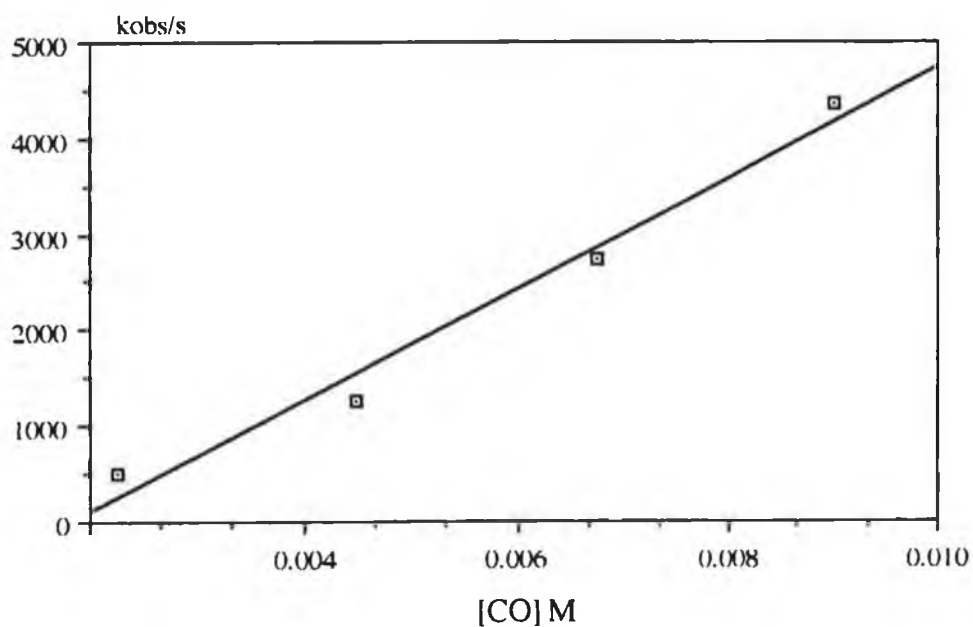


The second order rate constant k_2 for the reaction of $\text{CpMn(CO)}_2(\text{S})$ with CO was calculated to be $5.8 \times 10^5 \text{ dm}^3\text{mol}^{-1}\text{s}^{-1}$ at 298K. This is similar to the value obtained by Creaven *et al.* ($3.4 \times 10^5 \text{ dm}^3\text{mol}^{-1}\text{s}^{-1}$), at an uncorrected CO concentration [30]. The process is irreversible under CO, and CpMn(CO)_3 is formed, confirmed by UV/vis (Figure 3.3.2.3) ($\lambda_{\text{max}} = 330\text{nm}$). The data for the determination of the effect of CO on the lifetime of the solvated intermediate is tabulated in Table 3.3.2.1. The plot of observed rate constants (k_{obs}) versus CO concentration is shown in Figure 3.3.2.6.

Table 3.3.2.1: Data for the determination of the effect of [CO] on the lifetime of the primary photoproduct, $[\text{CpMn}(\text{CO})_2(\eta^2\text{-C}_8\text{H}_{14})] = 8.41 \times 10^{-4} \text{ M}$.

CO (E3) [M]	kobs/s
2.25	494
4.50	1255
6.75	2739
9.00	4354

Figure 3.3.2.6: Plot of kobs (s^{-1}) versus [CO] for $\text{CpMn}(\text{CO})_2(\text{S})$ with CO in cyclohexane at 298K.



$$\text{Slope} = 5.8 (\pm 0.6) \times 10^5 \text{ dm}^3 \text{ mol}^{-1} \text{ s}^{-1}$$

$$\text{Intercept} = -1000 \pm 320 \text{ s}^{-1}$$

$$\text{Correlation} = 0.99$$

3.3.2.3 Activation Parameters for the reaction of $\text{CpMn(CO)}_2(\text{S})$ with CO.

The activation parameters for the reaction of $\text{CpMn(CO)}_2(\text{S})$ with CO were calculated using the second order rate constant, and the values are tabulated in Table 3.3.2.2. The experimental data is shown in Table 3.3.2.3 with Arrhenius and Eyring plots in Figures 3.3.2.7 and 3.3.2.8 respectively.

The activation energy for the reaction is 47 kJmol^{-1} , which is higher than expected for the interaction of a highly reactive metal photofragment with a ligand [43]. The activation entropy of $14 \text{ Jmol}^{-1}\text{K}^{-1}$ indicated a possible dissociative mechanism for the transition state. This is supported by the proposed dissociation of S, to produce a 16 electron intermediate, followed by ligand replacement [30, 43].

Table 3.3.2.2: Activation parameters for the reaction of $\text{CpMn(CO)}_2(\text{S})$ with CO.

$$E_a^\ddagger = 47 \pm 2 \text{ kJmol}^{-1}$$

$$\Delta H^\ddagger = 45 \pm 2 \text{ kJmol}^{-1}$$

$$\Delta S^\ddagger = 14 \pm 25 \text{ Jmol}^{-1}\text{K}^{-1}$$

$$\Delta G^\ddagger = 41 \pm 2 \text{ kJmol}^{-1}$$

Table 3.3.2.3: Experimental data for the determination of the activation parameters for the reaction of $\text{CpMn(CO)}_2(\text{S})$ with CO.

Temp (K)	(1/T)E3 (1/K)	kobs (/s)	ln(kobs/[CO])	ln((kobs/T)/[CO])
284	3.52	1661	12.12	6.47
288	3.47	2148	12.38	6.72
293	3.41	2983	12.71	7.03
298	3.36	4546	13.13	7.43
303	3.30	6208	13.44	7.73
308	3.24	8086	13.71	7.98
313	3.19	10157	13.94	8.19

Arrhenius Plot

Slope = -5700 ± 210

Intercept = 32.1 ± 0.1

Correlation = 0.99

$$E_a^\ddagger = 47 \pm 2 \text{ kJmol}^{-1}$$

Eyring Plot

Slope = -5400 ± 210

Intercept = 25.4 ± 0.1

Correlation = 0.99

$$\Delta H^\ddagger = 45 \pm 2 \text{ kJmol}^{-1}$$

$$\Delta S^\ddagger = 14 \pm 25 \text{ Jmol}^{-1}\text{K}^{-1}$$

Figure 3.3.2.7: Arrhenius plot for the reaction of $\text{CpMn(CO)}_2(\text{S})$ with CO.

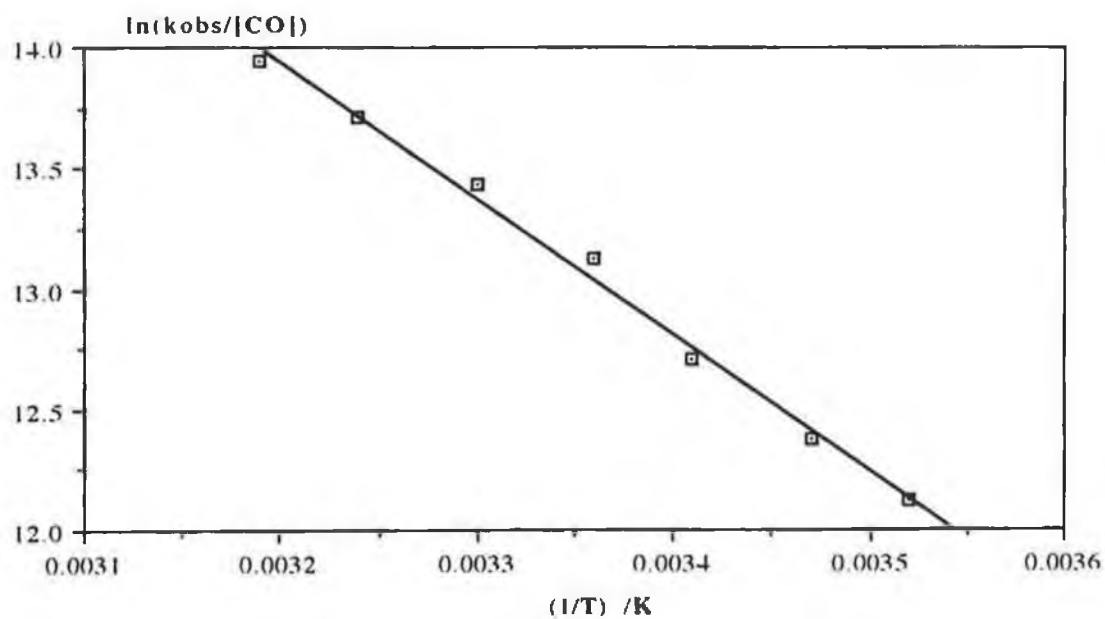
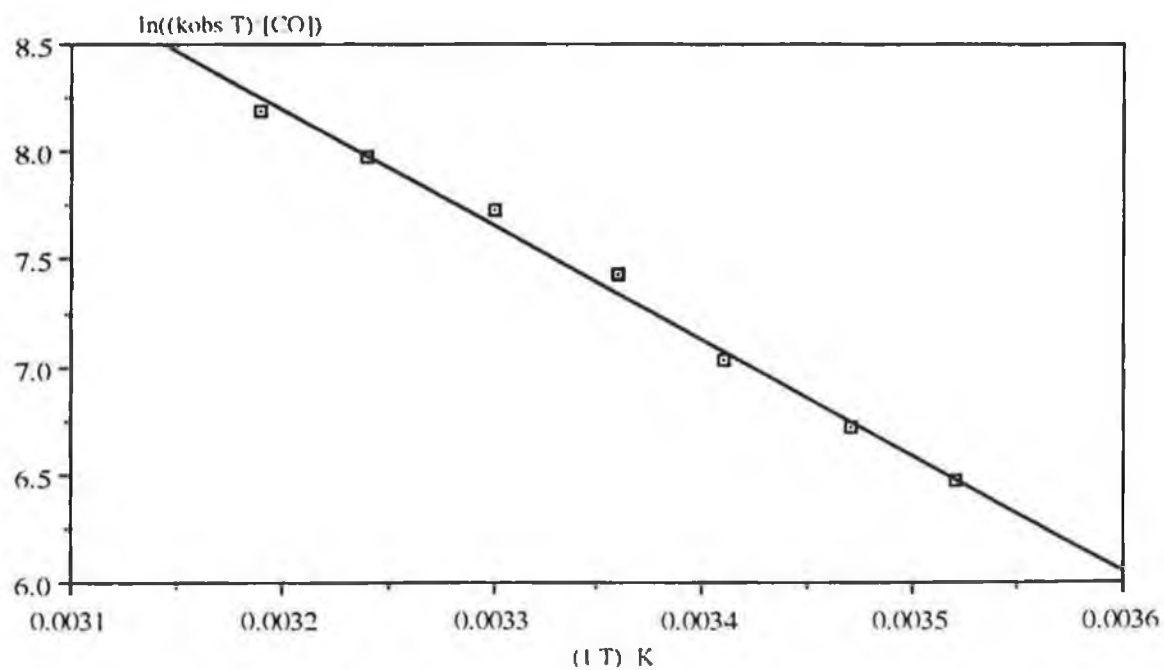


Figure 3.3.2.8: Eyring Plot for the reaction of $\text{CpMn(CO)}_2(\text{S})$ with CO.



3.3.2.4 Formation of $(\text{CO})_2\text{CpMn}(\mu\text{-CO})\text{MnCp}(\text{CO})(\eta^2\text{-C}_8\text{H}_{14})$.

Under an argon atmosphere, the solvated intermediate $\text{CpMn}(\text{CO})_2(\text{S})$ interacts with unphotolysed parent in solution, to form $\text{Cp}_2\text{Mn}_2(\text{CO})_4(\eta^2\text{-C}_8\text{H}_{14})$. For this system, the increase in observed rate constants with increasing parent concentration supports the formation of such species. Identification of the exact nature of this second transient species is difficult because of its very short lifetime. The photoproduct possibly contains a bridging carbonyl between the two metal centres, to form the complex $(\text{CO})_2\text{CpMn}(\mu\text{-CO})\text{MnCp}(\text{CO})(\eta^2\text{-C}_8\text{H}_{14})$ as shown in Reaction 3.3.2.4. Similar dinuclear complexes containing bridging carbonyl ligands have been reported [30, 42]. Figure 3.3.2.9 is the transient UV/vis difference spectrum recorded at $4400\mu\text{s}$ with maxima at 330 and 520nm. The transient UV/vis difference spectra for $\text{MeCp}_2\text{Mn}_2(\text{CO})_4(\mu\text{-CO})$ and its non-methylated derivative exhibited maxima at 360 and 530nm [41, 43]. The shift in band positions supports the formation of a different dinuclear species. This is true because the parent complex is different in this case.

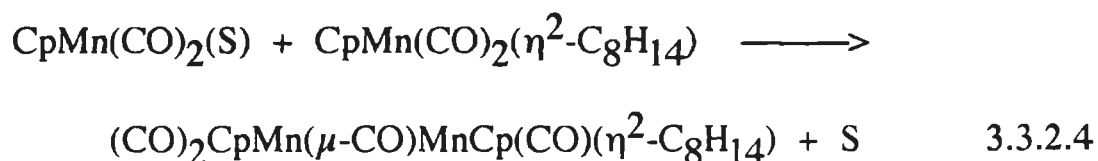
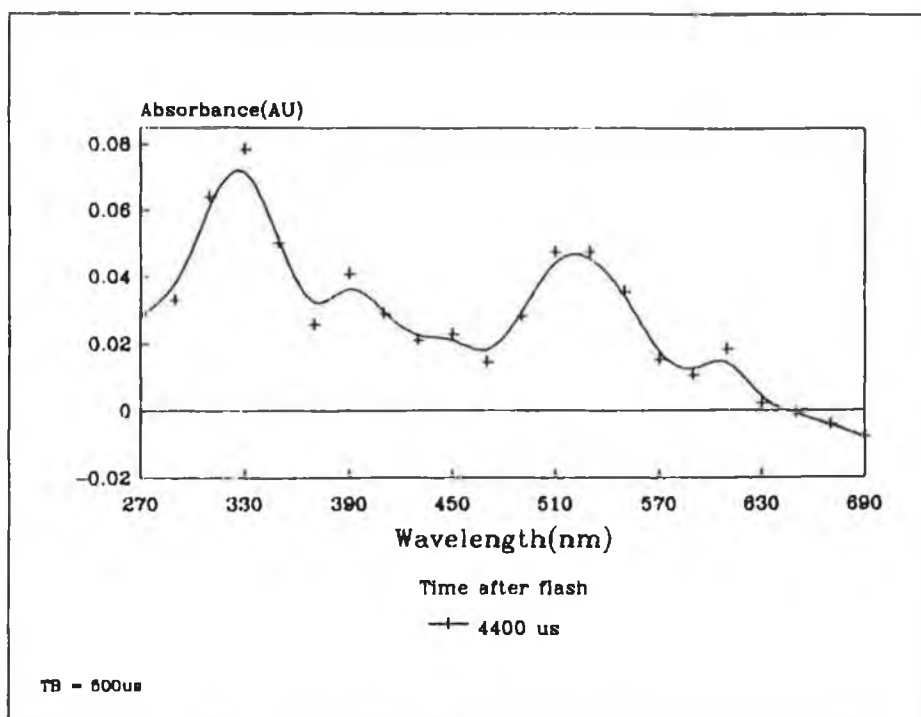


Figure 3.3.2.9: Transient UV/vis difference spectrum of $(\text{CO})_2\text{CpMn}(\mu\text{-CO})\text{MnCp}(\text{CO})(\eta^2\text{-C}_8\text{H}_{14})$ in cyclohexane 4400 μs after the flash.



The transient in Figure 3.3.2.10 shows the grow-in of the dinuclear species. The observed rate constants and $\text{CpMn}(\text{CO})_2(\eta^2\text{-C}_8\text{H}_{14})$ concentrations are tabulated in Table 3.3.2.4 with the corresponding plot in Figure 3.3.2.11. The second order rate constant for the formation of the dinuclear species is $2.7 \times 10^5 \text{ dm}^3\text{mol}^{-1}\text{s}^{-1}$ at 298K. This is an order of magnitude slower than that for the bridging carbonyl analogues, and possibly reflects a stronger interaction between the coordinatively unsaturated photofragment and the solvent.

Figure 3.3.2.10: Grow-in of the dinuclear $(\text{CO})_2\text{CpMn}(\mu\text{-CO})\text{MnCp}(\text{CO})(\eta^2\text{-C}_8\text{H}_{14})$ species from the reaction of $\text{CpMn}(\text{CO})_2(\text{S})$ with $\text{CpMn}(\text{CO})_2(\eta^2\text{-C}_8\text{H}_{14})$ at 360nm.

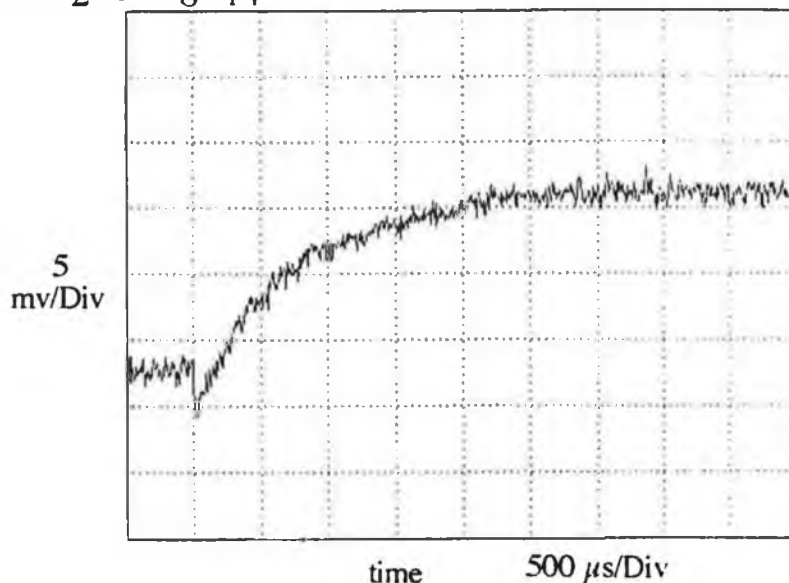


Table 3.3.2.4: Data for the determination of the second order rate constant for the formation of the dinuclear species at 298K.

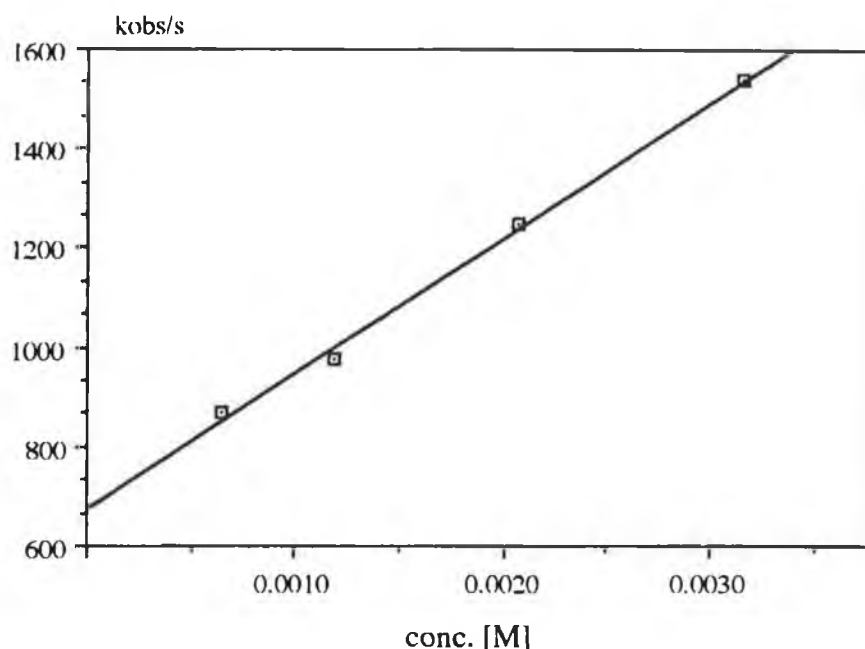
conc. (E3) [M]	kobs/s
0.64	867
1.19	979
2.07	1252
3.15	1539

$$\text{Slope} = 2.7 (\pm 0.3) \times 10^5 \text{ dm}^3\text{mol}^{-1}\text{s}^{-1}$$

$$\text{Intercept} = 680 (\pm 30) \text{ s}^{-1}$$

$$\text{Correlation} = 0.99$$

Figure 3.3.2.11: Plot showing change in k_{obs} with various $\text{CpMn(CO)}_2(\eta^2\text{-C}_8\text{H}_{14})$ concentrations.



Transient signals corresponding to the decay of the dinuclear complex were observed on a long timebase, and the effect of CO concentration on this decay was investigated. As CO concentration increased, the lifetime of the dinuclear species was reduced, providing possible evidence for the formation of CpMn(CO)_3 and parent (Reaction 3.3.2.5). The data and corresponding plot are shown in Table 3.3.2.5 and Figure 3.3.2.12. The rather short lifetime of the dinuclear intermediate ($\sim 10\text{ms}$) compared to $\sim 50\text{ms}$ for the CO bridged dinuclear complex again supports the formation of an unstable intermediate. The second order rate constant for the reaction of the dinuclear intermediate with CO was calculated to be $1.7 \times 10^4 \text{ dm}^3 \text{ mol}^{-1} \text{ s}^{-1}$ at 298K, almost three times faster than that for the reaction of CO with $(\text{MeCp})_2\text{Mn}_2(\text{CO})_5$ [42].

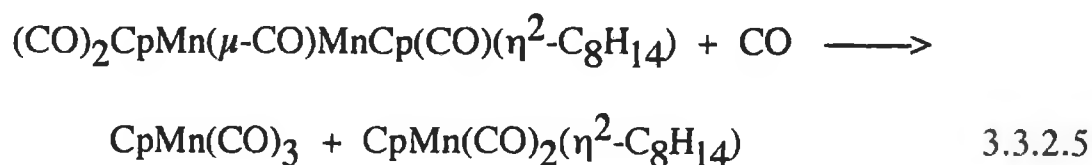


Table 3.3.2.5: Data for the determination of the effect of CO concentration on the lifetime of the dinuclear species.

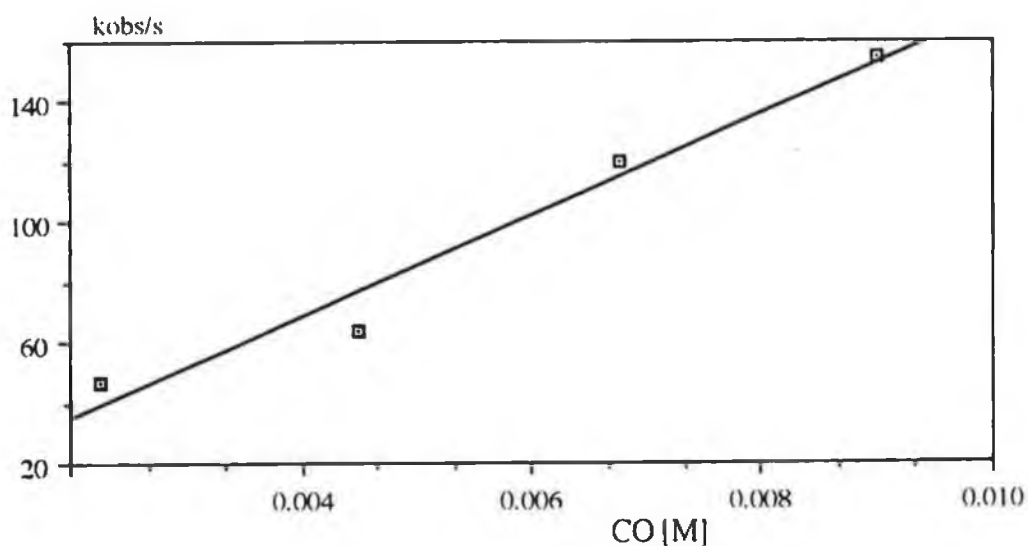
conc. (E3) [M]	kobs/s
2.25	47.1
4.50	64.1
6.75	120.3
9.00	154.4

$$\text{Slope} = 1.7 (\pm 0.2) \times 10^4 \text{ dm}^3 \text{ mol}^{-1} \text{ s}^{-1}$$

$$\text{Intercept} = 1.9 (\pm 11) \text{ s}^{-1}$$

$$\text{Correlation} = 0.98$$

Figure 3.3.2.12: Plot showing the effect of CO concentration on the decay of the dinuclear species.



3.3.2.5 Activation Parameters for the formation of $(\text{CO})_2\text{CpMn}(\mu\text{-CO})\text{MnCp}(\text{CO})(\eta^2\text{-C}_8\text{H}_{14})$.

Activation parameters for the reaction of $\text{CpMn}(\text{CO})_2(\text{S})$ with $\text{CpMn}(\text{CO})_2(\eta^2\text{-C}_8\text{H}_{14})$ were determined. The activation parameters are shown in Table 3.3.2.6. The experimental data is shown in Table 3.3.2.7 with Arrhenius and Eyring plots in Figures 3.3.2.13 and 3.3.2.14.

The activation energy for the reaction is 46 kJmol^{-1} . The activation entropy of $19 \text{ Jmol}^{-1}\text{K}^{-1}$ indicates a dissociative transition state. This supports the idea of steric difficulties encountered on interaction of the two bulky groups.

Table 3.3.2.6: Activation parameters for the formation of the dinuclear species.

$$E_a^\ddagger = 46 \pm 2 \text{ kJmol}^{-1}$$

$$\Delta H^\ddagger = 43 \pm 2 \text{ kJmol}^{-1}$$

$$\Delta S^\ddagger = 19 \pm 25 \text{ Jmol}^{-1}\text{K}^{-1}$$

$$\Delta G^\ddagger = 38 \pm 2 \text{ kJmol}^{-1}$$

Table 3.3.2.7: Data for the determination of the activation parameters for the formation of the dinuclear species.

Temp (K)	(1/T)E3 (1/K)	kobs (/s)	ln(kobs/[P])	ln((kobs/T)/[P])
283	3.53	674	13.34	7.69
288	3.47	851	13.57	7.91
293	3.41	1170	13.89	8.21
298	3.36	1673	14.25	8.55
303	3.30	2422	14.62	8.90
308	3.24	3169	14.89	9.16
313	3.19	4122	15.15	9.40

Arrhenius Plot

Slope = -5500 ± 175

Intercept = 32.8 ± 0.1

Correlation = 0.99

$$E_a^\ddagger = 46 \pm 2 \text{ kJmol}^{-1}$$

Eyring Plot

Slope = -5200 ± 160

Intercept = 26.1 ± 0.1

Correlation = 0.99

$$\Delta H^\ddagger = 43 \pm 2 \text{ kJmol}^{-1}$$

$$\Delta S^\ddagger = 19 \pm 25 \text{ Jmol}^{-1}\text{K}^{-1}$$

Figure 3.3.2.13: Arrhenius plot for the formation of the dinuclear species.

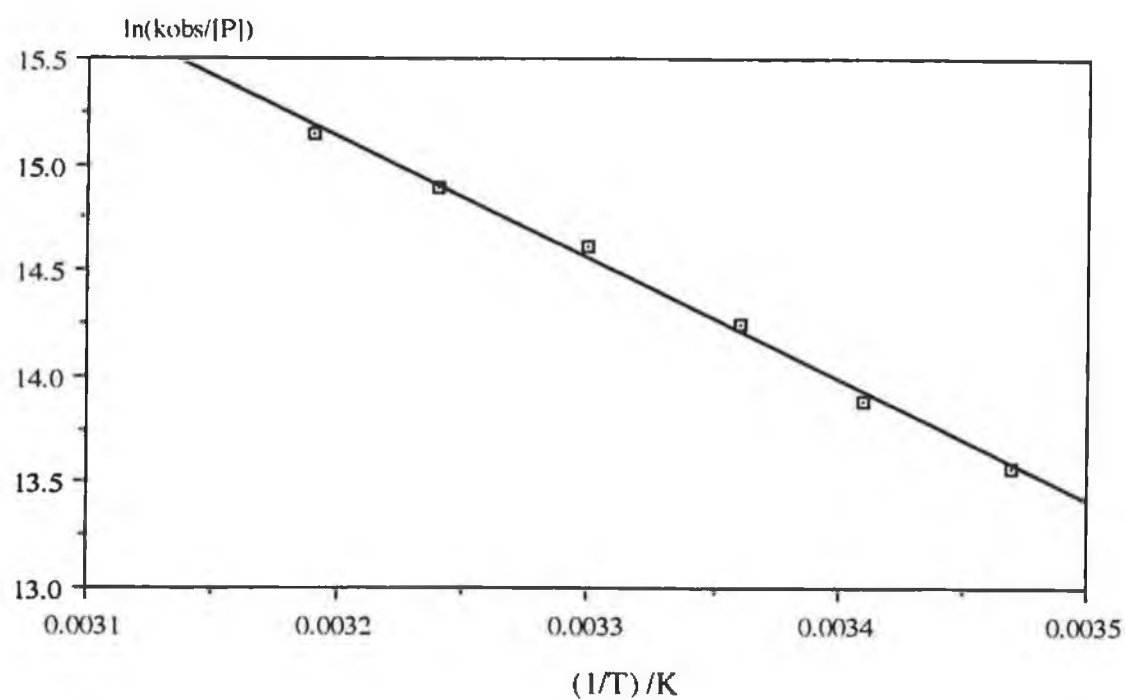
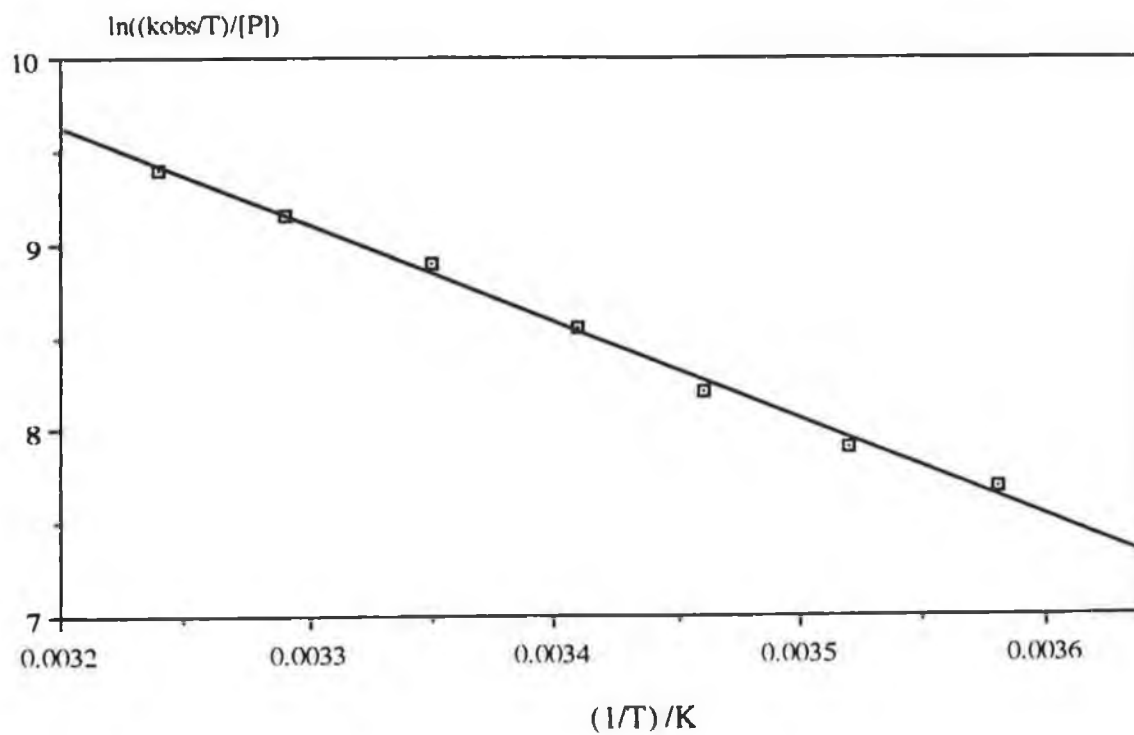


Figure 3.3.2.14: Eyring plot for the formation of the dinuclear species.

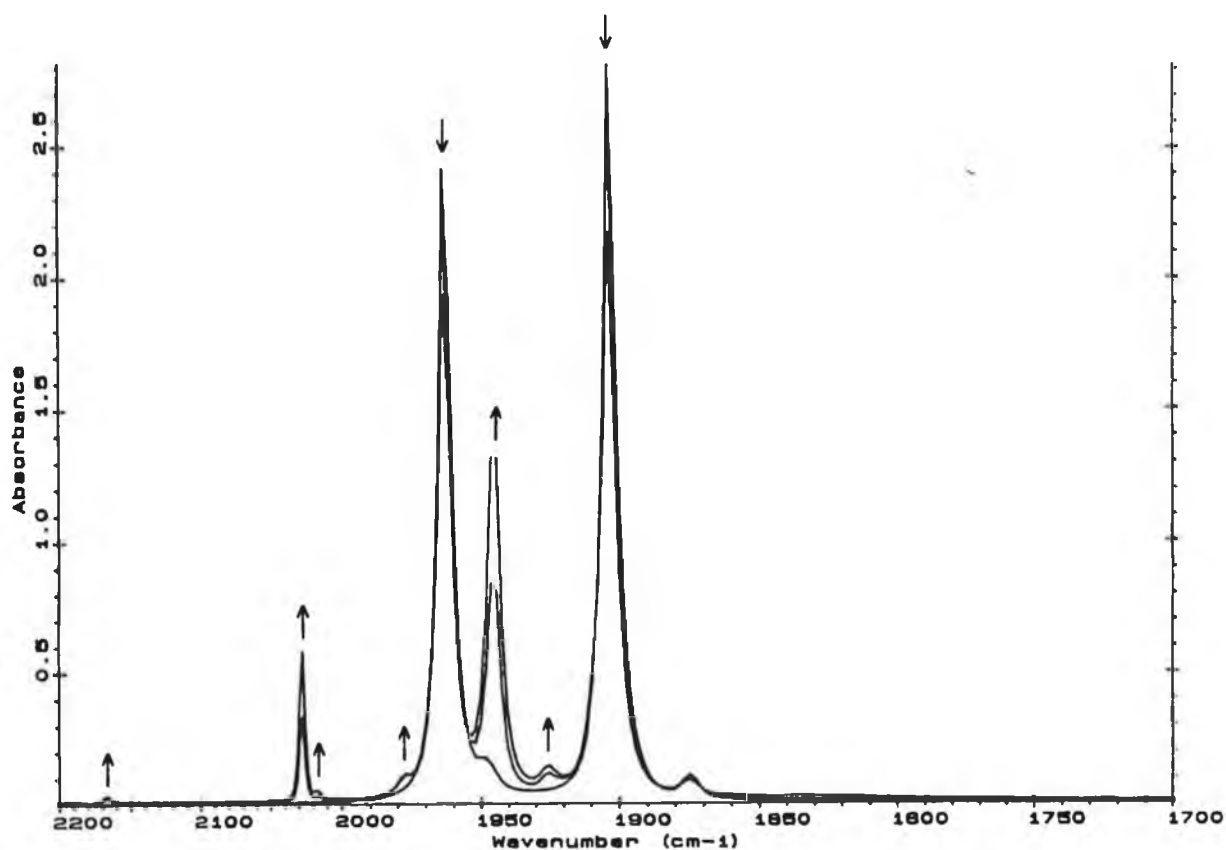


3.3.2.6 Infrared Monitored Photolysis of $\text{CpMn(CO)}_2(\eta^2\text{-C}_8\text{H}_{14})$.

Infrared experiments on photolysed cyclohexane solutions of $\text{CpMn(CO)}_2(\eta^2\text{-C}_8\text{H}_{14})$ under one atmosphere of CO indicated the considerable reduction of parent vibrations at 1963 and 1903 cm^{-1} concomitant with the production of two strong sharp peaks at 2028 and 1945 cm^{-1} respectively. IR analysis of CpMn(CO)_3 in cyclohexane $\nu(\text{CO})$ 2028 and 1945 cm^{-1} has conclusively proved the production of the tricarbonyl in flash photolysis experiments under carbon monoxide atmospheres.

In an argon atmosphere formation of the tricarbonyl is also observed, but not with the high conversion seen in experiments with CO present. Figure 3.3.2.15 shows more concentrated sample, with several new bands at 2167, 2028, 2017, 1976, 1945, and 1926 cm^{-1} . Those at 2028 and 1945 cm^{-1} are attributed to CpMn(CO)_3 , with ^{13}CO satellites at 2017 and 1926 cm^{-1} . The weak vibration at 2167 cm^{-1} corresponds to free CO [44]. Detection of IR vibrations for the dinuclear intermediate is made difficult by the strong absorption bands for the parent and tricarbonyl, as well as its inherent instability, and also, in the presence of CO, formation of the dinuclear species is inhibited. No evidence of a bridging carbonyl was found in the low frequency region of the spectrum, possibly as a result of the unstable nature of the intermediate.

Figure 3.3.2.15: Infrared spectral changes observed on photolysis of $\text{CpMn(CO)}_2(\eta^2\text{-C}_8\text{H}_{14})$ in argon degassed cyclohexane.



3.3.2.7 Summary.

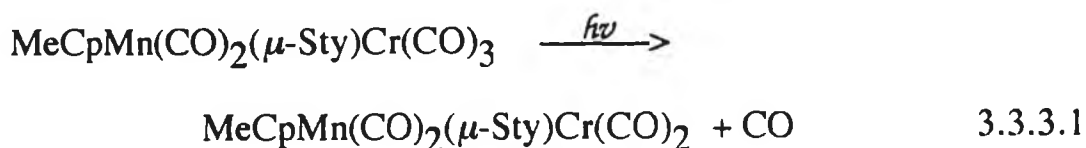
Laser flash photolysis of $\text{CpMn(CO)}_2(\eta^2\text{-C}_8\text{H}_{14})$ in cyclohexane produced the solvated dicarbonyl $\text{CpMn(CO)}_2(\text{S})$ and free *cis*-cyclooctene. This reacted with free CO to form the corresponding CpMn(CO)_3 complex. In argon atmospheres the solvated intermediate reacted with the parent

molecule to produce the short-lived dinuclear species. Similarities in the transient UV/vis absorption spectrum between this and previously identified manganese dinuclear complexes [30, 42], has led us to postulate that this dimanganese complex may also possess a carbonyl bridge between the two metal centres. However, determination of the exact structure is difficult because of its unstable nature. The rate of decay of this species under CO was almost three times faster than that for the reaction of $\text{Cp}_2\text{Mn}_2(\text{CO})_5$ with CO, indicating its very unstable nature. Possible reaction of $(\text{CO})_2\text{CpMn}(\mu\text{-CO})\text{MnCp}(\text{CO})(\eta^2\text{-C}_8\text{H}_{14})$ with CO produced $\text{CpMn}(\text{CO})_3$ and parent. Infrared investigations confirmed the generation of $\text{CpMn}(\text{CO})_3$ in both argon and carbon monoxide environments.

3.3.3 Laser Flash Photolysis of $\text{MeCpMn(CO)}_2(\mu\text{-Sty})\text{Cr(CO)}_3$ in Cyclohexane Solution.

Having looked at the photochemical reactions of StyCr(CO)_3 and $\text{CpMn(CO)}_2(\eta^2\text{-C}_8\text{H}_{14})$, it was of interest to determine the photochemistry in a combined system, where the manganese and chromium centres are linked *via* a bridging styrene ligand, as in $\text{MeCpMn(CO)}_2(\mu\text{-Sty})\text{Cr(CO)}_3$. StyCr(CO)_3 and $\text{CpMn(CO)}_2(\eta^2\text{-C}_8\text{H}_{14})$ were used as models to explain the photoprocesses observed in this novel hetero-binuclear complex. This complex has two potentially photoactive sites, one centred on manganese and the other on chromium. Irradiation may lead to a series of reactions as shown in Reactions 3.3.3.1 and 3.3.3.2.

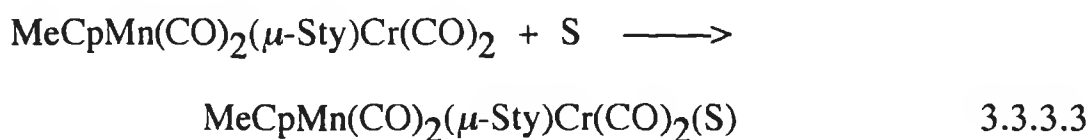
The reactivity of this complex was compared to that observed for the individual systems in various CO and argon environments. The olefin attached to the manganese atom, *via* an η^2 - interaction, will be less electron rich because of the presence of the electron withdrawing (arene) Cr(CO)_3 moiety, and as a result may accept more electron density from the manganese in back donation. This results in a stronger bond between the two, reflected in the carbon-carbon double bond length of 1.407 Å (Chapter 4).



and/or



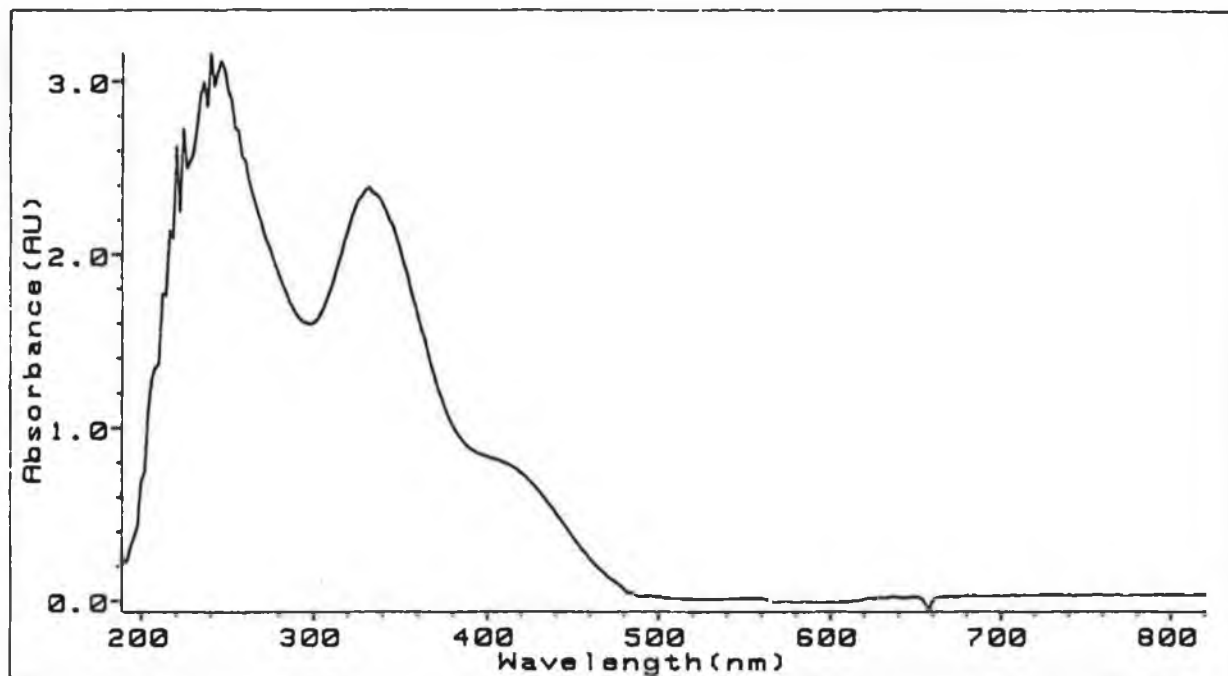
The solvent possibly coordinates to the photofragments as shown in Reaction 3.3.3.3 and 3.3.3.4.



3.3.3.1 Electronic Excitation Spectrum of $\text{MeCpMn(CO)}_2(\mu\text{-Sty})\text{Cr(CO)}_3$.

The UV/vis spectrum of $\text{MeCpMn(CO)}_2(\mu\text{-Sty})\text{Cr(CO)}_3$ is shown in Figure 3.3.3.1. It is very similar to that reported for StyCr(CO)_3 (Figure 3.3.1.1), possessing a window of low absorption at 290nm, and a prominent absorption band with maximum at 330nm with $\text{Mn} \rightarrow \pi^*\text{L}$ CT character. A low energy absorption band with maximum at 400nm (as observed for StyCr(CO)_3) was also observed. In $\text{MeCpMn(CO)}_2\text{L}$ complexes, the lowest energy absorption is very dependent on the substituents of L. Binding of the ligand results in a higher $\text{Mn} \rightarrow \pi^*\text{L}$ CT. However, it should be noted that weak LF transitions may contribute to these absorptions and also, interpretation of the UV/vis data is complicated by the fact that the molar extinction coefficients for manganese complexes are significantly lower than those for chromium complexes. The extinction coefficient of $\text{MeCpMn(CO)}_2(\mu\text{-Sty})\text{Cr(CO)}_3$ in cyclohexane was calculated as $7392 \text{ dm}^3\text{mol}^{-1}\text{cm}^{-1}$ at 354nm.

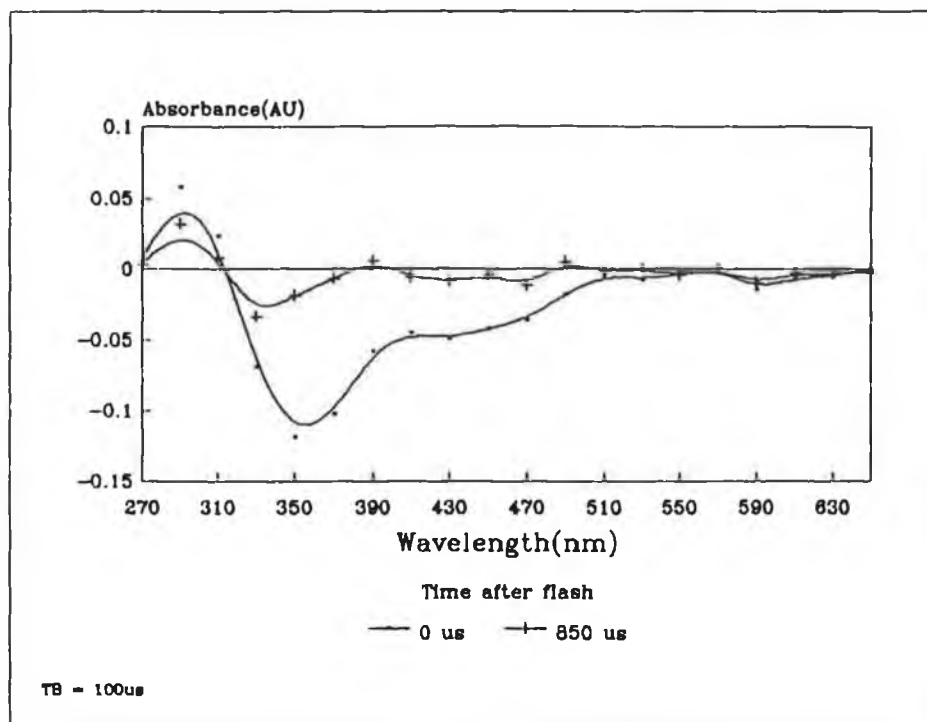
Figure 3.3.3.1: UV/vis spectrum of $\text{MeCpMn(CO)}_2(\mu\text{-Sty})\text{Cr(CO)}_3$ in cyclohexane.



3.3.3.2 Primary Photoproduct.

The transient UV/vis difference spectrum obtained (under an argon atmosphere) at $0\mu\text{s}$, and $850\mu\text{s}$ after the flash is shown in Figure 3.3.3.2. The spectrum at $0\mu\text{s}$ is analogous to the spectrum obtained (at $0\mu\text{s}$) for flash photolysis of StyCr(CO)_3 (Figure 3.3.1.2). The featureless absorption spectrum observed in the 580nm region indicates the absence of the solvated manganese photofragment $(\text{MeCp})\text{Mn(CO)}_2(\text{S})$.

Figure 3.3.3.2: Transient UV/vis difference spectrum observed on flash photolysis of $\text{MeCpMn(CO)}_2(\mu\text{-Sty})\text{Cr(CO)}_3$ in cyclohexane under argon.

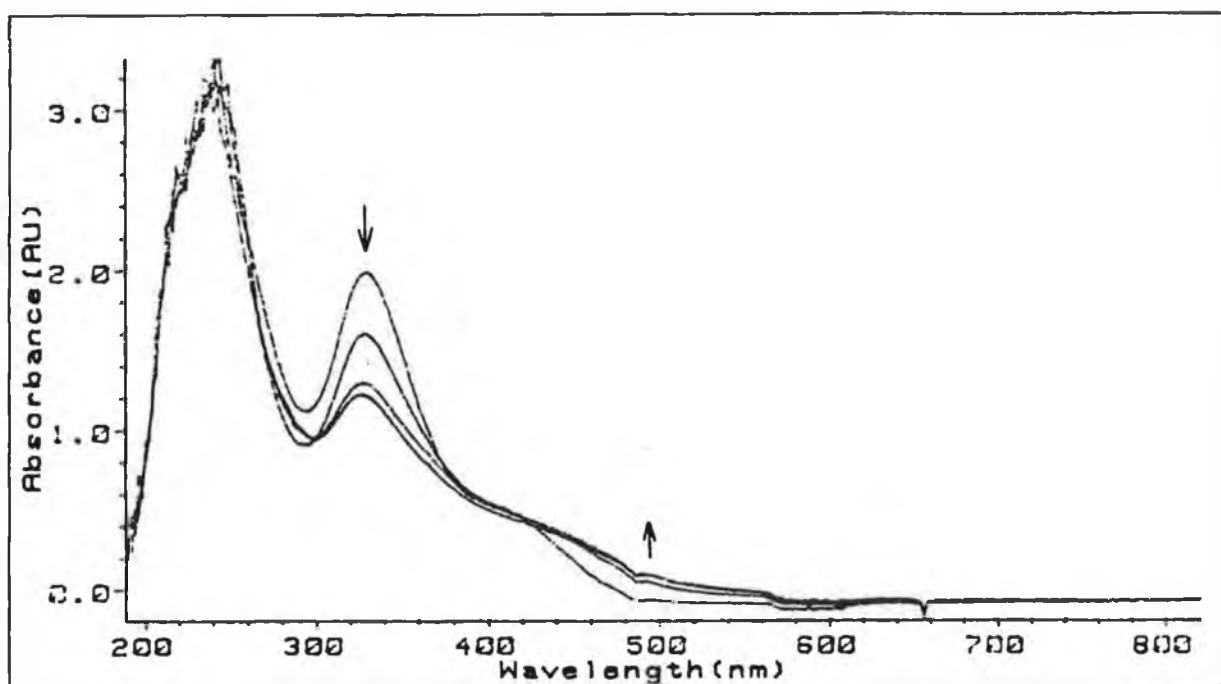


On the basis of these transient UV/vis spectra, it appears that the primary photoprocess is labilisation of CO from the chromium centre. This photochemical sequence is supported by the knowledge that chromium complexes are more photoreactive than manganese complexes [14, 52]. The complex formed in the flash had a risetime too quick to be detected on our system, and the mechanism of its decay was investigated.

The reaction was not reversible under either CO or argon atmospheres. Figure 3.3.3.3 shows the changes observed in the UV/vis spectrum during the course of a flash photolysis experiment under one atmosphere of argon. The band at 330nm, and shoulders at 410 and 260nm all decrease in intensity. Similar behaviour is also observed under one atmosphere of CO.

Prolonged irradiation under argon showed a complete reduction in intensity of the bands at 410 and 330nm, with the formation of new bands at 280 and 240nm. Infrared spectral changes (Section 3.3.3.6) were consistent with rupture of the μ -styrene bridge between the manganese and chromium centres, with the eventual production of MeCpMn(CO)_3 and StyCr(CO)_3 .

Figure 3.3.3.3: Changes observed in the UV/vis spectrum on flash photolysis of $\text{MeCpMn(CO)}_2(\mu\text{-Sty})\text{Cr(CO)}_3$ in cyclohexane under 1 atm. argon.



The dependence of the lifetime of the primary photoproduct on CO concentration was investigated. The transient UV/vis difference spectrum on flash photolysis of $\text{MeCpMn(CO)}_2(\mu\text{-Sty})\text{Cr(CO)}_3$ under CO is shown in Figure 3.3.3.4. The initial spectrum at $0\mu\text{s}$, and the spectrum $175\mu\text{s}$ later, indicate chromium-centred photochemistry. At $0\mu\text{s}$, the absorption at 290nm corresponds to $\text{MeCpMn(CO)}_2(\mu\text{-Sty})\text{Cr(CO)}_2(\text{S})$, formed within the laser

flash, while the negative absorption centred around 340nm corresponds to the depleted parent. The spectrum 175 μ s later exhibits the decay of the solvated intermediate (290nm), with regeneration of the parent (340nm). As observed under an argon atmosphere, there is little evidence for the formation of $\text{MeCpMn(CO)}_2(\text{S})$ because of the lack of spectral information around 580nm. A typical transient signal for the decay of the solvated dicarbonyl $\text{MeCpMn(CO)}_2(\mu\text{-Sty})\text{Cr(CO)}_2(\text{S})$ under CO, is shown in Figure 3.3.3.5.

Figure 3.3.3.4: Transient UV/vis absorption difference spectrum for $\text{MeCpMn(CO)}_2(\mu\text{-Sty})\text{Cr(CO)}_3$ under 1 atm. CO in cyclohexane.

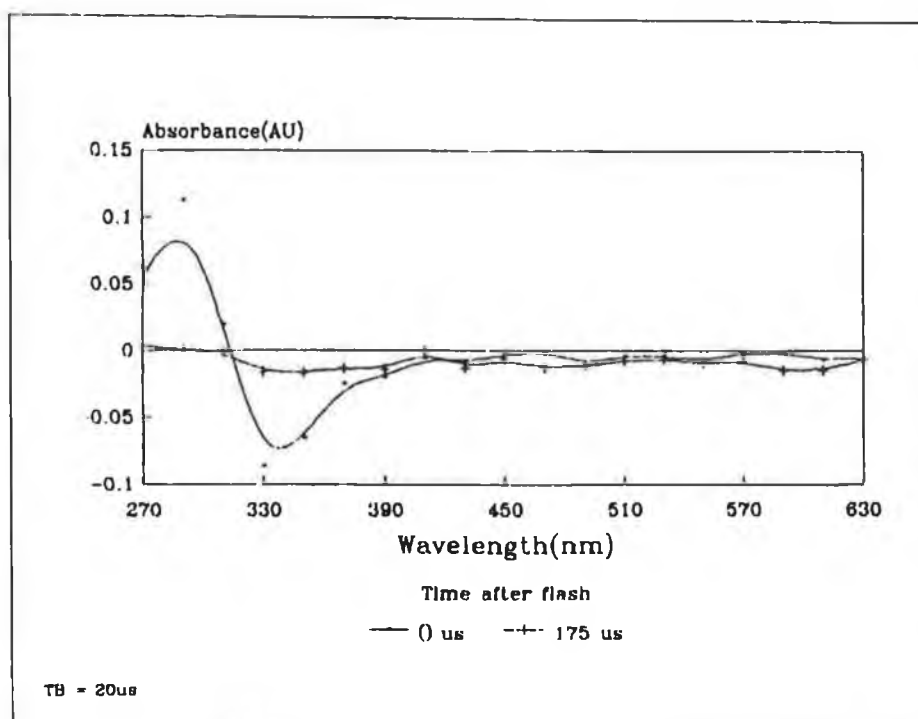
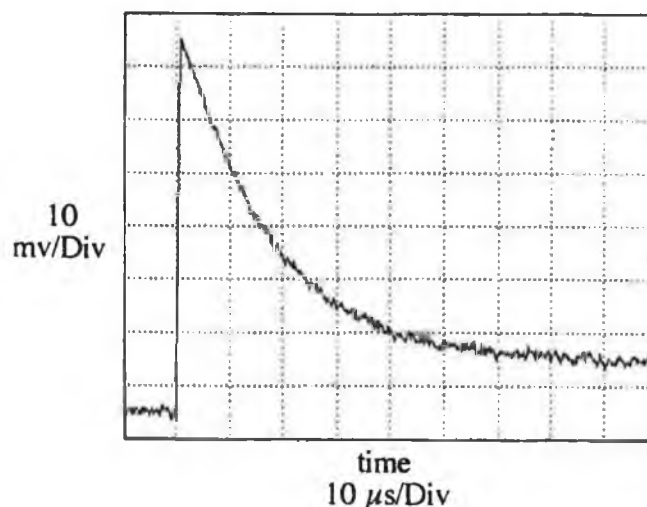


Figure 3.3.3.5: Transient decay for $\text{MeCpMn(CO)}_2(\mu\text{-Sty})\text{Cr(CO)}_2(\text{S})$ under CO [$0.9 \times 10^{-2}\text{M}$] monitored at 290nm.



Knowing the relative recombination rates for $\text{StyCr(CO)}_2(\text{S})$ and $\text{CpMn(CO)}_2(\text{S})$ with CO (Section 3.3.1.2 and 3.3.2.2), identification of the primary photoprocess may be kinetically ascertained by determining the recombination rate with CO.

It is worth noting at this point that the photochemistry of MeCpMn(CO)_3 is similar to that for CpMn(CO)_3 [14, 42, 45]. Crocock [42] reported that the rate for the reaction of $\text{MeCpMn(CO)}_2(\text{S})$ with CO was twice that for the analogous reaction with $\text{CpMn(CO)}_2(\text{S})$, possibly because of the steric effect of a methyl group attached to the Cp ring.

The lifetime of the solvated photoproduct depended on the concentration of CO present. The data for determination of the effect of CO concentration on the lifetime is tabulated in Table 3.3.3.1.

Table 3.3.3.1: Kinetic data for the determination of the effect of CO concentration on the lifetime of the transient species.

CO (E3) [M]	k _{obs} /s
2.25	15900
4.50	31200
6.75	51100
9.00	67300

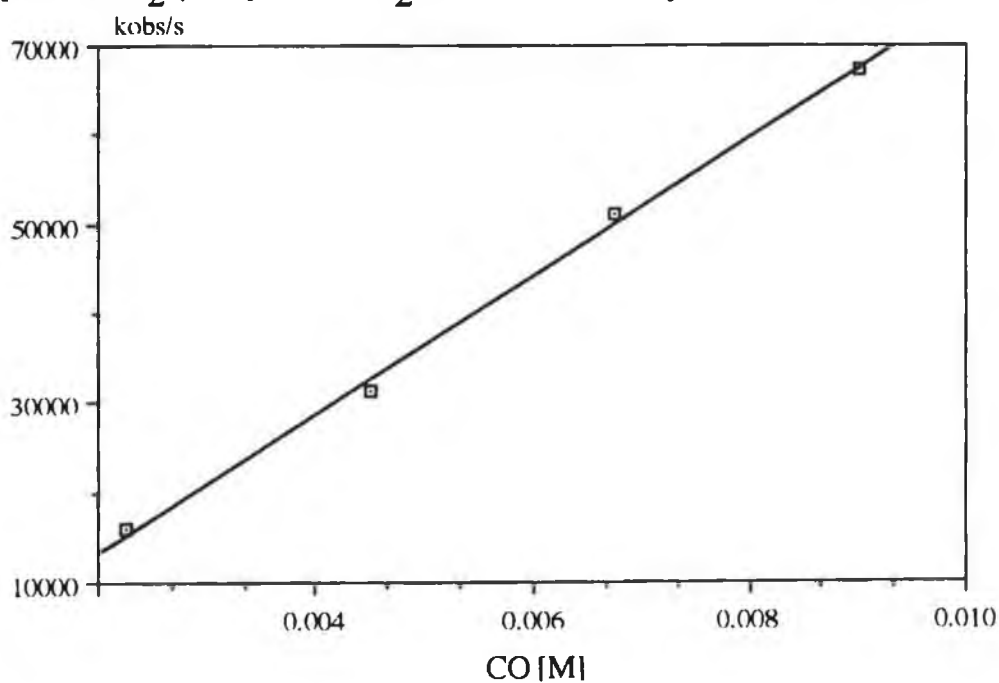
$$\text{Slope} = 7.7 (\pm 0.3) \times 10^6 \text{ dm}^3 \text{ mol}^{-1} \text{ s}^{-1}$$

$$\text{Intercept} = -2.2 (\pm 1.7) \times 10^3 \text{ s}^{-1}$$

$$\text{Correlation} = 0.99$$

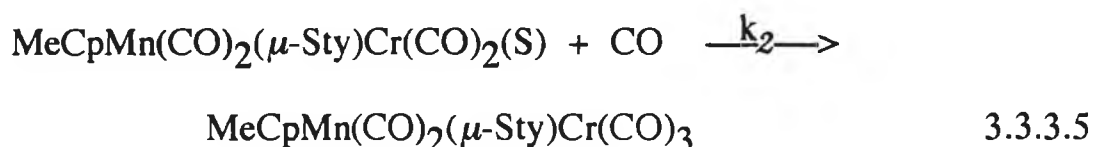
The observed rate of reaction k_{obs} was plotted against CO concentration. The corresponding plot is shown in Figure 3.3.3.6.

Figure 3.3.3.6: Plot of k_{obs} versus CO concentration for the reaction of $\text{MeCpMn(CO)}_2(\mu\text{-Sty})\text{Cr(CO)}_2(\text{S})$ with CO in cyclohexane at 298K.



The second order rate constant (k_2) for the reaction of $\text{MeCpMn(CO)}_2(\mu\text{-Sty})\text{Cr(CO)}_2(\text{S})$ with CO is $7.7 \times 10^6 \text{ dm}^3\text{mol}^{-1}\text{s}^{-1}$. This is the same within experimental error of the value obtained for the reaction of $\text{StyCr(CO)}_2(\text{S})$ with CO of $7.1 \times 10^6 \text{ dm}^3\text{mol}^{-1}\text{s}^{-1}$.

Considering the kinetic data obtained, and also the transient absorption spectral information, it was concluded that the primary photoprocess was photoejection of a CO molecule from the chromium centre, according to Reaction 3.3.3.1. The $\text{MeCpMn(CO)}_2(\mu\text{-Sty})\text{Cr(CO)}_2$ photofragment rapidly coordinates to cyclohexane, as shown in Reaction 3.3.3.3. This weakly coordinated solvent molecule is displaced by a molecule of CO (under a CO atmosphere) to regenerate the parent complex (Reaction 3.3.3.5).



Overall, the reactivity of the chromium photofragment is unchanged when attached to the manganese centre.

3.3.3.3 Activation Parameters for the reaction of CO with $\text{MeCpMn(CO)}_2(\mu\text{-Sty})\text{Cr(CO)}_2(\text{S})$.

Activation parameters for the reaction of CO with $\text{MeCpMn(CO)}_2(\mu\text{-$

Sty)Cr(CO)₂(S) were calculated. The second order rate constant k_2 was used in the calculations ($k_2 = k_{\text{obs}}/[\text{CO}]$), where $[\text{CO}] = 0.9 \times 10^{-2}\text{M}$. The activation parameters are listed in Table 3.3.3.2. The experimental data is given in Table 3.3.3.3 and the corresponding plots in Figures 3.3.3.7 and 3.3.3.8 for the Arrhenius and Eyring graphs respectively.

Table 3.3.3.2: Activation parameters for the reaction of MeCpMn(CO)₂(μ -Sty)Cr(CO)₂(S) with CO.

$E_a^\ddagger = 34 \pm 2 \text{ kJmol}^{-1}$
$\Delta H^\ddagger = 32 \pm 2 \text{ kJmol}^{-1}$
$\Delta S^\ddagger = -7 \pm 25 \text{ Jmol}^{-1}\text{K}^{-1}$
$\Delta G^\ddagger = 34 \pm 2 \text{ kJmol}^{-1}$

The activation energy for the reaction is very similar to the value obtained for the reaction of StyCr(CO)₂(S) with CO (37 kJmol⁻¹). The activation entropy is more negative, but is still close to zero indicating an interchange mechanism.

Table 3.3.3.3: Experimental data for the determination of the activation parameters for the reaction of $\text{MeCpMn(CO)}_2(\mu\text{-Sty})\text{Cr(CO)}_2(\text{S})$ with CO.

Temp (K)	(1/T)E3 (1/K)	kobs (/s)	ln(kobs/[CO])	ln((kobs/T)/[CO])
284	3.52	34189	15.15	9.50
288	3.47	39466	15.29	9.63
293	3.41	47853	15.48	9.80
298	3.36	64857	15.79	10.09
303	3.30	84265	16.05	10.34
313	3.19	126480	16.46	10.71

Arrhenius Plot

Slope = -4100 ± 200

Intercept = 29.6 ± 0.1

Correlation = 0.99

$E_a^\ddagger = 34 \pm 2 \text{ kJmol}^{-1}$

Eyring Plot

Slope = -3800 ± 200

Intercept = 22.9 ± 0.1

Correlation = 0.99

$\Delta H^\ddagger = 32 \pm 2 \text{ kJmol}^{-1}$

$\Delta S^\ddagger = -7 \pm 25 \text{ Jmol}^{-1}\text{K}^{-1}$

Figure 3.3.3.7: Arrhenius plot for the reaction of $\text{MeCpMn(CO)}_2(\mu\text{-Sty})\text{Cr(CO)}_2(\text{S})$ with CO.

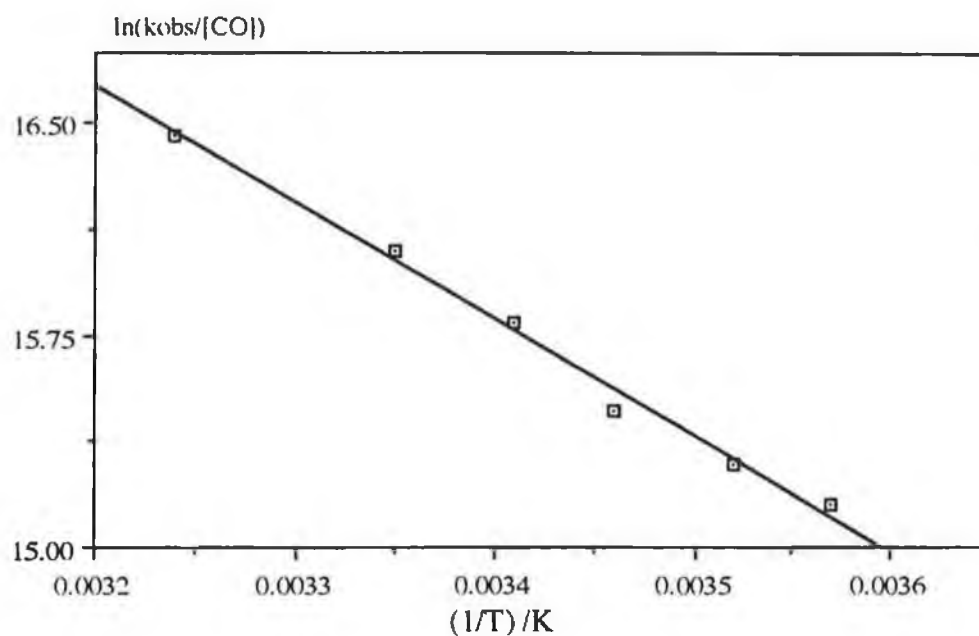
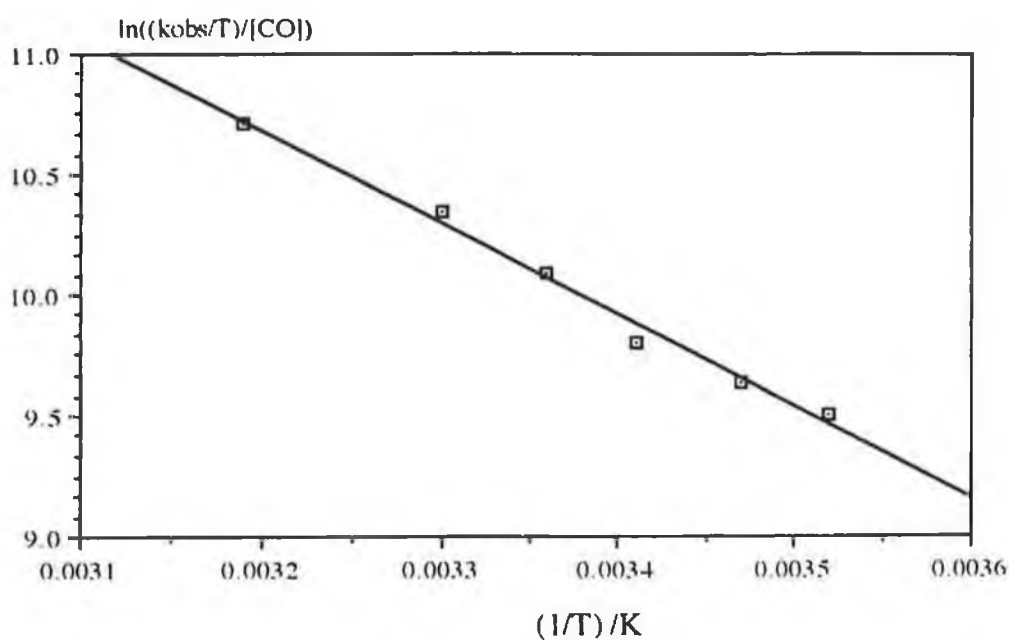


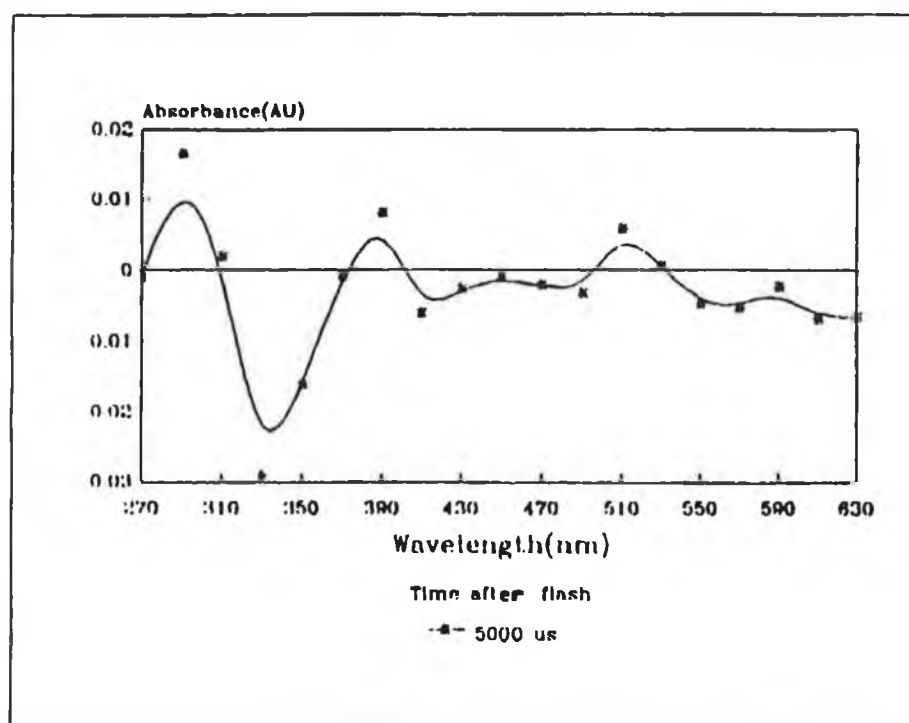
Figure 3.3.3.8: Eyring plot for the reaction of $\text{MeCpMn(CO)}_2(\mu\text{-Sty})\text{Cr(CO)}_2(\text{S})$ with CO.



3.3.3.4 Formation of $\{\text{MeCpMn}(\text{CO})_2(\mu\text{-Sty})\text{Cr}(\text{CO})_2\}_2(\mu\text{-CO})$.

Under one atmosphere of argon the formation of a second transient species was observed. The transient UV/vis difference spectrum of this species is shown in Figure 3.3.3.9. Absorption maxima are located at 290, 390 and 510nm. In the model compound $\text{StyCr}(\text{CO})_3$, the second transient species had absorption maxima at 290 and 390nm (Figure 3.3.1.9), where the photoproduct was attributed to a combination of $\text{StyCr}(\text{CO})_2(\text{cyclohexane})$ and $\text{StyCr}(\text{CO})_3$.

Figure 3.3.3.9: Transient UV/vis absorption spectrum of the second species.



To investigate if the formation of this second species was dependent on the concentration of $\text{MeCpMn}(\text{CO})_2(\mu\text{-Sty})\text{Cr}(\text{CO})_3$, experiments were carried out with various parent concentrations and the observed rate constants

determined. An estimate of the second order rate constant for the reaction was determined from the slope of a plot of k_{obs} (s^{-1}) versus concentration of $\text{MeCpMn(CO)}_2(\mu\text{-Sty})\text{Cr(CO)}_3$. The data is tabulated in Table 3.3.3.4 and the corresponding plot shown in Figure 3.3.3.10.

Table 3.3.3.4: Data for the determination of the effect of $\text{MeCpMn(CO)}_2(\mu\text{-Sty})\text{Cr(CO)}_3$ concentration on k_{obs} for the formation of the second species, at 298K.

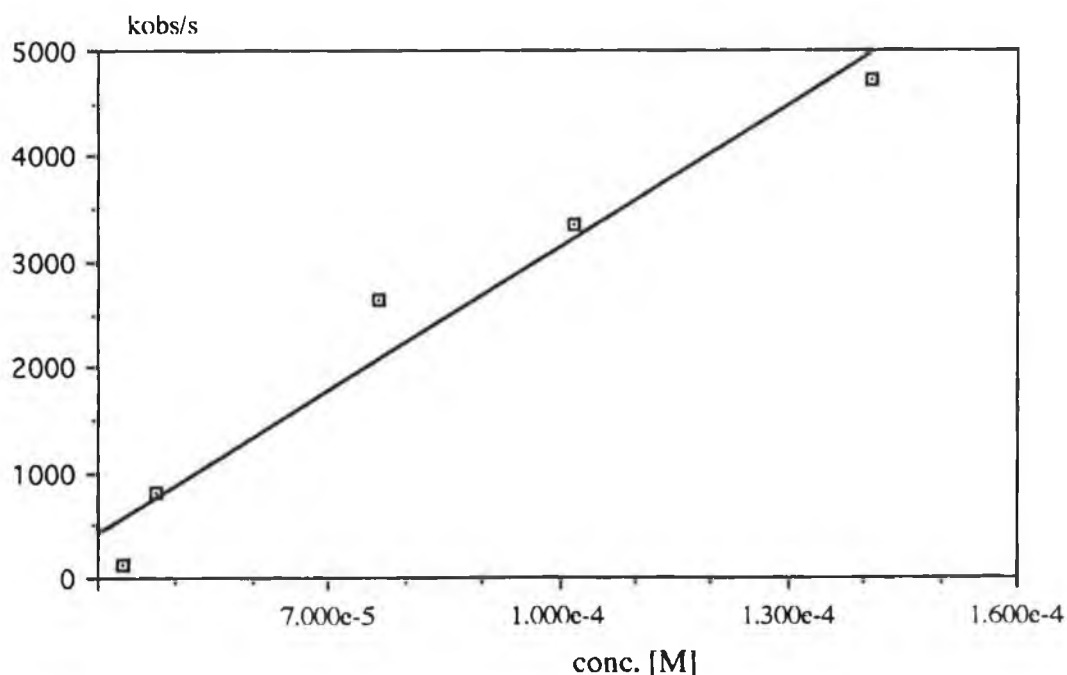
conc. (E4) [M]	kobs/s
0.43	136.6
0.47	803.5
0.77	2633.5
1.02	3362
1.41	4730

$$\text{Slope} = 4.6 (\pm 0.5) \times 10^7 \text{ dm}^3\text{mol}^{-1}\text{s}^{-1}$$

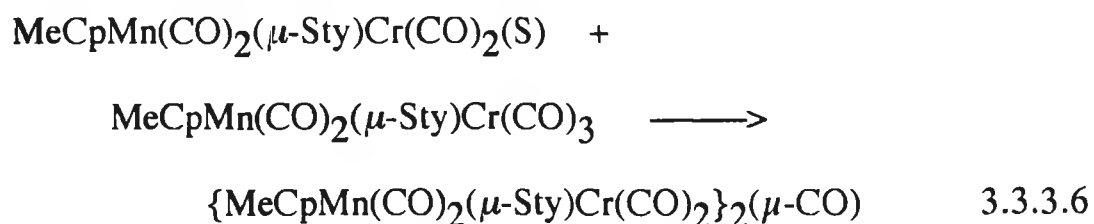
$$\text{Intercept} = -1370 \pm 450$$

$$\text{Correlation} = 0.98$$

Figure 3.3.3.10: Plot showing the change in k_{obs} with various concentrations of $\text{MeCpMn(CO)}_2(\mu\text{-Sty})\text{Cr(CO)}_3$.

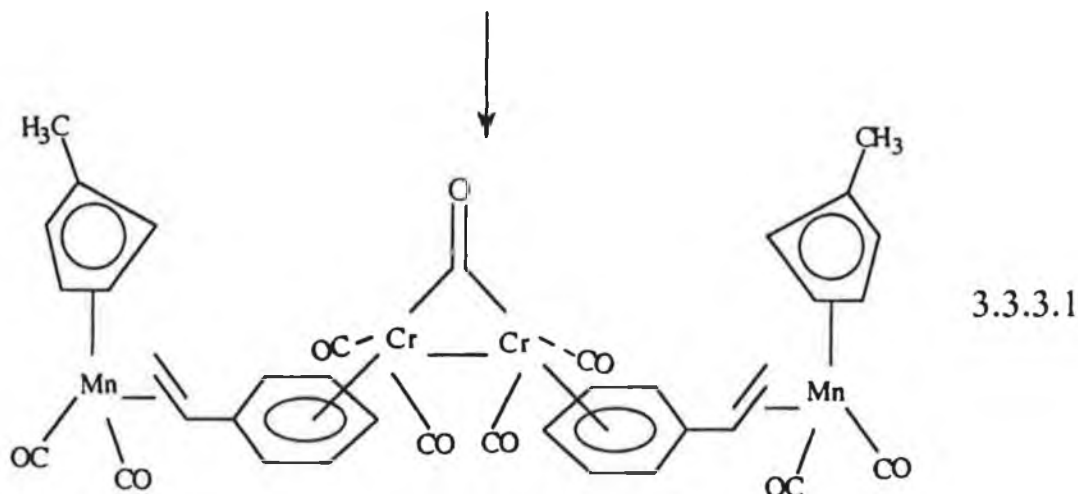
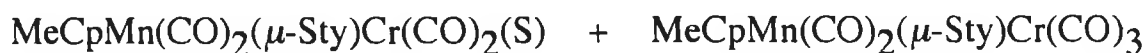


The formation of the second species linearly depended on the concentration of $\text{MeCpMn(CO)}_2(\mu\text{-Sty})\text{Cr(CO)}_3$, affording a second order rate constant of $4.76 \times 10^7 \text{ dm}^3\text{mol}^{-1}\text{s}^{-1}$. It is proposed that the $\text{MeCpMn(CO)}_2(\mu\text{-Sty})\text{Cr(CO)}_2$ photofragment combines with the dinuclear parent to form a short-lived 'tetranuclear' intermediate, as shown in Reaction 3.3.3.6.



Comparison of the second order rate constant with that obtained for the

corresponding reaction in the chromium model ($\text{StyCr}(\text{CO})_3$), points towards a chromium centred intermediate. However, the structure to this 'tetranuclear' intermediate is uncertain. The second order rate constant supports the idea of a 'tetranuclear' complex, possibly bridged by a chromium-chromium bond and a bridging carbonyl as shown in Scheme 3.3.3.1. However, determination of the exact structure and bonding of this 'tetranuclear' complex is made difficult, because of the many possibilities which may occur, and also, the fact that these coordination complexes do not absorb strongly in the visible region.



3.3.3.5 Activation Parameters for the formation of $\{\text{MeCpMn}(\text{CO})_2(\mu\text{-Sty})\text{Cr}(\text{CO})_2\}_2(\mu\text{-CO})$.

Activation parameters for the reaction of $\text{MeCpMn}(\text{CO})_2(\mu\text{-Sty})\text{Cr}(\text{CO})_2(\text{S})$ with $\text{MeCpMn}(\text{CO})_2(\mu\text{-Sty})\text{Cr}(\text{CO})_3$ were determined using the second

order rate constant k_3 , where $k_3 = (k_{\text{obs}}/[\text{MeCpMn}(\text{CO})_2(\mu\text{-Sty})\text{Cr}(\text{CO})_3])$. The values obtained were tabulated in Table 3.3.3.5. The experimental data is given in Table 3.3.3.6 with the Arrhenius and Eyring plots in Figures 3.3.3.11 and 3.3.3.12 respectively.

Table 3.3.3.5: Activation parameters for the formation of the second species.

$$E_a^\ddagger = 37 \pm 2 \text{ kJmol}^{-1}$$

$$\Delta H^\ddagger = 34 \pm 2 \text{ kJmol}^{-1}$$

$$\Delta S^\ddagger = 11 \pm 25 \text{ Jmol}^{-1}\text{K}^{-1}$$

$$\Delta G^\ddagger = 31 \pm 2 \text{ kJmol}^{-1}$$

The activation parameters are higher than those observed for the formation of $(\text{CO})_2(\text{Sty})\text{Cr}(\mu\text{-Sty})\text{Cr}(\text{CO})_3$ (Table 3.3.1.5). For the 'tetranuclear' complex, the slightly positive nature of the activation entropy suggests a dissociative mechanism for the transition state. This may be accounted for in terms of the steric problems encountered when the large solvated intermediate interacts with the bulky parent. The activation energy for the reaction is quite high at 37 kJmol^{-1} .

Infrared monitoring of the sample solution after flash photolysis under argon, has produced evidence for the formation of both $\text{MeCpMn}(\text{CO})_3$ and $\text{StyCr}(\text{CO})_3$ (Section 3.3.3.6).

Table 3.3.3.6: Experimental data for the determination of the activation parameters for the formation of the dinuclear species at 298K, $[\text{MeCpMn}(\text{CO})_2(\mu\text{-Sty})\text{Cr}(\text{CO})_3] = 1.85 \times 10^{-4} \text{ M}$.

Temp (K)	(1/T)E3 (1/K)	kobs (/s)	ln(kobs/[P])	ln((kobs/T)/[P])
283	3.53	1903	16.15	10.50
288	3.47	2548	16.44	10.78
293	3.41	3203	16.67	10.99
298	3.36	4442	17.00	11.30
303	3.30	5270	17.17	11.45
308	3.24	7117	17.47	11.74
313	3.19	8508	17.65	11.90

Arrhenius Plot

Slope = -4400 ± 100

Intercept = 31.9 ± 0.1

Correlation = 0.99

$E_a^\ddagger = 37 \pm 2 \text{ kJmol}^{-1}$

Eyring Plot

Slope = -4100 ± 100

Intercept = 25.1 ± 0.1

Correlation = 0.99

$\Delta H^\ddagger = 34 \pm 2 \text{ kJmol}^{-1}$

$\Delta S^\ddagger = 11 \pm 25 \text{ Jmol}^{-1}\text{K}^{-1}$

Figure 3.3.3.11: Arrhenius plot for the formation of the second species.

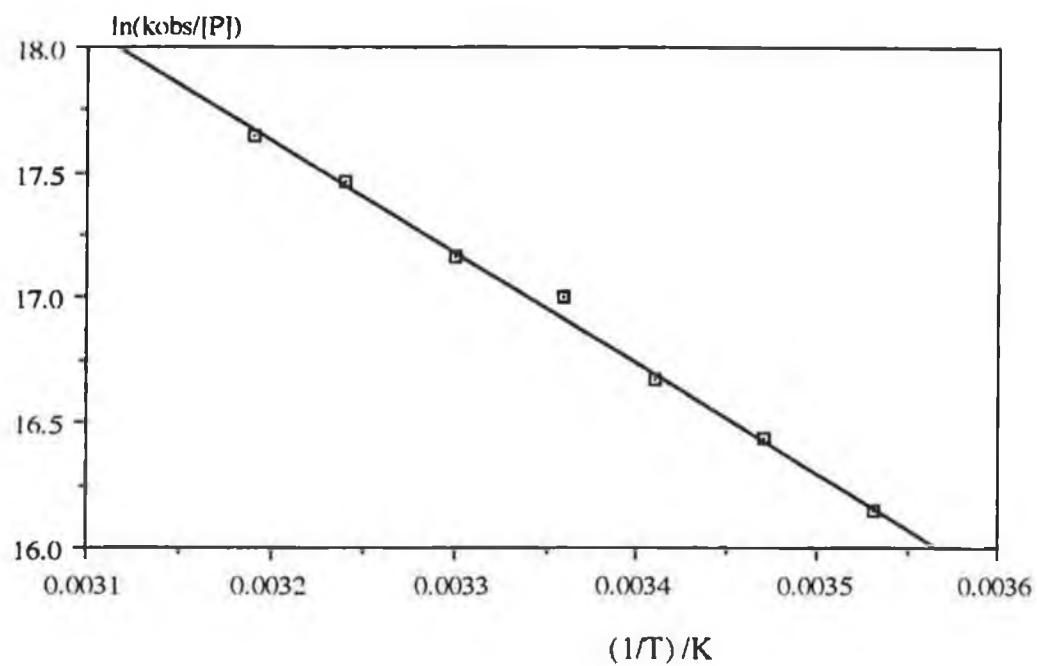
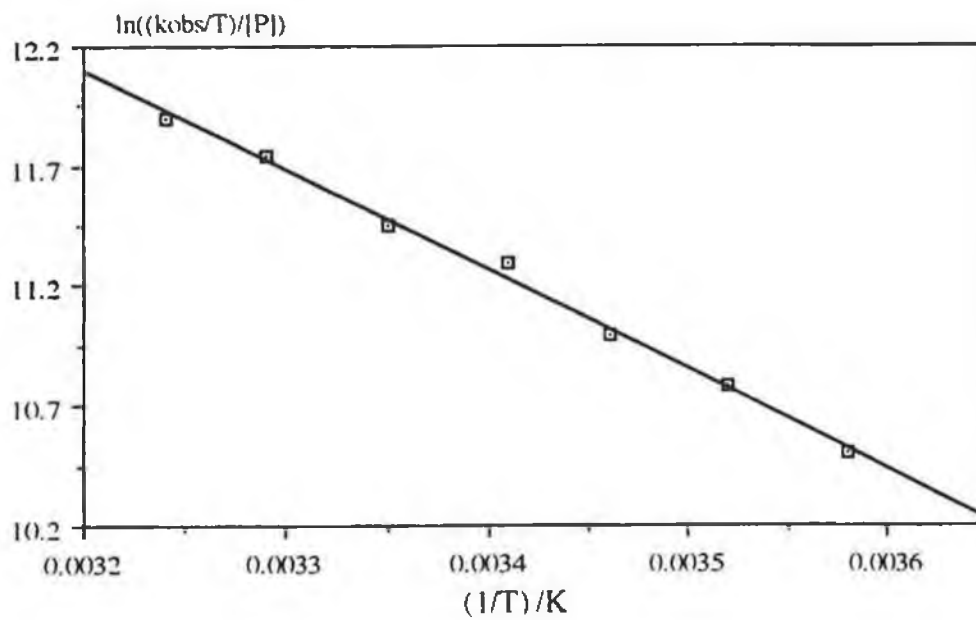


Figure 3.3.3.12: Eyring plot for the formation of the second species.



3.3.3.6 Infrared Monitored Photolysis of $\text{MeCpMn(CO)}_2(\mu\text{-Sty})\text{Cr(CO)}_3$.

Infrared monitoring of a sample of $\text{MeCpMn(CO)}_2(\mu\text{-Sty})\text{Cr(CO)}_3$ after a flash photolysis experiment, produced evidence for the formation of both MeCpMn(CO)_3 and StyCr(CO)_3 . In one atmosphere of CO, parent $\nu(\text{CO})$ vibrations at 1977, 1971, 1919, and 1916cm^{-1} decreased in intensity with the production of two new $\nu(\text{CO})$ bands at 2024 and 1941cm^{-1} (MeCpMn(CO)_3), and 1980 and 1914cm^{-1} (StyCr(CO)_3). Under argon, similar trends were observed over a longer time period. Based on the kinetic and UV/vis data, there is little evidence to suggest that this is a primary photoprocess.

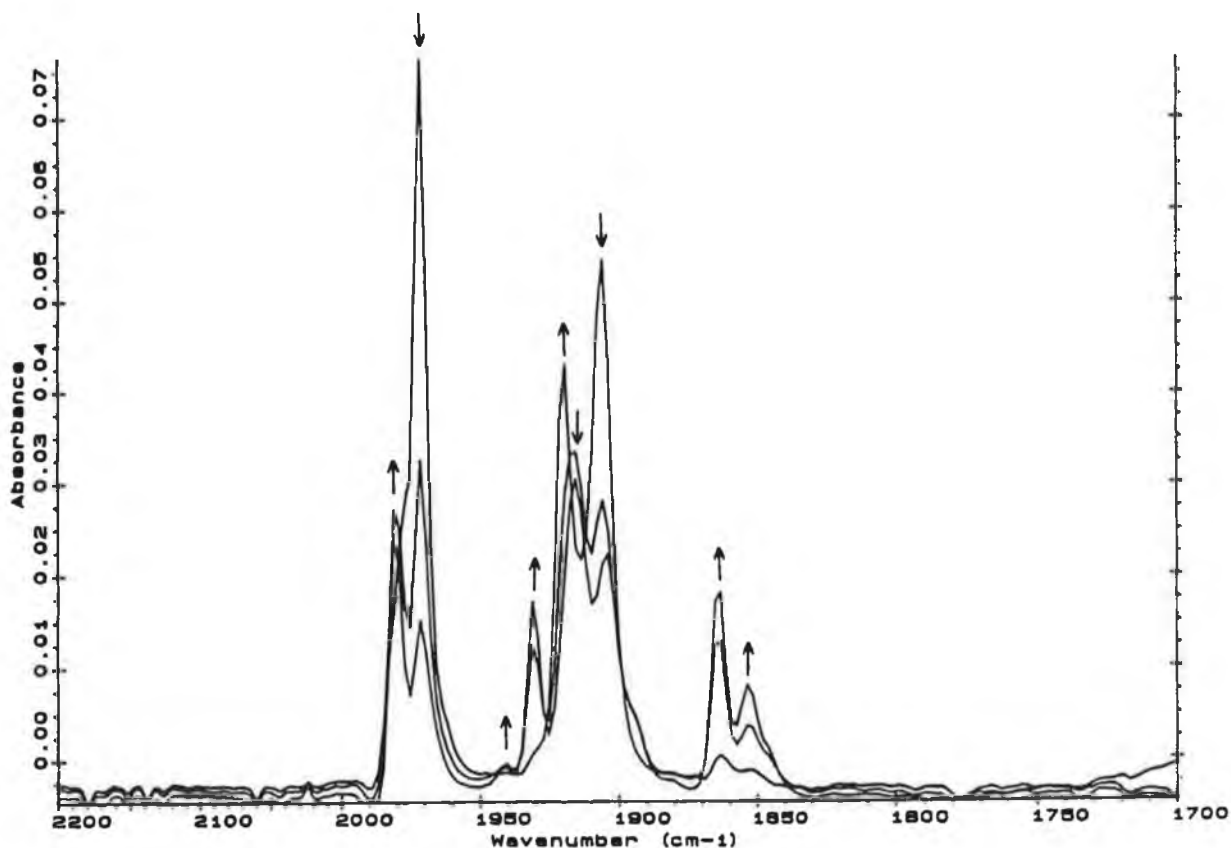
In argon degassed solutions, the unstable 'tetranuclear' complex possibly falls apart and the MeCpMn(CO)_2 photofragment scavenges CO molecules to form the tricarbonyl. Elucidation of the exact pathway for this process is made difficult by the low extinction coefficient of the MeCpMn(CO)_2 photofragment in cyclohexane, and also the variety of possibilities which exist.

An argon degassed sample of $\text{MeCpMn(CO)}_2(\mu\text{-Sty})\text{Cr(CO)}_3$ with excess pyridine present was irradiated with UV light (see Chapter 5) and monitored by infrared spectroscopy. The parent $\nu(\text{CO})$ absorption bands decreased in intensity concomitant with the production of several new $\nu(\text{CO})$ bands, as shown in Figure 3.3.3.13. After irradiating for 2 seconds, new

$\nu(\text{CO})$ vibrations were observed at 2024, 1941 cm^{-1} (very weak) ($\text{MeCpMn}(\text{CO})_3$), and 1930, 1864 cm^{-1} ($\text{MeCpMn}(\text{CO})_2(\text{Py})$). The $\nu(\text{CO})$ stretches at 1904 and 1853 cm^{-1} correspond well to those obtained for $\text{StyCr}(\text{CO})_2(\text{Py})$ (Section 3.3.1.6), but may also be due to the formation of $\text{MeCpMn}(\text{CO})_2(\mu\text{-Sty})\text{Cr}(\text{CO})_2(\text{Py})$. The $\nu(\text{CO})$ stretches at 1980 and 1915 cm^{-1} correspond to the cleaved $\text{StyCr}(\text{CO})_3$.

The evidence obtained supports the idea of rupture of the manganese- η^2 -olefin bond, as well as photoactivity on the chromium centre.

Figure 3.3.3.13: IR spectral changes for the reaction of $\text{MeCpMn}(\text{CO})_2(\mu\text{-Sty})\text{Cr}(\text{CO})_3$ with excess pyridine in argon degassed cyclohexane.



3.3.3.7 ^1H NMR Monitored Photolysis of $\text{MeCpMn(CO)}_2(\mu\text{-Sty})\text{Cr(CO)}_3$.

An argon degassed solution of $\text{MeCpMn(CO)}_2(\mu\text{-Sty})\text{Cr(CO)}_3$ in perdeuteriopyridine was photolysed with UV light (see Chapter 5) and changes in the proton nmr spectrum recorded. The emergence of a multiplet centered at 6.3 ppm (δ) and a singlet at 4.2 ppm, corresponding to vinylic and Cp protons respectively, provide evidence of Mn-olefin bond breakage, to produce $\text{MeCpMn(CO)}_2(\text{NC}_5\text{D}_5)$ and free StyCr(CO)_3 . IR analysis of a small volume of the nmr sample (in cyclohexane) had $\nu(\text{CO})$ bands in excellent agreement with those in already quoted (Section 3.3.3.6). Multiplets centered at 3.6 and 2.3 ppm appear to be the result of production of $\text{MeCpMn(CO)}_2(\mu\text{-Sty})\text{Cr(CO)}_2(\text{NC}_5\text{D}_5)$.

3.3.3.8 Summary.

Laser flash photolysis of $\text{MeCpMn(CO)}_2(\mu\text{-Sty})\text{Cr(CO)}_3$ in cyclohexane under either CO or argon atmospheres results in photoejection of a CO molecule from the chromium centre as the primary photoprocess. The lifetime of the dicarbonyl linearly depended on the CO concentration. Under argon, a 'tetranuclear' species was proposed *via* the interaction of $\text{MeCpMn(CO)}_2(\mu\text{-Sty})\text{Cr(CO)}_2(\text{cyclohexane})$ with parent. Cleavage of the Mn-olefin bond occurred on prolonged irradiation. This occurred in both CO and argon atmospheres, confirmed by the detection of MeCpMn(CO)_3 and

StyCr(CO)_3 using infrared spectroscopy. The chromium centre appears to possess the dominant photoactivity, while that of the manganese was 'hindered' on coordinating the $-\text{StyCr(CO)}_3$ ligand.

3.3.3.9 Conclusion.

The fast reaction solution photochemistry of the complexes StyCr(CO)_3 , $\text{CpMn(CO)}_2(\eta^2\text{-C}_8\text{H}_{14})$, and $\text{MeCpMn(CO)}_2(\mu\text{-Sty})\text{Cr(CO)}_3$ was investigated. Laser flash photolysis at 355nm with UV/vis monitoring of StyCr(CO)_3 , revealed two transient species. As was observed for the analogous (arene) Cr(CO)_3 complexes [13], the primary photoproduct was the dicarbonyl solvated intermediate. The lifetime of this species was reduced on adding CO to the system. Under an argon atmosphere, the second transient species $(\text{CO})_2(\text{Sty})\text{Cr}(\mu\text{-Sty})\text{Cr(CO)}_3$ was formed *via* interaction of $\text{StyCr(CO)}_2(\text{S})$ with StyCr(CO)_3 . This dinuclear complex is relatively stable, and has been isolated [8b].

Attempted homopolymerisation of StyCr(CO)_3 by UV irradiation was unsuccessful, possibly because of the expected instability of the product, and also the ease at which the parent monomer reforms.

Laser flash photolysis of $\text{CpMn(CO)}_2(\eta^2\text{-C}_8\text{H}_{14})$ in cyclohexane solution produced $\text{CpMn(CO)}_2(\text{S})$ and free *cis*-cyclooctene. The lifetime of the solvated dicarbonyl photofragment linearly depended on the CO concentration in solution. The reaction of $\text{CpMn(CO)}_2(\text{S})$ with $\text{CpMn(CO)}_2(\eta^2\text{-C}_8\text{H}_{14})$ under an argon atmosphere, led to the formation of

$(\text{CO})_2\text{CpMn}(\mu\text{-CO})\text{MnCp}(\text{CO})(\eta^2\text{-C}_8\text{H}_{14})$. $\text{CpMn}(\text{CO})_2(\eta^2\text{-C}_8\text{H}_{14})$ was eventually converted to its tricarbonyl analogue in both argon and carbon monoxide environments.

Photochemical investigation of the manganese-chromium dinuclear complex $\text{MeCpMn}(\text{CO})_2(\mu\text{-Sty})\text{Cr}(\text{CO})_3$ exhibited two transient species. The first species observed corresponds to $\text{MeCpMn}(\text{CO})_2(\eta^2\text{-C}_8\text{H}_8)\text{Cr}(\text{CO})_2(\text{S})$, confirmed by the transient spectral information, and also, comparison of the kinetic data for this system with the model manganese and chromium complexes studied. In argon atmospheres this species reacts with parent to produce a 'tetranuclear' intermediate. Cleavage of the Mn-olefin bond also occurs on prolonged irradiation of the sample (under a CO or argon atmosphere), forming the respective tricarbonyls.

Comparison of the photochemistry of the model compounds $\text{CpMn}(\text{CO})_2(\eta^2\text{-C}_8\text{H}_{14})$ and $\text{StyCr}(\text{CO})_3$ with the manganese-chromium dinuclear complex suggested that the greatest photoactivity was located on the chromium centre of the latter. On comparison of the UV/vis spectra for the model compounds at 355nm, the extinction coefficient for $\text{StyCr}(\text{CO})_3$ is much higher than that for $\text{CpMn}(\text{CO})_2(\eta^2\text{-C}_8\text{H}_{14})$. Therefore in a combined system, as in $\text{MeCpMn}(\text{CO})_2(\mu\text{-Sty})\text{Cr}(\text{CO})_3$, the relative photon absorption by the chromium centre will be much higher, compared to the photon absorption by the manganese centre, at this wavelength. Based on this, it is possible that rupture of the manganese-olefin bond occurs on a much smaller scale (relative to photoejection of CO from the chromium centre), but is not detected until the later stages of an experiment, when the

concentration of this cleaved manganese fragment increases. This possibly explains the relatively higher photoactivity observed at the chromium centre over that at the manganese centre, for $\text{MeCpMn(CO)}_2(\mu\text{-Sty})\text{Cr(CO)}_3$.

3.4 REFERENCES

- 1 Parshall, G. W.; *Homogeneous Catalysis*, Wiley-Interscience, New York, 1980, Chapter 3 and references therein.
- 2 (a) Herberhold, M.; *Metal- π -Complexes*, **Vol. 1**: Complexes with Di- and Oligo-olefinic ligands, Elsevier, Amsterdam, 1966; (b) Herberhold, M.; *Metal- π -Complexes*, **Vol. 2**: Complexes with Monoolefinic Ligands, 1974; (c) Strohmeier, W.; *Angew Chem. Internat. Edit.* **3**, 730, 1964.
- 3 Yamamoto, A.; *Organotransition Metal Chemistry: Fundamental Concepts and Applications*, Wiley-Interscience, New York, 1985.
- 4 Von Gustorf, E. K.; Grevels, F. W.; *Topics in Current Chemistry, Forsch. Chem. Forsch.* **13**, 366, 1969.
- 5 Balzani, V.; Carassati, V.; *Photochemistry of Coordination Compounds*, Academic Press, New York, 1970
- 6 Semmelhack, M. F.; *Org. Synth. Today Tomorr., Proc. IUPAC Symp. Org. Synth.*, Mar. 1980, Pergamon Press, Oxford, pp 66-69.
- 7 (a) Trahanovsky, W. S.; Hall, R. A.; *J. Organomet. Chem.* **96**, 71, 1975; (b) Trahanovsky, W. S.; Hall, R. A.; *J. Am. Chem. Soc.* **99**(14), 4850, 1977.
- 8 (a) Nesmeyanov, A. N.; Krivykh, V. V.; Petrovskii, P. V.; Kaganovich, V. S.; Rybinskaya, M. I.; *J. Organomet. Chem.* **93**, C8, 1975; (b) Nesmeyanov, A. N.; Krivykh, V. V.; Petrovskii, P. V.; Kaganovich, V. S.; Rybinskaya, M. I.; *J. Organomet. Chem.* **162**, 323, 1978.
- 9 Trembovler, V. N.; Baranetskaya, N. K.; Fok, N. V.; Zaslavskaya, G. B.; Yavorskii, B. M.; Setkina, V. N.; *J. Organomet. Chem.* **117**, 339,

1976.

- 10 Rausch, M. D.; Moser, G. A.; Zaiko, E. J.; Lipman, A. L. Jr.; *J. Organomet. Chem.* **23**, 185, 1970.
- 11 Knox, G. R.; Leppard, D. G.; Pauson, P. L.; Watts, W. E.; *J. Organomet. Chem.* **34**, 347, 1972.
- 12 Khand, I. U.; Mahaffy, C. A.; Pauson, P. L.; *J. Chem. Res. (S)* 352, 1978; *Chem. Res. (M)* 4454, 1978.
- 13 Creaven, B. S.; George, M. W.; Ginzburg, A. G.; Hughes, C.; Kelly, J. M.; Long, C.; McGrath, I. M.; Pryce, M. T.; *Organometallics*, **12**, 3127, 1993.
- 14 Bitterwolf, T. E.; Lott, K. A.; Rest, A. J.; Mascetti, J.; *J. Organomet. Chem.* **419**, 113, 1991.
- 15 Butler, I. S.; Uhm, H. L.; *Comments Inorg. Chem.* **7**(1), 1, 1988.
- 16 Traylor, T. G.; Stewart, K.; *Organometallics*, **3**, 325, 1984.
- 17 Nasielski, J.; Denisoff, O.; *J. Organomet. Chem.* **102**, 65, 1975.
- 18 Howell, J. A. S.; Burkinshaw, P. M.; *Chem. Rev.* **83**, 557, 1983.
- 19 Grevels, F. W.; Jacke, J.; Klotzbucher, W. E.; Ozcar, S.; Skibbe, V.; *Pure Appl. Chem.* **68**(7), 1017, 1988.
- 20 Fischer, E. O.; Herberhold, M.; *Experientia Suppl.* **9**, 259, 1964.
- 21 (a) Strohmeier, W.; Gerlach, K. L.; *Chem. Ber.* **94**, 398, 1961; (b) Strohmeier, W.; Von Hobe, D.; *Chem. Ber.* **94**, 2031, 1961; (c) Strohmeier, W.; Von Hobe, D.; Schonauer, G.; Laporte, H.; Z. *Naturforsch.* **17b**, 502, 1962.
- 22 Braterman, P. S.; Black, J. D.; *J. Organomet. Chem.* **39**, C3, 1972.
- 23 Angelici, R. J.; Loewen, W.; *Inorg. Chem.* **6**, 682, 1967.
- 24 (a) Collman, J. P.; Hegedus, L. S.; Norton, J. R.; Finke, R. G.;

- Principles and Applications of Organotransition Metal Chemistry*,
University Science Books, Mill Valley, CA, 1987; (b) Lewis, K. E.;
Golden, D. M.; Smith, G. P.; *J. Am. Chem. Soc.* **106**, 3905, 1984.
- 25 Antonova, A. B.; Kovalenko, S. V.; Korniyets, E. D.; Johansson, A.
A.; Struchkov, Y. T.; Ahmedov, A. I.; Yanovsky, A. I.; *J.*
Organomet. Chem. **244**, 35, 1983.
- 26 Herrmann, W. A.; Plank, J.; Ziegler, M. L.; Weidenhammer, K.; *J.*
Am. Chem. Soc. **101**(11), 3133, 1979.
- 27 Klassen, J. K.; Selke, M.; Sorensen, A. A.; Yang, G. K.; *J. Am.*
Chem. Soc. **112**, 1267, 1990.
- 28 Giordano, P. J.; Wrighton, M. S.; *Inorg. Chem.* **16**, 160, 1977.
- 29 Zheng, Y.; Wang, W.; Lin, J.; She, Y.; Fu, K.-J.; *J. Phys. Chem.* **96**,
7650, 1992.
- 30 Creaven, B. S.; Dixon, A. J.; Kelly, J. M.; Long, C.; Poliakoff, M.;
Organometallics, **6**, 2600, 1987.
- 31 Holloway, C. E.; Melnik, M.; *J. Organomet. Chem.* **396**, 129, 1990.
- 32 Andrianov, V. G.; Struchkov, Y. T.; Kolobova, N. E.; Antonova, A.
B.; Obezyuk, N. S.; *J. Organomet. Chem.* **122**, C33, 1976.
- 33 Kelly, J. M.; Long, C.; *J. Organomet. Chem.* **231**, C9, 1982.
- 34 Wrighton, M. S.; Haverty, J. L.; *Z. Naturforsch.* **30b**, 254, 1975.
- 35 Gilbert, A.; Kelly, J. M.; Budzwait, M.; Von Gustorf, E. K.; *Z.*
Naturforsch. **31b**, 1091, 1976.
- 36 Farrell, G. *Ph.D. Thesis*, Dublin City University, 1992.
- 37 Lees, A. J.; Adamson, A.; *Inorg. Chem.* **20**, 4381, 1981.
- 38 Dobson, G.R.; Spradling, M. D.; *Inorg. Chem.* **29**, 880, 1990.
- 39 Zhang, S.; Dobson, G. R.; *Inorg. Chim. Acta* **165**, L11, 1989.

- 40 Geoffrey, M. L.; Wrighton, M. S.; *Organometallic Photochemistry*, Academic Press, New York, 1979.
- 41 Crocock, E. B.; Long, C.; Howie, R. A.; in press.
- 42 Crocock, E. B.; *Ph. D. Thesis*, Dublin City University, 1992.
- 43 Creaven, B. S.; *Ph. D. Thesis*, Dublin City University, 1990.
- 44 Hepp, A. F.; Paw Blaha, J.; Lewis, C.; Wrighton, M. S.;
Organometallics, **3**, 174, 1984.
- 45 Black, J. D.; Boylan, M. J.; Braterman, P. S.; *J. Chem. Soc., Dalton Trans.* 673, 1981.
- 46 Brookhart, M.; Green, M. L. H.; *J. Organomet. Chem.* **250**, 395, 1983.
- 47 Kaim, W.; Gross, R.; *Inorg. Chem.* **25**, 498, 1986.
- 48 Gross-Lannert, R.; Kaim, W.; Lechner, U.; Roth, E.; Volger, C. Z.;
Anorg. Allg. Chem. **47**, 579, 1989.
- 49 Pittman, C. U. Jr.; Grube, P. L.; Ayers, O. E.; McManus, S. P.;
Rausch, M. D.; Moser, G. A.; *J. Polym. Sci. A-1*, **10**, 379, 1972.
- 50 Margerison, D.; East, G. C.; *Introduction to Polymer Chemistry*, Pergamon Press, Oxford, 1967.
- 51 Pittman, C. U. Jr.; Marlin, G. V.; Rounsefell, T. D.; *Macromolecules*, **6**(1), 1, 1973.
- 52 Hill, R. H.; Wrighton, M. S.; *Organometallics*, **6**, 632, 1987.
- 53 Geoffroy, G. L.; Wrighton, M. S.; *Organometallic Photochemistry*, Academic Press, New York, 1979.

Chapter 4

The Crystal and Molecular Structure of $\text{MeCpMn(CO)}_2(\mu\text{-Sty})\text{Cr(CO)}_3$.

4.1 Introduction.

X-ray crystallography is a technique used in determining the structure of complexes. The technique is based on the diffraction patterns of X-rays produced by interaction with matter. When X-rays strike a material, the resultant wave is diffracted in several directions. Each diffracted wave has a certain phase and amplitude with respect to the incident X-rays. In a regular repeating system such as a crystal, diffraction patterns are produced, from which structural information may be obtained [1].

We have determined the crystal and molecular structure of the manganese-chromium dinuclear complex $\text{MeCpMn(CO)}_2(\mu\text{-Sty})\text{Cr(CO)}_3$. The structure of this complex was determined because, firstly, we wanted to prove the existence of the μ -styrene bridge between the chromium and manganese centres. Secondly, to see if rotation about the μ -styrene bridge was possible, and perhaps bring the metal centres closer together. This is of interest because, if one end of the dinuclear complex can possibly rotate with respect to the other end, one may get intramolecular cyclisation (between the chromium centre and the manganese centre) on photoejection of a CO molecule. An intermolecular reaction is more likely in a rigid structure.

4.2 Data collection for $\text{MeCpMn(CO)}_2(\mu\text{-Sty})\text{Cr(CO)}_3$.

The manganese-chromium dinuclear complex $\text{MeCpMn(CO)}_2(\mu\text{-Sty})\text{Cr(CO)}_3$ was synthesised by photochemical displacement of a CO molecule from MeCpMn(CO)_3 in THF, and subsequent coordination to the olefinic group of StyCr(CO)_3 (see Chapter 5). Collection of the crystallographic diffraction data was carried out at the University of Aberdeen [2].

A crystal of $\text{MeCpMn(CO)}_2(\mu\text{-Sty})\text{Cr(CO)}_3$, (0.2 x 0.5 x 0.5mm) was selected for crystal diffraction analysis on a Nicolet P3 four circle diffractometer. The crystallographic data was collected, and the structure was solved using the Patterson heavy atom method. The program attempts to find the heavy atoms, and follows this up with a partial structure expansion to find the remaining non-hydrogen atoms. The program proposes a structure which may be refined.

Using $\text{MoK}\alpha$ radiation ($\lambda = 0.71069\text{\AA}$), 3518 reflections were measured of which 96 were rejected and 3167 were considered observed, having $I < 2\sigma(I)$. The data was obtained by Ω scan for 2θ in the range $0 - 60^\circ$. Scan rates were in the range 1.0 to $29.3 \text{ deg } \omega \text{ min}^{-1}$. The index ranges were 0 to 8 , 0 to 27 and -11 to 11 for h , k , and l respectively. Internal standards were 3 , 0 , 2 and 1 , 5 , -3 stable to ± 2.41 and 1.81 ($1 \times \sigma$) % response. The space group $\text{P2}_1/c$ was established, and $Z = 4$.

The structure was solved by the Patterson heavy atom method with partial structure expansion to find all non-hydrogen atoms using SHELXS-86 [3]. The atomic coordinates were refined with full matrix least squares refinement using SHELX-76 [4]. Hydrogen atoms were located in their

calculated positions and refined with respect to the carbon atoms to which they were attached. Standard isothermal parameters (U_{iso}) were used; 0.5\AA^2 for non-aromatic hydrogens and 0.13\AA^2 for aromatic hydrogens. During refinement, the methyl group on the cyclopentadienyl ring was treated as a rigid rotor. The crystals are monoclinic with unit cell dimensions; $a = 7.281(4)\text{\AA}$, $b = 23.637(14)\text{\AA}$, $c = 10.502(5)\text{\AA}$, $\beta = 99.19^\circ$, $V = 1784.20\text{\AA}^3$, $d(\text{calcd}) = 1.55(5)\text{ g/cm}^3$, $d(\text{meas}) = 1.6\text{ g/cm}^3$, $F(000) = 872$. R values were calculated to be $R = 0.0457$ and $R_w = 0.0442$ where $\{w = 1.5694/(\sigma(2F) + 0.000534F^2)\}$. Atomic scattering factors for both manganese and chromium were taken from the International Tables for X-ray Crystallography [5].

Density measurements were carried out using the gradient tube method [6]. The molecular structure can be seen in Figure 4.2.1 with atom numbering included. Figure 4.2.2 shows a SCHAKAL [7] representation of the unit cell. Figure 4.2.3 is a projection of the molecular structure onto the space-filled model. Selected bond lengths, and a complete list of bond angles, are given in Table 4.2.1 and Table 4.2.2 respectively. The final atomic coordinates for all non-hydrogen atoms are given in Table 4.2.3, and those for the hydrogen atoms in Table 4.2.4. The anisotropic temperature factors for the non-hydrogen atoms are listed in Table 4.2.5.

Figure 4.2.1: SCHAKAL drawings of the molecular structure of $\text{MeCpMn(CO)}_2(\mu\text{-Sty})\text{Cr(CO)}_3$.

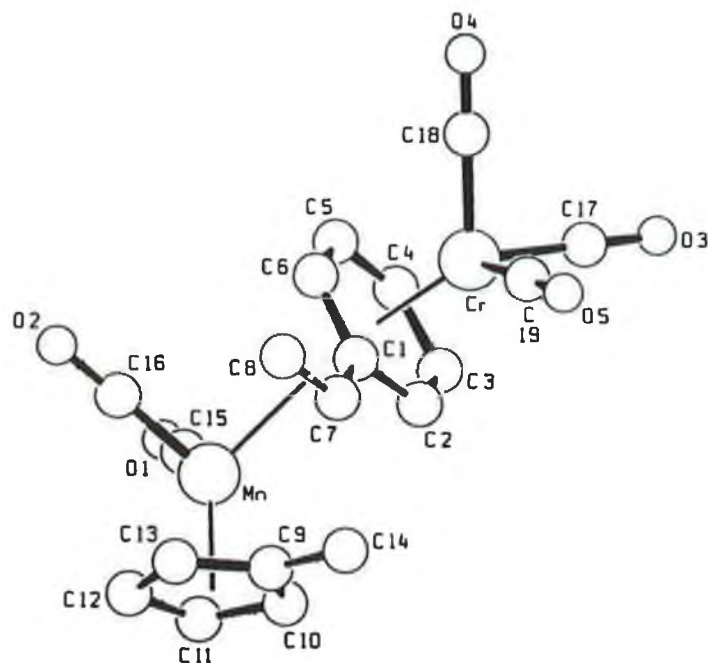
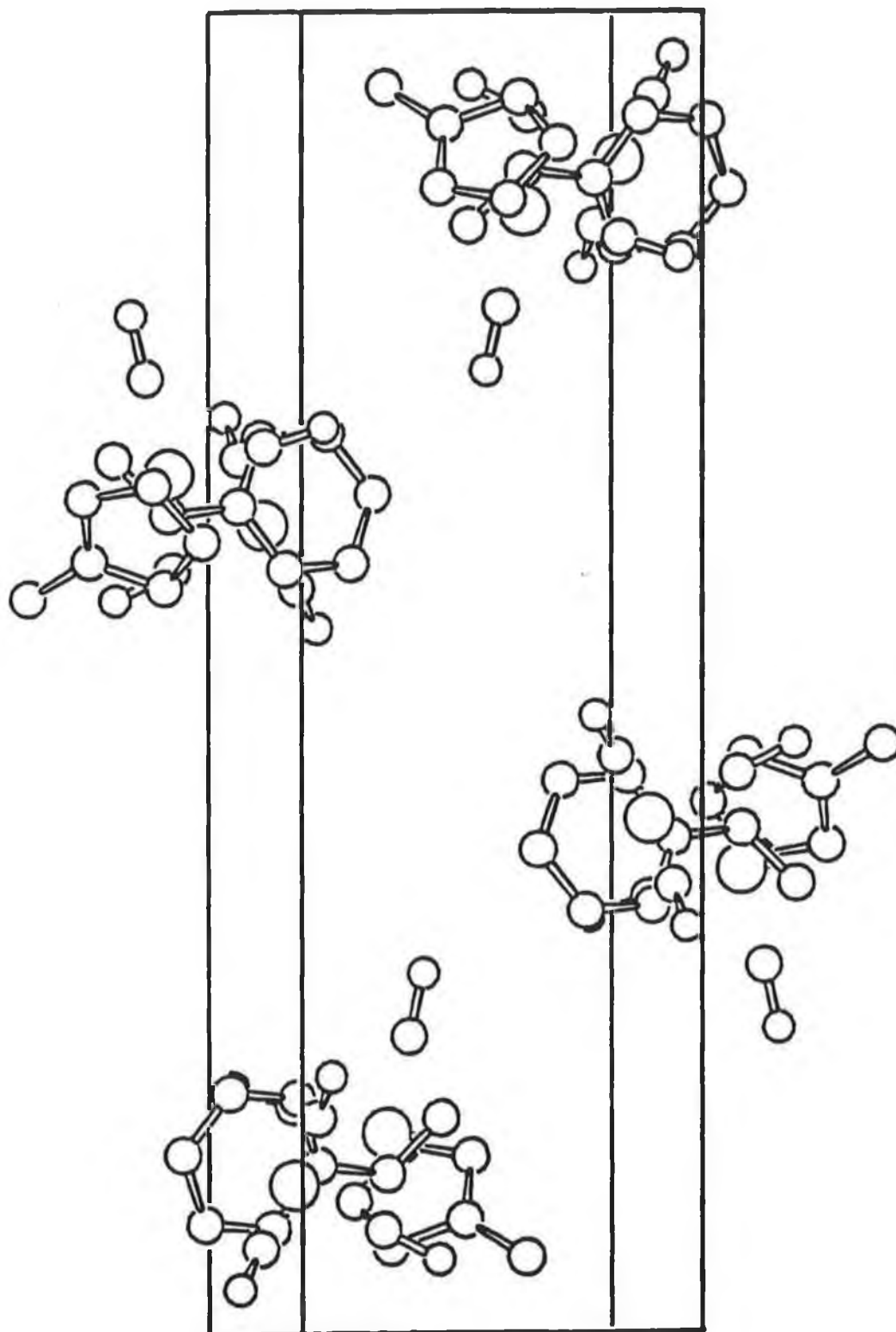


Figure 4.2.2: A SCHAKAL representation of the unit cell of $\text{MeCpMn(CO)}_2(\mu\text{-Sty})\text{Cr(CO)}_3$, (Metal-to-Carbon bonds omitted as are Hydrogen atoms for clarity).



4.3 Molecular structure of $\text{MeCpMn(CO)}_2(\mu\text{-Sty})\text{Cr(CO)}_3$.

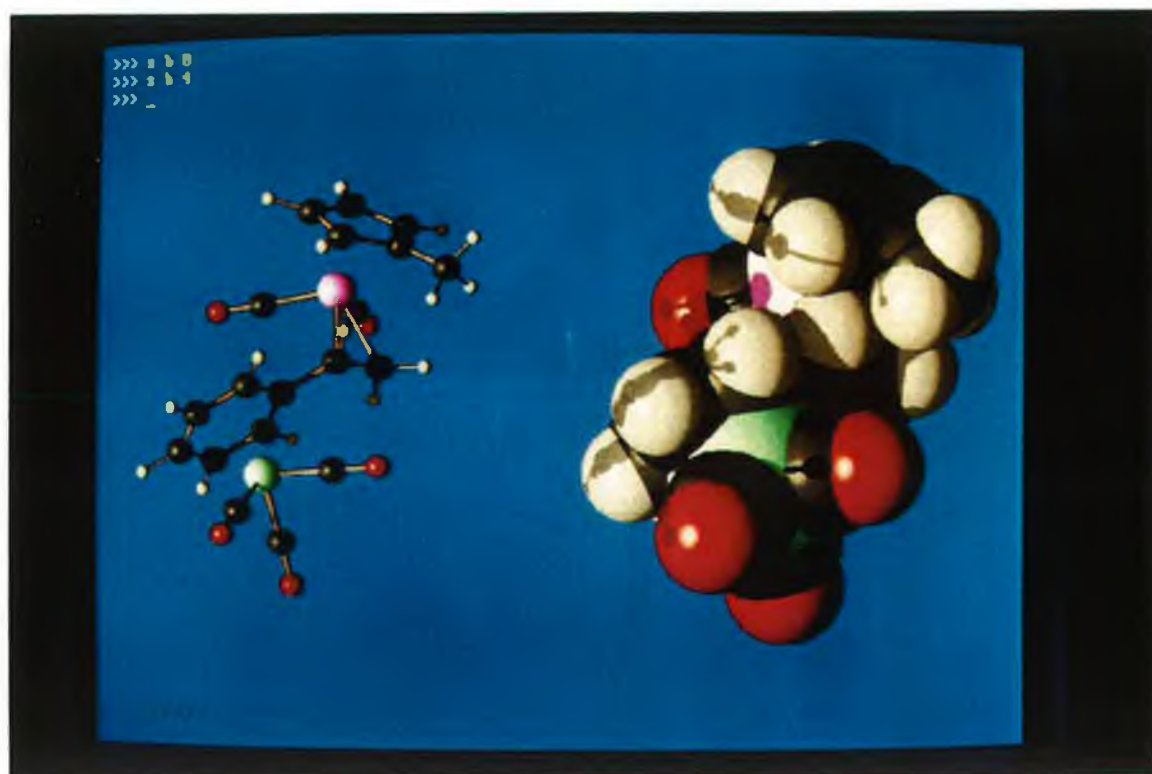
The StyCr(CO)_3 ligand is coordinated uniquely *via* the olefin group attached to the aromatic ring. The complex contains one molecule per asymmetric unit as represented in Figure 4.2.1. The distance between the carbon atoms of the double bond and the manganese atom are 2.147(5)Å and 2.162(4)Å. This is similar to the values 2.145(5)Å and 2.168(6)Å, for $\text{Cp(CO)}_2\text{Mn(PhCH=CHP(O)(OEt)}_2)$ obtained by Antonova *et al.* [8]. These values are shorter than those reported for other η^2 complexes; 1.976(6)Å and 2.242(6)Å for the η^2 -anthronylketene analogue [9]; 2.193(2)Å and 2.201(3)Å for the η^2 -*cis*-cyclooctene complex [10]. The η^2 coordinated ligands with inequivalent bond distances are as a result of large substituents on one of the vinylic carbons. In our case the arenechromium unit on C(7) results in the longer bond length. The carbon-carbon double bond length is 1.407(7)Å, which is significantly longer than that for the free ligand (1.30(6)Å [11]), or the average length of 1.34Å [3]. The corresponding value obtained for the η^2 -*cis*-cyclooctene complex was 1.388(4)Å. The longer bond lengths are as a result of stronger interaction between the central metal atom and the ligand.

The bond angle between the metal and the olefinic ligand C(7)-Mn-C(8) is 38.1(2)°, while that for η^2 -*cis*-cyclooctene is 36.7(1)° [10], methylvinylketone 37.5(3)° [12] and anthronylketene 39.5(2)° [9]. The more acute bond angle is also an indicator of the weakness of the interaction.

The Mn-C(CO) bond distances 1.768(6) and 1.792(6)Å are typical, and are similar to 1.772(2)Å, 1.781(2)Å and 1.786(2)Å reported by Fitzpatrick *et*

al. for CpMn(CO)_3 [13]. The average Mn-C(Cp) bond length is 2.156(5)Å, compared to 2.149(6)Å for the *cis*-cyclooctene analogue. The average C-C bond length in the Cp ring is 1.409(8)Å, and is similar to the corresponding values in the *cis*-cyclooctene (1.394(6)Å) and methylvinylketone (1.393(16)Å) complexes. The C(9)-C(14) bond length is 1.499(7)Å in the title compound, which is close to that for the C(Cp)-C(methyl) bond in $\text{MeCpMn(CO)}_2(\eta^2\text{-C}_8\text{H}_{14})$ (1.513(6)Å) [10].

Figure 4.2.3: Projection of the molecular structure of $\text{MeCpMn(CO)}_2(\mu\text{-Sty})\text{Cr(CO)}_3$ onto a space-filled diagram.



Interestingly, the methyl group on the Cp ring is *trans*- to a carbonyl in $\text{MeCpMn(CO)}_2(\mu\text{-Sty})\text{Cr(CO)}_3$, whereas it is *cis*- to a carbonyl in $\text{MeCpMn(CO)}_2(\eta^2\text{-C}_8\text{H}_{14})$. Frequently, when the coordinated ligand is a good π^* acceptor, the methyl substituent on the Cp ring orients itself *cis*- to a carbonyl ligand (or *trans*- to the unique ligand). The reason for it assuming a position *trans*- to a carbonyl in the dinuclear complex is most likely electronic in origin. This orientation is rather unusual as the (arene) Cr(CO)_3 moiety on the unique ligand is electron withdrawing. This should have the effect of reducing electron density on the olefin, now a good π^* acceptor, to produce the complex with the methyl group *cis*- to a carbonyl. However, the electron withdrawing nature of the (arene) Cr(CO)_3 group is not reflected here. The absence of this effect was also observed in the synthesis of some cobalt derivatives, using StyCr(CO)_3 as a directing agent [14]. The methyl group is also located out from the mean plane of the Cp ring. The Mn-C(9)-C(14) bond angle is $129.8(4)^\circ$, in agreement with that quoted for the Mn-C(Cp)-C(methyl) bond angle of $128.7(4)^\circ$ in $\text{MeCpMn(CO)}_2(\text{NC}_6\text{H}_5)$, where the σ -donor pyridine ligand is also *cis*- to the methyl group [15].

The crystal structure of StyCr(CO)_3 [11] revealed a disorder of orientation of the styrene about the $-\text{Cr(CO)}_3$ moiety. Two 'fractional' ligands existed and some of the atoms were too close together for successful refinement. The parameters indicated (†) were adjusted in a semi-rigid treatment of the 'fractional' ligands in least squares refinement. Coordination of StyCr(CO)_3 to the MeCpMn(CO)_2 photofragment, *via* the μ -styrene bridge, effectively prevented this disorder. Rotation of one end of the molecule with respect to

the other was not observed. This supports the idea of an intermolecular reaction when the molecule is coordinatively unsaturated (as observed in Section 3.3.3.4).

In the dinuclear complex, the average Cr-C(ring) bond length is 2.226(5)Å, in good agreement with 2.215(4)Å[†] in free StyCr(CO)₃. The average Cr-C(CO) bond length is 1.829(6)Å. The C(1)-C(7) bond length is 1.478(7)Å, unaffected from that in the free ligand (1.477(6)Å)[†]. The C(1)-C(7)-C(8) bond angle the dinuclear complex is 125.1(5)°. The vinylic carbon C(7) is out of the plane of the arene ring. The angle between the perpendiculars of the two aromatic ring planes is 68.02°. All other bond distances and angles are in the normal ranges.

Table 4.2.1: Selected bond lengths (Å) for $\text{MeCpMn(CO)}_2(\mu\text{-Sty})\text{Cr(CO)}_3$.

C1 —Cr	2.268(4)	C2 —Cr	2.221(4)
C3 —Cr	2.211(5)	C4 —Cr	2.221(5)
C5 —Cr	2.208(5)	C6 —Cr	2.231(4)
C17 —Cr	1.823(5)	C18 —Cr	1.840(5)
C19 —Cr	1.825(6)	C7 —Mn	2.162(4)
C8 —Mn	2.147(5)	C9 —Mn	2.202(5)
C10 —Mn	2.168(5)	C11 —Mn	2.137(5)
C12 —Mn	2.125(5)	C13 —Mn	2.151(5)
C15 —Mn	1.792(6)	C16 —Mn	1.768(6)
C2 —C1	1.420(7)	C6 —C1	1.407(6)
C7 —C1	1.478(7)	C3 —C2	1.391(7)
C4 —C3	1.416(7)	C5 —C4	1.388(7)
C6 —C5	1.405(6)	C8 —C7	1.407(7)
C10 —C9	1.435(7)	C13 —C9	1.397(7)
C14 —C9	1.499(7)	C11 —C10	1.397(7)
C12 —C11	1.409(8)	C13 —C12	1.419(8)
O1 —C15	1.140(6)	O2 —C16	1.162(6)
O3 —C17	1.154(5)	O4 —C18	1.153(5)
O5 —C19	1.157(6)		

Table 4.2.2: A complete list of bond angles ($^{\circ}$) for $\text{MeCpMn(CO)}_2(\mu\text{-Sty})\text{Cr(CO)}_3$. (continued overleaf)

C2 -Cr -C1	36.8(2)	C3 -Cr -C1	66.3(2)
C3 -Cr -C2	36.6(2)	C4 -Cr -C1	78.2(2)
C4 -Cr -C2	66.3(2)	C4 -Cr -C3	37.3(2)
C5 -Cr -C1	65.9(2)	C5 -Cr -C2	77.9(2)
C5 -Cr -C3	66.4(2)	C5 -Cr -C4	36.5(2)
C6 -Cr -C1	36.4(2)	C6 -Cr -C2	66.1(2)
C6 -Cr -C3	78.5(2)	C6 -Cr -C4	66.3(2)
C6 -Cr -C5	36.9(2)	C17 -Cr -C1	147.7(2)
C17 -Cr -C2	111.6(2)	C17 -Cr -C3	89.6(2)
C17 -Cr -C4	95.9(2)	C17 -Cr -C5	125.3(2)
C17 -Cr -C6	161.7(2)	C18 -Cr -C1	123.9(2)
C18 -Cr -C2	159.6(2)	C18 -Cr -C3	145.1(2)
C18 -Cr -C4	108.4(2)	C18 -Cr -C5	86.8(2)
C18 -Cr -C6	93.6(2)	C18 -Cr -C17	88.2(2)
C19 -Cr -C1	88.2(2)	C19 -Cr -C2	94.3(2)
C19 -Cr -C3	123.8(2)	C19 -Cr -C4	160.3(2)
C19 -Cr -C5	146.4(2)	C19 -Cr -C6	110.1(2)
C19 -Cr -C17	88.0(2)	C19 -Cr -C18	91.0(2)
C8 -Mn -C7	38.1(2)	C9 -Mn -C7	91.5(2)
C9 -Mn -C8	92.0(2)	C10 -Mn -C7	90.2(2)
C10 -Mn -C8	113.4(2)	C10 -Mn -C9	38.3(2)
C11 -Mn -C7	122.2(2)	C11 -Mn -C8	151.3(2)
C11 -Mn -C9	64.0(2)	C11 -Mn -C10	37.9(2)
C12 -Mn -C7	153.0(2)	C12 -Mn -C8	144.7(2)
C12 -Mn -C9	63.8(2)	C12 -Mn -C10	63.8(2)
C12 -Mn -C11	38.6(2)	C13 -Mn -C7	124.3(2)
C13 -Mn -C8	106.7(2)	C13 -Mn -C9	37.4(2)
C13 -Mn -C10	63.5(2)	C13 -Mn -C11	64.5(2)
C13 -Mn -C12	38.7(2)	C15 -Mn -C7	89.8(2)
C15 -Mn -C8	108.4(2)	C15 -Mn -C9	147.5(2)
C15 -Mn -C10	109.2(2)	C15 -Mn -C11	88.1(2)
C15 -Mn -C12	105.2(2)	C15 -Mn -C13	143.8(2)
C16 -Mn -C7	109.2(2)	C16 -Mn -C8	77.0(2)
C16 -Mn -C9	122.3(2)	C16 -Mn -C10	154.6(2)

Table 4.2.2 (cont'd): A complete list of bond angles ($^{\circ}$) for $\text{MeCpMn(CO)}_2(\mu\text{-Sty})\text{Cr(CO)}_3$.

C16 -Mn -C11	128.4(2)	C16 -Mn -C12	94.0(2)
C16 -Mn -C13	91.5(2)	C16 -Mn -C15	87.7(2)
C2 -C1 -Cr	69.8(2)	C6 -C1 -Cr	70.3(2)
C6 -C1 -C2	118.3(4)	C7 -C1 -Cr	129.8(3)
C7 -C1 -C2	118.6(5)	C7 -C1 -C6	123.0(5)
C1 -C2 -Cr	73.4(3)	C3 -C2 -Cr	71.3(3)
C3 -C2 -C1	121.2(5)	C2 -C3 -Cr	72.1(3)
C4 -C3 -Cr	71.8(3)	C4 -C3 -C2	119.8(5)
C3 -C4 -Cr	71.0(3)	C5 -C4 -Cr	71.2(3)
C5 -C4 -C3	119.3(5)	C4 -C5 -Cr	72.2(3)
C6 -C5 -Cr	72.4(3)	C6 -C5 -C4	121.3(5)
C1 -C6 -Cr	73.2(3)	C5 -C6 -Cr	70.7(3)
C5 -C6 -C1	120.1(5)	C1 -C7 -Mn	115.8(3)
C8 -C7 -Mn	70.4(3)	C8 -C7 -C1	125.1(5)
C7 -C8 -Mn	71.5(3)	C10 -C9 -Mn	69.5(3)
C13 -C9 -Mn	69.3(3)	C13 -C9 -C10	106.8(5)
C14 -C9 -Mn	129.8(4)	C14 -C9 -C10	125.5(5)
C14 -C9 -C13	127.5(5)	C9 -C10 -Mn	72.1(3)
C11 -C10 -Mn	69.9(3)	C11 -C10 -C9	108.7(5)
C10 -C11 -Mn	72.3(3)	C12 -C11 -Mn	70.3(3)
C12 -C11 -C10	107.8(5)	C11 -C12 -Mn	71.1(3)
C13 -C12 -Mn	71.6(3)	C13 -C12 -C11	107.9(5)
C9 -C13 -Mn	73.3(3)	C12 -C13 -Mn	69.6(3)
C12 -C13 -C9	108.7(5)	O1 -C15 -Mn	176.1(4)
O2 -C16 -Mn	178.7(5)	O3 -C17 -Cr	179.5(4)
O4 -C18 -Cr	178.2(5)	O5 -C19 -Cr	179.1(5)

Table 4.2.3: Atomic coordinates $\times 10^4$ for non-hydrogen atoms with e.s.d.'s in parentheses for $\text{MeCpMn(CO)}_2(\mu\text{-Sty})\text{Cr(CO)}_3$. $U_{\text{eq}} \times 10^3$.

$$\{U_{\text{eq}} = (1/3)\Sigma_i\Sigma_j U_{ij}a_i^* \cdot a_j^* \cdot a_i \cdot a_j\}.$$

	x/a	y/b	z/c	U_{eq}
Cr	706(1)	1120(1)	3905(1)	33(1)
Mn	4142(1)	1508(1)	8708(1)	36(1)
C1	1801(7)	1265(2)	6025(4)	38(1)
C2	607(8)	787(2)	5871(4)	44(1)
C3	-1202(8)	826(2)	5206(4)	47(1)
C4	-1871(7)	1349(2)	4665(5)	48(1)
C5	-692(7)	1814(2)	4779(4)	43(1)
C6	1138(7)	1778(2)	5445(4)	39(1)
C7	3705(7)	1197(2)	6747(4)	46(1)
C8	5089(8)	1618(3)	6890(4)	59(2)
C9	6242(8)	851(2)	9315(4)	46(1)
C10	4418(8)	648(2)	9428(5)	54(2)
C11	3672(9)	993(3)	10297(5)	60(2)
C12	4994(9)	1415(3)	10729(4)	61(2)
C13	6564(8)	1327(2)	10108(4)	53(1)
C14	7577(9)	569(3)	8568(5)	67(2)
C15	1746(8)	1715(2)	8521(4)	45(1)
C16	4712(7)	2236(2)	8708(5)	53(1)
C17	-415(7)	639(2)	2661(4)	41(1)
C18	1016(8)	1622(2)	2617(5)	46(1)
C19	2912(8)	776(2)	3769(4)	46(1)
O1	243(5)	1860(2)	8469(4)	62(1)
O2	5077(6)	2715(2)	8732(5)	86(1)
O3	-1112(6)	332(2)	1876(3)	66(1)
O4	1162(6)	1937(2)	1801(4)	72(1)
O5	4309(6)	555(2)	3699(4)	77(1)

Table 4.2.4: Coordinates $\times 10^4$ for hydrogen atoms in $\text{MeCpMn(CO)}_2(\mu\text{-Sty})\text{Cr(CO)}_3$.

	x/a	y/b	z/c
H2	1108	386	6278
H3	-2090	457	5103
H4	-3284	1387	4169
H5	-1184	2212	4346
H6	2033	2145	5517
H7	4059	794	7203
H8a	6495	1491	6819
H8b	4778	2013	6385
H10	3731	288	8926
H11	2328	945	10594
H12	4834	1748	11406
H13	7804	1585	10229
H14a	6969	378	7665
H14b	8483	268	9131
H14c	8370	938	8381

Table 4.2.5: Anisotropic temperature factors $\times 10^3$ with e.s.d.'s in parentheses for $\text{MeCpMn(CO)}_2(\mu\text{-Sty})\text{Cr(CO)}_3$.

	U11	U22	U33	U23	U13	U12
Cr	37(1)	32(1)	28(1)	0(1)	3(1)	-2(1)
Mn	39(1)	40(1)	27(1)	-1(1)	3(1)	-2(1)
C1	47(3)	41(3)	24(2)	-6(2)	5(2)	5(2)
C2	62(4)	40(3)	31(2)	2(2)	13(2)	0(3)
C3	52(3)	50(3)	41(3)	-3(2)	19(3)	-11(3)
C4	39(3)	55(3)	51(3)	-3(3)	12(2)	2(3)
C5	46(3)	41(3)	42(3)	-3(2)	6(2)	8(2)
C6	42(3)	37(3)	37(2)	-10(2)	5(2)	-1(2)
C7	55(3)	57(3)	24(2)	-5(2)	3(2)	13(3)
C8	47(3)	101(5)	32(3)	9(3)	10(2)	-4(3)
C9	52(3)	48(3)	35(2)	2(2)	2(2)	10(3)
C10	65(4)	47(3)	47(3)	13(3)	1(3)	2(3)
C11	70(4)	67(4)	49(3)	19(3)	25(3)	10(3)
C12	80(4)	74(4)	28(3)	2(3)	4(3)	19(4)
C13	53(4)	61(4)	40(3)	-1(3)	-13(3)	8(3)
C14	70(4)	69(4)	63(4)	2(3)	15(3)	21(3)
C15	52(4)	46(3)	36(3)	-8(2)	9(2)	-7(3)
C16	42(3)	55(4)	57(3)	-3(3)	-4(3)	0(3)
C17	47(3)	40(3)	35(2)	1(2)	0(2)	-3(2)
C18	58(4)	39(3)	41(3)	-5(2)	12(2)	-2(3)
C19	47(3)	50(3)	38(3)	-6(2)	-2(2)	-3(3)
O1	43(2)	76(3)	67(3)	-4(2)	12(2)	10(2)
O2	81(3)	51(3)	119(4)	0(3)	-4(3)	-24(2)
O3	85(3)	55(3)	48(2)	-11(2)	-17(2)	-9(2)
O4	106(4)	59(3)	55(2)	20(2)	28(2)	-4(2)
O5	49(3)	98(3)	82(3)	-19(3)	6(2)	15(2)

4.4 REFERENCES

- 1 Woolfson, M. M.; *An Introduction to X-Ray Crystallography*, Cambridge University Press, Cambridge, 1970.
- 2 This work was carried out by Dr. R. A. Howie, University of Aberdeen, Meston Walk, Aberdeen, Scotland.
- 3 Sheldrick, G. M.; *Acta Cryst.* **A46**, 467, 1990.
- 4 Sheldrick, G. M.; SHELX 76, Program for Crystal Structure Determination (1976), University of Cambridge, England.
- 5 *International Tables for X-Ray Crystallography*, Reidel D. (Publishing Company), Dordrecht, Netherlands. **Vol. IV**, 1974.
- 6 (a) *International Tables for X-Ray Crystallography*, Reidel D. (Publishing Company), Dordrecht, Netherlands. **Vol. III**, 1985; (b) Low, B. W.; Richards, F. M.; *J. Am. Chem. Soc.* **74**, 1660, 1952.
- 7 Keller, E. SCHAKAL 88, Program for Graphical Representation of Molecular and Crystallographic Models, University of Freiburg, Germany, 1988.
- 8 Antonova, A. B.; Kovalenko, S. V.; Korniyets, E. D.; Johansson, A. A.; Struchkov, Y. T.; Ahmedov, A. J.; Yanovsky, A. I.; *J. Organomet. Chem.* **244**, 35, 1983.
- 9 Herrmann, W. A.; Plank, J.; Ziegler, M. L.; Weidenhammer, K.; *J. Am. Chem. Soc.* **101**(11), 3133, 1979.
- 10 Crocock, B.; Long, C.; Howie, R. A.; in press.
- 11 Brown, G. M.; Frazier, C. C.; *Acta Cryst.* **C45**, 1158, 1989.
- 12 Le Borgne, G.; Gentric, E.; Grandjean, D.; *Acta Cryst.* **B31**, 2824, 1975.

- 13 Fitzpatrick, P. J.; Le Page, Y.; Sedman, J.; Butler, I. S.; *Inorg. Chem.* **20**, 2852, 1981.
- 14 Khand, I. U.; Mahaffy, C. A.; Pauson, P. L.; *J. Chem. Res. (S)* 352, 1978; *Chem. Res. (M)* 4454, 1978.
- 15 Crocock, B.; Long, C.; Howie, R. A.; *Acta Cryst.* **C48**, 1004, 1992.

Chapter 5

Experimental Section.

5.1 Materials.

Metal hexacarbonyls, MeCpMn(CO)_3 , CpMn(CO)_3 , (Riedel de-Haen or Strem), triphenylphosphine, di-*n*-butyl ether, *cis*-cyclooctene, toluene Sure/seal) (Aldrich), naphthalene and sodium metal (BDH), were used as supplied. Tetrahydrofuran (BDH), was heated to reflux over lithium aluminium hydride, distilled under argon, and stored over calcium hydride. The monomers; styrene, methylmethacrylate, and α -methylstyrene (BDH) were washed according to literature procedures [1] to remove inhibitors, and stored at -5°C . Azobisisobutyronitrile (AIBN) (Merck) was recrystallised from methanol before use. Cyclohexane, spectroscopic grade (Aldrich) was used as supplied. Pyridine, Gold label (Aldrich) was stored over type 4A molecular sieve before use. Solvents for chromatography and recrystallisation were reagent grade, and were argon degassed before use. Argon and carbon monoxide (IIG) were used as supplied. Nitrogen (oxygen free) or argon gases (IIG or Air Products) were used as supplied. Nuclear magnetic resonance solvents (Aldrich), 99.9 atom per cent were used as supplied.

5.2 Equipment and Procedures.

5.2.1: Infrared, UV/visible. and Proton Magnetic Resonance Spectral Investigations.

Infrared spectra were recorded on a Nicolet 205 FTIR spectrometer. The wavenumber accuracy was $\pm 4\text{cm}^{-1}$. Polymers were cast as films on sodium chloride plates from chloroform solution and their spectra recorded. In photolysis experiments with IR monitoring, argon degassed solutions

(0.2mm sodium chloride cells) were irradiated using an Oriel 100 watt high pressure mercury lamp, and changes in the carbonyl stretching region ($2200\text{-}1700\text{cm}^{-1}$) were monitored. A Corning filter ($> 80\%$ transmission at $360 < \lambda < 370\text{nm}$) was placed between the irradiation source and the sample. UV/vis spectra were recorded on a Hewlett Packard 8452A Photodiode array spectrophotometer. Peak positions were accurate to $\pm 2\text{nm}$. Proton magnetic resonance spectra were recorded on a Bruker model AC 400 MHz spectrometer.

5.2.2: Gel Permeation Chromatography.

Gel permeation chromatography (GPC) is a technique used for the characterisation of polymer molecular weight [2]. Separation is based on molecular size, determined by the ability of the molecules to penetrate the pore structure of the gel separation media. Calibration curves are prepared by injecting polymer standards of known molecular weight range, and plotting $\log(\text{molecular weight})$ versus retention volume. A polymer sample is then injected and from the retention volume its molecular weight may be determined. The method of Universal Calibration was used [2a], which allows for the determination of copolymer molecular weights of similar composition to the standards.

The separation column used was a PL-GEL ($10\mu\text{m}$ MIXED $300 \times 7.5\text{mm}$) with a PL-GEL ($10\mu\text{m}$ 100\AA $50 \times 7.5\text{mm}$) pre-column. A $20\mu\text{l}$ injection loop was used. A Waters R401 Differential Refractometer detector (interfaced to a BBC microcomputer) was used. This detector was very sensitive to changes in temperature, flow rate and mobile phase. THF (reagent grade) was used as the mobile phase, and was degassed by filtering

through 0.45 μ m Millipore filters and placing in an ultrasound bath for 10 minutes before use. Toluene was used as the internal standard to correct for deviations in the flow rate. The output from the detector was analysed using GPC software (Polymer Laboratories Ltd.). The calibration curve obtained for the polystyrene standards is shown in Figure 5.2.1 with the corresponding data in Table 5.2.1. Standards and samples were prepared in THF at concentrations of 0.2% w/v. The average molecular weight distribution and the root-mean-square (rms) end-to-end distances for the various homopolymers and copolymers are tabulated in Tables 5.2.2 and 5.2.3 respectively. Also included are the weights of the various monomers and AIBN used in their syntheses.

Figure 5.2.1: GPC calibration curve for polystyrene standards.

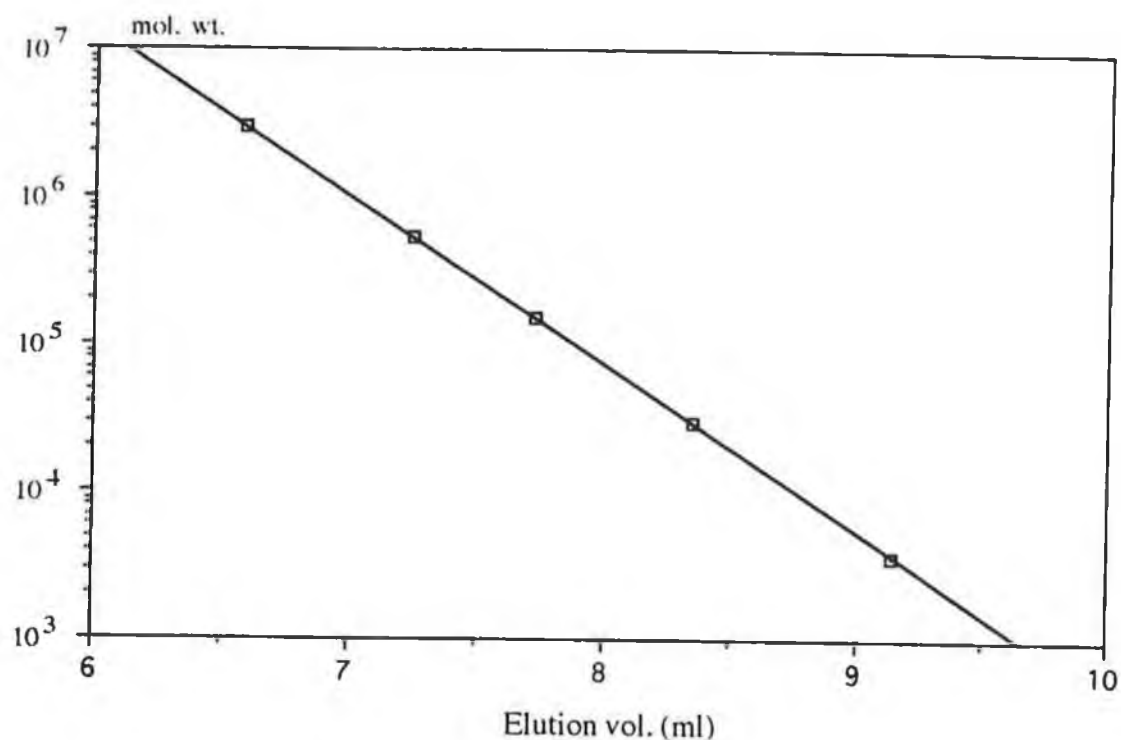


Table 5.2.1: Data for polystyrene calibration curve.

Elution vol. (cm ³)	Molecular Weight (amu)		
	Standards	Linear Fit	
		Calculated	Ratio
9.14	3.250	3709	0.88
8.35	34,500	29251	1.18
7.72	170,000	151815	1.12
7.24	470,000	532367	0.88
6.59	2,850,000	2911326	0.98

Table 5.2.2: Experimental data for the synthesis and rms end-to-end distance determination for the various homopolymers.

Pol. (% AIBN)	Monomer (g)	Rxn. time (hr)	Mw/Mn	rms Dist. (Å)
PS (5)	10.20	2	8.73	63
PS (4)	10.10	2	7.13	94
PS (3)	10.10	2	4.89	113
PS (2)	10.00	2	3.93	236
PS (1)	10.10	2	2.84	283
PMMA (5)	5.36	2	2.96	96
PMMA (3)	5.21	2	2.14	173
PMMA (2)	5.29	2	1.83	258
PMMA (1)	5.21	2	1.61	313
P- α -MS	5.50	0.17	1.36	85.4
P- α -MS	5.52	0.5	1.49	108.4
P- α -MS	5.50	1	1.59	145.9
P- α -MS	5.50	2.5	1.26	167
P- α -MS	5.50	12	1.34	179.4
P- α -MS	5.30	22	1.30	207.4

Table 5.2.3: Experimental data for the synthesis and rms end-to-end distance determination for the various copolymers (1% AIBN).

(S:Monomer)	Styrene (g)	Comonomer (g)	Mw/Mn	rms Dist. (Å)
5;1	3.05	1.72 (I)	2.11	114
10;1	3.05	0.86 (I)	3.22	129
20;1	2.09	0.29 (I)	3.90	200
30;1	3.40	0.31 (I)	3.28	194
3;1	0.52	0.4 (II)	2.51	124
5;1	0.43	0.2 (II)	2.06	175
10;1	0.87	0.2 (II)	2.34	182
20;1	2.60	0.3 (II)	2.52	175
30;1	3.90	0.3 (II)	3.03	203

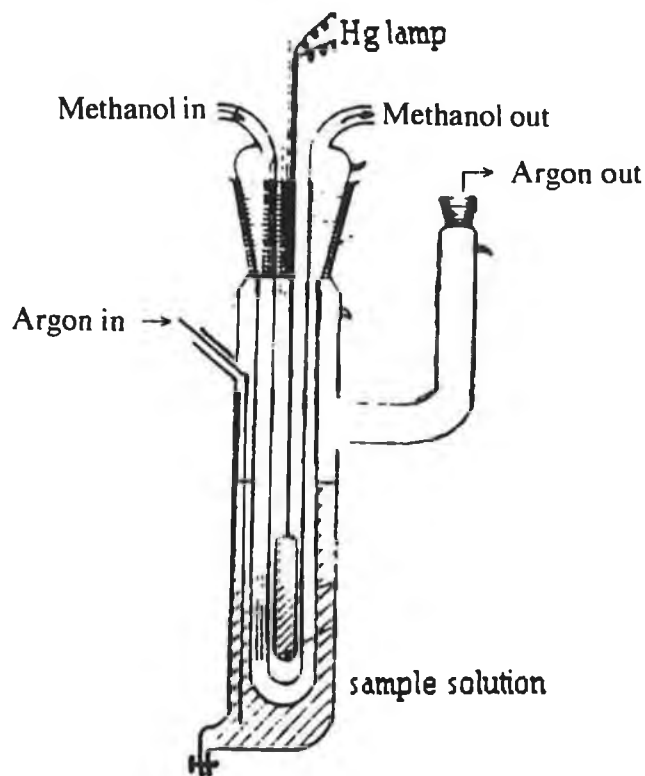
(I): *p*-DPPS

(II): StyCr(CO)₃

5.2.3: Photolysis Experiments.

Preparative photolysis experiments were performed using an Applied Photophysics 400 W medium pressure mercury vapour lamp. The lamp was housed in a double-walled quartz jacket through which methanol at -5°C was circulated to prevent heating of the solution, as shown in Figure 5.2.3. The sample solution was placed in the external chamber. A continuous stream of argon or nitrogen was passed through the solution to remove the carbon monoxide liberated. The products were purified using various procedures.

Figure 5.2.3: Photolysis apparatus used in the synthesis of substituted manganese carbonyl derivatives.



5.2.3.1: Preparation of $\text{CpMn(CO)}_2(\eta^2\text{-C}_8\text{H}_{14})$.

The yellow $\text{CpMn(CO)}_2(\eta^2\text{-cis-C}_8\text{H}_{14})$ complex was prepared by photoejection of a CO molecule from CpMn(CO)_3 in THF, and subsequent displacement of the solvent by *cis*- C_8H_{14} . CpMn(CO)_3 , (0.9mmoles) was added to 150ml THF in the photoreaction vessel and irradiating for 3 hours at -5°C , monitoring the decarbonylation reaction by infrared spectroscopy. The tricarbonyl $\nu(\text{CO})$ vibrations at $2020(\text{m})$ and $1933(\text{s})\text{cm}^{-1}$ diminished on irradiating, concomitant with the production of two new stretches at $1927(\text{s})$ and $1851(\text{s})\text{cm}^{-1}$ corresponding to the cherry-red

$\text{CpMn(CO)}_2(\text{THF})$ adduct. When the reaction was complete, the lamp was turned off and the solution degassed for a further 20 minutes to ensure removal of any free carbon monoxide. The solution was quickly transferred under argon to a flask containing a 20 molar excess of *cis*-cyclooctene. The solvent was removed under reduced pressure and a yellow oily residue remained. This was dissolved in a minimum volume of argon degassed methanol, filtered through cotton wool and stored at -80°C for 72 hours. The resultant yellow precipitate was filtered and dried. IR (*n*-hexane): $\nu(\text{CO})$ 1905(s), 1964(s) cm^{-1} . The yellow powder was reasonably air-stable, but decomposed rapidly in aerated solution.

5.2.3.2: Preparation of $\text{MeCpMn(CO)}_2(\mu\text{-Sty})\text{Cr(CO)}_3$.

MeCpMn(CO)_3 , (2.33mmoles) was dissolved in THF and irradiated as before. The parent $\nu(\text{CO})$ vibrations at 2017(m) and 1929(s) cm^{-1} decreased in intensity with the production of two new vibrations at 1923(s) and 1847(m) cm^{-1} , corresponding to the burgundy coloured $\text{MeCpMn(CO)}_2(\text{THF})$ adduct. The solution was transferred under argon to a flask containing an equimolar amount of StyCr(CO)_3 , which had been dissolved in a minimum volume of THF. This was allowed to stir in the dark for 30 minutes, after which the solvent was removed under reduced pressure. The yellow residue was chromatographed on neutral alumina, using hexane/ether as the mobile phase. The unreacted MeCpMn(CO)_3 eluted first with a 9:1 hexane/ether mix. The polarity was increased (5:1) and unreacted StyCr(CO)_3 eluted. A final yellow band was eluted using a 1:1 mix of hexane/ether, which was later identified as the required product.

The solvent was removed under reduced pressure and an orange-brown solid remained. Crystals were grown from ether/hexane in the dark over a period of 3-5 days. The reaction of $\text{MeCpMn(CO)}_2(\text{THF})$ with StyCr(CO)_3 proceeded in $\sim 15\%$ yield. The crystals were reasonably air-stable in solid form, but rapidly decomposed in solution. IR (pentane): $\nu(\text{CO})$ 1982(m), 1974(s), 1919(s), and 1910(s) cm^{-1} . Proton NMR (CDCl_3): $\delta(\text{CH}_3)$ 1.92 (3H, s), $\delta(\text{C-H}_{\text{vinyl}})$: $\delta(\text{H}_\text{A})$ 3.55-3.57 (1H, dd), $\delta(\text{H}_\text{B})$ 2.74-2.76 (1H, d), $\delta(\text{H}_\text{C})$ 2.41-2.44 (1H, d); $\delta(\text{C}_6\text{H}_5)$ 4.35-4.45 (5H, m), $\delta(\text{C}_5\text{H}_4)$ 5.13-5.47 (4H, m) (See inset, Figure 5.3.1 for explanation of vinylic protons).

5.2.4: Laser flash photolysis with UV/vis monitoring.

A schematic diagram of the flash photolysis system used is shown in Figure 5.2.4.1. The excitation source is a Q-switched Nd-YAG laser, with a fundamental frequency at 1064nm. This may be doubled, tripled or quadrupled to generate second (532nm), third (355nm), or fourth (266nm) harmonic frequencies. At 355nm, the power was approximately 30mJ per pulse. This energy may be changed by altering the voltage across the amplifier flash tube. The pulse diameter is approximately 4mm, and its duration $<10\text{ns}$. The monitoring light source is an Applied Photophysics 40804 air cooled 250W Xenon arc lamp. The laser beam is directed onto the sample cuvette *via* two Pellin-Broca prisms, and is in the cross-beam configuration with the UV/vis monitoring beam. A power meter placed between the two prisms is used to trigger the oscilloscope. UV/vis filters were used ($\lambda > 400\text{nm}$ or $\lambda > 345\text{nm}$) between the monitoring source and the sample to prevent excessive photolysis of the sample. The monitoring beam passes through the sample and is directed to the entrance slit of an

Applied Photophysics f/3.4 monochromator. The light detector is a Hamamatsu five stage photomultiplier operated at 850 volts. Changes in absorbance are output to a transient digitizer (oscilloscope) *via* a variable load resistor. The Hewlett Packard HP 54510A oscilloscope is interfaced to an Olivetti PCS286 microcomputer *via* an IEEE bus.

In a laser flash photolysis experiment, a transient species is produced whose absorbance is recorded as a function of time. The initial amount of light transmitted is measured as a function of the voltage (I_0) accross the photomultiplier tube when the shutter is open. When the laser pulse strikes the sample, the oscilloscope records the change in voltage with time, from the photomultiplier tube. This corresponds to a change in absorbance with time at the monitoring wavelength. Point-by-point spectra may be accumulated by recording transients at a series of monitoring wavelengths (at fixed intervals), at a certain time after the flash.

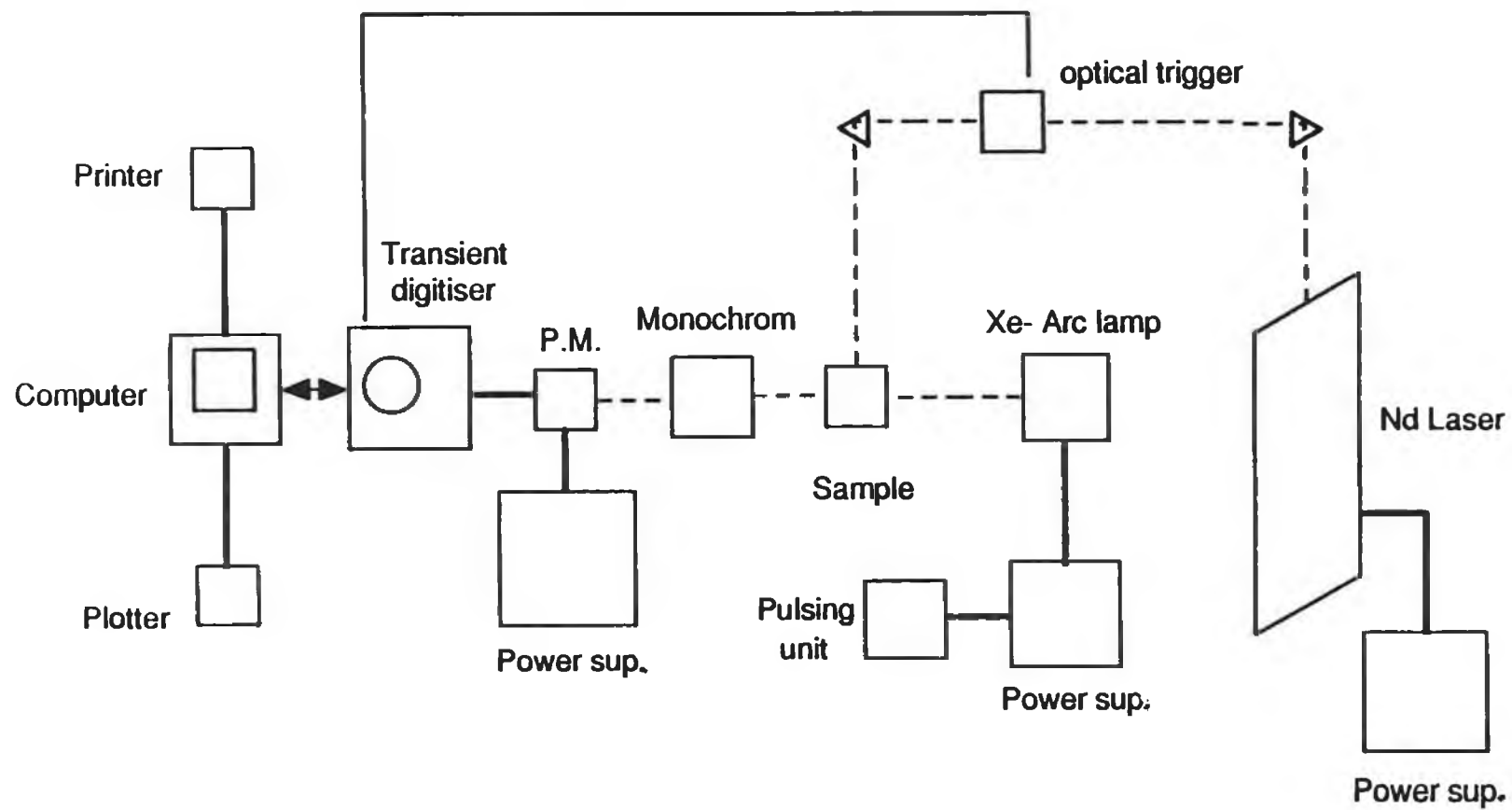


Figure 5.2.4.1: Schematic diagram of the laser flash photolysis system.

5.2.4.1: Sample preparation for flash photolysis experiments.

Laser flash photolysis of metal hexacarbonyls in the presence of various polymers was carried out in toluene solution. Samples were adjusted to an absorbance of ~1.0 absorbance units (at 355nm) so that the reaction kinetics of the three different metal systems (with various extinction coefficients) could be compared. In the copolymer systems, an argon flush method was used in the degassing procedure because, the concentration of ligand was so high that any impurities present had minimal effect on the reaction kinetics. In the homopolymer systems, solutions were degassed by three cycles of freeze-pump-thaw followed by a liquid pumping phase, to remove moisture and oxygen. One atmosphere of argon was then placed over the solution.

Flash photolysis of the half-sandwich compounds was carried out in cyclohexane. Solution absorbances were between 0.5 and 2.5 absorbance units at 355nm. Concentrations were calculated using the extinction coefficients obtained for the various complexes. All solutions were degassed by three or four cycles of freeze-pump-thaw followed by a liquid pump. Argon, or the required carbon monoxide pressure was added to prevent boiling of the solvent and also to check reaction reversibilities. The concentration of CO in cyclohexane was determined to be $9.0 \times 10^{-3} \text{ mol dm}^{-3}$ at one atmosphere of CO at 298K [3].

5.2.4.2: Determination of Activation Parameters.

The activation parameters were calculated from the Arrhenius and Eyring equations. The Arrhenius equation is given by:

$$\ln k = \ln A - E_a^\ddagger/RT$$

where E_a^\ddagger is the activation energy of the activated complex, A is a frequency factor, and R is the universal gas constant. Plotting the observed rate constant, k_{obs} (s^{-1}) against $1/T$ gives a straight line of slope equal to $-E_a^\ddagger/R$.

The Eyring equation is given by:

$$k_2 = (kT/h)(e^{-\Delta G^\ddagger/RT})$$

where k is the Boltzmann constant, h is Planck's constant, and ΔG^\ddagger is the Gibbs free energy of activation. Knowing that $\Delta G^\ddagger = \Delta H^\ddagger - T\Delta S^\ddagger$, where ΔH^\ddagger and ΔS^\ddagger are the enthalpy and entropy changes of activation respectively, the following is obtained:

$$\ln k/T = \ln k/h + \Delta S^\ddagger/R + \Delta H^\ddagger/RT$$

Plotting $\ln k_{\text{obs}}/T$ versus $1/T$ gives a straight line. From the slope and intercept both ΔH^\ddagger and ΔS^\ddagger may be calculated where:

$$\text{Slope} = -\Delta H^\ddagger/R$$

$$\text{Intercept} = \ln k/h + \Delta S^\ddagger/R$$

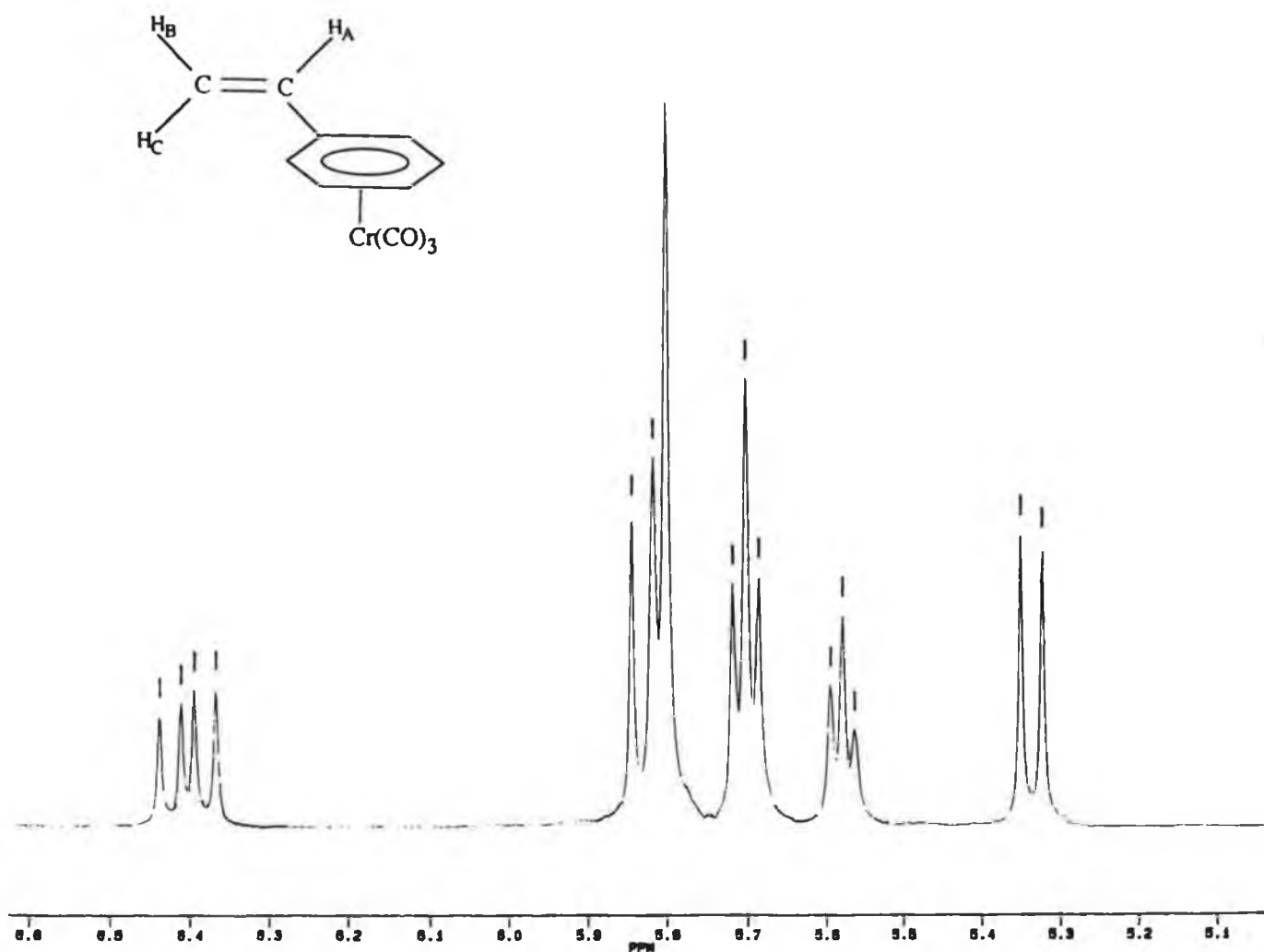
An experiment was one of monitoring the increase in k_{obs} as the temperature was raised in increments of 5K from approximately 280K to 323K.

5.3 Synthetic Procedures.

5.3.1: Synthesis of StyCr(CO)₃.

StyCr(CO)₃ was prepared by the method of Khand *et al.* [4] with slight modifications. Cr(CO)₆ (22.7mmol), and styrene (65 mmol) with inhibitor present, were added to a mixture of di-*n*-butyl ether (90ml) and THF (25ml). The solution was argon degassed for 30 minutes and then heated to reflux. The reflux was maintained for four days under a continuous stream of argon. The resultant orange solution was cooled, filtered and the solvent removed under reduced pressure. A vacuum pump was required to remove all the solvent to dryness. The residue was dissolved in *n*-hexane with heating, and filtered to remove any polymer present, which is insoluble in *n*-hexane. The solvent was removed and the complex was recrystallised from *n*-hexane at -20°C. The orange product was obtained in ~20% yield, as an air stable material. However, it quickly decomposed in solution. IR (C₆H₁₂): $\nu(\text{CO})$ 1980(s), 1915(s)cm⁻¹. IR lit. value [5] (C₆H₁₂): $\nu(\text{CO})$ 1980, 1913cm⁻¹. Proton NMR (C₃D₆O) $\delta(\text{H}_\text{A})$ 6.36-6.43 (1H, quartet), $\delta(\text{H}_\text{B})$ 5.56-5.59 (1H, t), $\delta(\text{H}_\text{C})$ 5.32-5.34 (1H, d), $\delta(\text{C}_6\text{H}_5)$ 5.68-5.71 (2H, t), 5.80-5.81 (2H, d) and 5.84 (1H, s). Figure 5.3.1 shows a proton NMR spectrum of StyCr(CO)₃ (aromatic region).

Figure 5.3.1: ^1H NMR spectrum of StyCr(CO)_3 in $\text{C}_3\text{D}_6\text{O}$.



5.3.2: Preparation of *p*-Diphenylphosphinostyrene (*p*-DPPS).

The synthesis of *p*-DPPS involved the inverse addition of *p*-styryl-magnesium bromide to chlorodiphenylphosphine at 0°C [6]. Direct addition of the phosphine resulted in polymerisation of the monomer. The Grignard reagent was prepared in an oxygen free environment.

5.3.2.1: Preparation of the *p*-Styrylmagnesium bromide.

A dry three-necked flask was fitted with an argon inlet, pressure equalising dropping funnel and a reflux condenser with a calcium chloride drying tube, and the flask was then flushed with argon for 20 minutes. 5.0g magnesium turnings was added, along with 50ml THF with stirring under a constant stream of argon. 1.0cm³ ethyl bromide was added and the temperature maintained below 40°C throughout the reaction. 4-Bromostyrene (100mmol) was added dropwise, and the Grignard reagent stirred under argon for 1 hour. The product was filtered under argon immediately before use.

5.3.2.2: Preparation of *p*-Diphenylphosphinostyrene.

A dry three-necked flask was fitted with an argon inlet, thermometer and rubber septum and flushed as before. Chlorodiphenylphosphine (70mmol) was added along with 50 cm³ THF. The temperature was reduced to 0°C, and *p*-styrylmagnesium bromide was added slowly *via* syringe. The resultant mixture was brought to room temperature and stirred for 45 minutes under argon. Unreacted Grignard reagent was removed by adding to aqueous NH₄Cl, followed by extraction with THF and drying over magnesium sulphate. Polymeric impurities were removed by precipitation in pet. ether, and filtering. The product precipitated from solution on addition of dry ethanol. The crude product was recrystallised from ethanol. IR (KBr): $\nu(\text{C}=\text{C})$ 1621cm⁻¹, m. pt.: 77-78°C.

5.4 Synthesis of the Homopolymer Complexes.

5.4.1: Styrene and Methyl Methacrylate Homopolymers.

Styrene and methyl methacrylate were individually homopolymerised by free radical initiation using AIBN. Mixtures of monomer and AIBN were argon degassed for 15 minutes before heating to 80°C for two hours. The glassy homopolymers produced were dissolved in a minimum volume of chloroform and repeatedly precipitated from pet. ether (40-60). The white polymers were dried *in vacuo* overnight. A range of molecular weights were prepared by varying the percentage AIBN added. Relatively low molecular weight distributions were obtained. The data, including rms end-to-end distances is tabulated in Table 5.2.2.

5.4.2: Anionic Polymerisation of α -Methylstyrene.

α -Methylstyrene does not undergo free-radical polymerisation but may be efficiently homopolymerised using anionic or cationic initiators. Anionic polymerisation involves the transfer of an electron from an electron donor to a monomer molecule to form a radical anion. Propagation takes place through addition of monomer molecules to the active centres. The polymers continue to grow to form a 'living' polymer, and termination will not occur (unless any oxidising impurities enter the system) until a terminating species is added.

α -Methylstyrene was homopolymerised using sodium naphthalide as the initiator in THF at -80°C. Sodium naphthalide is formed from naphthalene and metallic sodium in THF. This reacts very quickly with vinyl groups to produce radical ions which quickly dimerise, and are capable of propagating

anionically at both ends. The initiation step is rapid, all the polymer chains beginning to 'grow' at the same time. The propagation reaction is slower in comparison and when all the monomer is used up, other monomers may be added and the propagating reaction continues until terminated.

Preparation of sodium naphthalide.

A dry three-necked round-bottomed flask was fitted with an argon inlet, a reflux condenser and a calcium chloride drying tube. The flask was flushed with argon for 20 minutes. Then 1.53g of naphthalene in 50ml dry THF was added, followed by 1.5g of sodium wire, stirring continuously. After 10-20 minutes the deep green colour of the initiator was evident. The solution was stirred for 2 hours under a constant stream of argon.

Homopolymerisation of α -Methylstyrene.

A dry three-necked flask was fitted with an argon inlet, a calcium chloride drying tube, and a rubber septum. The system was argon flushed for 20 minutes. The required weight of monomer (~5.0g) in THF was added, and the temperature gradually lowered to -80°C , by immersing in a THF-liquid nitrogen slurry. Sodium naphthalide initiator was added *via* syringe, whereupon a deep red colour immediately formed, indicating the production of α -methylstyrene anions. At a later stage the 'living' polymers were terminated using methanol (4cm^3). The polymer solution was brought to room temperature and the solvent reduced to a minimum volume. The polymers were precipitated in pet. ether and dried *in vacuo*. Various molecular weights were obtained by varying the propagation time from a few minutes to several hours. Polymerisations proceeded in > 90% yield

producing polymers of very narrow molecular weight distribution. The experimental data is tabulated on Table 5.2.2.

5.5 Synthesis of the Copolymer Complexes.

5.5.1: Preparation of Styrene: *p*-Diphenylphosphinostyrene Copolymers.

Copolymers of styrene (S) and *p*-diphenylphosphinostyrene (*p*-DPPS) were prepared in 5:1, 10:1, 20:1 and 30:1 mole ratios of styrene to *p*-DPPS. The polymerisation reaction was initiated using AIBN (1%) as described for the homopolymers. The white copolymers were precipitated in pet. ether from chloroform. IR analysis (copolymer cast as film on NaCl plates from CHCl₃) revealed spectra very similar to polystyrene with a weak phosphine-aryl absorption at 1434cm⁻¹. The percentage phosphorus in each was determined by microanalysis [7]. The experimental data is tabulated in Table 5.2.3.

5.5.2: Preparation of Styrene: StyCr(CO)₃ Copolymers.

Polystyrene-bound chromiumtricarbonyl was prepared by the copolymerisation of styrene (S) and StyCr(CO)₃ using AIBN as the initiator. Copolymers were prepared in mole ratios of 3:1, 5:1, 10:1, 20:1 and 30:1 styrene to StyCr(CO)₃ respectively. The olive-coloured copolymers were precipitated in pet. ether from chloroform and dried. The UV/vis spectrum of the copolymers was very similar to that for (benzene)Cr(CO)₃ (in toluene). IR analysis (cast film) revealed spectra similar to polystyrene except for the intense absorptions in the ν(CO) region

at 1965 and 1883 cm^{-1} . The concentration of chromium in each copolymer was determined from the extinction coefficient of (benzene) $\text{Cr}(\text{CO})_3$ in toluene. The experimental data for the synthesis and rms end-to-end distance determination is shown in Table 5.2.3.

5.6 REFERENCES

- 1 Perrin, D. D.; Armarego, W. L. F.; Perrin, D. R.; *Purification of Laboratory Chemicals*, Pergamon Press, New York, 1980.
- 2 (a) Collins, E. A.; Bares, J.; Billmeyer, F. W. Jr.; *Expts. in Polymer Science*, Wiley Interscience, New York, 1973; (b) Brydson, J. A.; *Plastic Materials*, Buttersworth Scientific, London, 1982.
- 3 (a) Makranczy, J.; Begyery-Balog, K.; Ruzs, L.; Patyi, L.; *Hung. J. Ind. Chem.* **4**, 629, 1976; (b) Gjaldback, J. C.; *Acta Chem. Scand.* **6**, 623, 1952; (c) *IUPAC Solubility Data Series*, Pergamon Press, Oxford, England. **Vol. 43**, 1990.
- 4 Khand, I.U.; Mahaffy, C. A.; Pauson, P. L.; *J. Chem. Res. (S)* 352, 1978; *Chem. Res. (M)* 4454, 1978.
- 5 Rausch, M. D.; Moser, G. A.; Zaiko, E. J.; Lipman, A. L. Jr.; *J. Organomet. Chem.* **23**, 185, 1970.
- 6 Rabinowitz, R.; Marcus, R.; *J. Org. Chem.* **26**, 4157, 1961.
- 7 Microanalytical Laboratory, University College Dublin, Dublin 4.

APPENDIX A

Table 1A: Experimental data for the determination of the activation parameters for the formation of $\text{W(CO)}_5(\text{PPh}_3)$, $[2.92 \times 10^{-2} \text{ M PPh}_3]$ in toluene.

Temp (K)	$(1/T)E_3$ (1/K)	kobs (/s)	ln(kobs)	ln(kobs/T)
289	3.46	13.04	2.56	-3.09
293	3.41	13.80	2.62	-3.05
308	3.25	22.35	3.10	-2.62
313	3.19	29.67	3.39	-2.35
318	3.14	38.15	3.65	-2.12
323	3.10	51.08	3.93	-1.84

Arrhenius Plot

$$\text{Slope} = -3660 \pm 320$$

$$\text{Intercept} = 15.0 \pm 0.2$$

$$\text{Correlation} = 0.99$$

$$E_a^\ddagger = 26 \pm 3 \text{ kJmol}^{-1}$$

Eyring Plot

$$\text{Slope} = -3320 \pm 320$$

$$\text{Intercept} = 8.3 \pm 0.2$$

$$\text{Correlation} = 0.99$$

$$\Delta H^\ddagger = 24 \pm 2 \text{ kJmol}^{-1}$$

$$\Delta S^\ddagger = -143 \pm 25 \text{ Jmol}^{-1}\text{K}^{-1}$$

Table 2A: Experimental data for the determination of the activation parameters for the formation of $\text{W(CO)}_5(\text{MePh-PPh}_2)$ [$1.94 \times 10^{-2}\text{M}$ MePh-PPh_2] in toluene.

Temp (K)	(1/T)E3 (1/K)	kobs (/s)	ln(kobs)	ln(kobs/T)
295	3.39	16.74	2.81	-2.86
304	3.29	23.39	3.15	-2.56
308	3.24	32.15	3.47	-2.26
318	3.19	42.29	3.74	-2.00
318	3.14	60.04	4.09	-1.66
323	3.09	75.45	4.32	-1.45

Arrhenius Plot

Slope = -5230 ± 320

Intercept = 20.4 ± 0.1

Correlation = 0.99

$$E_a^\ddagger = 44 \pm 3 \text{ kJmol}^{-1}$$

Eyring Plot

Slope = -4910 ± 335

Intercept = 13.7 ± 0.1

Correlation = 0.99

$$\Delta H^\ddagger = 41 \pm 3 \text{ kJmol}^{-1}$$

$$\Delta S^\ddagger = -84 \pm 25 \text{ Jmol}^{-1}\text{K}^{-1}$$

Table 3A: Experimental data for the determination of the activation parameters for the reaction of $\text{W(CO)}_5(\text{toluene})$ with (5:1);(S:*p*-DPPS), $[2.32 \times 10^{-2} \text{M PPh}_3]$.

Temp (K)	(1/T)E3 (1/K)	kobs (/s)	ln(kobs)	ln(kobs/T)
299	3.34	71.26	4.26	-1.43
303	3.30	82.48	4.41	-1.30
308	3.24	98.05	4.58	-1.14
313	3.19	112.99	4.72	-1.01
318	3.14	139.78	4.94	-0.82
323	3.10	168.58	5.12	-0.07

Arrhenius Plot

Slope = -3380 ± 125

Intercept = 15.6 ± 0.1

Correlation = 0.99

$$E_a^\ddagger = 28 \pm 1 \text{ kJmol}^{-1}$$

Eyring Plot

Slope = -3070 ± 102

Intercept = 8.8 ± 0.1

Correlation = 0.99

$$\Delta H^\ddagger = 26 \pm 1 \text{ kJmol}^{-1}$$

$$\Delta S^\ddagger = -125 \pm 25 \text{ Jmol}^{-1} \text{K}^{-1}$$

Table 4A: Experimental data for the determination of the activation parameters for the reaction of $\text{W(CO)}_5(\text{toluene})$ with (10:1);(S:*p*-DPPS), $[2.55 \times 10^{-2} \text{M PPh}_3]$.

Temp (K)	(1/T)E3 (1/K)	kobs (/s)	ln(kobs)	ln(kobs/T)
290	3.44	80.96	4.39	-1.27
296	3.37	102.57	4.63	-1.06
303	3.30	115.22	4.74	-0.96
308	3.24	156.12	5.05	-0.67
318	3.14	220.00	5.39	-0.36
323	3.10	270.90	5.60	-0.17

Arrhenius Plot

Slope = -3405.1 ± 65.57

Intercept = 16.099 ± 0.02

Correlation = 0.99

$$E_a^\ddagger = 28.31 \pm 0.55 \text{ kJmol}^{-1}$$

Eyring Plot

Slope = -3107.4 ± 57.18

Intercept = 9.4115 ± 0.02

Correlation = 0.99

$$\Delta H^\ddagger = 25.83 \pm 0.48 \text{ kJmol}^{-1}$$

$$\Delta S^\ddagger = -119.29 \pm 25 \text{ Jmol}^{-1}\text{K}^{-1}$$

Table 5A: Experimental data for the determination of the activation parameters for the reaction of $\text{W(CO)}_5(\text{toluene})$ with (20:1);(S:*p*-DPPS), $[1.00 \times 10^{-2} \text{M PPh}_3]$.

Temp (K)	(1/T)E3 (1/K)	kobs (/s)	ln(kobs)	ln(kobs/T)
299	3.34	104.88	4.65	-1.04
303	3.30	124.50	4.82	-0.88
308	3.24	152.35	5.02	-0.70
318	3.14	237.00	5.46	-0.29
323	3.09	276.65	5.62	-0.15

Arrhenius Plot

Slope = -3930 ± 104

Intercept = 17.8 ± 0.1

Correlation = 0.99

$$E_a^\ddagger = 33 \pm 1 \text{ kJmol}^{-1}$$

Eyring Plot

Slope = -3610 ± 110

Intercept = 11.0 ± 0.1

Correlation = 0.99

$$\Delta H^\ddagger = 30 \pm 1 \text{ kJmol}^{-1}$$

$$\Delta S^\ddagger = -106 \pm 25 \text{ Jmol}^{-1}\text{K}^{-1}$$

Table 6A: Experimental data for the determination of the activation parameters for the reaction of $\text{W(CO)}_5(\text{toluene})$ with (30:1);(S:*p*-DPPS), $[1.89 \times 10^{-2} \text{M PPh}_3]$.

Temp (K)	(1/T)E3 (1/K)	kobs (/s)	ln(kobs)	ln(kobs/T)
299	3.34	261.29	5.56	-0.13
303	3.30	364.64	5.89	0.18
308	3.24	443.30	6.09	0.36
318	3.14	539.93	6.29	0.54
323	3.09	664.84	6.49	0.73

Arrhenius Plot

Slope = -4225 ± 285

Intercept = 19.8 ± 0.1

Correlation = 0.99

$$E_a^\ddagger = 35 \pm 3 \text{ kJmol}^{-1}$$

Eyring Plot

Slope = -3880 ± 275

Intercept = 13 ± 0.1

Correlation = 0.99

$$\Delta H^\ddagger = 32 \pm 3 \text{ kJmol}^{-1}$$

$$\Delta S^\ddagger = -90 \pm 25 \text{ Jmol}^{-1}\text{K}^{-1}$$

APPENDIX B

Table 1B: Experimental data for the determination of the activation parameters for the formation of $\text{Mo(CO)}_5(\text{PPh}_3)$, $[1.27 \times 10^{-2} \text{M PPh}_3]$.

Temp (K)	$(1/T)E_3$ (1/K)	kobs (/s)	ln(kobs)	ln(kobs/T)
296	3.38	228.36	5.43	-0.26
303	3.30	320.76	5.77	0.05
308	3.24	420.57	6.04	0.31
318	3.19	519.40	6.25	0.50
318	3.14	625.93	6.43	0.67
323	3.09	751.31	6.62	0.84

Arrhenius Plot

Slope = -4125 ± 81

Intercept = 19.4 ± 0.1

Correlation = 0.99

$$E_a^\ddagger = 34 \pm 1 \text{ kJmol}^{-1}$$

Eyring Plot

Slope = -3825 ± 85

Intercept = 13 ± 0.1

Correlation = 0.99

$$\Delta H^\ddagger = 32 \pm 1 \text{ kJmol}^{-1}$$

$$\Delta S^\ddagger = -92 \pm 25 \text{ Jmol}^{-1}\text{K}^{-1}$$

Table 2B: Experimental data for the determination of the activation parameters for the formation of $\text{Mo(CO)}_5(\text{MePh-PPh}_2)$, $[1.01 \times 10^{-2} \text{M MePh-PPh}_2]$.

Temp (K)	(1/T)E3 (1/K)	kobs (/s)	ln(kobs)	ln(kobs/T)
299	3.34	333.40	5.81	0.11
303	3.30	445.41	6.09	0.38
308	3.24	571.84	6.34	0.61
313	3.19	695.56	6.54	0.79
318	3.14	864.90	6.76	1.00
323	3.09	1013.79	6.92	1.14

Arrhenius Plot

Slope = -4350 ± 225

Intercept = 20.4 ± 0.1

Correlation = 0.99

$$E_a^\ddagger = 36 \pm 2 \text{ kJmol}^{-1}$$

Eyring Plot

Slope = -4030 ± 230

Intercept = 14.0 ± 0.1

Correlation = 0.99

$$\Delta H^\ddagger = 34 \pm 2 \text{ kJmol}^{-1}$$

$$\Delta S^\ddagger = -84 \pm 25 \text{ Jmol}^{-1}\text{K}^{-1}$$

Table 3B: Experimental data for the determination of the activation parameters for the reaction of Mo(CO)₅(toluene) with (5:1):(S:*p*-DPPS), [1.53 x 10⁻²M PPh₃].

Temp (K)	(1/T)E3 (1/K)	k _{obs} (/s)	ln(k _{obs})	ln(k _{obs} /T)
298	3.35	831.22	6.72	1.02
304	3.29	1241.96	7.12	1.40
308	3.24	1631.49	7.39	1.66
313	3.19	1952.83	7.57	1.83
318	3.14	2267.52	7.72	1.96
323	3.09	2910.82	7.97	2.20

Arrhenius Plot

Slope = -4590 ± 325

Intercept = 22.2 ± 0.1

Correlation = 0.99

$$E_a^\ddagger = 38 \pm 3 \text{ kJmol}^{-1}$$

Eyring Plot

Slope = -4325 ± 325

Intercept = 15.6 ± 0.1

Correlation = 0.99

$$\Delta H^\ddagger = 36 \pm 3 \text{ kJmol}^{-1}$$

$$\Delta S^\ddagger = -68 \pm 25 \text{ Jmol}^{-1}\text{K}^{-1}$$

Table 4B: Experimental data for the determination of the activation parameters for the reaction of $\text{Mo(CO)}_5(\text{toluene})$ with (10:1);(S:*p*-DPPS), $[2.20 \times 10^{-2} \text{M PPh}_3]$.

Temp (K)	(1/T)E3 (1/K)	kobs (/s)	ln(kobs)	ln(kobs/T)
300	3.33	1978.00	7.59	1.88
308	3.24	2534.39	7.83	2.10
313	3.19	3507.43	8.16	2.41
318	3.14	4562.08	8.44	2.68
323	3.09	5209.08	8.55	2.78

Arrhenius Plot

$$\text{Slope} = -4300 \pm 435$$

$$\text{Intercept} = 21.9 \pm 0.1$$

$$\text{Correlation} = 0.99$$

$$E_a^\ddagger = 36 \pm 4 \text{ kJmol}^{-1}$$

Eyring Plot

$$\text{Slope} = -4045 \pm 425$$

$$\text{Intercept} = 15.3 \pm 0.1$$

$$\text{Correlation} = 0.98$$

$$\Delta H^\ddagger = 34 \pm 4 \text{ kJmol}^{-1}$$

$$\Delta S^\ddagger = -70 \pm 25 \text{ Jmol}^{-1}\text{K}^{-1}$$

Table 5B: Experimental data for the determination of the activation parameters for the reaction of Mo(CO)₅(toluene) with (20:1);(S:*p*-DPPS), [1.17 x 10⁻²M PPh₃].

Temp (K)	(1/T)E3 (1/K)	kobs (/s)	ln(kobs)	ln(kobs/T)
297	3.36	1483.38	7.30	1.61
303	3.30	1854.26	7.52	1.81
308	3.24	2708.86	7.90	2.17
313	3.19	3399.65	8.13	2.38
318	3.14	4012.75	8.29	2.53
323	3.09	4586.55	8.43	2.65

Arrhenius Plot

Slope = -4380 ± 290

Intercept = 22.0 ± 0.1

Correlation = 0.99

$E_a^\ddagger = 36 \pm 3 \text{ kJmol}^{-1}$

Eyring Plot

Slope = -4050 ± 285

Intercept = 15.2 ± 0.1

Correlation = 0.99

$\Delta H^\ddagger = 34 \pm 3 \text{ kJmol}^{-1}$

$\Delta S^\ddagger = -71 + 25 \text{ Jmol}^{-1}\text{K}^{-1}$

Table 6B: Experimental data for the determination of the activation parameters for the reaction of Mo(CO)₅(toluene) with (30:1);(S:*p*-DPPS), [1.34 x 10⁻²M PPh₃].

Temp (K)	(1/T)E3 (1/K)	kobs (/s)	ln(kobs)	ln(kobs/T)
296	3.37	1469.90	7.29	1.60
303	3.30	1537.89	7.33	1.62
308	3.24	2913.42	7.97	2.24
313	3.19	3148.73	8.05	2.30
318	3.14	5694.45	8.64	2.88
323	3.09	5849.27	8.67	2.89

Arrhenius Plot

Slope = -5620 ± 770

Intercept = 26.1 ± 0.2

Correlation = 0.96

$$E_a^\ddagger = 47 \pm 7 \text{ kJmol}^{-1}$$

Eyring Plot

Slope = -5300 ± 775

Intercept = 19.3 ± 0.2

Correlation = 0.96

$$\Delta H^\ddagger = 44 \pm 7 \text{ kJmol}^{-1}$$

$$\Delta S^\ddagger = -37 \pm 25 \text{ Jmol}^{-1}\text{K}^{-1}$$

APPENDIX C

Table 1C: Experimental data for the determination of the activation parameters for the formation of $\text{Cr}(\text{CO})_5(\text{PPh}_3)$, $[1.97 \times 10^{-2} \text{M PPh}_3]$.

Temp (K)	(1/T)E3 (1/K)	kobs (/s)	ln(kobs)	ln(kobs/T)
297	3.36	525.32	6.26	0.57
303	3.30	780.16	6.66	0.94
308	3.24	1132.16	7.03	1.30
313	3.19	1380.65	7.23	1.48
318	3.14	1632.53	7.39	1.63
323	3.09	1914.16	7.56	1.78

Arrhenius Plot

Slope = -4765 ± 390

Intercept = 22.4 ± 0.1

Correlation = 0.99

$$E_a^\ddagger = 40 \pm 3 \text{ kJmol}^{-1}$$

Eyring Plot

Slope = -4450 ± 390

Intercept = 15.6 ± 0.1

Correlation = 0.99

$$\Delta H^\ddagger = 37 \pm 3 \text{ kJmol}^{-1}$$

$$\Delta S^\ddagger = -68 \pm 25 \text{ Jmol}^{-1}\text{K}^{-1}$$

Table 2C: Experimental data for the determination of the activation parameters for the formation of $\text{Cr(CO)}_5(\text{MePh-PPh}_2)$, $[1.18 \times 10^{-2} \text{M MePh-PPh}_2]$.

Temp (K)	$(1/T)E_3$ (1/K)	kobs (/s)	ln(kobs)	ln(kobs/T)
299	3.34	751.86	6.62	0.92
303	3.30	857.16	6.75	1.03
308	3.24	1083.26	6.98	1.25
313	3.19	1559.95	7.35	1.60
318	3.14	2159.77	7.67	1.91
323	3.09	2658.80	7.88	2.10

Arrhenius Plot

Slope = -5300 ± 320

Intercept = 24.2 ± 0.1

Correlation = 0.99

$$E_a^\ddagger = 44 \pm 3 \text{ kJmol}^{-1}$$

Eyring Plot

Slope = -5000 ± 320

Intercept = 17.5 ± 0.1

Correlation = 0.99

$$\Delta H^\ddagger = 42 \pm 3 \text{ kJmol}^{-1}$$

$$\Delta S^\ddagger = -52 \pm 25 \text{ Jmol}^{-1}\text{K}^{-1}$$

Table 3C: Experimental data for the determination of the activation parameters for the reaction of $\text{Cr(CO)}_5(\text{toluene})$ with (5:1);(S:*p*-DPPS), $[3.95 \times 10^{-3} \text{M PPh}_3]$.

Temp (K)	(1/T)E3 (1/K)	kobs (/s)	ln(kobs)	ln(kobs/T)
297	3.36	640.04	6.46	0.76
304	3.29	865.36	6.76	1.04
310	3.22	1376.99	7.22	1.49
314	3.19	1691.85	7.43	1.68
318	3.14	1951.29	7.57	1.81
324	3.08	2375.48	7.77	1.99

Arrhenius Plot

Slope = -4895 ± 300

Intercept = 22.9 ± 0.1

Correlation = 0.99

$E_a^\ddagger = 41 \pm 3 \text{ kJmol}^{-1}$

Eyring Plot

Slope = -4610 ± 315

Intercept = 16.3 ± 0.1

Correlation = 0.99

$\Delta H^\ddagger = 38 \pm 3 \text{ kJmol}^{-1}$

$\Delta S^\ddagger = -62 \pm 25 \text{ Jmol}^{-1}\text{K}^{-1}$

Table 4C: Experimental data for the determination of the activation parameters for the reaction of $\text{Cr(CO)}_5(\text{toluene})$ with $(10:1);(\text{S};p\text{-DPPS})$, $[8.9 \times 10^{-3} \text{M PPh}_3]$.

Temp (K)	$(1/T)E_3$ (1/K)	kobs (/s)	ln(kobs)	ln(kobs/T)
295	3.38	1203.92	7.09	1.40
303	3.30	1684.44	7.42	1.71
308	3.24	2337.52	7.75	2.02
313	3.19	3065.01	8.02	2.28
318	3.14	4000.09	8.29	2.53
324	3.08	5118.34	8.54	2.76

Arrhenius Plot

Slope = -4980 ± 135

Intercept = 23.9 ± 0.1

Correlation = 0.99

$E_a^\ddagger = 41 \pm 1 \text{ kJmol}^{-1}$

Eyring Plot

Slope = -4680 ± 130

Intercept = 17.2 ± 0.1

Correlation = 0.99

$\Delta H^\ddagger = 39 \pm 1 \text{ kJmol}^{-1}$

$\Delta S^\ddagger = -55 \pm 25 \text{ Jmol}^{-1}\text{K}^{-1}$

Table 5C: Experimental data for the determination of the activation parameters for the reaction of $\text{Cr(CO)}_5(\text{toluene})$ with (20:1);(S:*p*-DPPS), $[6.2 \times 10^{-3} \text{M PPh}_3]$.

Temp (K)	(1/T)E3 (1/K)	kobs (/s)	ln(kobs)	ln(kobs/T)
298	3.35	1399.02	7.24	1.55
303	3.30	1638.55	7.40	1.69
308	3.24	1947.86	7.57	1.84
314	3.18	2245.55	7.71	1.96
318	3.14	2655.86	7.88	2.12
324	3.08	3221.59	8.07	2.29

Arrhenius Plot

Slope = -3025 ± 105

Intercept = 17.4 ± 0.1

Correlation = 0.99

$E_a^\ddagger = 25 \pm 1 \text{ kJmol}^{-1}$

Eyring Plot

Slope = -2695 ± 110

Intercept = 10.6 ± 0.1

Correlation = 0.99

$\Delta H^\ddagger = 22 \pm 1 \text{ kJmol}^{-1}$

$\Delta S^\ddagger = -110 \pm 25 \text{ Jmol}^{-1}\text{K}^{-1}$

Table 6C: Experimental data for the determination of the activation parameters for the reaction of $\text{Cr}(\text{CO})_5(\text{toluene})$ with (30:1);(S;*p*-DPPS), $[5.42 \times 10^{-3} \text{M PPh}_3]$.

Temp (K)	(1/T)E3 (1/K)	kobs (/s)	ln(kobs)	ln(kobs/T)
296	3.38	1406.97	7.24	1.55
303	3.30	1979.75	7.59	1.88
309	3.23	2593.41	7.86	2.13
313	3.19	3011.56	8.01	2.26
318	3.14	3810.59	8.24	2.48
324	3.08	4766.03	8.47	2.69

Arrhenus Plot

Slope = -4090 ± 55

Intercept = 21.1 ± 0.1

Correlation = 0.99

$E_a^\ddagger = 34 \pm 1 \text{ kJmol}^{-1}$

Eyring Plot

Slope = -3780 ± 65

Intercept = 14.3 ± 0.1

Correlation = 0.99

$\Delta H^\ddagger = 31 \pm 1 \text{ kJmol}^{-1}$

$\Delta S^\ddagger = -78 \pm 25 \text{ Jmol}^{-1} \text{K}^{-1}$

APPENDIX D

Table 1D: Experimental data for the determination of the activation parameters for the reaction of (3:1);(S:StyCr(CO)₂(S)) with [2 x 10⁻² M] PPh₃.

Temp (K)	(1/T)E3 (1/K)	kobs (/s)	ln(kobs)	ln(kobs/T)
283	3.53	40.67	3.71	-1.94
288	3.47	54.74	4.00	-1.66
298	3.35	78.43	4.36	-1.33
303	3.30	132.62	4.89	-0.83
308	3.24	225.40	5.42	-0.31
313	3.19	361.18	5.89	0.14

Arrhenius Plot

Slope = -6230 ± 735

Intercept = 25.6 ± 0.3

Correlation = 0.97

$E_a^\ddagger = 52 \pm 3 \text{ kJmol}^{-1}$

Eyring Plot

Slope = -5930 ± 725

Intercept = 18.9 ± 0.3

Correlation = 0.97

$\Delta H^\ddagger = 50 \pm 3 \text{ kJmol}^{-1}$

$\Delta S^\ddagger = -41 \pm 25 \text{ Jmol}^{-1}\text{K}^{-1}$

Table 2D: Experimental data for the determination of the activation parameters for the reaction of (5:1);(S:StyCr(CO)₂(S) with [2 x 10⁻² M] PPh₃.

Temp (K)	(1/T)E3 (1/K)	kobs (/s)	ln(kobs)	ln(kobs/T)
298	3.35	136.12	4.91	-0.78
303	3.30	276.72	5.62	-0.09
308	3.24	552.82	6.31	0.59
313	3.19	1119.83	7.20	1.28
318	3.14	1502.62	7.32	1.56

Arrhenius Plot

Slope = -12400 ± 1100

Intercept = 46.5 ± 0.2

Correlation = 0.98

$$E_a^\ddagger = 103 \pm 3 \text{ kJmol}^{-1}$$

Eyring Plot

Slope = -11400 ± 800

Intercept = 37.6 ± 0.2

Correlation = 0.99

$$\Delta H^\ddagger = 95 \pm 3 \text{ kJmol}^{-1}$$

$$\Delta S^\ddagger = 115 \pm 25 \text{ kJmol}^{-1}$$

Table 3D: Experimental data for the determination of the activation parameters for the reaction of (10:1);(S:StyCr(CO)₂(S)) with $[2 \times 10^{-2} \text{ M}]$ PPh₃.

Temp (K)	(1/T)E3 (1/K)	kobs (/s)	ln(kobs)	ln(kobs/T)
298	3.35	1164	7.06	1.36
303	3.30	2139	7.67	1.95
308	3.24	3239	8.08	2.35
313	3.19	5318	8.57	2.83
318	3.14	7091	8.86	3.10
323	3.09	13033	9.47	3.69

Arrhenius Plot

Slope = -8800 ± 410

Intercept = 36.6 ± 0.1

Correlation = 0.99

$$E_a^\ddagger = 73 \pm 3 \text{ kJmol}^{-1}$$

Eyring Plot

Slope = -8500 ± 395

Intercept = 29.9 ± 0.1

Correlation = 0.99

$$\Delta H^\ddagger = 71 \pm 3 \text{ kJmol}^{-1}$$

$$\Delta S^\ddagger = 51 \pm 25 \text{ Jmol}^{-1}\text{K}^{-1}$$

Table 4D: Experimental data for the determination of the activation parameters for the reaction of (20:1);(S:StyCr(CO)₂(S)) with [2 x 10⁻² M] PPh₃.

Temp (K)	(1/T)E3 (1/K)	kobs (/s)	ln(kobs)	ln(kobs/T)
298	3.35	4855	8.48	2.79
303	3.30	7200	8.88	3.14
308	3.24	12541	9.41	3.70
313	3.19	15640	9.66	3.91
318	3.14	29774	10.30	4.54
323	3.09	42550	10.66	4.88

Arrhenius Plot

Slope = -8400 ± 400

Intercept = 36.6 ± 0.1

Correlation = 0.99

$$E_a^\ddagger = 70 \pm 3 \text{ kJmol}^{-1}$$

Eyring Plot

Slope = -8120 ± 410

Intercept = 30 ± 0.1

Correlation = 0.99

$$\Delta H^\ddagger = 68 \pm 3 \text{ kJmol}^{-1}$$

$$\Delta S^\ddagger = 52 \pm 25 \text{ Jmol}^{-1}\text{K}^{-1}$$

Table 5D: Experimental data for the determination of the activation parameters for the reaction of (30:1);(S:StyCr(CO)₂(S)) with $[2 \times 10^{-2} \text{ M}] \text{PPh}_3$.

Temp (K)	(1/T)E3 (1/K)	kobs (/s)	ln(kobs)	ln(kobs/T)
299	3.34	5626	8.64	2.94
303	3.30	7606	8.94	3.22
308	3.24	11546	9.35	3.62
313	3.19	11479	9.58	3.83
318	3.14	27646	10.28	4.47
323	3.09	41477	10.63	4.89

Arrhenius plot

Slope = -7900 ± 520

Intercept = 35.0 ± 0.1

Correlation = 0.99

$$E_a^\ddagger = 66 \pm 4 \text{ kJmol}^{-1}$$

Eyring Plot

Slope = -7600 ± 520

Intercept = 28.3 ± 0.1

Correlation = 0.99

$$\Delta H^\ddagger = 63 \pm 4 \text{ kJmol}^{-1}$$

$$\Delta S^\ddagger = 37 \pm 25 \text{ Jmol}^{-1}\text{K}^{-1}$$